2011

Arterial Tissue Perforation Using Ultrasonically Vibrating Wire Waveguides

Mark Wylie
Technological University Dublin, mark.wylie@tudublin.ie

ARTERIAL TISSUE PERFORATION USING ULTRASONICALLY VIBRATING WIRE WAVEGUIDES

Mark Wylie

B.Eng Tech, B.E

Dublin Institute of Technology

School of Manufacturing and Design Engineering

Doctor of Philosophy (PhD)

Supervisors: Dr. Graham Gavin & Dr. Garrett McGuinness

2011

ABSTRACT

Chronic Total Occlusions (CTOs) are fibrous and calcified atherosclerotic lesions which completely occlude the artery. They are difficult to treat with standard dilation procedures as they cannot be traversed easily. Their treatment is also associated with a high risk of arterial perforation. Low frequency ultrasonic vibrations delivered via wire waveguides represent a minimally invasive treatment for CTOs and other tissue ablation applications. These devices typically operate at 20–50 kHz delivering wire waveguide distal tip amplitudes of vibration of 0-60 μm. The diseased tissue is ablated or disrupted by repetitive direct mechanical contact and cavitation. This research assesses the susceptibility of arterial tissue to perforation and residual damage under the action of ultrasonically energised wire waveguides. Using Finite Element Analysis (FEA), a linear acoustic model of the wire waveguide distal tips can predict the pressures for a range of operating parameters typically used for these devices. High mesh densities (140 EPW) were required to solve the entire acoustic field, including complex wave interactions. The FEA model was used to aid in the further design and modification of an ultrasonic apparatus and wire waveguide (0–34.3 μm at 22.5 kHz). Using a test rig, the effects of distal tip amplitudes of vibration, feedrate and angled entry on the perforation forces, energy and temperature were measured. The perforation forces reduced (≈ 60%, 6.13 N - 2.46 N mean) when the wire waveguide was energised at low amplitudes of vibrations (< 27.8 μm). There were no significant change in tissue perforation forces above this or when the waveguide was operating above the cavitation threshold. Histological analysis also showed tissue removal. While this knowledge is useful in the prediction and avoidance of perforations during CTO operations; it is also envisaged that this information can aid in the design and development of generic ultrasonic wire waveguide tissue cutting tools.

DECLARATION

I certify that this thesis, which I now submit for examination for the award of Doctor of Philosophy (PhD), is entirely my own work and has not been taken from the work of others, save and to the extent that such work has been cited and acknowledged within the text of my work.

This thesis was prepared according to the regulations for postgraduate study by research of the Dublin Institute of Technology and has not been submitted in whole or in part for another award in any institute.

The work reported on in this thesis conforms to the principles and requirements of the Institute's guidelines for ethics in research.

The Institute has permission to keep, lend or copy this thesis in whole or in part, on condition that any such use of the material of the thesis is duly acknowledged.

Signature _____ Date_____

Candidate

ACKNOWLEDGEMENTS

My sincere thanks go to my project supervisors Dr. Graham Gavin and Dr. Garrett McGuinness for their excellent guidance and encouragement throughout the duration of this project.

I would like to thank Dr. Marek Rebow, Head of Research in Engineering, Dublin Institute of Technology and Mr. John Lawlor, Head of School of Manufacturing and Design Engineering, Dublin Institute of Technology for their outstanding support and useful advice.

I would also like to thank my colleagues for their constant encouragement and assistance with all types of technical problems. Dr. Jacinta Brown and Dr. Helen Lambkin for their support and guidance and use of their laboratory facilities in Dublin Institute of Technology. Finally, I am forever indebted to my family and friends for their understanding, endless patience and encouragement when it was most required.

TABLE OF CONTENTS

LIST OF FIGURES

LIST OF TABLES

CHAPTER

1 INTRODUCTION

1.1 Catheter delivered ultrasonic wire waveguides in cardiovascular treatments

Cardiovascular surgery has benefited from the advances in Minimally Invasive Surgery (MIS) and it is now possible to perform some surgical interventions on an outpatient basis without the use of traumatic open thoracic surgery. There is a rapid development and refinement of surgical instruments used in this surgical field, in particular MIS has seen unprecedented success in Percutaneous Transluminal Interventions (PTI), delivering dilation devices (balloon and stent) and other cutting tools to an atherosclerotic lesion site for restoring antegrade blood flow to the artery.

However, totally blocked arteries known as Chronic Total Occlusions (CTOs) can be identified in approximately 16% of all patients undergoing angioplasty. They pose a significant challenge to standard minimally invasive interventional techniques that require a guidewire to cross the lesion prior to placement of dilation devices. The ability of a guidewire to cross the lesion appears to be critical to the outcome of standard dilation procedures; a key success indicator in 80% of all cases [1]. This problem has led to an impetus in the development of new devices for unblocking CTOs.

Catheter delivered external transducer systems which deliver ultrasonic vibrations via a wire waveguide can be applied in cardiovascular treatments for thrombus dissolution and for ablation and disruption of hard fibrous calcified atherosclerotic tissues, such as CTOs [2, 3]. This method is reported to selectively remove both inelastic diseased tissue and thrombus through a combination of direct contact and cavitation, with minimal disruption to the surrounding healthy elastic arterial wall, as shown in Figure 1-1. These systems use long slender shafts for navigating the vascular system but typically terminate with an enlarged distal tip (1.1 – 2.0 mm diameter) [2, 4, 5]. Because the wire waveguides typically vibrate in the low ultrasonic frequency range (20-50 kHz), they are also often referred to as high frequency mechanical vibrations. The wire waveguide distal tip vibrations commonly used are approximately 0 - 60 µm in amplitude [2, 5-8].

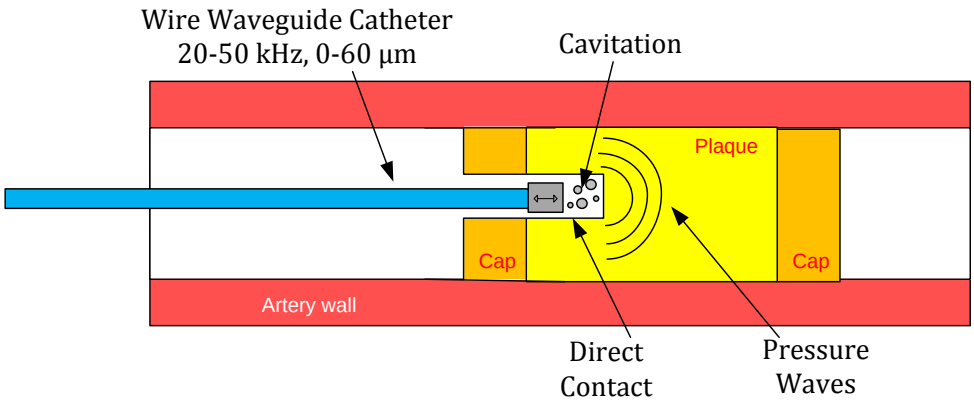

Figure 1-1 : Ultrasonic wire waveguide recanalising a CTO.

In 2005 and 2007, a device using high frequency mechanical vibrations (≈ 20 kHz) delivered via a wire waveguide was approved for use in the recanalisation of CTOs, in Europe and the United States, respectively [9, 10].

Calcifications and fibrous tissue formation is commonly present in CTOs and they are associated with an increased potential for arterial wall perforation during treatment with traditional devices when compared to sub-totally occluded vessels. This may be a result of the distal section of the guidewire or subsequent device being deflected by the hard diseased lesion cap toward the surrounding healthy elastic artery wall or by entering a false lumen [11, 12].

1.2 Research aim and objectives

Most work to date using catheter delivered external transducer systems which deliver ultrasonic vibrations via a wire waveguide has focused on end clinical outcomes, such as, thrombus dissolution, hard fibrous and calcified atherosclerotic tissue ablation and removal.

Minimally invasive cardiovascular devices operate close to healthy vascular tissue and may be associated with a risk of tissue damage or perforation of the surrounding soft healthy arterial wall. While the literature discusses the ability of high frequency mechanical waveguides to selectivity ablate and disrupt diseased tissues, its effects on soft vascular wall tissue have not yet been quantified. No work has been done assessing the resistance of such soft tissue to perforation or cutting using these devices despite the fact this may be of benefit in minimising the risk of perforation during CTO procedures. In addition, greater knowledge of this technology in soft tissue perforation may

lead to the development of generic soft tissue cutting tools which can be used in MIS and other applications.

Using an ultrasonic wire waveguide apparatus, modified as part of this work, the effects of high frequency mechanical vibrations transmitted through wire waveguides on porcine vascular tissue perforation forces, using clinically relevant operating parameters and conditions, is examined.

1.2.1 Aim

The specific aim of this research is to:

"To determine if the ultrasonically energised wire waveguide permits perforation of soft arterial tissue at lower forces, introducing a risk of arterial perforation during CTO recanalisation."

1.2.2 Objectives

This research was realised by conducting a number of parallel but related studies:

i. Numerical analysis of wire waveguide distal tip acoustic conditions.
ii. Ultrasonic apparatus modification and test rig design and development for tissue testing.
iii. Tissue testing using the ultrasonic apparatus and test rig.

1.2.2.1 Numerical analysis of wire waveguide distal tip acoustic conditions

A method of modelling the acoustic conditions surrounding the wire waveguide distal tip is presented as part of this work, using linear acoustic fluid-structure Finite Element Analysis (FEA) (ANSYS). This method is then used as a design tool to aid in the selection of ultrasonic apparatus operating parameters for a tissue testing programme.

1.2.2.2 Ultrasonic wire waveguide apparatus and test rig for tissue testing

A wire waveguide ultrasonic apparatus, developed previously, is modified for a suite of soft tissue tests [13]. A test rig is designed and developed to accommodate this ultrasonic apparatus, which can advance the ultrasonic apparatus towards tissue samples in a controlled manner (feedrate and entry angle). A tissue-wire waveguide force measurement system is also developed. The acoustic field is measured using a hydrophone and a cavitation detection system. Temperature sensing equipment (embedded thermocouples) is also included in the test rig development. A data acquisition system interfaces with a PC and allows for measurement and recording of the above.

1.2.2.3 Tissue testing using the ultrasonic apparatus and test rig

The characterised ultrasonic apparatus is then used to test the perforation forces using ultrasonically vibrating wire waveguide on soft tissue ablation and disruption over a range of distal tip amplitudes of vibration, both above and below the cavitation threshold. The tissue tests are conducted in three phases.

In an effort to more closely mimic surgical *in vivo* conditions the effects of feedrate and angled entry to the tissue on the perforation forces are examined. The temperature increase in the tissue is also measured. Finally a histological analysis is used to assess tissue perforation and damage mechanisms.

1.3 Organisation of thesis

Chapter 2

This review focuses on the use of an ultrasonic wire waveguide device for thrombolysis and angioplasty, with specific applications to CTOs. Experimental and clinical data on device configuration and operating parameters are then compiled. This chapter is a more comprehensive analysis of the state of the art of therapeutic ultrasound and ultrasonic cutting tools for tissue cutting and ablating applications. This review investigates the evolution of this energy delivery, examining both past and present applications and potential future trends. The design requirements for tissue testing using an in-house ultrasonic apparatus, as part of this research, will be extracted from the literature review. This review also highlights the lack of experimental knowledge and quantitative data in wire waveguide ablation and disruption of soft tissue.

Chapter 3

This chapter outlines a methodology for predicting the acoustic pressures generated by an ultrasonically vibrating wire waveguide in a fluid, both directly at the wire waveguide distal tip and the entire acoustic field. Verification of the model is achieved through a mesh convergence and sensitivity analysis and

comparison with analytical solutions. The accuracy of the model for a range of typical operating parameters is determined. This method is then validated by comparing the predicted results of the acoustic field with that of experimental results conducted by others representing a wire waveguide in a peripheral artery.

A number of wire waveguide distal tips are modelled for a range of amplitudes of vibrations. Using a cavitation pressure threshold, it was then possible to predict the amplitudes of vibration required to cause cavitation. Spatially, the cavitation region for a range of wire waveguide distal geometries could also be determined.

Chapter 4

The requirements for an ultrasonic apparatus for this research programme are outlined here. An existing design of an ultrasonic apparatus developed and manufactured previously is refined and improved upon so that it is suitable for a tissue testing programme. The characterisation methods of the ultrasonic apparatus are also outlined, verifying some of the major design requirements. A test rig and sensing equipment used for this research are also outlined. An approach for examining the force profile of the wire waveguide-tissue interaction using a cantilever beam arrangement is proposed. Using a miniature hydrophone and an ultrasonic B-mode diagnostic scanner, Passive Cavitation Detection (PCD) for the acoustic field generated by the vibrating wire waveguide is also conducted.

Chapter 5

Tissue testing using the characterised ultrasonic apparatus and test rig is presented here. The testing was conducted in three phases.

i. Phase one was an initial pilot study to determine the effects of ultrasonic activation of the wire waveguides on perforation forces. These preliminary tests showed that the ultrasonic apparatus and test rig was capable of performing tissue tests. The effects of amplitude of vibration on the maximum perforation forces were investigated. Based on these results, phase two and phase three tissue tests were then designed.

ii. Phase two tissue testing involved a closer examination and analysis of the perforation forces and energies using improved wire waveguides. The effects of cavitation on perforation forces and energies were also investigated here.

iii. Finally, phase three tissue testing is intended to be closer to conditions encountered *in vivo*, such as angled entry perforation and perforation over a range of feedrates. The temperature rise is also recorded for a range of feedrates and amplitudes of vibrations.

Chapter 6

Finally, the major findings and conclusions for the entire research programme are presented here. A summary of results and potential future research and recommendations are also presented.

1.4 Contributions

The following methods and results represent a novel contribution in the emerging field of ultrasonic soft tissue ablation and disruption using wire waveguides. The contributions of this thesis are:

1. This thesis contains an experimental study of ultrasonically energised wire waveguides on arterial tissue perforation. A study of this type has not been conducted before. These results are relevant to wire waveguide application in CTOs and are important in establishing suitable operating parameters, end effector designs and in guiding surgical technique. This is realised through the presentation and analysis of:

    - Force profile data of soft arterial tissue perforation using ultrasonically vibrating wire waveguides with clinically relevant operating parameters.
    - Perforation initiation force, perforation initiation energy, the total perforation energy.
    - Effects of angled entry, feedrates and amplitudes of vibration on perforation forces and temperature increase, similar to conditions encountered *in vivo*.
    - Histological examination of tissues perforated with ultrasonically vibrating wire waveguides.

2. A computational numerical method capable of predicting the pressures in the acoustic field surrounding the ultrasonically vibrating wire waveguide. This model may be used as a tool for designing ultrasonic wire waveguide devices. This methodology includes:

- Verification of the model by performing mesh density analysis and comparison with accepted analytical solutions for a range of clinically relevant operating parameters.
- Validation of the model against experimental measurements from the literature of an ultrasonic wire waveguide operating in simulated *in vivo* conditions (peripheral artery).
- Presentation of predicted pressure profiles, using this validated model, for a range of distal tip geometries and amplitudes of vibration.
- Operation parameters required to cause cavitation can, therefore, be predicted with the inclusion of a cavitation threshold parameter. The extent of the cavitation region in the medium can also be predicted.

3. A method of designing and developing an experimental test rig with an integrated ultrasonic wire waveguide apparatus, including:

- A method of measuring the perforation forces and temperatures in the soft tissue using a custom cantilever force measurement device.
- A method of experimentally measuring cavitation for these devices using a Passive Cavitation Detection (PCD) via a hydrophone and B-mode

ultrasonic scanner, thus establishing an inertial cavitation threshold for the medium (water) at a typical frequency used for these devices.

- A method of manufacturing wire waveguides which can deliver amplitudes of vibration and transmit for sufficient periods of time for tissue ablation and disruption.

1.4.1 Publications

1.4.1.1 International refereed journals

- A Linear Finite Element Acoustic Fluid-Structure Model of Ultrasonic Angioplasty *in vivo*. **Mark P. Wylie**, Garrett McGuinness and Graham Gavin. *International Journal of Numerical Methods in Biomedical Engineering*. Volume 26, Issue 7, pages 828 – 842, July 2010.

- Ablation of Chronic Total Occlusions using Kilohertz-Frequency Mechanical Vibrations in Minimally Invasive Angioplasty Procedures.
  G.B. McGuinness, **Mark P. Wylie**, G.P. Gavin. *Critical Reviews in Biomedical Engineering.* Volume 38, Issue 6, pages 511 – 531, July 2010.

- Increased Susceptibility of Arterial Tissue to Wire Perforation with the Application of High Frequency Mechanical Vibrations.
  Mark P. Wylie, Garrett B. McGuinness and Graham P. Gavin. *IEEE Transactions on Biomedical Engineering*. Manuscript accepted December 2011. DOI 10.1109/TBME.2012.2184286

1.4.1.2 Conference proceedings

- Numerical Investigation of the Effects of Ultrasonic Angioplasty: Thermal Heating and Acoustic Streaming.

  Mark P. Wylie, Garrett McGuinness and Graham Gavin. *Northern Ireland Biomedical Engineering Society Conference*, Belfast, Northern Ireland, March, 2008. Conference abstract.

- A Numerical Acoustic Fluid-Structure *in Vivo* Model of Ultrasonic Angioplasty in a Peripheral Artery.

  Mark P. Wylie, Garrett McGuinness and Graham Gavin. *Conference on Computational & Mathematical Biomedical Engineering*, Swansea, UK, June, 2009. Conference paper.

- Ultrasonic Angioplasty: Assessing the Risk of Arterial Perforation.

  Mark P. Wylie, Garrett McGuinness and Graham Gavin. *UK Society for Biomaterials Conference*, Belfast, Northern Ireland, July, 2009. Conference paper.

- Therapeutic Ultrasound Angioplasty: The Risk of Arterial Perforation. An *In Vitro* Study.

  Mark P. Wylie, Garrett McGuinness and Graham Gavin. *IEEE Engineering in Medicine Conference*, Minneapolis, USA, September, 2009. Conference paper.

- Perforation of Arterial Tissue using Low Frequency Ultrasound Delivered via NiTi Waveguides.

  Mark P. Wylie, Garrett McGuinness and Graham Gavin. *Bioengineering In Ireland Conference,* Galway, Ireland, January, 2011. Conference abstract.

- Soft Tissue Cutting with Ultrasonic Mechanical Waveguides.

  Mark. P. Wylie, Garrett McGuinness and Graham. P. Gavin. *International Congress on Ultrasonics*, Gdansk, Poland, September, 2011. Conference paper.

CHAPTER

2 LITERATURE REVIEW

2.1 The cardiovascular system and cardiovascular disease

The cardiovascular system comprises of the heart, its connecting blood vessels and the lymphatic system. The purpose of the cardiovascular system is to distribute nutrients, gases and hormones throughout the body [14]. It actively regulates flow velocity and pressure by dilation and contraction of the vessels.

Cardiovascular disease encompasses a number of disorders which generally act to inhibit the performance of the cardiovascular system by means of blood flow reduction through the arterial vessels. Narrowing of the artery lumen not only reduces blood flow but also increases the risk of blood clot formation due to a substantial decrease in the lumens cross sectional area. Narrowing of the lumen can be attributed to a cardiovascular disease of the artery known as atherosclerosis. Indeed, most cardiovascular diseases are a direct result of an underlying atherosclerotic condition of the arteries [15].

2.1.1 The artery and atherosclerosis

The arterial wall can be thought to comprise of at least 3 distinct layers; the tunica intima, tunica media and tunica adventitia. The intima, or inner wall, is the thinnest layer and consists of a sheath of endothelial cells. They provide a low resistance to blood flow in the artery and prevent adhesion to the arterial wall.

The media contains many elastic fibres (elastin), smooth muscle cells and some collagen fibrils depending on its location in the vascular system [16]. The elastin allows for elastic material behaviour while the collagen provides the load bearing structural strength [17]. Typically, there are only a few collagenous fibres in the media [17]. The adventitia contains many dispersed collagenous fibres and is surrounded by tough perivascular connective tissue. The mechanical properties of healthy arterial tissue are comparable to that of rubber [18]. They display creep under constant load and stress relaxation under constant extension but stiffen once physiological strain range level has been exceeded.

Atherosclerosis is a gradual chronic cardiovascular disease of the arteries which is specifically localised to the intima of the artery [15]. It creates an obstruction to blood flow in the artery and is the most common cause of acute myocardial infarction [19]. Atherosclerosis can affect the large and medium sized muscular arteries (such as coronary, iliac and femoral) and also large elastic arteries (such as the aorta) [15]. It is thought that narrowing of the lumen from atherosclerosis is a result of the inflammatory response from the repeated injury of the endothelial cells which line the inner intima [20].

This lesion manifests itself first as a thin fatty streak on the arterial wall. With time, the lesion can become fibrous and calcified [21]. Advanced stages of this disease are known to include fibrocalcific tissue with calcified caps, hence the name, atherosclerosis, which comes from the Greek word *athero,* meaning gruel or paste [22].

The properties of atherosclerotic lesions vary depending on the pathogenesis of the lesion. Some studies have examined the mechanical properties of the various types of atherosclerotic lesions and elucidate to the fact that there is a large variability in the properties of lesion types from patient to patient and also specific anatomical location [23]. Early stages of the disease are often softer than normal arterial tissue [24] and exhibit time dependent behaviour under constant mechanical loading (i.e. viscoelastic behaviour) [25]. As time progresses, the lesion can become harder and more brittle, as a result of fibrous plaque and calcification formation [26]. Maher *et al.* has conducted studies on the tensile and compressive strength of fresh human carotid atherosclerotic plaques, concluding also that calcified plaque material is the stiffest lesion tissue type while echolucent plaques were the least stiff [23].

2.1.2 Treatments for atherosclerotic lesions

There are pharmacological approaches such as vasodilators and beta blockers which help to relieve some symptoms of atherosclerosis. The vasodilators stimulate the smooth muscle cells which act to enlarge the lumen [27]. Other drugs that are also administered include antihypertensive drugs and lipid lowering drugs. Examples include thiazide diuretics, beta blockers, angiotensin converting enzyme inhibitors, calcium channel blockers, aspirin, metformin and insulin [28]. Beyond a certain degree of severity, atherosclerotic lesions require a surgical intervention and are commonly treated by minimally invasive Percutaneous Transluminal Intervention (PTI). The most common dilation procedure is the balloon and stent which was conceived in the early 1970s.

2.1.3 Minimally invasive surgical techniques

Minimally Invasive Surgical (MIS) techniques for treatment of atherosclerotic lesions first require the use of intravascular catheters and guidewires. The guidewires are applied percutaneously to the vascular system. This method of delivery, if successful, has a significant reduction in trauma when compared to conventional open thoracic surgery. The majority of current guidewires have a main shaft diameter of 0.35 mm or less [29]. They are manoeuvred through the vessel to explore the lesion site and act as a rail for the follow up surgical device. They may fall under two classifications [30].

i. Non-hydrophilic – Lower frictional resistance, better manoeuvrability.
ii. Hydrophilic – Most suited to provide tactile feedback.

Guidewires can be used to probe the lesion site, examining if there is a viable path through the lumen. They can be classified according to their stiffness (soft, intermediate and stiff). Soft guidewires are typically used for advancement of the catheter and crossing occlusions of small lumens. Intermediate guidewires are used in tortuous vessels or recently occluded vessels and stiff wires are used for advancing through totally occluded lesions [29]. Atherosclerotic lesions which can be successfully traversed by a guidewire can then be treated by the standard balloon and stent. For the lesions which cannot be traversed, an armoury of alternative less well established methods are available [31-34]. The premise behind the majority of these devices is to unblock the artery to a state whereby it can be traversed and then treated by a secondary follow up device, such as the balloon and stent.

2.1.3.1 Balloon and stent

For balloon dilation procedures, initially a guidewire is fed to the lesion location and traverses the blockage. X-ray and ultrasound diagnostic imaging systems are often employed to guide the balloon into position; contrast media is also often used. The angioplasty balloon is inflated which dilates the artery by mechanical strain. This may be a stand-alone procedure but more often will be accompanied by a metal structure known as a stent (90% of the time [35]). The stent is left in the artery to support the arterial wall and to tack the diseased material back from the arterial flow path. An illustration of the procedure is shown in Figure 2-1. This procedure has a high success rate for common lesion types.

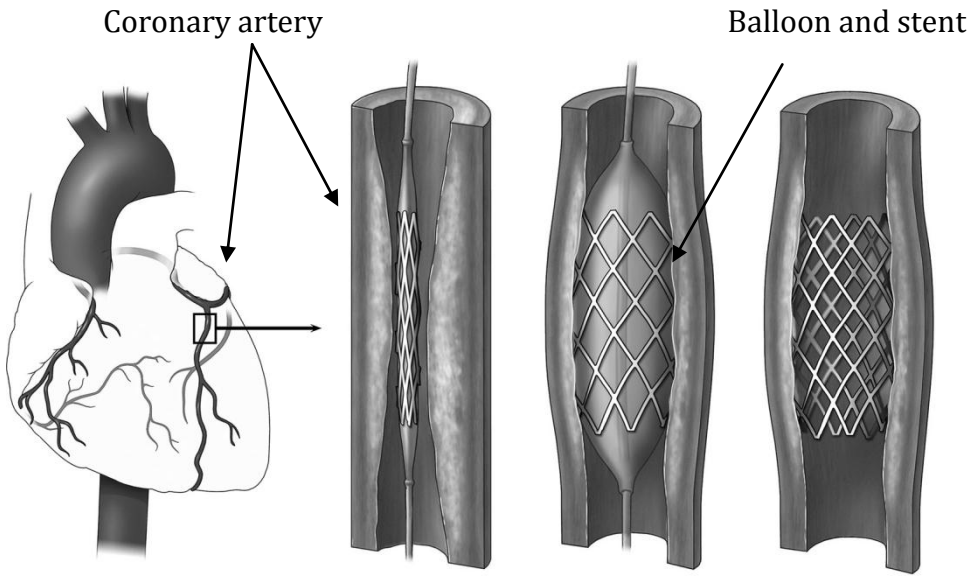

Figure 2-1: Balloon and stent procedure [36].

2.1.4 Complications associated with common PTI

Although the balloon and stent is a highly accepted form of intervention there are some limitations. Success rates are lesion specific [37] and damage of the surrounding healthy artery may also occur. In some cases, emergency surgery is required. More advanced lesions can be unstable and potentially hazardous.

2.1.4.1 Eccentric lesions

The lesion is considered eccentric when it fails to involve the entire inner artery circumference [38], as shown below in Figure 2-2. Eccentric lesions are more predominant with early stages of lesion formation. In a study conducted by Mintz *et al.,* 55% of all atherosclerotic lesions examined by angiography were eccentric [38]. The eccentric lesions may yield sub optimal results if the balloon is to expand stretching and damaging the healthy arterial wall while failing to alter the plaque impinging on the lumen [37].

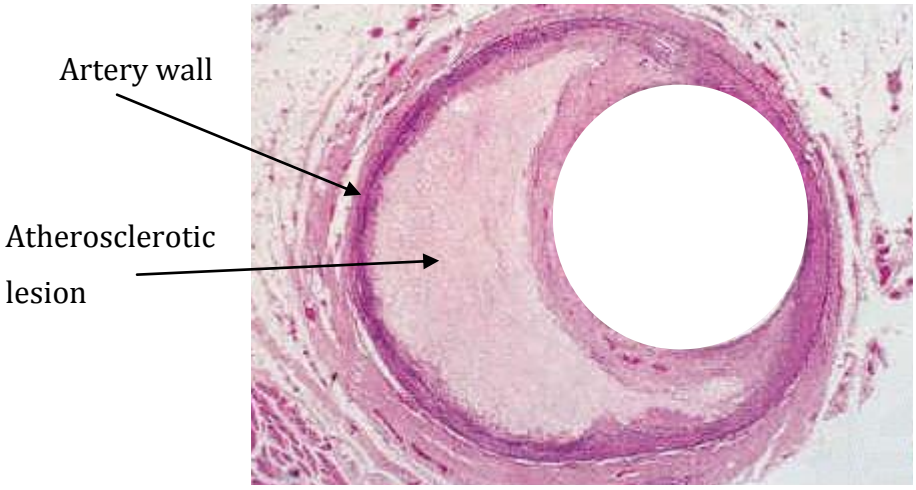

Figure 2-2 : Eccentric atherosclerotic lesion, H&E stain [39].

2.1.4.2 Restenosis

As a result of the surrounding healthy arterial tissue being strained from balloon inflation, the patient may suffer from a restenosis of the artery. This is effectively an inflammatory response of the healthy arterial tissue. This is the formation of scar tissue which can cause inflammation of the arterial wall thus reducing the blood flow once again. It can occur within the first 6 months after surgery, and has up to a 40 % chance of occurring after balloon angioplasty [40] cited in [41]. Stents can act to reduce restenosis but 25% of all patients with stent implantations still suffer from restenosis [41].

2.1.5 Chronic Total Occlusions (CTOs)

Advanced stages of atherosclerosis may result in a complete blockage of the lumen, otherwise known as Chronic Total Occlusions (CTOs). CTOs are defined as occlusions of the artery which are more than one month old [42]. They are also classified as having a length of occlusion greater than 15 mm [43]. Depending on their duration, they broadly consist of various degrees of fibro-athermanous plaque and thrombus [42, 43].

2.1.5.1 Traversing the lesion

Early stage atherosclerotic lesions can be treated by PTI, such as balloon and stent. However, CTOs are challenging as they do not lend themselves to being accessed and traversed by the guidewire, as can be seen in Figure 2-3. Guidewire access and ability to cross the lesion is critical to the success of standard dilation procedures and has been reported to be the key success

indicator in 80% of cases [1]. Forcing the guidewire may only cause deflection towards the artery wall or into adjoining bifurcations. Excessive force may also cause the plaque to fracture, creating large segments of broken plaque in the artery lumen.

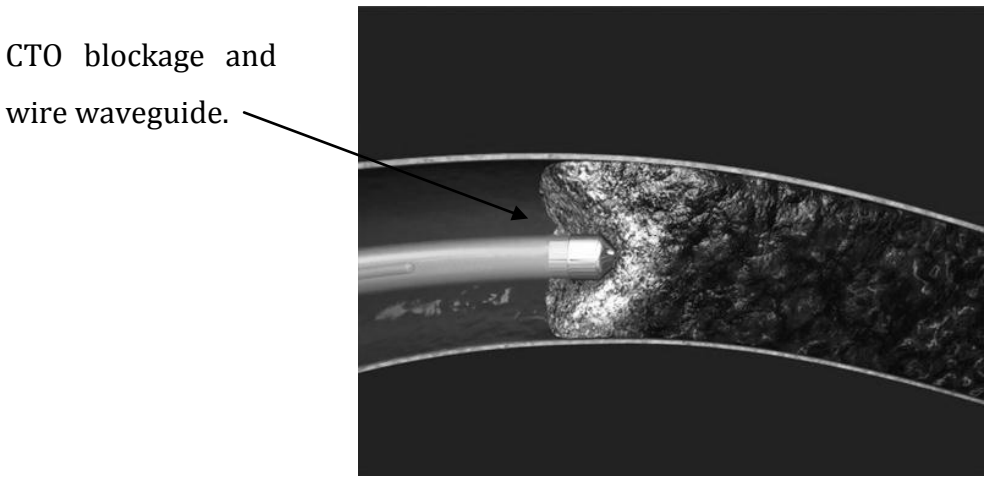

Figure 2-3: Guidewire encounter with a CTO [44].

2.1.5.2 Increased risk of arterial wall perforation

CTOs are often difficult to engage safely with minimally invasive procedures and are associated with an increased potential for arterial wall perforation during treatment with traditional devices when compared to sub-totally occluded vessels. This may be a result of the distal section of the guidewire or subsequent device being deflected by the hard diseased lesion cap toward the surrounding healthy elastic artery wall or by entering a false lumen [11, 12]. A schematic of this occurrence is shown in Figure 2-4. Dissection of the coronary arteries with proximal vessel occlusion due to aggressive wiring and guide catheter techniques are also reported with CTOs engagement ([45] cited

in [11]). For these reasons CTOs are the number one cause for coronary artery bypass graft (CABG) surgery referral [43]. Because of this high risk surgery (CABG), an increasing number of vascular specialists are employing a percutaneous intervention-first policy for the treatment of CTOs [34].

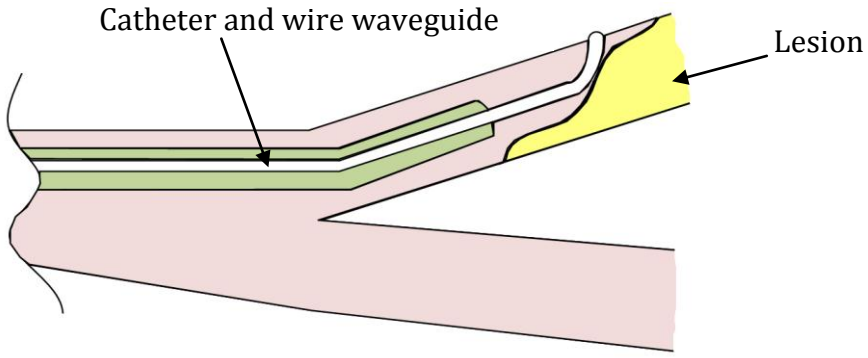

Figure 2-4 : Wire waveguide and guidewire encountering an atherosclerotic lesion and being deflected towards artery wall.

2.1.6 Devices and techniques for CTOs

Problematic atherosclerotic lesions, such as CTOs, traditionally required by-pass graft surgery, in most cases open thoracic surgery. This treatment can now be attempted by Minimally Invasive Surgery (MIS). There are MIS devices on the market that are specifically designed to target various lesion types and CTOs. Traditional dilation treatments are often attempted first by stiffer guidewires. Some devices specifically for CTOs have been successfully approved in the USA by the Food and Drug Administration (FDA) and also in the European Union (EU). These include the Safe Cross guidewire and FrontRunner catheter which operates using radio frequency energy, and the POLAR™ (Path Of Least Arterial Resistance) low frequency vibrational device which delivers lateral

movements at the distal end of standard guidewires in the frequency range of 16 – 100 Hz [1, 46]. A device known as the Silverhawk™ Plaque Excision system has been approved in both the US and the EU for use in debulking of coronary and peripheral atherosclerotic lesions. This device removes plaque using a small rotating blade at the distal end of a catheter. This device is passed along the lesion length a number of times, removing and capturing the removed plaque with each pass [47].

Rotational drilling devices for atherosclerotic lesions were developed in mid 1980's [48]. Some of these devices and recent designs for treating CTOs include the Rotablator and multi-wire crushing techniques [43, 49]. The Rotablator consists of a thin elastic wire, the distal end of which has the form of a burr. The proximal end is connected to a rotating drill and spun at speeds of 3000 revolutions per minute. This acts to clear the lumen by displacing the atherosclerotic material against the artery wall [48].

Slower speed rotary drilling machines have also been introduced and tested, an example of this is the WildCat by Avinger, which is specifically aimed towards Peripheral Artery Disease (PAD) [50]. LASER angioplasty is another technique used to unblock arteries. The device is advanced though the artery to the site of blockage. This operates by emitting pulsating beams of light which act to vaporise the plaque [51]. The first LASER device, the Excimer LASER, was approved in 1992 by the FDA. The device, however, is relatively costly [52].

2.1.6.1 Catheter delivered external ultrasound transducer wire waveguide treatment of CTOs

The use of low frequency, high power ultrasonic energy transmitted via wire waveguides has been proposed as a method to treat CTOs. Because of their low ultrasonic frequency of operation, these devices are also often described as high frequency mechanical vibrations or high frequency drilling [53]. Complex conditions exist at the wire waveguide distal tip and its interface with the surrounding tissue. This is due to the combined effects of ultrasound exposure and the dynamics of high frequency cyclic loading of the diseased tissue. One benefit of the ultrasonic treatment over other plaque removal devices such as the Silverhawk™ and Rotoblator is the preferential removal of the diseased tissue.

The first device of this type using high frequency mechanical vibrations (20 kHz) transmitted through wire waveguides for atherosclerotic lesion ablation and disruption has been approved in both the EU (2005) [9] and also by the FDA (2007) [10]. This device was intended to facilitate intra-lumen placement of conventional guidewires beyond peripheral artery CTOs. This is known as the CROSSER™ system and was approved based on substantial equivalence to that of a radiofrequency device (Intraluminal Therapeutics (ILT) Safe-Cross System) which is also used for CTO unblocking [54].

2.1.7 Summary of atherosclerosis and its treatments

- Atherosclerosis is a cardiovascular disease which inhibits blood flow through the artery. The lesion is soft initially but may become hard and calcified over time. Complete blockages are known as CTOs, they can comprise of fibrous tissue and calcifications.
- Atherosclerotic lesions are typically treated by a balloon and stent. However, their success relies on the ability to cross the lesion. CTOs are difficult or impossible to transverse and are, therefore, associated with complications, such as, increased risk of arterial perforation. They are the number one cause for coronary artery by-pass surgery referral.
- New devices and techniques have been developed as alternative therapies for problematic lesions such as CTOs. One such technique uses high frequency mechanical vibrations (≈ 20 kHz) transmitted via wire waveguides to unblock the stenosed artery.
- The first clinical device, the CROSSER™, which uses high frequency mechanical vibration delivered via a wire waveguide has been approved (EU and FDA) for use in the treatment of CTOs. The effects of the CROSSER™ on the surrounding soft arterial tissue have not yet been published.
- The soft tissue properties and subsequent response to the low frequency ultrasound is not known. Soft arterial tissues properties may change as a result of strain (physiological strain range) rendering the tissue more stiff.

2.2 Therapeutic ultrasound in medicine

Ultrasound in medicine can be generated by exploiting the piezoelectric effect of certain crystalline materials. These materials have the ability to change shape when a voltage is applied and vice-versa. Ultrasound generation produces sound waves at a frequency above the upper human hearing threshold (≈20 KHz) which propagate by longitudinal motion in compression/refraction cycles. In medicine, two principal forms of ultrasound energy can be used.

i. High-frequency low intensity ultrasonic waves in the megahertz range which for ultrasonic imaging.
ii. High intensity ultrasound at generally lower frequencies which can be used to ablate and disrupt hard materials or emulsify soft tissues and fat.

The latter of the two describes what is commonly known today as therapeutic ultrasound. The use of therapeutic ultrasound for clinical treatments is an emerging technology. The premise behind this technology is the selective disruption of tissue types on the basis of their mechanical properties and their response to the ultrasonic energy.

Its effectiveness and high success rates for a range of medical procedures [55] had led researchers to examine its uses in other areas and treatments. In order to understand the origins of the application of ultrasonically energised wire waveguides for cardiovascular tissue disruption and ablation, one must first describe the general trend of evolution from the early therapeutic ultrasonic devices. For this reason, the development of therapeutic ultrasonic devices is discussed in this section.

2.2.1 Classification of therapeutic ultrasonic devices

Therapeutic ultrasonic devices can be broadly classified according to frequency of operation, acoustic intensity range and delivery method. For this review, the devices are classified according to delivery method. The device used for this research would belong in the percutaneous catheter delivered external transducer system category but has similarities with some external transducer tipped cutting devices. The delivery methods include:

i. Transcutaneous delivered external transducer systems.
ii. Ultrasonic tissue cutting and drilling devices.
iii. Percutaneous catheter delivered external transducer systems.

2.2.1.1 Transcutaneous delivered external transducer systems

This describes the application of ultrasound generated by an extracorporeal transducer. This is a non-invasive means which couples the transducer directly to the body via ultrasonic transmission fluid or gel. The ultrasound is then focused to the target tissue to achieve the desired effect.

2.2.1.1.1 High Intensity Focused Ultrasound (HIFU)

HIFU primarily utilises cavitation as a mean of ablation or coagulation necrosis. Secondary ablation effects through heating are also observed [56]. This is an area of therapeutic ultrasound which is generating a lot of momentum not only for hard tissue ablation but also for soft tissue ablation using short but high intensity ultrasonic pulses (histotripsy).

2.2.1.1.2 Histotripsy

This therapy uses focused ultrasound to fractionate soft tissue through controlled tissue cavitation. Tests using histotripsy as a means of non-invasive thrombolysis have been conducted by Maxwell *et al*. Their results show effective thrombolysis only when cavitation was present. It was also observed that fluid flow generated by a cavitation cloud can attract, trap and further break down clot fragments [57].

2.2.1.1.3 Lithotripsy

Lithotripsy is also a form of extracorporeal HIFU. Shockwave lithotripsy is a procedure for treatment of kidney stones, a schematic of this procedure is shown in Figure 2-5. It uses a focused acoustic pulse to ablate the kidney stone.

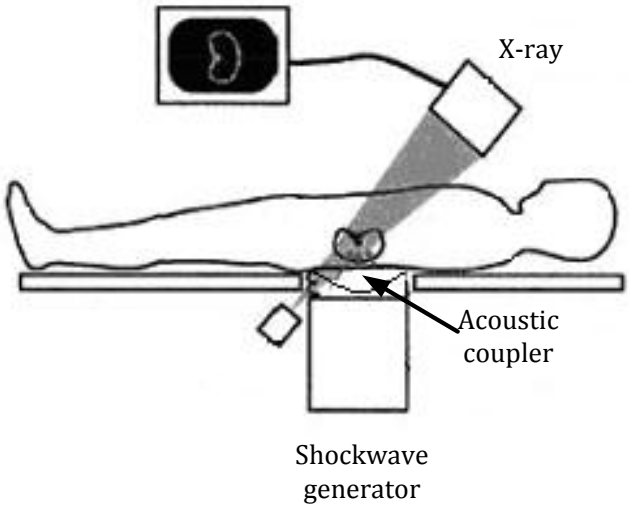

Figure 2-5 : Lithotripsy of a kidney stone.

2.2.1.2 Ultrasonic tissue cutting and drilling devices

2.2.1.2.1 Chisels and drills on hard tissue (bone)

Much work has been done in the area of ultrasonic bone cutting and removal. It is because of its success in this field that it has also expanded into other applications of mineralised tissue removal using probes, such as dentistry. The effectiveness of mineralised tissue removal using therapeutic ultrasound is described by Volkov in 1974 who used 25-30 kHz longitudinal mechanical vibrations to drive saws and scalpels when cutting bone [58]. In other work by Cardoni *et al.*, they examined a low frequency ultrasonic cutting tool for cutting bone which operates in the frequency range of 20-100 kHz [59]. They report that the benefits of using this device over conventional cutting scalpels include the reduction of swarf, reduced reaction forces and more precise cutting which is otherwise not achievable with other high speed rotational devices.

Khambay and Walmsley examined the effects of feedrate on the cutting forces when using an ultrasonically vibrating cutting tool on bone [60]. Using a harmonic chisel, the effect of feedrate on the cutting depth of bovine bone was examined. Results show that when the feedrate increases there is a corresponding increase in the downward force which is followed by a decrease in the force at feedrates greater than 56 mm/min. The depth of the cut increases up to a feedrate of 56 mm/min after which it decreases. They also report the effects of angle of approach to the bone with the cutting device, stating that both the longitudinal and downward forces do not change when the rake angle changes from 0 degrees to 10 degrees. The downward force decreases when the rake angle increases from 10 degrees to 20 degrees [60].

2.2.1.2.2 Phaco-emulsification

Phaco-emulsification refers to a procedure for removing ocular cataracts whereby the eyes internal lens is emulsified by a low frequency ultrasonic probe. This procedure was developed by Charles Kelmen who took inspiration after seeing this form of energy being used in dentistry [61]. A conventional phaco tip vibrates at ultrasonic frequencies typically between 25 KHz and 62 KHz [62].

For this procedure, heating of the distal tip and surrounding medium can be substantial and is considered an unwanted adverse effect. Therefore, the distal tip must be irrigated by coolant to prevent thermal damage within the eye. Cavitation effects using these devices can generate even more heat [62].

Phaco-emulsification is now known to cause collateral damage to the cornea and efforts are being made to reduce ultrasonic powers below the intensities required to cause cavitation [63]. Therefore, recent advances in this technology (SonicWave) propose the use of sonic frequencies (40-400 Hz) to eliminate or mitigate the effects of ultrasonic cavitation and heating during this procedure [64].

2.2.1.2.3 Scalpels and incisors on soft tissue

One of the first studies using an ultrasonically vibrated scalpel was documented as early as 1979 by Hodgens who describes the evolution of this device as being a descendant of the Cavitron-Kilmen Phaco-emulsfier [65]. He proffers that the potential value of this device, as well as ablation and dissection, is the reduction of blood loss during surgery from thermal cauterisation. This

scalpel operates by delivering amplitudes of vibration of 150 μm to the distal scalpel tip. Today, a number of ultrasonic incisors and scalpels are commercially available.

i. UltraCision

Koch *et al.* performed tests using an ultrasonic scalpel (UltraCision) on a suite of soft porcine tissues which operated at 55 kHz and produced amplitudes of vibration between 10 - 50 μm [66]. Heating of the tissue at 1.0 mm from the cutting interface of above 40 ^{0}C was measured. However, it was stated that perfusion of blood through the tissue reduced the heat efficiently at distances greater than 5.0 mm from the distal tip [66].

ii. Harmonic Ace

More recently, the application of a double sided scalpel (i.e. an incisor) has been developed and is gaining acceptance across the world in endoscopic surgery for dividing systematic vessels [67]. The design of the incisors typically includes a sharp blade distal tip which is ultrasonically vibrated coupled to a small narrow blade jaw which acts to clamp the tissue, see Figure 2-6 . The jaw is typically not ultrasonically vibrated. The Harmonic Ace ® (Ethicon Endo-Surgery Inc, Cincinnati, Ohio) is a good example of an ultrasonically energised shearing device.

The Harmonic Ace ® is FDA approved for use in dividing any vessels 5.0 mm or less in diameter [68]. In clinical tests using this device by Tanaka, its efficiency for shearing and sealing pulmonary vessels in clinical trials is

described [69]. Ethicon Endo-surgery also boasts an arsenal of different but similar products using this technology. They all operate at 55.5 kHz.

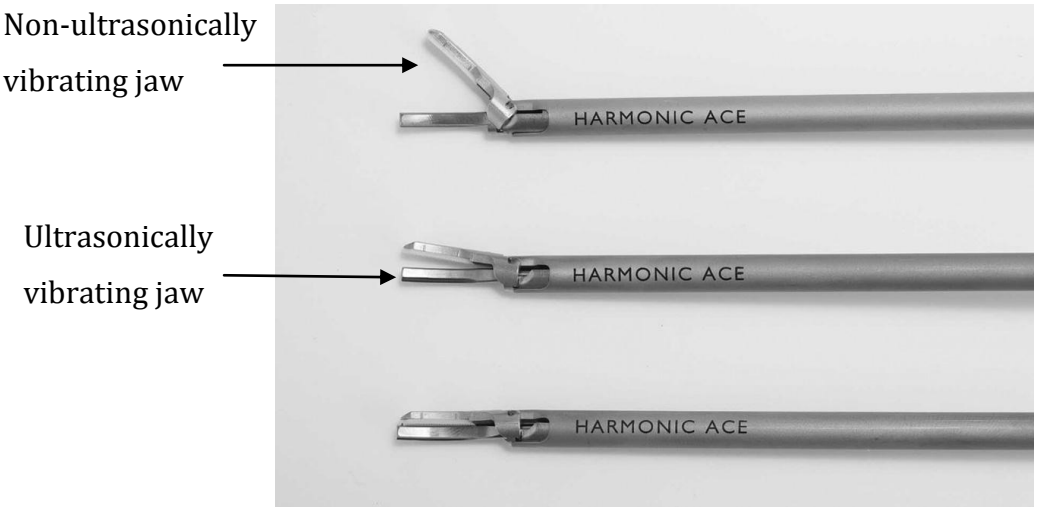

Figure 2-6: Harmonic ACE from Takana [69].

iii. LOTUS

The LOTUS ultrasonic scalpel also performs a similar function to the Harmonic Ace but instead of longitudinal vibrations at the distal tip there is torsional vibration which oscillates around an arc. It also operates at a lower frequency of 36 kHz [70].

2.2.1.3 Percutaneous catheter delivered external ultrasonic transducer systems

Using small incisions in the skin it is possible to apply ultrasonic wire waveguides through a catheter which is inserted percutaneously. It is currently only used in the delivery of a wire waveguide to the vascular system for surgery. The catheter and wire waveguide are passed through an insertion made in the artery to the lesion site, as shown in Figure 2-7 . The catheter is typically used to

guide the wire waveguide through the vascular system to lesion site. The transducer is external to the body but acts to transmit the energy through the wire waveguide to the distal tip.

2.2.1.3.1 Ultrasonic wire waveguide delivery for thrombolysis and angioplasty

In cardiovascular applications, this form of therapy has been applied for soft thrombus dissolution (thrombolysis) and hard brittle atherosclerotic tissue removal. It relies on the transmission of high frequency mechanical vibrations (low ultrasonic frequency range (20-50 kHz)) via wire waveguides. The waveguides must be able to transmit the energy through lengths of wire which are sufficiently long to navigate the arterial system and to reach the lesion site (≈ 1600 mm) [13].

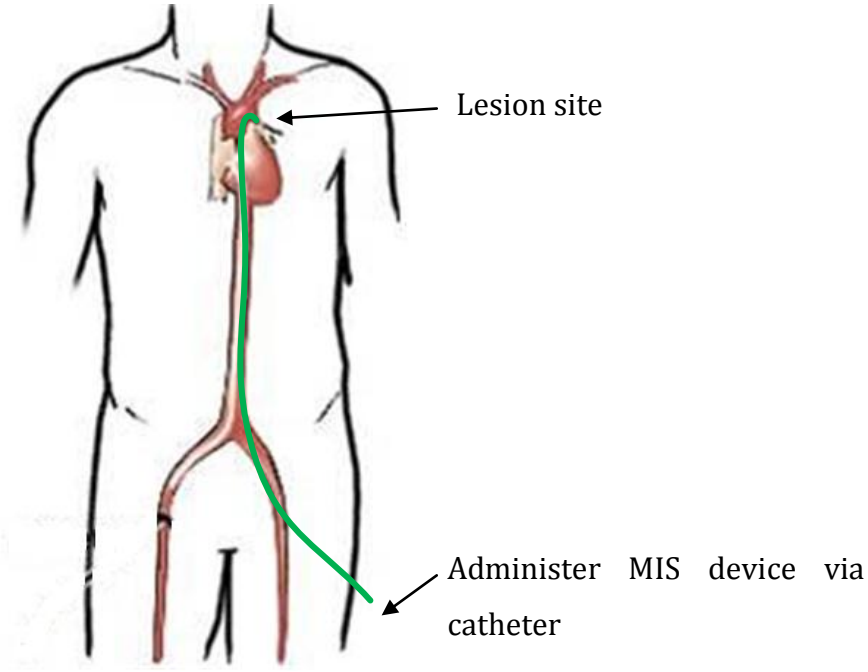

Figure 2-7 : Wire waveguide delivered through a catheter to lesion site.

They must also be sufficiently small in diameter so as to be flexible enough to pass through some of the smaller arteries in the body, such as the coronary arteries. Diameters typically range from 0.35- 2.0 mm [2, 5, 13]. In most cases, a large ball tip is also attached to the distal end to cause cavitation and create a larger lumen. Reports of ball tips in the region of 2.0 – 2.5 mm are also described [2, 5, 7, 71].

The wire waveguide can be fed to the lesion site through a catheter, energised and pushed through the lesion, removing tissue in the process and making a viable path to restore blood flow or allowing the vessel to be dilated further by a follow up device. Some early prototypes of these devices were designed and tested but were of little practical use because of their small wire waveguide lengths [2, 71-73]. Over time, through constant refinement of design, some of the more difficult design challenges were overcome and these problems were addressed.

2.2.1.3.2 Device configuration

The first practical devices for ultrasonic angioplasty *in vivo* were developed in the late 1980's. These devices generally comprise of three sub-systems. External generator (A), ultrasonic transducer (B) and a horn or transmission wire (C) are typically used. The generator delivers AC power input to the piezoelectric transducer; this converts the electrical energy to high frequency mechanical vibrations and is often amplified by using an acoustic horn. These are solid metal tapered rods that can be coupled to the distal end of the transducer. A flexible ultrasound transmission wire waveguide is often

coupled directly to the acoustic horn. Figure 2-8 shows this arrangement used by Rosenschein *et al.* [6].

A similar arrangement is also shown by Siegel *et al.* [74]. Their system was powered by a Blackstone Lithotripsy generator. This was then coupled to a transducer. Siegel's wire waveguide was ensheathed in a catheter which provided saline irrigation for cooling to the distal wire waveguide tip, their system schematic is shown in Figure 2-9. Both Rosenschein's and Siegel's systems operate in the low 20 kHz frequency range.

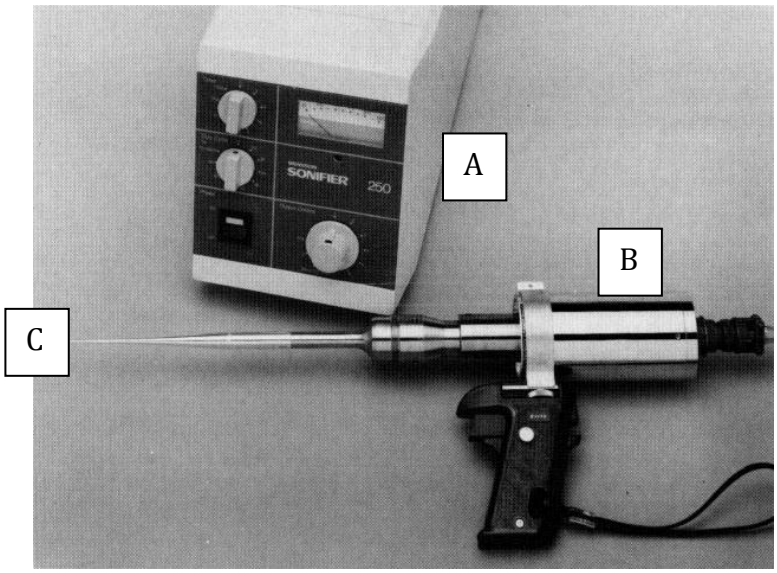

Figure 2-8 : Prototype of ultrasonic angioplasty device by Rosenschein *et al.* [6].

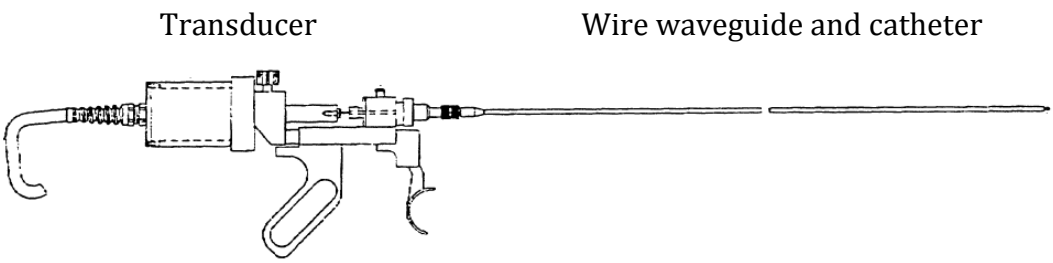

Figure 2-9 : Diagram of the ultrasonic device used for arterial plaque ablation by Seigel *et al.* [74].

The FDA and EU approved medical device for CTO recanalisation is very similar in many respects to these early devices. The CROSSER™ Catheter System consists of a re-usable electronic generator, a high-frequency transducer and a single-use CROSSER™ CTO recanalisation catheter (wire waveguide, length 1200- 1460 mm, 1.1 – 1.5 mm distal tip outer diameter [75]). An optional saline flush system, the Flowmate™ Injector is also available. According to the manufactures specifications, the recanalisation catheter operates at 20 kHz at a stroke depth of approximately 20 μm [44]. The complete system is shown in Figure 2-10.

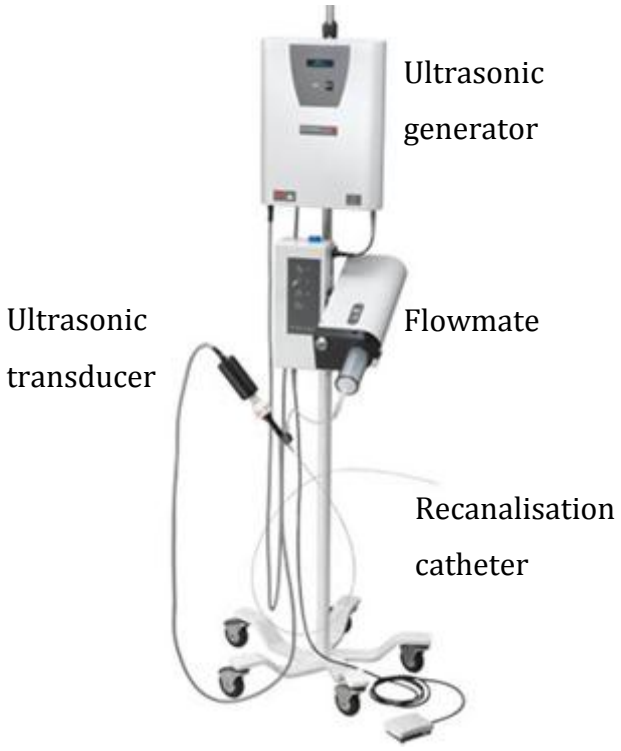

Figure 2-10 : The CROSSER™ Catheter System [44].

Detailed literature on the manufacturing and design of these devices is sparse. Patents are available which illustrate the mechanics behind the design but do not outline the manufacturing methods or a means to achieve similar devices [76-78]. Some of the design aspects involved in producing these ultrasonic devices is described by Gavin [13]. Gavin describes the use of an adapted Branson™ sonifier to achieve similar wire waveguide distal tip conditions to that used in the approved clinical and experimental devices. Gavin's work focused on the characterisation of the ultrasonic apparatus with particular emphasis on the wire waveguide and its connection methods to the acoustic horn. Gavin's ultrasonic apparatus was modified and used as part of this research programme for tissue testing. The modifications are described in further detail in Chapter 4.

2.2.2 Summary of therapeutic ultrasound and wire waveguide devices

- Therapeutic ultrasound generally operates in the low acoustic frequency range (20 - 100 kHz) but at much higher acoustic intensities to that of ultrasonic diagnostic imaging devices. Therapeutic ultrasound is generally used where selective tissue ablation and disruption is required.
- Therapeutic ultrasonic devices in medicine can be classified according to their method of delivery :

  i. Transcutaneous delivered external transducer,
  ii. Ultrasonic tissue cutting devices and
  iii. Percutaneous catheter delivered external transducer systems.

- Transcutaneous devices (such as HIFU) are non-invasive and are designed to generate cavitation at the tissue target site and generally operate at acoustic intensities many orders of magnitude greater than that of the other therapeutic delivery methods.
- Ultrasonic tissue cutting devices generally operate at frequencies below 100 kHz and are used for hard/soft tissue ablation and disruption. Benefits of using these devices over traditional non-ultrasonic devices include reduced cutting forces, increased tissue removal rates and more precise cutting. Feedrate has also been shown to have an impact on tissue removal rates.

- The UltraCision ultrasonic scalpel has been tested on cutting of porcine tissue with amplitudes of vibration between 10 -50 μm at 55 kHz. They report heating above 40 ^{0}C but state that perfusion of the blood reduces this temperature efficiently 5.0 mm from the distal tip.
- In phaco-emulsification, heating is described as being generated from the phaco tip. This may be due by internal friction of the vibrating probe. Fine *et al.* also describe additional heating caused by cavitation during phaco-emulsification [62].
- Percutaneous catheter delivered external transducer systems include the use of ultrasonically vibrating wire waveguides for ablation and disruption of cardiovascular tissues, with a specific clinical application of CTO ablation. The use of ultrasonically vibrating wire waveguides in cardiovascular treatments has been coined as “ultrasonic angioplasty” in some forums. It is also known as high frequency mechanical vibrating wire waveguide delivery.

2.3 Ablation and disruption mechanisms using wire waveguides

At the distal tip of the wire waveguide, both hard diseased tissue and thrombus are thought to be disrupted by a number of mechanisms; primarily direct mechanical ablation and cavitation and, to a lesser extent, acoustic streaming and pressure wave components [79]. In this section, the ablation and disruption mechanisms which are encountered using ultrasonic wire waveguide devices will be discussed. Figure 2-11 below illustrates the mechanisms which are responsible for the disruption and ablation of the tissue.

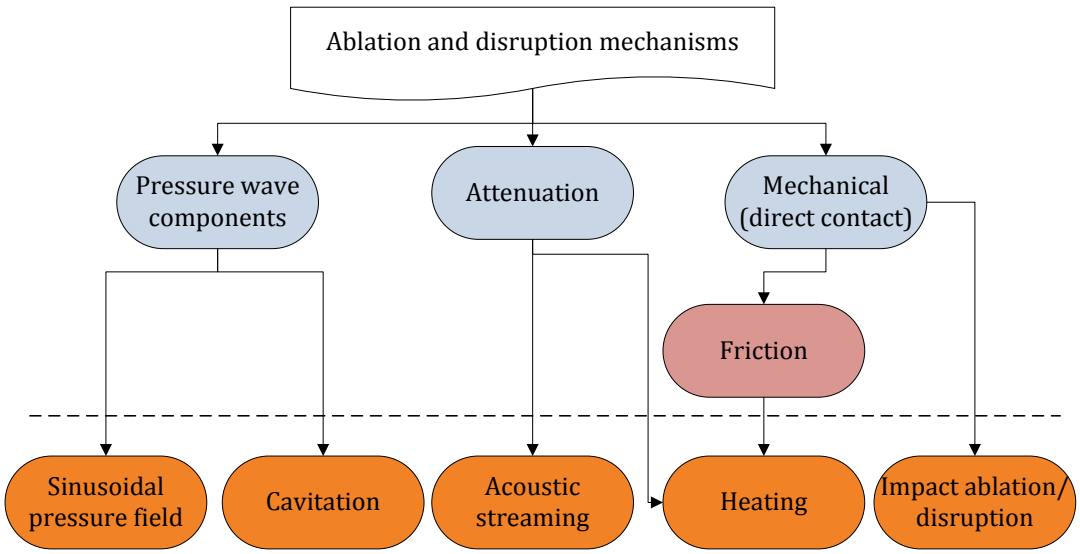

Figure 2-11: Ablation and disruption mechanisms.

2.3.1 Mechanical contact disruption and ablation

Mechanical contact ablation caused by the vibrating wire waveguide distal tip impacting the diseased atherosclerotic lesion in the artery is thought to play a critical role in material disruption and removal [80]. High frequency cyclic impacting of the tissue and wire waveguide can cause the tissue to fail. Indeed,

recent studies using the CROSSER™ system describe ablation mechanisms as a result of high frequency mechanical vibrations [81]. In soft tissue, Cimino and Bond suggest that the primary ablation mechanisms associated with tissue removal is predominantly related to direct mechanical impact of the acoustic horn, acoustic streaming and pressure wave components [82].

From the perspective of micromachining engineering materials, the key variable for effective ultrasonic cutting devices by mechanical disruption is amplitude of vibration at the cutting tip [83]. The removal rate also increases with frequency and is dependent on the size of the end probe area [82]. In brittle material removal, the ablated particles may also create a slurry at the distal wire tip, which may contribute to further tissue removal. The concentration of the slurry (particulate) at the tip has an effect on removal rate, raising the concentration of this tends to increase the removal rate [84].

2.3.2 Cavitation

Cavitation generated by the wire waveguide distal tip case occurs on the negative half of the acoustic cycle. As the wire waveguide is vibrating, it is causing high pressures at the amplitude maxima and low pressure at the amplitude minima. These low pressures can cause the rapid expansion of bubbles (dissolved gas coming out of solution). Following this, on the positive half of the cycle, the bubbles then collapse. It is during this phase that the disruptive effects of cavitation occur. Cavitation is usually considered to be an undesirable erosive effect in diagnostic ultrasound but deemed to be a crucial mechanism in both ultrasonic ablation of CTOs and ultrasonic thrombolysis [3, 7, 85-87]. The two main types of ultrasonic cavitation are:

i. Stable cavitation, where the radius of the cavitation bubbles oscillates around an equilibrium value over a considerable number of acoustic cycles without the generation of bubble collapse [88] and

ii. Inertial cavitation, where the bubble rapidly grows and collapses a number of times over a single acoustic cycle, and is commonly associated with damage mechanisms [89].

Cavitation is a threshold phenomenon [90]. The acoustic pressure threshold for inertial cavitation is much higher than that for stable cavitation. There is a considerable amount of information in the literature on cavitation thresholds [91-94]. These thresholds are sensitive to temperature, dissolved gasses and are frequency dependent.

For therapeutic ultrasound, the frequencies of interest typically range from 20-50 kHz [13] because the intensity required to produce cavitation rises rapidly above frequencies of 100 kHz [92]. Nyborg also describes the onset of cavitation for water, in the frequency range of 20-50 kHz [91]. With suitable gas nuclei present, above pressure amplitudes in the range of 0.1 - 0.2 MPa, inertial cavitation threshold is observed. The inertial cavitation for degassed water at room temperature, recorded by Perkins, is shown in Figure 2-12 [92]. For the frequency range typically used in therapeutic ultrasound (20 – 50 kHz), the inertial cavitation threshold is given as approximately 6 – 8 W/cm^2.

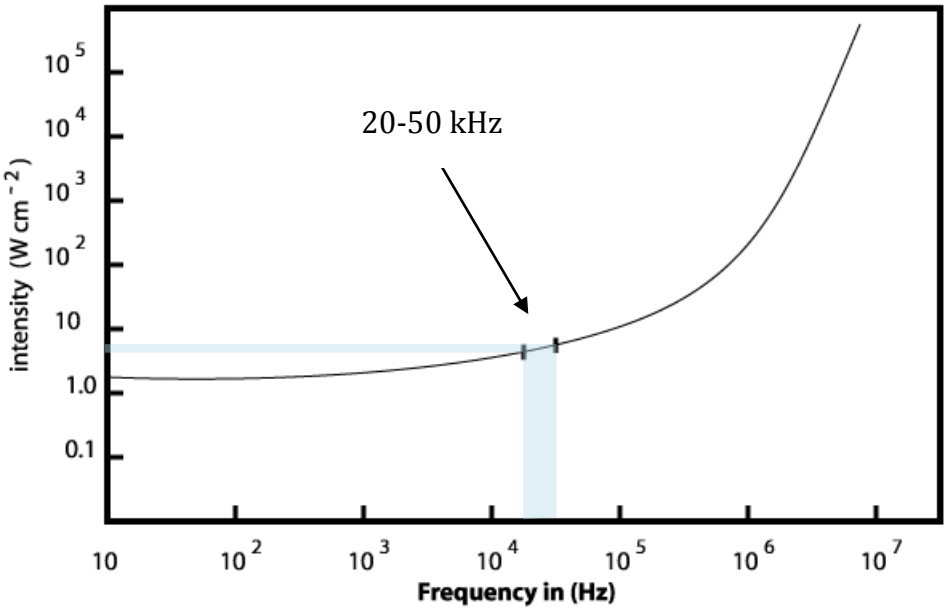

Figure 2-12: Inertial cavitation threshold for degassed water from Perkins [92].

2.3.2.1 Cavitation detection

Critical to the understanding and evaluation of these devices is the ability to detect the onset of cavitation. Cavitation can be observed to some degree by the naked eye. When using small diameter wire waveguides (and hence small localised cavitation regions) in often inaccessible locations near tissue, other methods must be employed. The event of cavitation can be examined indirectly by its effects on the surrounding environment:

i. A simple technique is the use of an aluminium foil (pitting method). Here the heterogeneous cavitation causes pitting on the thin foil section (≈ 20 μm thickness) and can been seen by the naked eye. Experiments using this method have been conducted by Tezel *et al.* at 20 KHz [95].

ii. Cavitation can be actively measured by using chemiluminescence of luminol. The cavitation bubbles in this case collapse creating radicals which oxidise luminol and emit a weak blue light [96].

iii. Cavitation also acts as a secondary sound source and can, therefore, be measured passively by analysing the acoustic frequency profile generated by the device using a hydrophone; this is known as Passive Cavitation Detection (PCD). The method is outlined in the ANSI Bubble Detection and Cavitation Monitoring Report [97] and is practiced by others [94] [93, 98, 99]. This will be discussed in further detail in the methodology section.

It is also possible to visualise cavitation by using an ultrasonic diagnostic imaging device. Cavitations can be identified in the ultrasound image display as highly echogenic microbubbles. This technique was employed by Rosenschein *et al.* who used a 7.5 MHz multi-element linear array ultrasound imaging transducer positioned at the wall of an arterial phantom [87].

2.3.3 Attenuation of the ultrasound

Attenuation of the acoustic energy describes all mechanisms which remove energy from the ultrasonic wave. This includes scattering and absorption, where the absorption relates to the amount of energy which is absorbed by the medium and converted into heat. In acoustics, the attenuation coefficient may be expressed in units of NPm^{-1} or dBm^{-1} and are frequency dependent [100]. Attenuation coefficients are non-linear and are only

approximations limited to a finite frequency range, as can be seen in Figure 2-13 (note x-axis in MHz units).

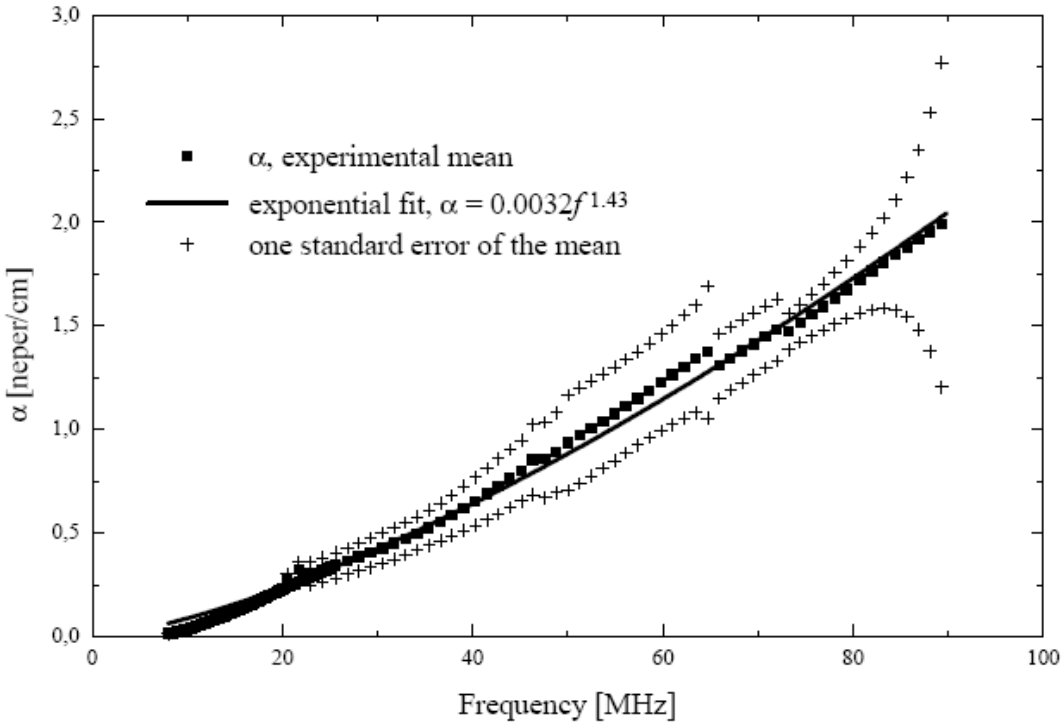

Figure 2-13: Experimental mean results for the attenuation coefficient as a function of frequency [101].

2.3.3.1 Heating

The generation of heat when using ultrasonic angioplasty devices is commonly reported [102, 103]. The thermal response from ultrasonically vibrating cutting tools on tissue (bone) has been described in similar applications (chisel) by Cardoni *et al*. The thermal increase has been decomposed into two contributing factors.

i. Absorption of the ultrasonic energy (i.e. attenuation).

ii. Friction between cutting tool and the tissue [59].

It has been suggested that when using ultrasonic angioplasty devices, the thermal injury to the tissues may be the result of conduction from the wire waveguide. This is caused by ultrasonic energy being converted to heat as it is transmitted through the waveguide to the tissue [87]. Siegel *et al.* describe the temperature increase at the probe distal tip (2.3 - 3.0 mm diameter) when using ultrasonic angioplasty on canine arteries at a frequency of 20 kHz. Five minutes of constant duty ultrasound produced a temperature increase from 22 to 50 ^{0}C at probe tip. 50% duty for the same duration produced only an 8 ^{0}C temperature rise [102]. Hartnell *et al.* also report similar temperature increases. Tests were conducted *in vitro* studies using 1.6 mm mushroomed tipped wire waveguides for thrombus ablation. For 15 minutes of activation and at an ambient temperature of 37 ^{0}C, an intra-luminal temperature rise of 9 ^{0}C and a wall temperature increase of 15 ^{0}C were measured [103].

The generally accepted safe limit for heating blood for short periods of time is 41 ^{0}C, after which cell death ensues [104], so irrigation at the distal tip is common. Efforts to combat heating have been made by integrating a saline flush into the system [72]. This also has the additional benefit flushing away ablated debris.

2.3.3.2 Acoustic streaming

Any medium or object in the path of an ultrasonic beam which absorbs some of the energy of the beam, will experience a force due to the change in momentum carried by the beam [100]. This is caused by the momentum loss of the acoustic beam by attenuation being taken up by the momentum of the fluid

mass, thus conservation of momentum is fulfilled [105]. The result of this is known as radiation force, but originally, this was coined as “Quartz Wind” because it was emitted from a quartz piezoelectric transducer [106]. The radiation force acts on the fluid medium and gives rise to a dipole streaming regime, known as acoustic streaming [107].

Acoustic streaming is commonly treated as a second order mathematical function, which means that the streaming speeds are proportional to the square of the source amplitude [106]. The streaming velocity is also a function of frequency [105]. The fluid flow from acoustic streaming gives rise to shear forces within the fluid which may cause cell and tissue damage [108], the extent of which is still unknown. Acoustic streaming has also been shown to enhance thermal convection thus reducing the localised heating effects by ultrasound [109] and [110] cited in [111].

The effects of acoustic streaming on material ablation are not yet known and it may have a greater effect on highly viscous thrombus rather than hard calcified plaques. In work by Lauer *et al.*, the affects of 1 MHz intermittent ultrasound on thrombus was examined. They concluded that acoustic streaming alone, without cavitation effects, was responsible for the increased thrombolysis [112].

2.3.4 Failure of soft tissues by therapeutic ultrasound

Although these ultrasonic devices are generally aimed towards diseased atherosclerotic hard tissue ablation and disruption and thrombolysis, there is a lack of clarity on the effects that this energy has on the soft healthy arterial wall. In other fields of therapeutic ultrasound, there is evidence to suggest that soft

tissue may be failing due to a combination of mechanisms such as soft tissue fragmentation, mechanical and thermal ablation (whereby the water content of the soft tissue is lowered as a result of thermal absorption rendering tissue susceptible to brittle failure) or fibre bundle de-striation [82, 113]. Fundamentally, the question of whether soft tissue is removed by ablation or fibres are torn and separated at the powers reported in ultrasonic therapy still remains unanswered.

2.3.5 Other considerations for failure of soft tissues

Relevant to this research is the quantification of the fracture and failure of soft tissues by non-ultrasonically energised cutting and perforating devices. Combining the knowledge of both fields (non-ultrasonic and ultrasonic) may help to give a better insight to the overall mechanics of soft tissue perforation when using ultrasound transmitted via wire waveguides. This section describes non-ultrasonic devices only.

A number of authors have presented work on perforation and cutting of soft tissues with standard needles and scalpels and have established methods for quantifying the energy needed to achieve this. McCarthy *et al.* [114] investigated the cutting of soft tissues with scalpels with the goal of establishing a 'blade sharpness index' for describing scalpels and other such implements. To quantify the cutting process, the force profile for the cut was measured and using the indentation distance into the tissue (δ_i), it was possible to calculate energy or work done. They describe cut initiation energy, E_i, required to initiate a cut in soft tissues, given in Equation 1 and illustrated in Figure 2-14. Given

that tissue deforms initially to some penetration depth, δ_i, under loading prior to failure, E_i, is defined as:

$$E_i = \int_{\delta i} F\, dx \qquad \text{Equation 1}$$

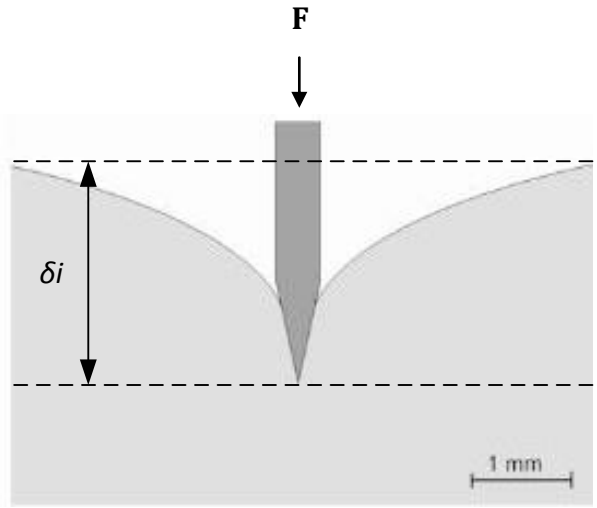

Figure 2-14 : Needle insertion into tissue by McCarthy *et al.* [114].

The force profile for needle insertion phases into human liver and kidney has been examined experimentally by Mahvash and Hayward. An experiment was designed to measure the force profile for a needle insertion into the tissue. They decompose the force profile into four phases, as shown in Figure 2-15 [115] cited in [116]. They describe the force profile as composing of:

i. Deformation – Initial deformation from contact with tissue.
ii. Steady state penetration – Energy threshold breached and crack initiates.
iii. Relaxation – Desired force achieved and force relaxes as a result of viscoelastic properties of the material.
iv. Extraction phase – Force due to the released stored elastic strain energy and friction.

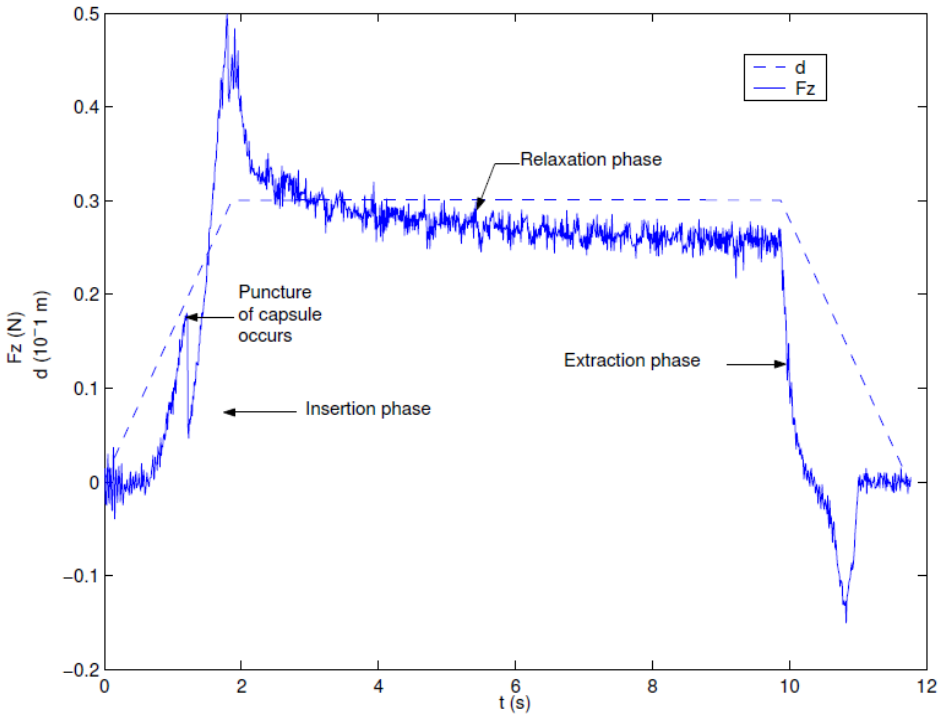

Figure 2-15: Needle insertion phases (force profile) into a human liver from Mahvash and Hayward [115].

Azar and Hayward [116] also describe the use of a general energy balance equation to describe all phases of the initial tissue deformation and perforation of porcine liver tissue during a needle insertion. Allowing for the investigation of the cut initiation energy and also the work done during insertion of the needle, accounting for friction, wedging and fracture work. Some work has been conducted on the effects of feedrate on the perforation forces of a needle into soft liver tissue. The feedrates range from 2 – 10 mm/sec and show an increase in perforation forces with increasing feedrates [117].

2.3.6 Summary of ablation and disruption mechanisms

- Cavitation, direct mechanical impact, acoustic streaming and other pressure wave components are described as ablation and disruption mechanisms for both ultrasonic thrombolysis and atherosclerotic plaques. It is not yet known the degree or contribution of which the mechanisms have on diseased tissue failure or indeed healthy soft tissue damage and perforation.
- Failure due to mechanical contact of the wire waveguide and tissue may be caused by the action of high frequency cyclic impacts on the tissue, pulverising and breaking down the brittle tissue or straining, moving and cutting of the soft tissue fibres.
- Non-contact tissue disruption and ablation may be related to inertial cavitation in the acoustic medium in regions close to or on the target tissue. Softer thrombus may be broken down by shear forces created by high streaming velocities.
- Cavitation thresholds for the low ultrasonic frequency range used in cathether delivered external transducer wire waveguide systems for water range from 0.1 MPa to - 0.2 MPa [91]. For a frequency of 22.5 kHz with acoustic properties of water with suitable gas nuclei this is approximately 2-3 W/cm^2. For degassed water this may be as high as ≈ 6 – 8 W/cm^2.
- Attenuation coefficients and cavitation thresholds are non-linear and dependent on the fundamental frequency of operation. There is a paucity

of information for these coefficients in the literature for the frequencies (and acoustic mediums) used in ultrasonic angioplasty.

- Heating of diseased and surrounding healthy tissue may be caused by a number of factors, including attenuation of the ultrasonic wave, frictional heating of the wire waveguide-tissue interaction and internal friction heating of the vibrating wire waveguide or tool. Heating when using ultrasonic angioplasty devices may cause thermal damage. These effects can be mitigated by using irrigation via the catheter. This may also act to flush away ablated debris.
- This research is focused on soft tissue failure due to high frequency vibrating wire waveguides at similar operating conditions to that used for unblocking CTOs and thrombolysis.
- Soft tissue perforation for a range of feedrates (2 – 10 mm/sec) using a needle show that increasing feedrates results in increased perforation force.
- Techniques which were used for analysing soft tissue failure using cutting forces and tissue indentation distances by standard non-ultrasonic cutting tools, such as needles are adopted for this research in assessing the perforation energies of the wire waveguide and tissue.

2.4 Experiences using catheter delivered external transducer wire waveguide delivery in cardiovascular applications.

2.4.1 In vitro

In 1965, Anschuetz and Bernard first suggested that this form of ultrasonic energy has potential to be applied to atherosclerotic plaque irradiation [118]. In the same year, Lane and Mino ablated human coronary atherosclerotic plaques post mortem [119] cited in [120]. This heralded the beginning of studies into the use of low frequency ultrasound to disrupt atherosclerotic lesions. These initial studies concluded that ultrasonic energy transmitted through flexible wire waveguides can offer effective treatment for the disruption of atherosclerotic lesions.

2.4.1.1 Ultrasonic thrombolysis

Relatively low frequency (26.5 KHz) ultrasonic waves transmitted via small diameter waveguides were first used to ablate an occluding thrombus *in vitro* by Trubenstein *et al.* in 1976 using a probe 21-29 cm in length [73] cited in [120]. Bige *et al.* also examined the use of ultrasound at 27 kHz for thrombolysis [121]. They voiced their concern that the ablated fragments can cause new thrombus formation. However, in a study performed by Philippe *et al.* , who analysed fragment size after thrombolysis, they found that 90% of the fragments to be less than 10μm [122].

2.4.1.2 Plaque disruption and ablation

The low frequency operation of these devices began to be the standard for any experimental work carried out. There are a number of reasons behind this. Suchkova *et al.* demonstrated greater acceleration in fibrinolysis using frequencies in the mid-kilohertz rather than in the megahertz range [123].

As far as safety is concerned, Siegel *et al.* reports that the microscopic particulate debris generated during plaque ablation are small and comparable to the particulates from other clinically used modalities, he also states that the clinical studies in humans show that this treatment can be used safely and effectively for peripheral angioplasty [2].

In an effort to discover the optimal amplitudes of vibration at distal tip for carrying out ultrasonic angioplasty on atherosclerotically occluded arteries, Chikada describes the use of an ultrasonic device for ultrasonic angioplasty of human cadaveric arteries [72]. A 2.5 mm diameter 5 cm long hollow probe was used which could deliver amplitudes of 210 μm at 100% power input. This operated at 24 kHz. Effective removal of the lesion is reported at distal tip amplitudes of vibration for soft atheroma (90-110 μm), mild atherosclerosis (110-130 μm) and calcified lesions (150 μm).

Fischell *et al.* experimented with ultrasound at 20 kHz using a ball tipped wire probe of 2.0 mm diameter on thoracic arteries from New Zealand white rabbits and human cadaver iliofemoral arteries. They performed the tests with their device on atherosclerotically occluded (fibrocalcific) arterial segments using a 50% pulsed cycle of 30 msec. Saline was infused via the catheter to prevent heating of the probe [124] .

Siegel *et al.* describe the initial experiences of using an ultrasonic device for occluded coronary arteries (xenografts in canine). The device operated at 19.5 kHz and delivered amplitudes of vibration between 15 - 30 μm to a 1.7 mm diameter ball tipped wire waveguide [2]. Similar operational characteristics would later be adopted by the CROSSER™ ultrasonic device [53]. In this paper, the forces applied to successfully recanalise the occluded arteries were given. Forces between 0.98 - 1.96 N were measured. The adverse effects of the ultrasonic probe in contact with the healthy canine arterial tissue were also observed as part of this study [72]. Incidences of restenosis in both short and long term outcomes were reported. It was found that higher distal tip amplitudes of vibration resulted in higher rates of restenosis.

2.4.2 In vivo

2.4.2.1 Ultrasonic thrombolysis

Studies *in vivo* suggest that catheter delivered ultrasound can be used for thrombolytic therapy without injuring the surrounding vessel wall [125]. In the mid 1990s clinical studies using catheter delivered ultrasound were performed on human coronary and peripheral arteries, Hamm *et al.* 1994 first published their successful treatment of intra-coronary thrombolysis using this method [126]. Later in 1997 Hamm *et al.* and Rosenschein *et al.* [127, 128] conducted a study on a number of patients for mechanical thrombolysis, although both these results were positive, they were not significantly better than the standard available treatment, balloon angioplasty [129].

2.4.2.2 Plaque disruption and ablation

A number of investigators had shown that this technique can be used safely and effectively for peripheral artery angioplasty *in vivo* [80, 86, 87, 130]. In 1989, Siegel *et al.* published their results on their initial clinical experience of a percutaneous catheter-delivered arterial recanalisation of human peripheral arteries. They used an ultrasonic probe operating at 20 kHz with a power output at transducer of 20-35 W/cm^2 [130]. The aim of the ultrasonic device was to reduce the degree of stenosis so that a follow up balloon device could be put into place and inflated, dilating the artery further. Three of four total occlusions were recanalised in 120 s or less. The results of this experiment were extremely positive, with no arterial emboli, dissection, spasm or arterial perforation observed. However Siegel concludes that one of the major limitations of this ultrasound system is difficulty of steering from lack of flexibility.

One of the largest clinical trial of ultrasonic angioplasty was conducted between 1993 and 1995 in Europe. This was known as CRUSADE (Coronary Revascularisation Ultrasound Angioplasty Device Evaluation) and it involved a total of 229 patients with 234 coronary lesions [120]. The ultrasonic angioplasty device operated at 19.5 kHz with 1.2 mm and 1.7 mm ball tips. A range of atherosclerotic lesion stages were treated and 82% of lesions were successfully crossed. 92% of these were then treated by adjunctive balloon angioplasty [120].

In an effort to examine the long term effects of this new procedure, Siegel *et al.* conducted a study which was intended to present follow-up data as well as short-term results on a larger clinical series of patients undergoing ultrasonic angioplasty [80]. The tests were carried out on peripheral arteries using a 2.0

mm or 3.0 mm ball tip. This operated at a frequency of 19.5 kHz; the device configuration is shown in Figure 2-16. It was reported that this method is useful for recanalisation of fibrous, calcific and thrombotic arterial occlusions and reduces arterial stenoses.

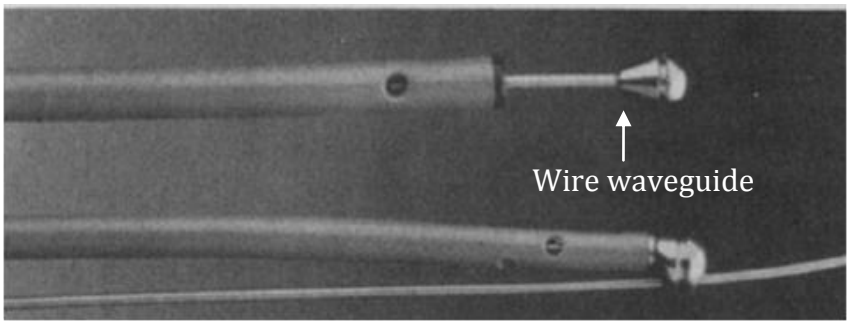

Figure 2-16 : 2.0 and 3.0 mm ball tipped titanium wire waveguide from Siegel *et al.* [80].

Drobinski *et al.* also published results of experiments carried out on total peripheral artery occlusions [86]. Clinical tests were conducted on coronary and peripheral arteries using a 130 cm long wire waveguide (0.8 mm wire with 2.0 mm ball distal tip) and show that up to 70% of the blockage can be removed by this method [86]. Crossing the occlusion was achieved in 6 minutes or less, with occlusion length ranging from 5-10 cm, feedrate (if continuous) < 17 mm/min, the amplitudes of vibration at wire waveguide distal tip are 50 μm.

More recently, up to and following the approval of the CROSSER™ system, studies have been conducted using the clinically approved device. According to the manufactures specification, the CROSSER™ system operates at 20 kHz approximately which delivers stroke depths of 20 μm [4, 44, 53]. They describe that the high frequency, low amplitude, longitudinal stroke pulverizes a channel through the CTO by mechanical impact [53].

In this study they describe some necessary design changes which had to be made to the wire waveguide in order to access the lesion site [53]. The aims of this study were to first access the safety of the device and identify any possible opportunities for device improvement. The initial wire was a feasibility stage wire design (1.3 mm diameter uncoated wire) which was then reduced to a hydrophilically coated 1.1 mm diameter wire waveguide which dramatically improved deliverability. They reported an increase in clinical success from 40-76% as a result. Another study using the CROSSER™ system highlighted that it was effective with ostial and distal lesions, tapered and abrupt lesion morphologies [4]. Recent clinical trials (CENTRAL), completed in 2011, using the CROSSER™ system investigates the efficacy of the device to navigate through the central lumen [131].

2.4.3 Additional benefits of using ultrasonic angioplasty

Episodes of arterial spasm resulting in myocardial infarction have been encountered when using balloon angioplasty [132], however it was found that the ultrasonic energy induces smooth muscle relaxation, a secondary effect which may improve safety of arterial recanalisation by reducing vaso-constriction during catheterisation. Fischell *et al.* suggested that air bubble stimulation generated by the ultrasound could be the mechanism behind the beneficial vaso-relaxation they observed [124]. This phenomenon was also observed by Chokshi *et al.* [133]. In a study conducted by Demer *et al.* on follow up balloon dilation of the artery after ultrasound wire waveguide treatment, incidences of increased distensibility of calcific atherosclerotic arteries after treatment using the ultrasound are reported [5].

2.4.4 Summary of clinical and experimental studies using ultrasonic wire waveguides

- The wire waveguide devices typically operate in the low ultrasonic frequency range (20 - 50 kHz) and deliver longitudinal amplitudes of vibration at the wire waveguide distal tip between 0- 60 μm. The wire waveguides shafts are typically slender (0.35 – 2.0 mm) but are often tipped with enlarged spheres 1- 2.5 mm in diameter. A review of the operating parameters is shown in Table 2-1.
- The forces required to recanalise occluded arteries is given by Siegel *et al.* [2] as 0.98 – 1.96 N using amplitudes of vibration between 15 – 30 μm with a 1.7 mm wire waveguide ball distal tip. These operating parameters are similar to the CROSSER™ catheter.
- The EU and FDA approved device for CTOs, the CROSSER™, delivers amplitudes of vibration in the region of 20 μm to a distal tip of 1.1 or 1.5 mm in diameter.
- CTOs are associated with increased risk of arterial perforation, possibly a result of the guidewire being deflected towards the arterial wall.
- Recent clinical trials (CENTRAL) are investigating the efficacy of the CROSSER™ device to navigate through the central lumen. The purpose of the trial may be a response to the risk of arterial perforation in the treatment of CTOs generally.
- To date there has been no study on the effects, if any, of the wire waveguide on perforation of the artery wall.

Description	Frequency (kHz)	Distal tip amplitude of vibration (µm)	Wire waveguide details	Investigator
Thrombolysis ***In vitro***	26.5	25-30	Hollow wire 210-290 mm length	Trubestein [73]
Thrombolysis ***In vitro***	20	63.5 – 111	Titanium wire 0.72 mm shaft, 2.0 mm ball tip	Ariani *et al.* [71]
Atherosclerotic lesion ***In vitro***	20	50± 25	Titanium wire 0.5 mm with 2.0 mm ball tip	Demer *et al.* [5]
Atherosclerotic lesion ***In vitro***	22.5	130/200	Titanium wire 1.98/2.46 mm ball tip	Makin *et al.* [7]
Atherosclerotic lesion ***In vitro***	19.5	15-30	1.7 mm ball tip	Siegel *et al.* [2]
Atherosclerotic lesion ***In vitro***	24	90 – 150	Titanium 2.5 mm hollow wire	Chikada [72]
Atherosclerotic lesion ***In vitro***	20	N/A	Titanium 2.0 mm wire tip	Fischell *et al.* [124]
Atherosclerotic lesion ***In vivo***	20	150± 25	Aluminium alloy 1.6 mm wire tip	Rosenschein *et al.* [6]
Atherosclerotic lesion ***In vivo***	20	10	1.1 – 1.7 mm wire tip	CROSSER™ System [75]
Atherosclerotic lesion ***In vivo***	19.5	55.5	Titanium 2.0 - 3.0 mm wire tip	Siegel *et al.* [80]
Atherosclerotic lesion ***In vivo***	N/A	50	Titanium 0.8 mm shaft, 2.0/2.5 mm ball tipped wire	Drobinski *et al.* [86]

Table 2-1 : Review of operating parameters for thrombolysis and angioplasty, *in vitro* and *in vivo*.

2.5 Performance evaluation of the devices

While some investigators examine the efficacy of their device in terms of clinical outcomes [4, 131], other investigators investigate the fundamentals of the device operation. This includes:

i. Wire waveguide materials and mechanics.
ii. Acoustic pressure field generated by the wire waveguide distal tip.

2.5.1 Wire waveguides materials and mechanics

Titanium and Nickel Titanium alloys (Nitinol) and high mechanical Q Aluminium were traditionally used as wire waveguide material because of their super elastic strength [87]. The mechanical quality factor (Q) of the wire waveguide material is proportional to the ratio of stored energy dissipated per unit material volume per cycle of vibration. A reduction in the quantity of the energy dissipated as thermal energy is associated with high material Q values. High Q values are also associated with lower attenuation of the ultrasound per unit length of wire waveguide [87]. In comparison, Aluminium has Q values in the region of 50,000 while Titanium has roughly half (24,000) [87].

The wire waveguide performance has been analysed experimentally by a number of investigators [71, 134]. Ariani *et al.* describe a method of measuring the amplitudes of vibration at the distal tip of the wire waveguide for power input settings by means of an optical microscope [71]. This method of distal tip amplitude of vibration measurement was also performed by Gavin *et al.* for a similar ultrasonic apparatus [134]. Other methods using a LASER measurement

system has also been investigated. In terms of accuracy, however, both methods yield very similar results [135].

2.5.2 Acoustic pressure field (theoretical)

The vibrating wire in a fluid causes an oscillating acoustic pressure field around the distal tip. This field is caused by compression/rarefaction waves radiating from the source which produce sinusoidal forces on the surrounding tissue. Variations in density in the acoustic medium through which the wave propagates can cause reflection. The reflected wave may combine with the incident wave to produce a standing wave structure. Standing waves in tissue can cause free moving cells to gather at the nodes of the wave structure. In blood, this effect may cause it to coagulate at these locations [108]. Assuming linear wave propagation, for an incompressible fluid with no mean flow, and neglecting shear stresses, the lossless acoustic wave equation (Equation 2) can be written as [136]:

$$\frac{1}{c^2}\frac{\partial^2 P}{\partial t^2} - \left(\nabla^2 P\right) = 0 \qquad \text{Equation 2}$$

The speed of sound in the medium, c, can be calculated using Equation 3:

$$c = \sqrt{\frac{k}{\rho}} \qquad \text{Equation 3}$$

Where the bulk modulus of the material is given by k and material density is given by ρ. The spatial-average-temporal-average acoustic intensity at the waveguide radiating face, I_{SATA}, can be derived from the measurement of acoustic pressure under the assumption of plane progressive wave propagation (a situation in which particle velocity and acoustic pressure are in phase). Under these assumptions, the peak intensity can be calculated using Equation 4 [91]:

$$I_{SATA} = \frac{P_{max}^2}{2\rho c} \qquad \text{Equation 4}$$

It should be noted that the above wave equation is a linear approximation. Wave velocity is a function of the particle velocity (or acoustic pressure). High pressure components of the wave travel more quickly than the lower pressure regions, eventually overtaking them and generating a shock front, a non-linear effect [137].

2.5.3 Reflection of the acoustic wave

Standing waves in the acoustic field are caused by the reflection which occurs at the interface of layers/materials of different acoustic impedances. For therapeutic ultrasound the reflected sound power for various tissue types and the tissue-air interface encountered *in vivo* can be calculated. The sound power reflection coefficient (α_r) is given in Equation 5 [138]:

$$\alpha_r = \left(\frac{\rho_2 c_2 - \rho_1 c_1}{\rho_2 c_2 + \rho_1 c_1}\right)^2 \qquad \text{Equation 5}$$

Thus, assuming no energy loss, the total reflection of the incident energy must correspond to a unity value of reflection coefficient. The speed of sound for air and blood/tissue was taken as 340 m/s and 1580 m/s respectively and with densities of 1.2 kg/m^3 and 1050 kg/m^3 respectively [100]. Using Equation 5 and the material properties given, the sound power reflection can be calculated to be 99.9% at a tissue-air interface.

2.5.4 Flat vibrating wire tip in a fluid

Also applicable to this work is the solution for the pressure, P_{max}, at a small piston source (circular radiating face) from Wu and Nyborg [106]. This closely represents experimental waveguides/transducers with flat circular radiating faces. Figure 2-17 shows a diagram of a radiating piston which illustrated the parameters used in Equation 6. Where the amplitude of displacement is given by ξ_0.

$$P_{max} = 2\pi^2 \rho R f^2 \xi_0 \qquad \text{Equation 6}$$

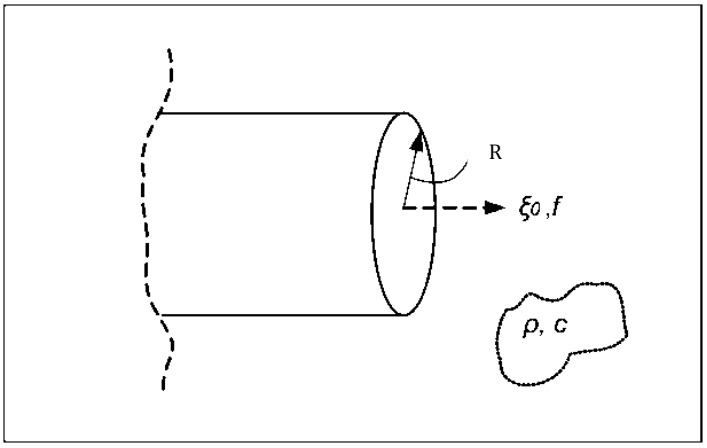

Figure 2-17: Illustration of parameters used in calculation of acoustic pressures and acoustic intensities.

2.5.5 Radiused vibrating wire tip in a fluid

Analytical solutions for the acoustic pressures for a pulsating sphere in a fluid and the more representative oscillating sphere in a fluid also exist. The analytical solution proposed by Morse [139] for the pressure field near an oscillating sphere in a fluid is given in Equation 7 and associated Figure 2-18. Although this linear solution is limited to a simple geometry, it has been suggested by Nyborg [136] as a useful approximation to predict pressure amplitudes and subsequent cavitation associated with the frequencies and conditions encountered in ultrasound angioplasty.

$$P_{max} = 2\pi^2 \rho R f^2 \xi_0 \times \frac{R^2 |cos\theta|}{r^2} \qquad \text{Equation 7}$$

Where the radius of the sphere is given by R, the radial distance from centre of sphere is given by r and the angle between the direction of oscillation and radius-vector is given by θ.

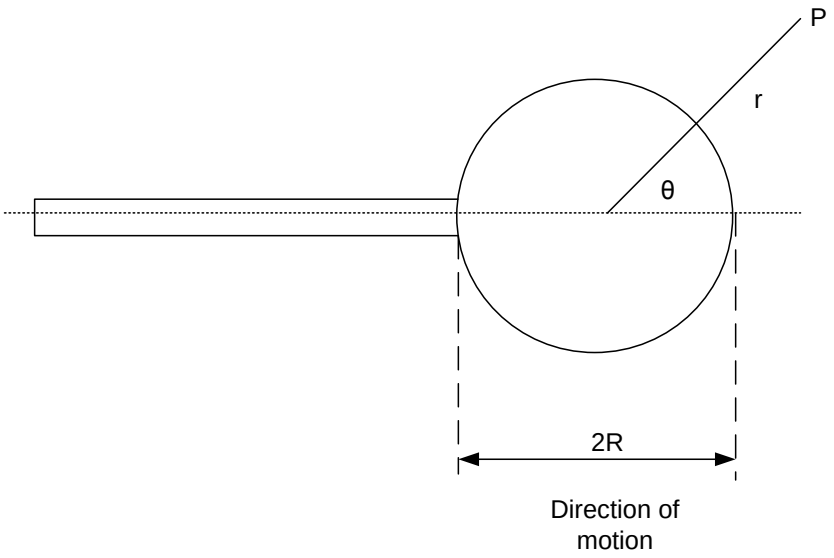

Figure 2-18: Idealised model of waveguide spherical tip.

2.5.6 Acoustic pressure field (experimental)

The significance of the pressure amplitude at the waveguide tip, the role it plays in cavitation and pressures developed in surrounding fluids and tissues has led a number of researchers to investigate this phenomenon experimentally [7, 123, 140].

Makin and Everbach investigated the acoustic pressures developed by an ultrasonically vibrating wire waveguide submerged in a liquid with acoustic properties similar to that of blood [7]. The experiment consisted of a 2.46 mm diameter spherical tipped wire waveguide oscillating in a cylinder of fluid (peripheral arterial phantom) at 22.5 kHz. Their experiment comprised of an ultrasonic emitter-receiver submerged in a tube within a 355 mm high acrylic tank with an internal diameter of 203 mm. The tank was filled with water or a glycerine-water mix. The experiment was described as having a 355 mm high tank filled to 345 mm with fluid (i.e. 10 mm of air at top of cylinder). A schematic of this experimental set up is shown in Figure 2-19.

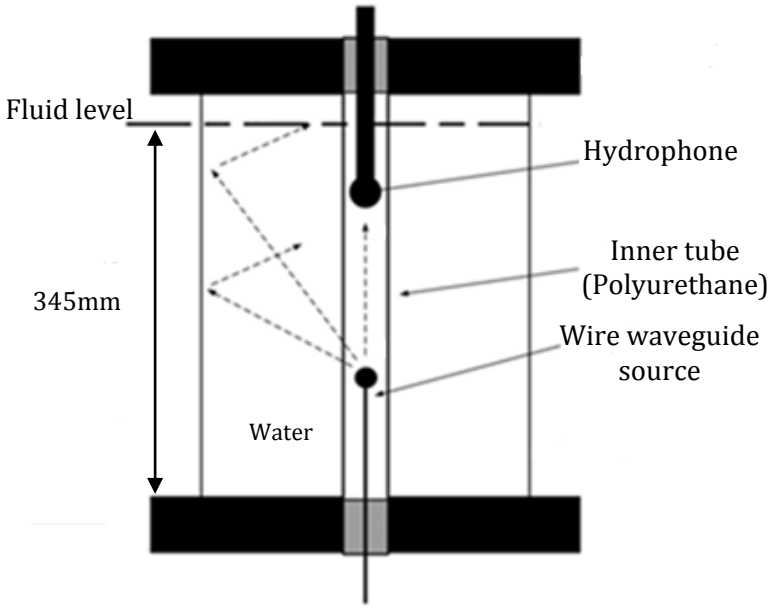

Figure 2-19 : Schematic of experimental set up by Makin and Everbach.

Pressures were measured in the range of 12-250 mm from the vibrating tip using an acoustic hydrophone; measurements in the vicinity of the tip were restricted due to the limitations of their measuring equipment (potentially damaging their sensor). Their results demonstrate two important effects of the ultrasound:

i. Despite not being able to directly measure pressures at the wire waveguide distal tip, the authors were able to measure cavitation activity with a 20 MHz focused transducer. They concluded that not only was cavitation evident, but that the amount of cavitation was related to distal tip amplitude of vibration and also to the tip geometry.
ii. Their results also showed a standing wave in the acoustic domain of significant amplitude. They concluded that because the acrylic walls were acoustically transparent at the frequency used this standing wave was caused by an impedance mismatch between the liquid representative of blood and the surrounding air.

2.5.7 Summary of performance evaluation of these devices

- The distal tip amplitudes of vibration are a function of wire waveguide length, input displacement and losses in the wire waveguide. Nodes and anti-nodes exist along the wire waveguide. The amplitudes of vibration at the wire waveguide distal tip can be determined both experimentally (microscope, image capture software) and analytically.
- The maximum acoustic pressures and the Spatial-Average-Temporal-Average acoustic intensities can be analytically determined for a flat and radiused wire waveguide distal tip. Analytical solutions given in this chapter do not account for non-linearity of the ultrasonic sound propagation or complex geometries of the wire waveguide and are, therefore, limited.
- *In vivo,* complex acoustic conditions exist because of the impedance mismatch between tissue and fluids. Surrounding tissues such as bone can cause high sound power reflection. Indeed, the tissue-air interface from the body and surrounding air atmosphere can act to reflect as much as 99.9 % of the sound power.
- It is possible to experimentally measure the pressure in the acoustic field generated by a wire waveguide distal tip using a hydrophone but pressures in regions < 12 mm to the distal tip cannot be measured by this experimentally. High pressures and cavitation in this proximity can critically damage the hydrophone.

2.6 Computational numerical analysis

2.6.1 Finite Element Analysis

Finite Element Analysis (FEA) is a numerical method of solving partial differential equations to determine approximate solutions for field variables, such as pressure, strain, temperature, electromagnetism etc. This technique is used to simulate an object or system (static and dynamic analysis) by representing a geometrically similar model. This method divides the model into discrete elements or finite elements (i.e. a mesh). Material properties, structures and loads are then applied to these elements. A finer mesh will act to improve resolution but subsequently increases computational effort. FEA can be advantageous over experimental methods as it can model complex geometries and be used to recover results where experimental methods cannot. Numerical models are often simplified representations of actual systems and are limited by adequate knowledge of material properties and response, input parameters etc. Many commercially available FEA packages offer extensive post processing options, allowing for the analysis of many different aspects of the solved model.

2.6.2 FEA for ultrasonic applications

It is possible to apply this numerical method to examine certain aspects of ultrasound and its propagation through media such as blood and tissue. Some investigators have attempted to model some of the effects of ultrasound, such as acoustic streaming and heating [141-144]. Other research has been performed on modelling the operation of the ultrasonic angioplasty devices, i.e. piezoelectric effect and wire waveguide motion [145, 146]. There is some work

on the effects of dynamic loading due to high frequency mechanical impact on the tissue. Some acoustic models have been created in biological media using FEA, but generally these are at sonic or subsonic levels [147, 148].

2.6.3 Linearity

Ultrasound is fundamentally a non-linear propagation of sound waves [149]. A non-linear partial differential equation is used to describe an ultrasonic wave propagating in biological tissue. This derives from the non-linear pressure-density relationship and variance in speed of sound with pressure amplitude during compression/rarefaction cycles which has a greater influence at higher frequencies and at greater intensities. In high frequency ultrasonics, there are some non-linear material properties which also need to be taken into account for tissues. These include the amplitude dependent attenuation, harmonic generation, increased energy dissipation, acoustic saturation and waveform distortion [150]. Some work has been done on soft tissue response to low ultrasonic frequencies by Palmeri [151]. It is stated that at the low ultrasonic frequencies (<100 kHz), soft tissues can be also be considered and modelled as linear elastic, isotropic solids [151] . Since the applied frequencies used in this work are in the sub 100 kHz range the properties of the media are modelled using linear assumptions.

The propagation speed of the wave as it passes through the medium is a function of the particle velocity of the tissue (medium). When the amplitude is infinitesimally small, the ultrasound propagation can be considered as a linear phenomenon [152]. When the pressure amplitude becomes significantly large this linear approximation no longer holds [152]. The application of the linear

material properties and assumption of linear wave propagation greatly reduces the computational time and power substantially.

2.6.4 Mesh density in ultrasonic acoustics

The accuracy of the model is related to the density of the mesh, i.e. the spatial resolution. Sufficient element density is required to avoid aliasing data between nodes and to capture the small perturbations in the high frequency acoustic field, as can be seen in Figure 2-20. In acoustics, the mesh density is often described as Elements Per Wavelength (EPW). Wavelength is inversely proportional to the frequency, so higher frequency ultrasonics requires more elements and therefore greater computational power.

There is some data on the EPW which should be used to accurately predict ultrasonic transmission from emitters and propagation through elastic media, such as tissue. EPWs of anywhere from 8-20 for ultrasonic transducers and waveguides are described in the literature [146, 153-155]. Information on the EPW for acoustic models for low frequency ultrasonics is sparse. Lewis *et al.* did some initial work on FEA acoustic modelling of ultrasonic cleaning baths with a mesh density of 20 EPW [156]. This value was taken from Mosser's modelling protocol of modelling of mechanical waves in wire waveguides, not the acoustic field [153].

In ultrasonic acoustics, more complex acoustic conditions exist and, therefore, more elements may be required to capture high frequency wave interactions. Model mesh convergence is typically applied to the models to ensure that the correct mesh density has been applied. A sensitivity analysis

may then be performed to ensure that the mesh density is accurate for a range of input parameters (i.e. frequency).

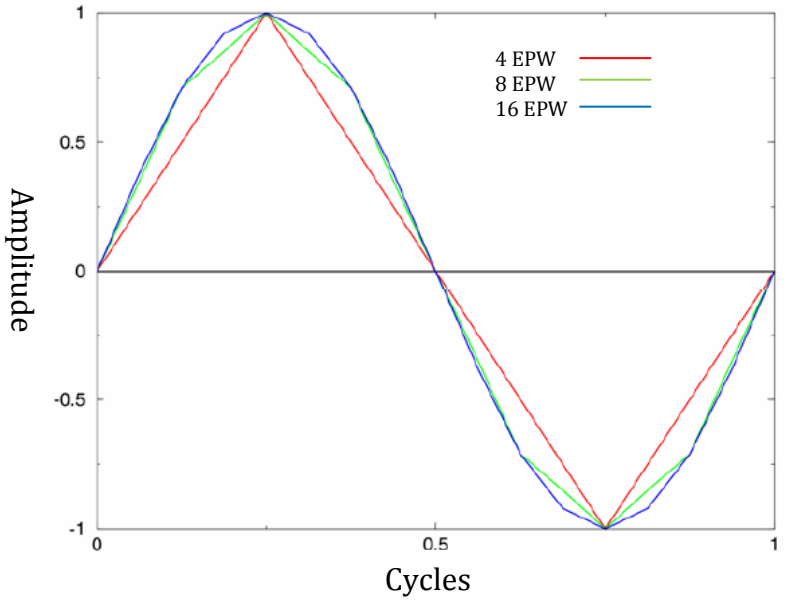

Figure 2-20: Effects of mesh density on resolution [157].

2.6.5 Acoustic FEA of ultrasound angioplasty

Previous FEA of ultrasonic wire waveguides has focussed on modelling how the wire waveguide transmits the ultrasonic waves to the distal tip. Gavin performed a modal and harmonic analysis to determine wire waveguide resonant characteristics, damping and stresses [13]. The same authors also modelled the pressure field in the fluid and the effect the presence of fluid had on the resonant response of waveguides. This FEA, however, did not perform a mesh density analysis of the acoustic domain and therefore may be subject to inaccuracies.

Local conditions at the wire waveguide distal tip make it extremely difficult if not impossible to measure the acoustic pressure field immediately at the vibrating wire distal tip. Makin *et al.*, describe their attempt to experimentally measure the acoustic pressures at the wire tip but state that measurements closer than 12 mm were not possible with their hydrophone [7]. High pressures and cavitation can critically damage the hydrophone so caution must be exercised. FEA offers an insight to the acoustic pressures both at the wire distal tip and indeed the entire acoustic field.

By creating models to determine the acoustic activity, the onset of cavitation can be predicted. These are areas in which pressures are sufficiently low to cause cavitation can be identified throughout the acoustic field. Complex geometries and multiple fluids can also be considered.

Relatively speaking, ultrasonic angioplasty is still in its infancy and through design and testing, improvements can be made. FEA is an ideal method for design improvements, acoustic FEA of the ultrasonic device can be used to examine the effects of the following on the acoustic field:

i. Frequency
ii. Amplitude of vibration
iii. Distal tip geometries
iv. Fluid and tissue properties

2.6.6 Summary of computational numerical analysis

- Ultrasound is a non-linear propagation of high frequency pressure waves. But for low ultrasonic frequency operation (<100 kHz), using linear assumptions FEA may provide accurate results.
- Acoustic FEA can be used to predict the pressures generated by a vibrating wire waveguide. If adequate mesh densities (Elements Per Wavelength (EPW)) are applied, these models may then be used to numerically solve the entire acoustic field, providing data which cannot be obtained experimentally.
- The correct mesh densities (EPW) for modelling the acoustic field generated by ultrasonic angioplasty devices at typical operating parameters have not yet been investigated. More complex acoustic conditions exist and, therefore, more elements are required to capture the high frequency wave interactions, especially in regions where there is high acoustic activity, i.e. reflection.
- Using the FEA with an inertial cavitation threshold for the acoustic medium, it is possible to determine the operating conditions necessary to generate cavitation. The region (spatial) in which cavitation occurs can also be determined.
- With a verified and validated model, this method can, therefore, be used to examine the effects of distal tip geometry, acoustic frequencies, tissue properties and amplitudes of vibration on the acoustic field.

2.7 Project outline

Using the background information established from the literature review, a method of approach to answering the research question, as outlined in Chapter 1, is presented.

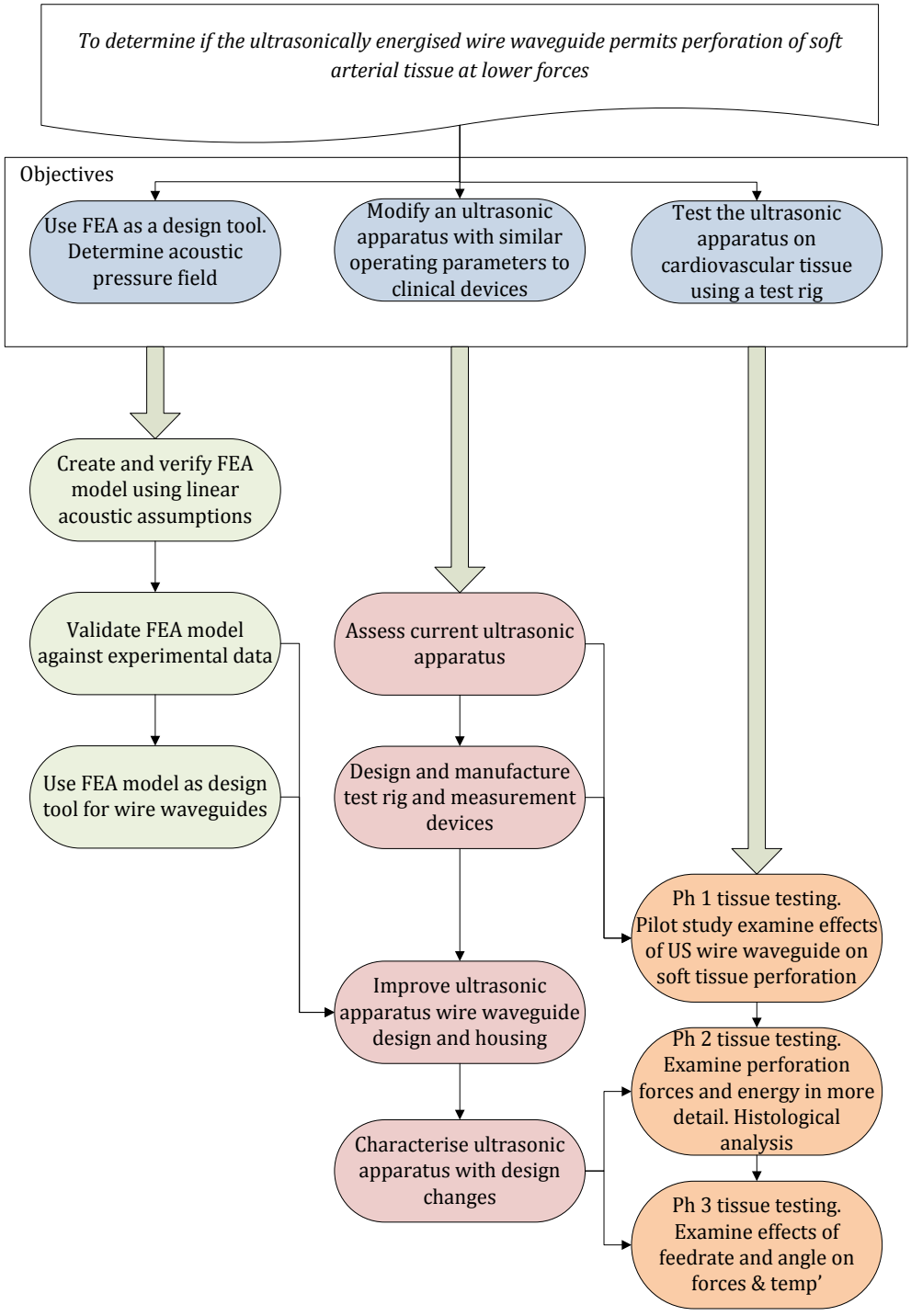

Figure 2-21 : Research aim and objectives.

CHAPTER

3 NUMERICAL ANALYSIS

3.1 Introduction

The goal of this work is to refine and extend the Finite Element Analysis (FEA) methodology, previously used by Gavin [13] to predict the waveguide mechanics and ultrasound transmission into the fluid, to simulate reflection at tissue interfaces and then compare these predictions with reference to experimental data from the literature. The method is then also applied to the prediction of ultrasound transmission for proposed new distal tip geometries. The acoustic FEA is capable of predicting distal tip acoustic pressures and the onset of cavitation, with the inclusion of an adequate threshold value.

FEA is used to model wire waveguide distal tip conditions in an effort to establish operating parameters for an ultrasonic apparatus modified as part of this work in a tissue testing programme. The modelling approach is conducted in three stages, also illustrated in Figure 3-2:

i. Determination of adequate mesh densities for the frequency range and amplitudes of vibration of interest by comparing the results with Morse's analytical solution for pressures generated by a vibrating sphere [139].
ii. Using this verified model, the pressures near the distal tip of the waveguide for proposed distal tip design improvements are predicted with the goal of understanding the effects of tip geometry, amplitude of vibration and frequency on the onset of cavitation.

iii. Finally, the model is validated against experimental results reported in the literature in peripheral arterial phantom [7].

3.2 Theoretical background

Ultrasound is a non-linear propagation of sound which is above the human hearing threshold. This derives from the non-linear pressure density relationship and variance in speed of sound with pressure amplitude. This has a greater effect at higher frequencies and at greater acoustic intensities.

For solving finite element acoustic fluid-structure interaction models, the Navier-Stokes equations of fluid momentum and the flow continuity equation must be considered along with the structural dynamics equation. Assuming linear wave propagation, for an incompressible fluid with no mean flow, and neglecting shear stresses, the lossless acoustic wave equation can be written as:

$$\frac{1}{c^2}\frac{\partial^2 P}{\partial t^2} - \left(\nabla^2 P\right) = 0 \qquad \text{Equation 8}$$

Where:

$$c = \sqrt{\frac{k}{\rho}} \qquad \text{Equation 9}$$

For a harmonically varying pressure:

$$\overline{P} = e^{j\omega t}$$ Equation 10

Where: $\overline{P}$ = Pressure amplitude

$\omega = 2\pi f$

$j = \sqrt{-1}$

f = Frequency of oscillation of the pressure

Equation 8 reduces to the Helmholtz equation:

$$\frac{\omega^2}{c^2}\overline{P} + \nabla^2 \overline{P} = 0$$ Equation 11

This governing equation for acoustic wave propagation can be discretized taking into account the coupling of acoustic pressure and structural motion at the fluid-structure interface [158].

Fluid: $$[M_F](\ddot{\vec{P}}) + [K_F](\vec{P}) = (\vec{F}_F) - \rho_0 [R]^T (\ddot{\vec{u}})$$ Equation 12

Structural: $$[M_S](\ddot{\vec{u}}) + [K_S](\vec{u}) = (\vec{F}_S) + [R](\vec{P})$$ Equation 13

Where: $(\ddot{\vec{P}})$ and $(\vec{P})$ = the 2nd derivative of nodal pressure and nodal pressure respectively and [R] = a coupling matrix that represents effective area associated with each node.

The equations given in Equation 12 and 13 can be combined into a single relationship that describes load quantities at all locations in the fluid and structure as shown in Equation 14.

Combined: $$\begin{bmatrix} M_S & 0 \\ \rho_0 R^T & M_F \end{bmatrix} \begin{pmatrix} \ddot{\vec{u}} \\ \ddot{\vec{P}} \end{pmatrix} + \begin{bmatrix} K_S & -R \\ 0 & K_F \end{bmatrix} \begin{pmatrix} \vec{u} \\ \vec{P} \end{pmatrix} = \begin{pmatrix} \vec{F}_S \\ \vec{F}_F \end{pmatrix}$$ Equation 14

3.3 Methodology

The general methodology for the FEA is outlined in Figure 3-2. Computational models were developed using a commercially available finite element package (ANSYS). Acoustic *Fluid29* elements are in the general acoustic field and all models were axisymmetric, making use of symmetrical conditions generally encountered in wire waveguide design. The *Fluid29* 2-D elements have four corner nodes with three degrees of freedom per node, x, y directions and pressure and are governed by the lossless wave equation. The model required the inclusion of an infinite absorbing boundary layer to define the outer limit of the acoustic model. An infinite acoustic boundary using fluid elements *Fluid129* is set up along the model boundary according to the following defined conditions i.e. this absorbing boundary must lie on an arc of radius greater than 0.2λ [158]. Where λ = c/f is the dominant wavelength. The acoustic properties of the fluid elements representing the blood was given as c = 1580m/s and ρ = 1050 kg/m^3 [100].

A Fluid-Structure Interface (FSI) defined where the wire waveguide distal tip and fluid meet. The interaction of the fluid nodes and structural nodes at the fluid-structure interface is such that the pressure in the acoustic field exerts an

applied force on the structural elements which produce an effective fluid load. The governing equations for both the fluid nodes and structural nodes are shown in Equation 14. Figure 3-1 shows an example of the model geometry and mesh. All models are solved for a harmonically varying distal tip displacement on the FSI. It has been shown by Gavin that is not necessary to include the wire waveguide structural elements [13]. The input displacement on the FSI specified the amplitude of vibration of the distal tip. A frequency sweep is also performed for a range of frequencies of interest. Pressure plots were then generated.

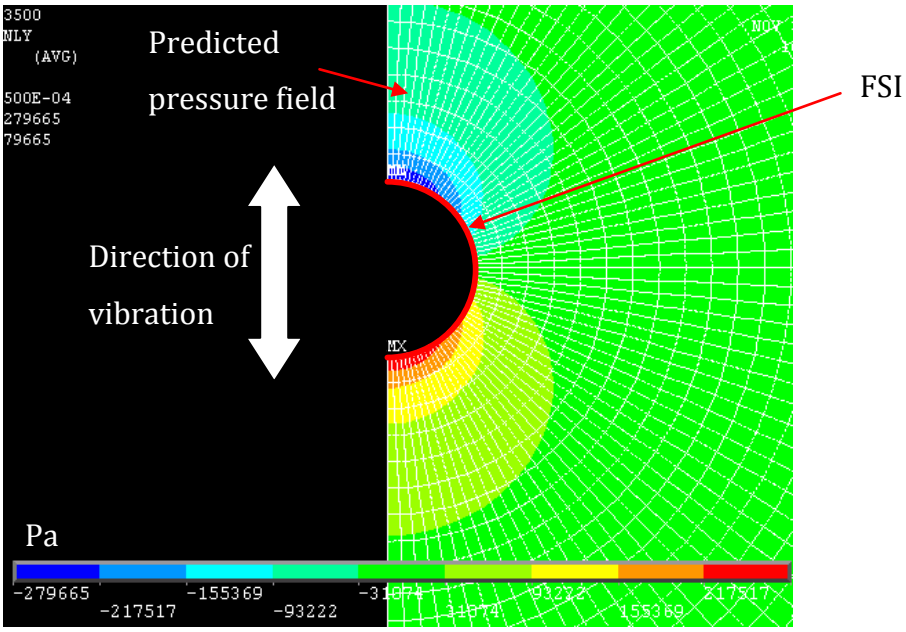

Figure 3-1 : Model geometry and mesh structure.

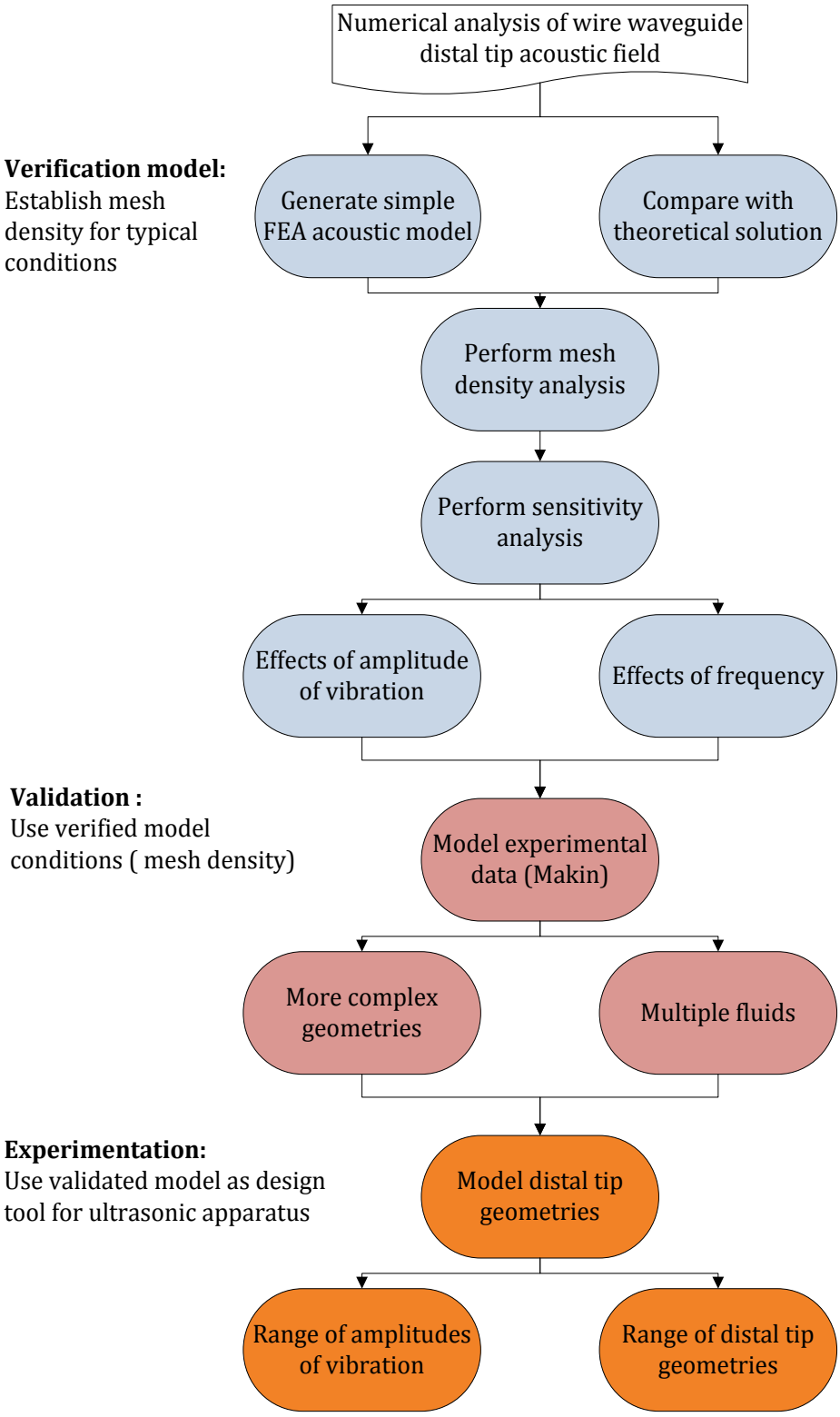

Figure 3-2 : FEA methodology.

3.3.1 Model verification: mesh density analysis

Understanding the effect of the mesh density on the model's ability to resolve the ultrasonic waves and pressures near the distal tip is critical. A simple acoustic axisymmetric model of the ultrasonic wire waveguide was developed that can predict the pressure field around the vibrating tip. A model was created of a spherical tipped wire waveguide vibrating in a fluid, which represented blood [100].

For controlled meshing the model geometry was created manually by assigning areas to connecting lines. Each line of known length is split according to the mesh density and subsequently meshed. The lines are split according to the wavelength for the frequency which is to be modelled. The model was meshed manually for each frequency of operation. The aim of this meshing technique is to create quadrilateral elements shapes with 1:1 aspect ratios.

A mesh density study was performed in which the number of elements per wavelength (EPW) was increased until the model correlated with the analytical solution for a oscillating spherical sphere [139]. Since the wavelength is frequency dependent, a range of frequencies and distal tip amplitudes of vibrations were modelled to verify that the models are still accurate in predicting acoustic pressures using this EPW count for the typical settings encountered using ultrasound angioplasty.

3.3.1.1 Model verification and mesh density analysis results

The mesh density analysis results are shown in Figure 3-3 and Table 3-1. The results clearly show the effects of insufficient mesh density when trying to

accurately predict the pressure amplitudes at the distal tip of the waveguide and in the acoustic field around the waveguide. The model was initially meshed with 20 EPW as reported by others in similar applications to be sufficient [146, 148, 155, 156] and then increased until a good correlation was achieved with the pressures directly ahead of the spherical ball tip as determined from the analytical solution. This was shown to amount to at least 140 EPW for the conditions of interest.

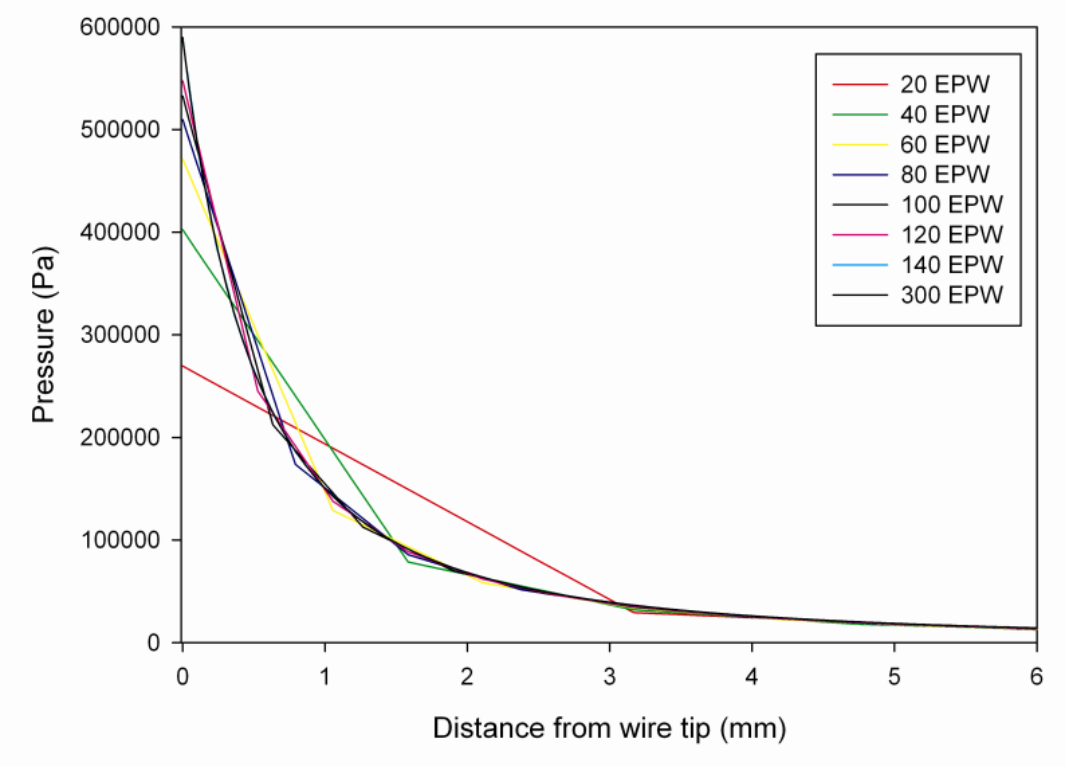

Figure 3-3 : Mesh density analysis for verification model. Pressure versus distance for a 2.0 mm diameter ball tip (amplitude of vibration of 25 µm) at 22.5 kHz and increasing EPW count (20-300 EPW).

For 20 EPW, the predicted maximum pressure at the distal tip was approximately 270 kPa, significantly lower than the distal tip pressure of approximately 600 kPa given by the analytical solution. 140 EPW were required

to closely predict the analytical pressures. These results highlight how suboptimum meshing can render models prone to errors and inaccuracies. The magnitude of the discrepancies between the Morse's analytical solution and FEA model for maximum pressures at the spherical ball tip surface can be seen in Table 3-1. It also shows that a percentage difference of approximately 2.5% can be achieved when compared with the analytical solution for an element count of 140 EPW. For increasing of the mesh density from 140 – 300 EPW a 0.5 % discrepancy exists in the difference between the FEA and the analytical solution. For the additional computational power required for increasing this mesh density, this discrepancy is agreeable.

EPW	**20**	**40**	**60**	**80**	**100**	**120**	**140**	**300**
FEA max pressure at tip (kPa)	269.5	402.2	471.1	509.5	532.6	547.2	587.0	589.5
% difference from analytical solution	53	29.7	17.7	11	7	4.5	-2.4	-2.9

Table 3-1 : Percentage difference of maximum pressure at distal tip versus pressures calculated by analytical solution (Morse [139]).

Since these devices are often used over a range of frequencies (20-50 kHz) and at distal tip amplitudes of vibration (≈ 0- 60 μm), a number of models were created using the upper range of distal tip amplitudes of vibration (40 μm), for a range of different frequencies, using the 140 EPW established from previous results. The results are shown in Figure 3-4. The purpose of this model was to examine the effects of frequency and distal tip amplitudes on the accuracy of the

model using the 140 EPW. This study also showed that 140 EPW produced pressure profiles with close agreement to the Morse analytical solution for the frequencies and distal tip displacements modelled.

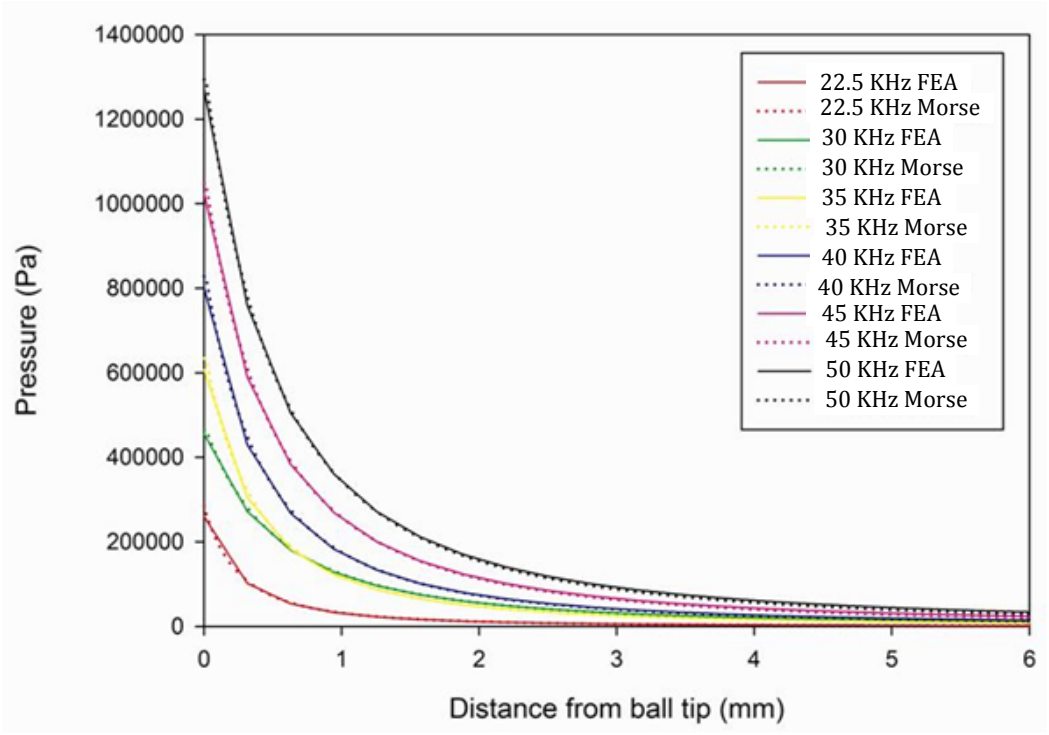

Figure 3-4 : Pressure versus distance from FEA model of 1.0 mm diameter radiused distal tip with 140 EPW and distal tip amplitudes of vibration of 40 µm for a range of frequencies vs. analytical solution (Morse [139]).

3.3.2 Model validation: *In vivo* model in a peripheral artery

Since both methods (FEA and analytical) do not account for the non-linear wave propagation of ultrasound, validation of the model was necessary. To validate the acoustic FEA for this application and to further understand the effects of the acoustic pressures during ultrasonic angioplasty, a model representative of Makin and Everbach's experimental study using a 22.5 kHz wire waveguide device is created [7], this is shown in Figure 3-5.

This is representative of a peripheral artery with an acoustic tissue-air interface typically encountered *in vivo*. Their experiment involved an ultrasonic emitter (wire waveguide, ball tipped 2.46 mm Ø) and receiver (hydrophone) submerged in a liquid glycerine/water blood acoustic analogue. The aim of this experiment was to measure the pressures over a number of distances from the vibrating wire waveguide. The pressures over this distance were then plotted. The surrounding air interface created a standing wave in the acoustic field plot.

A geometric representation of this experiment was created. The inner dimensions of the cylindrical tank which contained the liquid medium were developed by creating areas from connecting lines. The lines could then be split and meshed according to the mesh density (140 EPW). *Fluid29* elements were used for the liquid environment. These elements were assigned to have linear acoustic material properties ($c = 1580 m/s$ and $\rho = 1050 kg/m^3$). The FSI was created along the nodes where the wire waveguide and liquid meet. Again no structural elements were created to represent the wire waveguide since the displacement on the nodes of the FSI would suffice. *Fluid129* infinite acoustic boundary layer was also included in the model.

Where the previous FEA verification model focused on single fluid fields, the validation model required other complexities such as a liquid/air interface. The model incorporated liquid (blood) and air properties, geometries based on Makin and Everbach's experiment and frequency of operation. Makin and Everbach specified maximum amplitude of vibration of their wire waveguide distal tip of 65 μm at 100% power input but applied very low power inputs for their experiment. Based on similar equipment and set-ups the amplitude of vibration applied to the distal tip for the FEA is inferred to be 10% of total output ≈ 6.5 μm amplitude of vibration. These displacements were then applied to the nodes along the FSI in the y-direction.

The aim of this FEA was to examine if one could accurately predict the pressures recorded but also predict the standing wave (nodes and amplitudes) generated in Makin's experiment using linear assumptions. This would validate the mesh density study and examine whether or not ultrasound at these low acoustic intensities can be solved accurately by assuming linear acoustic relationships.

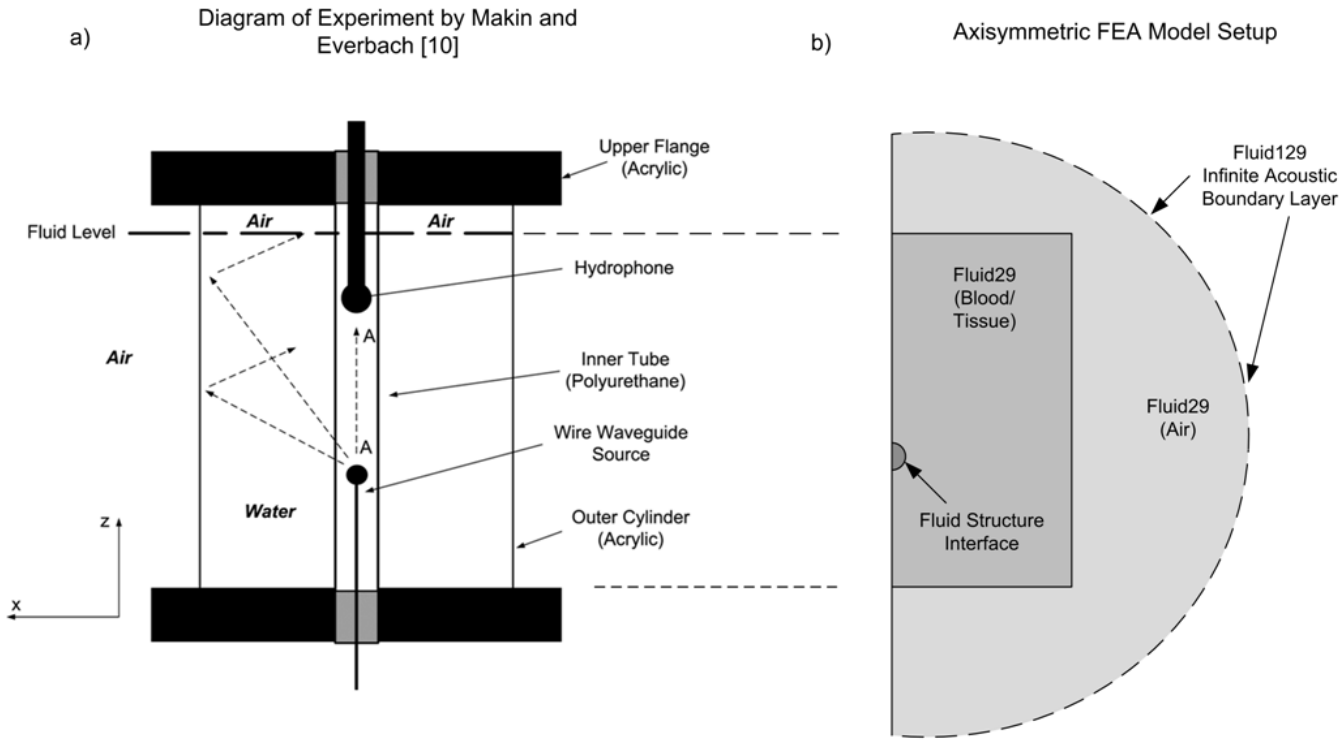

Figure 3-5 : a) Schematic of Makin and Everbach's experimental set up. b) Interpretation of the FEA acoustic model of Makin's experiment.

3.3.2.1 Model validation: *In vivo* model in a peripheral artery results

Using the mesh density of 140 EPW established by the verification model, the validation model shows a close correlation between the experimentally measured pressure data from the Makin experiment and the pressures predicted by the FEA model of this experiment. The results are plotted in Figure 3-6. The standing wave nodal locations show a very close correlation but some discrepancies exist in the pressure amplitudes. The pressure amplitude variations in the model may be due to a number of factors, including, inaccuracies of the inputted material acoustic properties (local variations) or non-linear effects.

Pressures presented here are at a distance 12 mm from the wire waveguide and are very small in comparison to the maximum pressures at the waveguide distal tip (1200 Pa Vs. 90 kPa). The largest deviation in pressure amplitude from the experimental and FEA is ≈ 400 Pa. In comparison to a model with a pressure range 0 – 90 kPa this amount of discrepancy is deemed agreeable for determining the critical pressures.

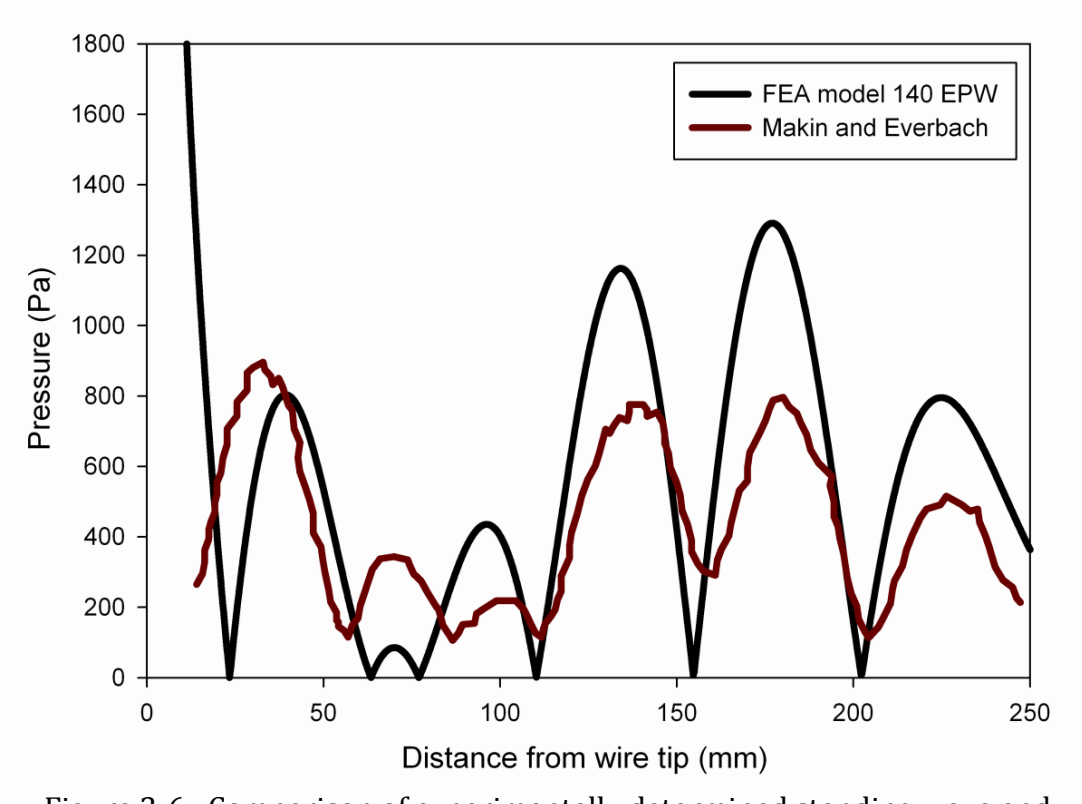

Figure 3-6 : Comparison of experimentally determined standing wave and predicted standing wave from FEA.

3.3.3 Acoustic pressure field versus waveguide parameters

Using the verified model with the appropriate mesh density, as determined from the above methodology, a number of tip geometries similar to those reported in the literature were modelled. The acoustic pressure field associated with each wire waveguide distal tip design was assessed for a range

of amplitudes of vibration based on those input settings commonly reported. The frequency of 22.5 kHz is applied to these models as this was the frequency used by Makin *et al*. The distal tip geometries modelled (diagrams included in figures) were:

i. Spherical ball tip, used for model verification
ii. Radiused tip (1.0 mm diameter)
iii. Flat tip (1.0 mm and 2.0 mm diameter)
iv. Inverted dome (1.0 mm diameter)

3.3.3.1 Acoustic pressure field versus wire waveguide distal tip geometry results

Using the verified model mesh density (i.e. 140 EPW), the pressures created by different wire waveguide distal tip geometries could now be investigated using FEA. Operating at a frequency of 22.5 kHz, the following results were achieved for the distal tip geometries modelled. Figure 3-7 shows the pressure results for the 1.0 mm radiused tip for a range of wire waveguide distal tip amplitude of vibrations (0 – 60 μm). The predicted pressures show clearly the effect that increasing distal tip displacement has on the waveguide performance. With the inclusion of a cavitation threshold relevant to the *in vivo* conditions, the onset of this critical event may be predicted. Assuming suitable gas nuclei present, according to Nyborg, cavitation is observed above pressures in the range of 0.1 – 0.2 MPa [136].

Figure 3-8 shows the predicted pressures for a 1.0 mm flat distal tip. For the 1.0 mm radiused distal tip, the maximum pressure is approximately 270 kPa (amplitudes of vibration of 60 μm). For the same amplitudes of vibration, a 1.0

mm flat distal tip produces nearly 550 kPa. The 1.0 mm inverted dome for the same amplitudes of vibration, as shown in Figure 3-9 produces nearly 1,100 kPa, an increase of close to 300% when compared to that of the 1.0 mm radiused wire for the same amplitude of vibration.

The effect of distal tip size was also assessed. For flat distal tips, doubling the diameter of the wire waveguide will have a proportionate effect on the pressure; with the 2.0 mm flat distal tip wire generating 1,100 kPa, as shown in Figure 3-10. Of interest, also, is that the wire distal tip geometry produces characteristic acoustic pressure decay profiles. Ideally, for the purpose of ablation of the diseased material directly ahead of the distal tip, it is desirable to project the maximum pressures directly ahead as opposed to latterly, where they may damage the surrounding healthy tissue. The walls of arteries may also harbour nuclei that could generate undesirable cavitation within the healthy artery wall; therefore, these pressures should be kept to a minimum.

The inverted dome results in a higher pressure distribution, with the walls of the dome acting as a barrier to the adjacent healthy artery wall where pressures are lower. Also, this shape acts to intensify the pressure by a focal mechanism. The spherical and radiused configurations display a wide dipole-like pressure distribution in all directions, spatially '*wasting*' some of the acoustic power that could be used to ablate the diseased material ahead. Any geometry, however, is limited by surgical interventional constraints, flexibility, risk of arterial perforation and, therefore, some wire waveguide distal tips may be associated with additional drawbacks.

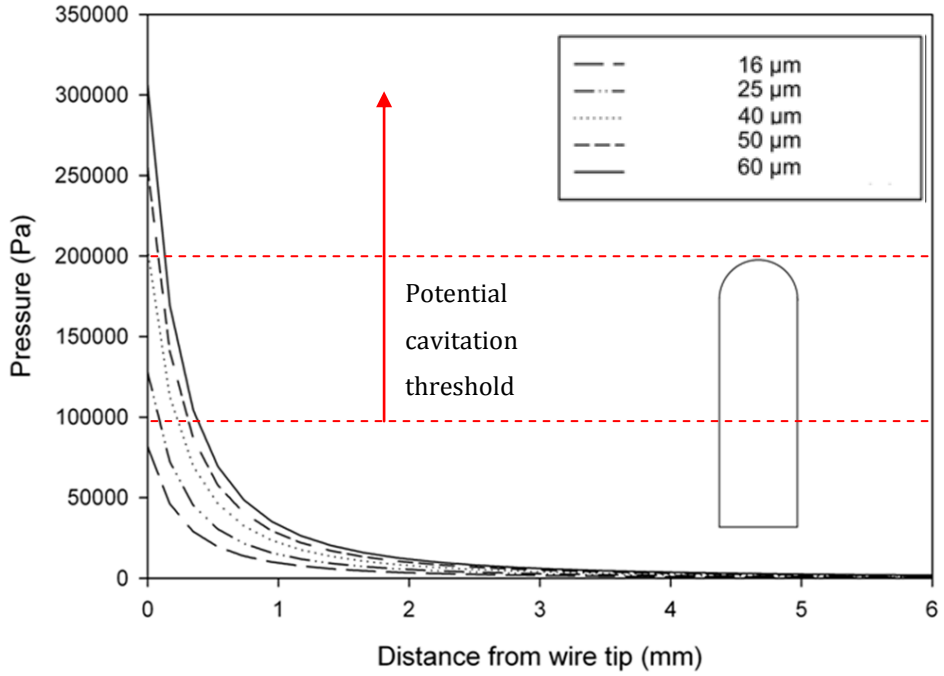

Figure 3-7 : Pressure versus distance of 1.0 mm radiused distal tip with 140 EPW at 22.5 kHz for amplitudes of vibrations 16 – 60 µm.

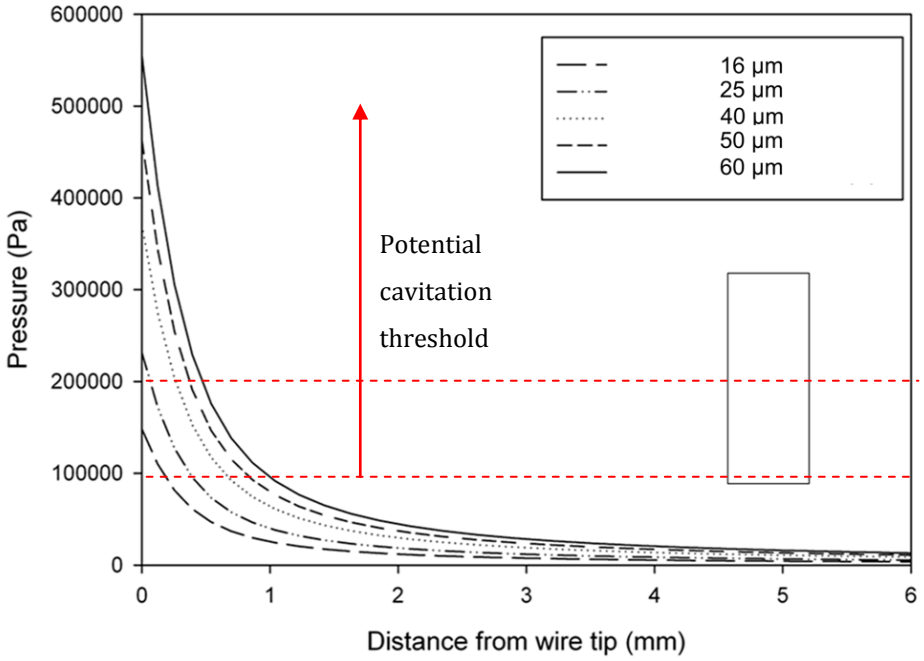

Figure 3-8 : Pressure versus distance of 1.0 mm flat distal tip with 140 EPW at 22.5 kHz for amplitudes of vibrations 16 – 60 µm.

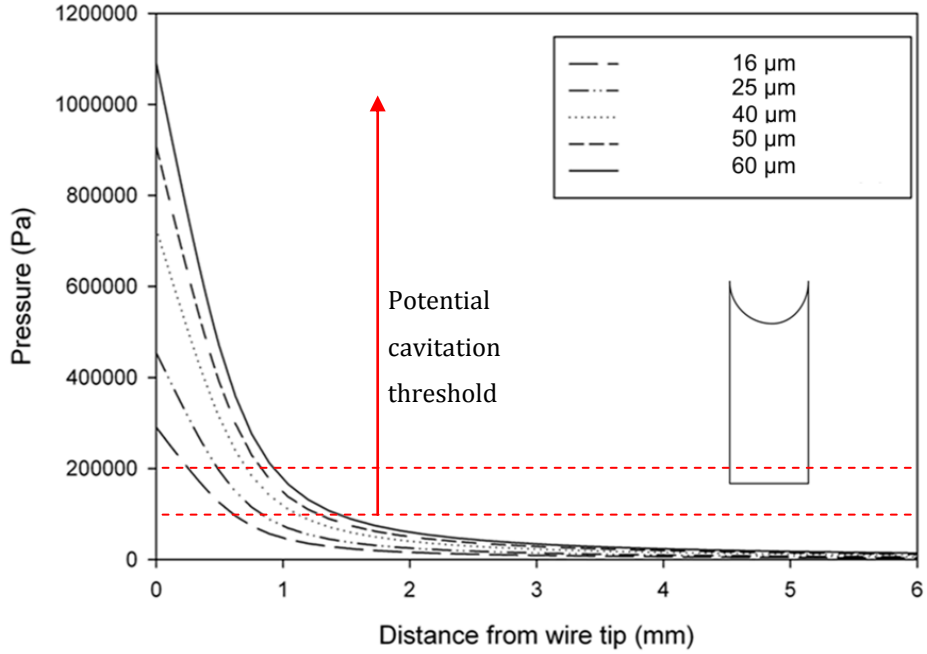

Figure 3-9 : Pressure versus distance of 1.0 mm inverted dome distal tip with 140 EPW at 22.5 kHz for amplitudes of vibrations 16 – 60 µm.

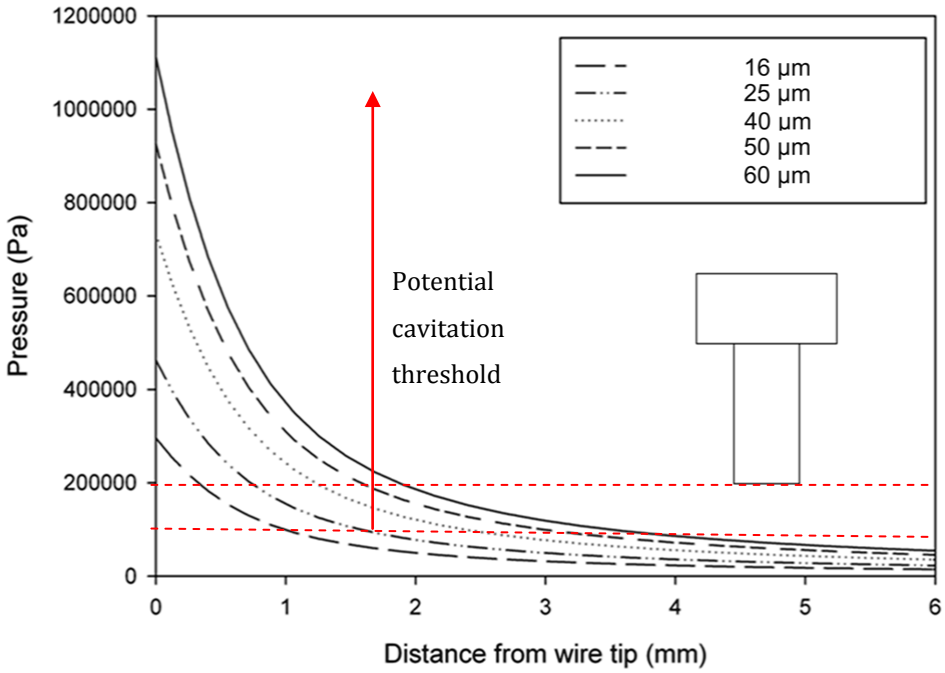

Figure 3-10 : Pressure versus distance of 2.0 mm flat distal tip with 140 EPW at 22.5 kHz for amplitudes of vibrations 16 – 60 µm.

3.4 Conclusions

A linear acoustic fluid-structure model can be used in the prediction of the pressure profiles and cavitation using ultrasonically vibrating wire waveguides. The model compared favourably with the analytical solution provided an adequate mesh density was utilised. This was determined to be approximately 140 EPW for the frequencies and amplitudes modelled here and encountered during use of these devices.

The model showed the relationship between distal tip amplitude of vibration, frequency and pressures developed. Increasing the frequency does increase the pressure substantially; however, the intensities to cause cavitation also increase. Most devices operate in the region up to 50 kHz and the EPW count was shown to be sufficient over the range. Unlike the analytical solution, the model was not restricted to simplified geometries.

The acoustic pressure results for the range of distal tips modelled showed that the geometries not only affected the distal tip surface pressure but also altered the overall acoustic profile around the distal tip, i.e. the pressure decay distance. This may play a critical role as it can be used to alleviate lateral pressures that may adversely affect healthy arterial tissue.

The model of the Makin and Everbach's experiment demonstrated that a linear acoustic modelling approach may be useful in the design of wire waveguide distal tip geometries and could be used to predict acoustic pressure profiles in relatively complex environments with tissue-air interfaces, such as the peripheral artery as demonstrated here.

The shape of the wire waveguide distal tip end-effectors plays a significant role in tissue tip interaction. Using the acoustic FEA as a design tool, the pressures created by a vibrating wire waveguide for a range of amplitudes of vibration for different distal tip geometries can be predicted. Using the cavitation threshold of 0.1 – 0.2 MPa, the wire waveguides and ultrasonic apparatus parameters which can achieve these pressures can be designed.

While a robust design methodology for predicting acoustic pressures and cavitation has been advanced, soft tissue interactions are not well understood and require careful experimental investigation. Chapter 4 introduces an ultrasonic apparatus and test rig designed to determine ultrasonic wire waveguide and tissue interaction perforation forces and heating. Tissue tests are then conducted using this apparatus and test rig.

CHAPTER

4 ULTRASONIC APPARATUS AND TEST RIG DEVELOPMENT

4.1 Introduction

An existing ultrasonic apparatus with similar operating parameters to clinical devices and other experimental ultrasonic wire waveguide devices was modified and further developed as part of this research for tissue testing. The apparatus was developed from an ultrasonic device previously used in other research by Gavin [13]. Gavin's research focused on wire waveguide mechanics. This ultrasonic apparatus was examined for its suitability in the tissue testing programme. An adaptation of this original apparatus was then developed and characterised for later use in the tissue testing programme (see Chapter 5). Some of the major changes to this original device include improved wire waveguide attachment methods and a new custom housing for additional wire waveguide support; this will be explained in further detail in Section 4.4.

This apparatus was used to study the waveguide distal tip and tissue interaction by replicating the following parameters commonly reported in the literature:

i. Operational frequency.

ii. Wire waveguide distal tip geometry.

iii. Amplitudes of vibration of wire waveguide distal tip.

The ultrasonic apparatus was incorporated into a bench top test rig. This would advance the apparatus at a specific feedrate and could measure forces and temperature rise in the tissue as the wire waveguide perforates the tissue. The test rig is also designed to accommodate a hydrophone for acoustic field pressure measurements. This system will be used then for cavitation detection. The development stages of both the ultrasonic apparatus and the test rig are shown in Figure 4-1. Existing work is shown in green; all other colours represent new work. The end objective was to have an ultrasonic apparatus and a test rig with known operational characteristics that could be used for the tissue testing programme.

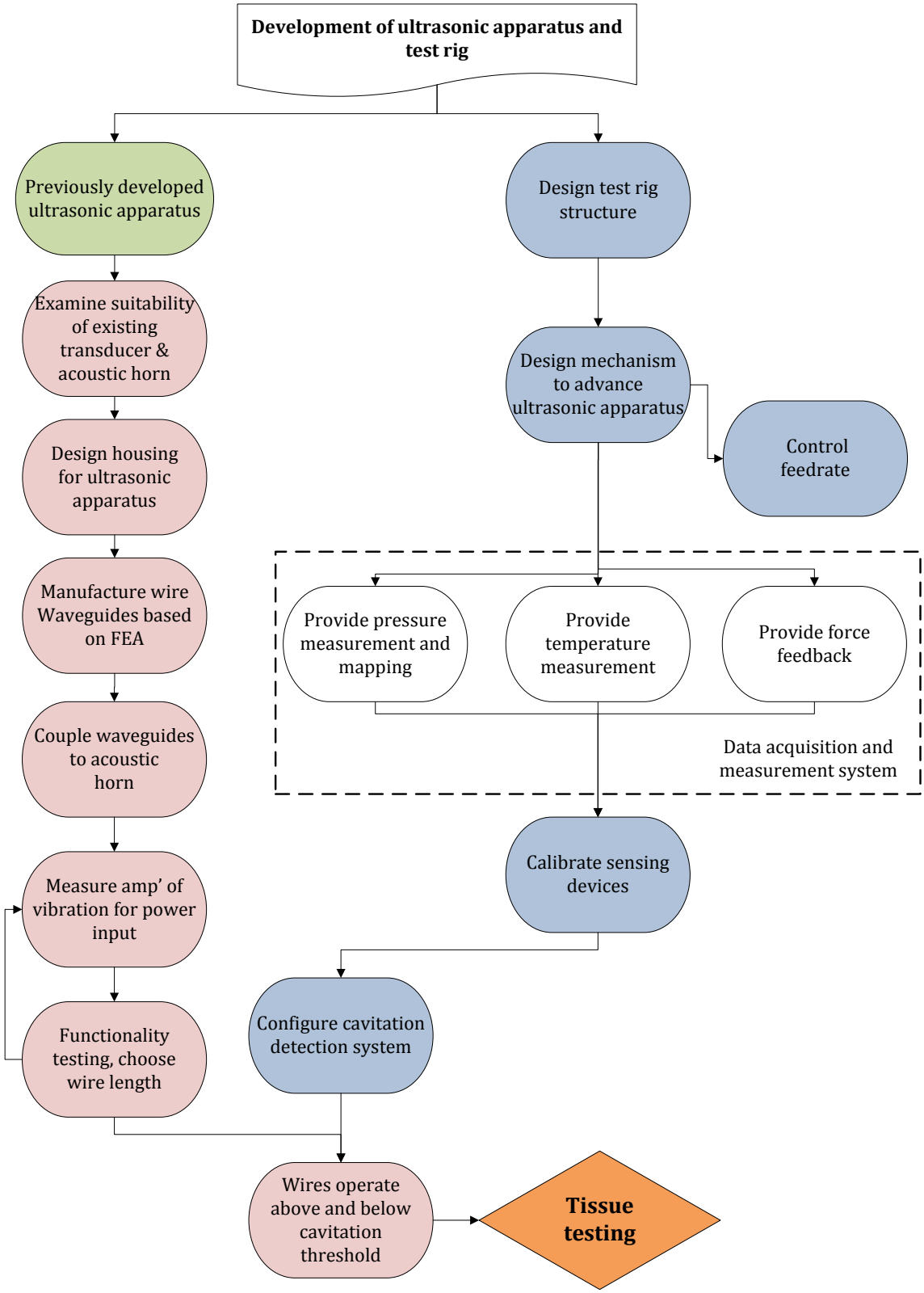

Figure 4-1: Development and design stages for ultrasonic apparatus and test rig.

4.1.1 Ultrasonic apparatus design requirements

The requirements for the ultrasonic apparatus which are to be used for tissue testing are outlined below. This was aimed to highlight key parameters required for the tissue testing but to also examine the current device for its suitability in the tissue testing programme. The requirements for the design of the ultrasonic apparatus are described in terms of functional, performance, design and operational requirements. The terms “shall”, “should” and “may” are used respectively to depict mandatory requirements, those that are to be considered but are not seen as mandatory and requirements that will be considered when all other requirements are satisfied.

	Functional requirements
F.1.	The apparatus *shall* be capable of transmitting ultrasonic frequency mechanical vibrations through wire waveguides.
F.2.	The input power settings to the transducer *shall* be variable and allow for a range of wire waveguide distal tip amplitudes of vibrations.
F.3.	The waveguides *shall* operate for a duration such that tissue testing can be performed.
F.4.	The apparatus *shall* allow for the attachment and testing of a range of wire waveguides with different wire waveguide distal tip geometries.
F.5.	The system *should* operate similar to that of the approved CROSSER™ device and other experimental ultrasonic wire waveguide devices for ultrasonic angioplasty as outlined in the literature review.

Table 4-1 : Functional requirements for ultrasonic apparatus design.

	Performance requirements
P.1.	The apparatus *shall* transmit energy at a single fixed frequency between 20- 50 kHz. *Response to F.5*
P.2.	The apparatus *should* be capable of using wire waveguides between 1.0 - 2.0 mm, both flat and round distal tips. *Response to F.5.*
P.3.	The apparatus *shall* be capable of transmitting ultrasonic mechanical vibrations to the wire waveguide distal tip for longer than 20 sec. *Response to F.3.*
P.4.	The apparatus *shall* be capable of delivering amplitudes of vibration between 0- 60 μm. *Response to F.5.*
P.5.	The wire waveguides *should* perform both above and below inertial cavitation threshold. *Response to F.3.*
P.6.	The energised apparatus (including waveguides) *should* be capable of performing no less than 100 tissue tests. *Response to F.3.*

Table 4-2 : Performance requirements for ultrasonic apparatus design.

	Design requirements
D.1.	The wire waveguides *should* be manufactured in such a way that the waveguides performance is repeatable. *Response to F.3.*
D.2.	The apparatus *may* allow for quick and easy replacement of the wire waveguide. *Response to F.4.*
D.3.	The apparatus *shall* be designed in such a way that it can be integrated to a test rig. *Response to F.3.*
D.4.	The apparatus *should* also be handheld and mobile. *Response to F.3 & F.5.*

Table 4-3 : Design requirements for ultrasonic apparatus design.

	Operational requirements
O.1.	The apparatus *shall* be safely handled by the operator. *Response to D4.*
O.2.	Activation and sonification of the apparatus *shall* not harm or damage the operator or others in close proximity.
O.3.	The cost of developing the apparatus and manufacturing multiple wire waveguides *should* be within the budget for this project.

Table 4-4 : Operational requirements for ultrasonic apparatus design.

4.2 Ultrasound generation

The ultrasonic apparatus used for this research was an adapted Branson™ Ultrasonic Sonifier model 150D™ system previously developed by Gavin and is shown in Figure 4-2. Gavin describes the selection of the sonifier for adaptation because of its operating frequency, variable power output and the system's ability to auto tune to the systems resonant frequency [13]. The system comprised of a portable generator and transducer package. This sonifier is designed to be used in chemical and biological processes to disrupt cells, homogenise or emulsify materials, disperse or mix compounds and accelerate reactions by means of ultrasonic energy transmitted via an acoustic horn. The operating frequency of the sonifier (as specified by the manufacturer) operated at the low ultrasonic frequency of 22.5 kHz (nom) [159]. The generator has an analogue dial which ranges from 1 – 10 and this is related to power output. These units are arbitrary units and the suffix "au" will be used to describe the power input settings in this document from here on.

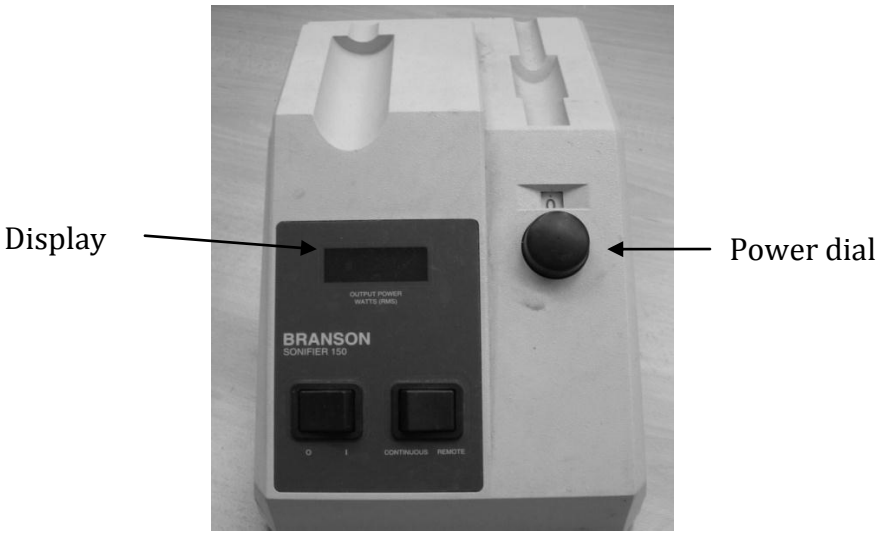

Figure 4-2 : Branson™ sonifier generator.

4.2.1.1 Sonifier (transducer)

The ultrasonic apparatus uses a piezoelectric transducer (Lead Zirconate Titanate) internal stack structure to produce longitudinal displacements. The piezoelectric effect was created by delivering a sinusoidal voltage input (950 Vrms) to the piezoelectric stack, converting electrical energy to high frequency mechanical vibrations [159]. The ultrasonic vibrations are then amplified by attaching an acoustic horn to the distal end of the transducer, as can be seen in Figure 4-3. The auto tuning function can perform a frequency sweep and find the resonant frequency of the system (converter and horn) and load (liquid environment).

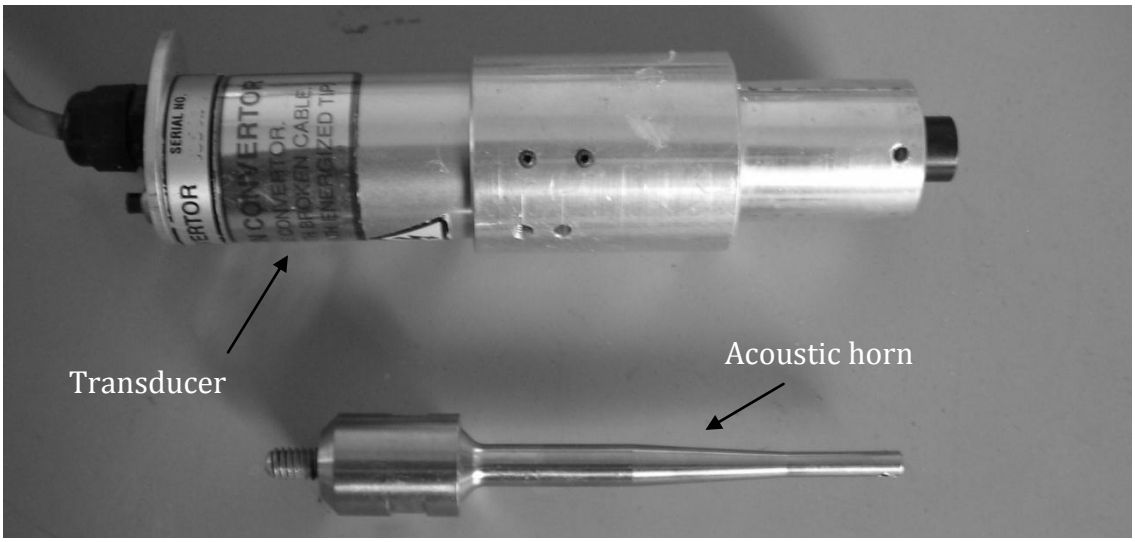

Figure 4-3 : Ultrasonic transducer and acoustic horn.

4.2.1.2 Acoustic horn

The acoustic horn, shown in Figure 4-3 above, screws into to the distal end of the ultrasonic transducer. The acoustic horn allows for amplification of the ultrasonic vibrations produced by the transducer. The output of the acoustic

horn (amplitude of vibration) will, therefore, be the input to the attached wire waveguide. Of the acoustic horns available, a Titanium alloy horn (Branson™ Microtip 5.0 mm series, pt #: 101-148-069) was most suited. This is an acoustic horn with a step and linear taper and was chosen as it has a specified maximum output amplitude of vibration of approximately 30-150 μm for setting 1 and 7 au respectively at the resonant frequency of 22.5 kHz when connected to the piezoelectric converter [160]. The acoustic horn can only be operated in a liquid environment, as the liquid acts to both cool and load the wire waveguide distal tip once energised. Operating the ultrasonic apparatus outside of a liquid environment will cause the ultrasonic apparatus to stall and may otherwise cause damage to the transducer [159].

4.2.1.3 Wire waveguide coupling to acoustic horn

Attaching a wire waveguide, essentially a mass, to the acoustic horn can affect the system's performance. The horns are finely tuned instruments, manufactured to high tolerances and altering their shape can cause the system to stall or under perform. However, with the use of short wire waveguide lengths, of relatively negligible mass, the auto tuning function of the ultrasonic transducer can still find system resonance. Short wire waveguide lengths also allowed for integration of the ultrasonic apparatus to the bench top test rig. The wire waveguides are much shorter than waveguides which are used in clinical surgery but for the investigation of the wire waveguide distal tip and tissue interaction, longer waveguides were not required, since only the amplitude of vibration was of interest.

Methods of attaching a wire waveguide to the distal end of the acoustic horn are available in the literature and in patent data sheets [13, 78, 161, 162]. Most methods rely on either a friction fit, crimp fit or heat shrunk interference fit between a female end screw and the male wire waveguide, as shown in Figure 4-4.

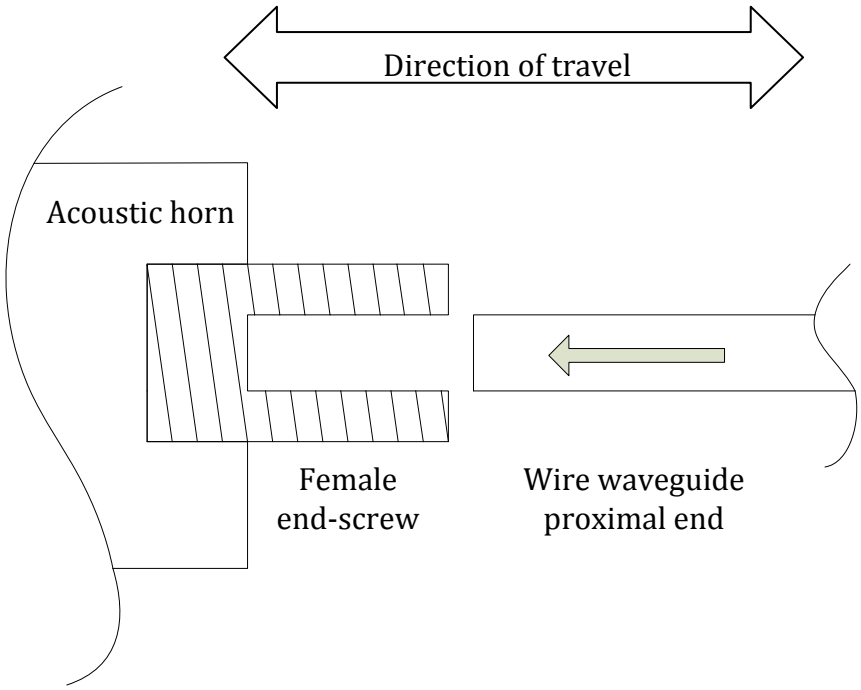

Figure 4-4 : Female end screw and wire waveguide coupling method.

The initial approach to manufacturing the wire waveguides was based on crimping the larger female screw radially around the male proximal end of the wire waveguide, as proposed by Gavin [13]. The wire waveguides were inserted approximately 6-8.0 mm into the female M3 grub screw and crimped, this was then screwed into the distal end of the acoustic horn. This technique produced low transmission success rates and short transmission periods before failure (if

the wire waveguides were successful in transmitting the ultrasonic vibrations). Failure generally occurred at the point where the wire waveguide and female screw were compressed by the crimping. The wire waveguide was still held in the female screw. However, it had snapped just as it protruded from the female screw. This may have been a result of stress concentration from damage to the wire waveguide at this point from crimping.

As part of this present work, in an effort to increase time to failure, a new wire waveguide manufacturing technique was developed. To avoid crimping the wire, a friction interference fit was employed. Testing using this method proved most satisfactory. If the interference fit was managed correctly, wires transmitted without failure for extended periods of time, ideal for tissue testing. The procedure for manufacturing the friction interference fit wire waveguides for 1.0 mm diameter wire, are as follows:

i. M3 Stainless Steel (SS) screws were placed in a radial clamp and centre drilled at high speed on a milling machine to a depth of 6-8.0 mm using a 0.95 mm jobber drill bit. These are now the female screw.

ii. Wire waveguides were cut in 200 mm length sections. The proximal end of the wire waveguides were then ground sharp, 45 degree radially, approximately 2-3.0 mm from the end.

iii. The wire waveguides were then placed vertically in a bench top vice, sharp side up, with approximately 10 mm of wire protruding.

iv. The M3 0.95 mm female screw was placed on top on the male wire waveguide, the sharp edge provided a lead in. This was then press fitted.

v. The waveguide could now be screwed into the acoustic horn using the female screw, as shown in Figure 4-5.

vi. It was found that crimping reduced contact surface area and resulted in premature failure of the wire waveguides at the crimping point. Waveguides would emit a high pitch singing moments before failure.

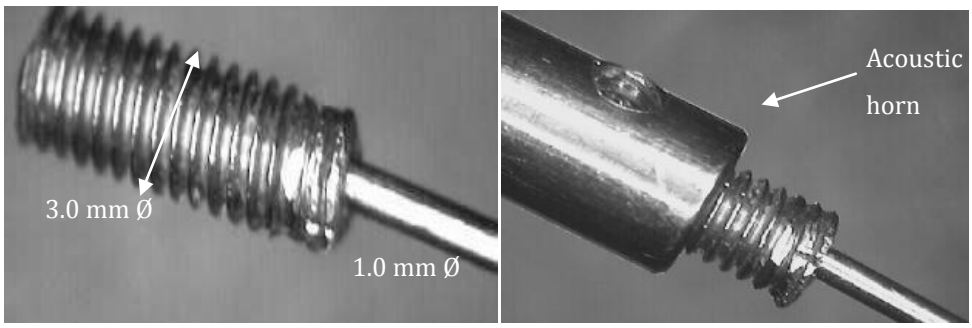

Figure 4-5 : Wire waveguide manufacture, (left) wire waveguide in M3 grub screw, (right) wire waveguide screwed into distal end of acoustic horn.

4.3 Wire waveguides design and performance

4.3.1 Materials

The medical grade surgical wire chosen for the wire waveguide material was a Nickel-Titanium (NiTi) alloy (Nitinol). This particular Nitinol alloy consists of 54.5 – 57 % Wt Nickel with balance % Wt Titanium, with some other

trace elements. It was chosen because of its super-elastic behaviour and proven success in this field as wire waveguide material [6, 13]. The wire waveguide material for tissue testing was obtained from EUROFLEX GmbH (Kaiser-Friedrich-Str. 7, D-75172 Pforzheim) in 1.0, 1.5 and 2.0 mm diameters. These wire diameters were chosen because the acoustic pressure profile for each diameter was previously established using FEA in Chapter 3.

4.3.2 Wire waveguide length

The nature of the energy transmission creates a standing wave with nodes and anti-nodes along the wire waveguide length (i.e. resonance and anti-resonance lengths)[13]. The maximum amplitudes of vibration at wire waveguide distal tip occur at a length of wire which terminates at a resonant length (i.e. the input from the acoustic horn is amplified). An anti-resonance length provides no amplification at the distal tip from the input at the acoustic horn. A schematic of the input and output of the wire waveguide is shown in Figure 4-6 [13, 163]. The resonant and anti-resonant lengths are a function of frequency and acoustic speed and can be calculated by using Equation 16.

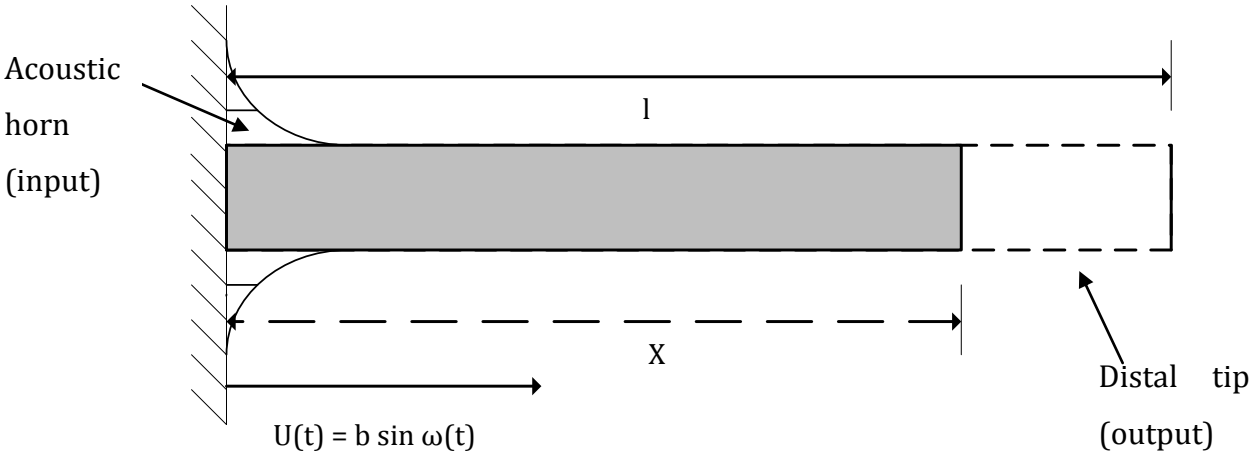

Figure 4-6: Diagram of a uniform rod, of length l, with an input displacement.

$$u(x,t) = b\left(cos\frac{\omega x}{c} + tan\frac{\omega l}{c}\ sin\frac{\omega x}{c}\right) sin\,\omega t$$ Equation 15

The resonant response of the wire waveguide can also be derived from the above solution and is shown in Equation 16. f_n denotes the resonant frequencies of longitudinal vibration for a rod of length l . The speed of sound the rod material is given by *c*.

$$f_n = \frac{nc}{4l} \quad n = 1, 3, 5 \ldots$$ Equation 16

Typically, the ultrasonic devices operate at a constant frequency. Based on this assumption, for fixed frequency transmission, the wire waveguide lengths for which resonance occurs (n = 1, 3, 5, 7….) and the lengths for which anti-resonance occurs (n = 0, 2, 4, 6, 8….) can be calculated using Equation 17.

$$l_n = \frac{nc}{4f}$$ Equation 17

Using the material properties for the wire waveguide, the acoustic speed can be determined by using Hooke's Law in Equation 18.

$$c = \sqrt{\frac{E}{\rho}}$$ Equation 18

Where E is the young's modulus of the wire material (75 GPa) and ρ is the density (6500 kg/m^3) of the medium. For the NiTi wire waveguides, c = 3396.83

m/s, therefore, the resonance lengths (n = 1, 3, 5, 7…) and anti-resonance lengths (n = 2, 4, 6, 8…) are as follows:

Node # (f = 22,500 Hz)	Position of node along wire waveguide (mm)
1	37.7
2	75.48
3	113.2
4	150.9
5	188.7
6	226.4

Table 4-5 : Wire waveguide lengths of resonance and anti-resonance.

It was necessary to use lengths of wire which could produce the required wire waveguide distal tip amplitudes of vibrations but would also be of suitable length for test rig integration and tissue tests (transmit energy for sufficient periods of time for a number of tests). The wire waveguide material fatigue strength greatly influences the maximum achievable amplitudes of vibration at the distal tip and also time to failure. The wire waveguide was prone to failure if the amplitudes of vibration were too great at the distal tip.

Initially wire waveguides of anti-resonant length of 150.9 mm were tested. Wires at this length had short periods of transmission time and failed within a matter of seconds. Wire length ± 2-3.0 mm from 150.9 mm caused system stall or intermittent transmission.

In previous work by Gavin, 144 mm wire waveguide length was used. The distal tip amplitude of vibration for power input was also characterised by Gavin for this wire waveguide length. Initial tissue tests were conducted using this length of wire waveguide but transmission and time to failure was also poor which prevented testing of large sample sizes using the same wire waveguide.

For this wire waveguide material, optimum lengths for consistent and reliable energy transmission were found to occur at lengths between resonance and anti-resonance lengths. For this apparatus and with test rig constraints, 132 mm was most suited. This length of wire waveguide was also favourable as it produced a range of amplitudes of vibration across the cavitation threshold, this will be elaborated on further in the cavitation detection section 4.8. The remaining tissue tests were, therefore, carried out using a 132 mm wire waveguide. A wire waveguide and acoustic horn can be seen in Figure 4-7.

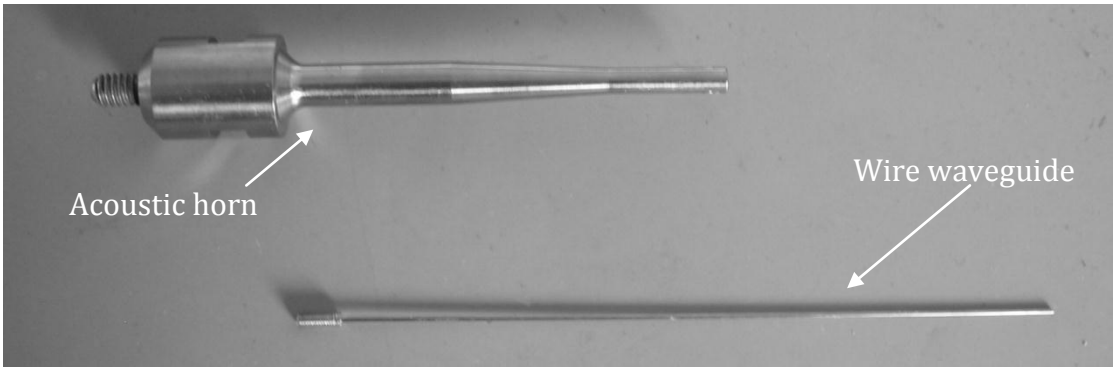

Figure 4-7 : Acoustic horn and 132 mm wire waveguide.

4.3.3 Wire waveguide distal tip

Wire waveguides for ablation and disruption of cardiovascular tissue, as described in the literature, often comprise of slender shafts which have larger distal tip finishes, such as sphere tip; they may be then supported by a catheter as shown in Figure 4-8. The objective of tissue testing was to examine the effects of the wire waveguide distal tip-tissue interaction. The wire waveguides used for tissue testing did not have a slender shaft, they replicated the wire waveguide distal tip, i.e. the shaft and distal tip diameter was constant. The wire waveguide distal tips for tissue testing were either ground flat or radiused.

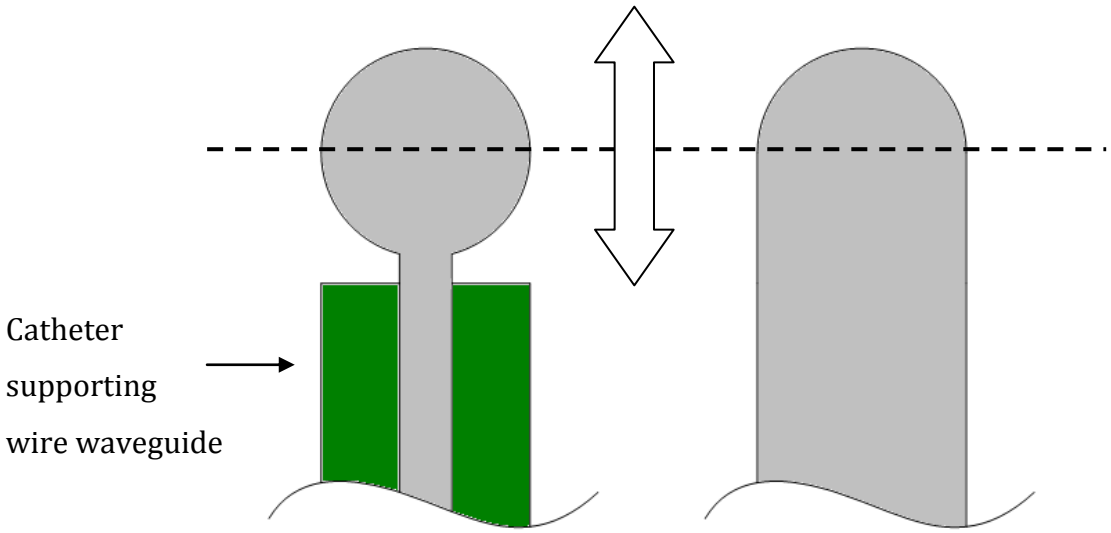

Figure 4-8 :(Left), wire waveguide in catheter with enlarged ball distal tip and slender shaft. (Right), wire waveguides used for testing representative of the enlarged ball distal tip.

4.3.3.1 Radiused

Radiused wire waveguide distal tips were machined and ground from the NiTi wires. They have the appearance of a dome tip (i.e. edges have been filleted) so they are not ground to a constant radius. To achieve this finish on the wire waveguides the following was performed. This process is illustrated in Figure 4-9 :

i. Large sand stone grinding bits (12 mm diameter) were drilled using a 1.0 mm ball nose jobber drill bit (A). This gave an internal form for the wire tip to be ground.

ii. The sand stone bit was secured in a Dremel high speed cutter. The Dremel was then held vertically in a vice.

iii. The Dremel was powered and set to maximum speed. The wires were fed into the drilled hole and the wire waveguide distal tip was ground as a result (B). The resulting distal tip finish is shown in Figure 4-10.

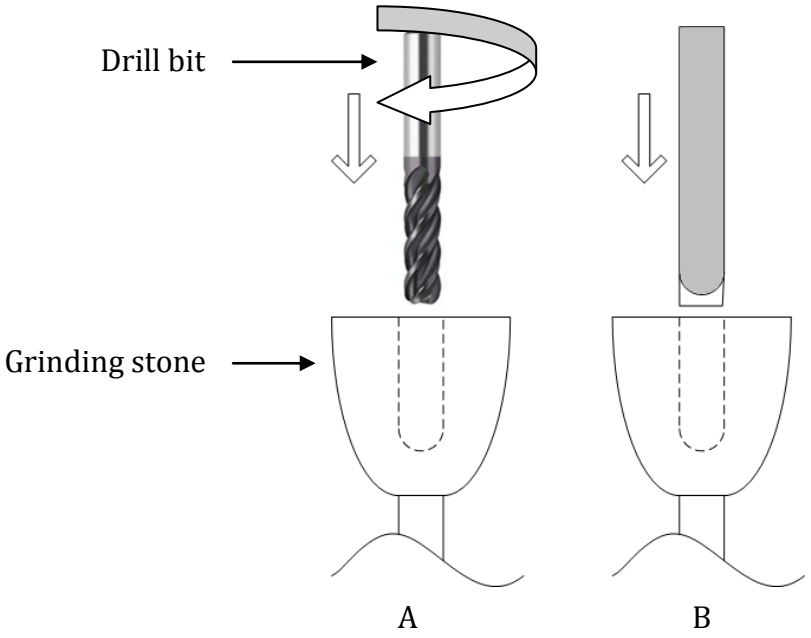

Figure 4-9 : Method for rounding wire waveguide distal tips.

Figure 4-10 : Radiused wire waveguide distal tip.

4.3.3.2 Flat

Flat wire waveguide distal tips, which were also required, were manufactured from the NiTi wire, as shown in Figure 4-11 and Figure 4-12. The wire waveguide distal tips were ground flat using a high speed rotating grinding stone. This form gave constant and highly repeatable geometries.

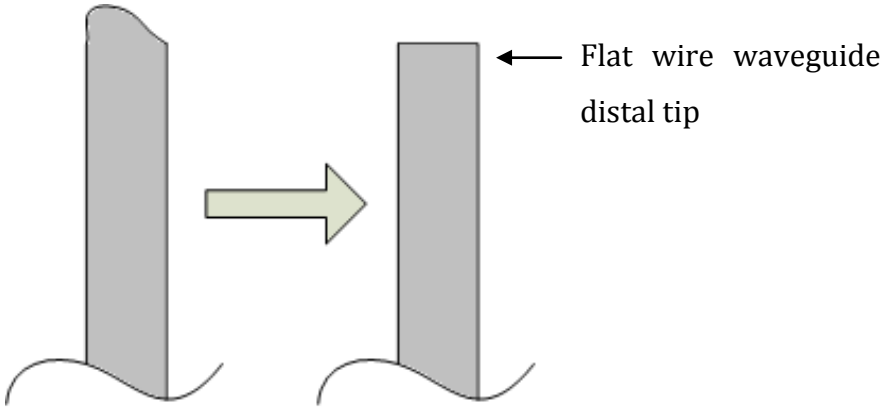

Figure 4-11 : Grinding wire waveguide distal tip flat.

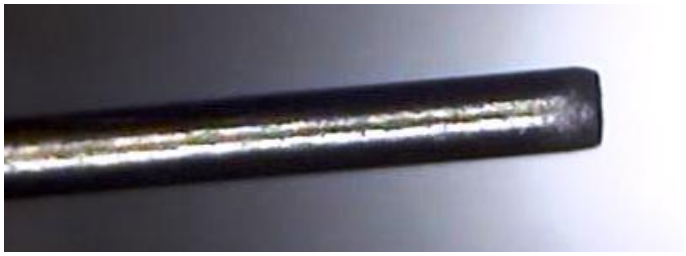

Figure 4-12 : Flat wire waveguide distal tip.

4.4 Housing for acoustic horn and wire waveguide

The housing for the ultrasonic apparatus was custom designed and built to hold the acoustic horn and transducer in a lightweight casing which protects the user from contact with the transducer and acoustic horn. It also encloses the horn in a liquid environment, essential for operation. This can be seen in Figure 4-13.

For ease of access and replacement of wire waveguides, the housing was manufactured as two split halves which could then be bolted together through holes incorporated into the design at mid section and also at the neck of the housing. One side of the housing was designed with a 1.0 mm ridge along the

inside of the shell wall. This could then be slotted into the opposite half which had a recessed 1.0 mm cut out, also seen in Figure 4-13. The housing was made from Acrylonitrile Butadiene Styrene (ABS) thermosetting plastic and manufactured on a Rapid Prototype Machine (RPM) creating a Fused Deposition Model (FDM). This was designed on SolidEdge CAD package and an STL file format was created which could be transferred to the RPM. The RPM finished product is a porous material. Since this is to contain a liquid, a sealer was impregnated into the plastic. This was then coated with polyester glass fibre filler (Isopon), formed and painted.

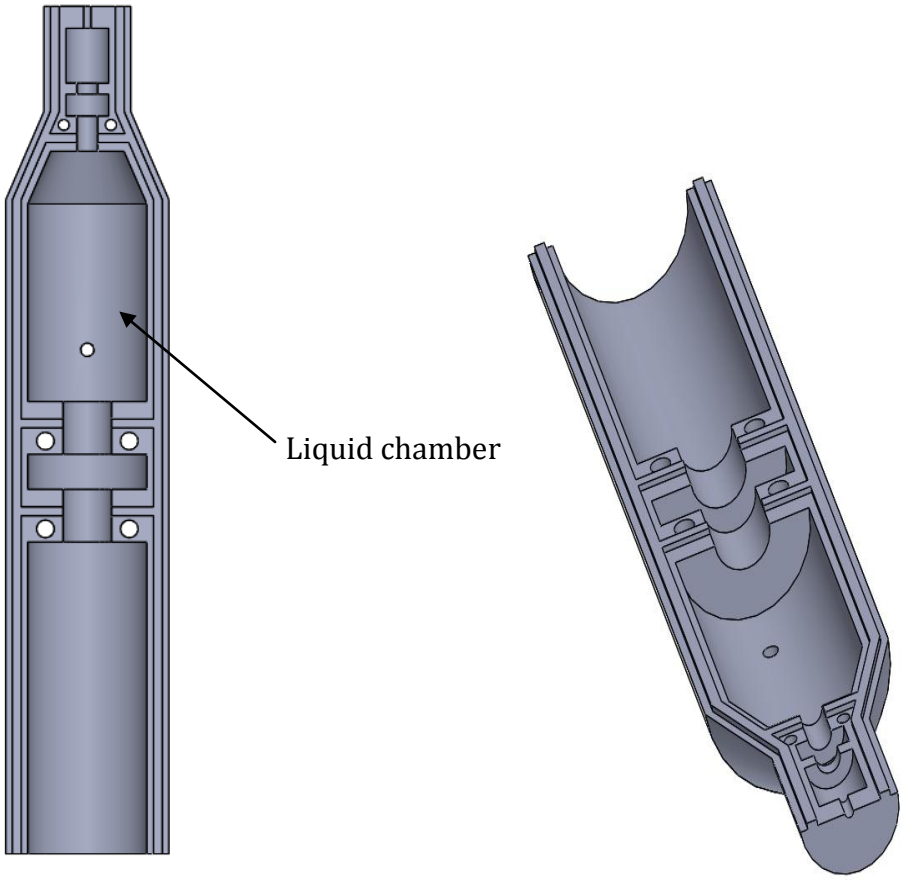

Figure 4-13 : ABS apparatus housing manufactured by RPM.

4.4.1 Assembly

The wire waveguides are screwed into the acoustic horn, which then exit the housing through a number of seals, as seen in Figure 4-14. A seal was installed on the acoustic horn where it enters the sealed liquid chamber. Another two seals were installed at the opposite end of the housing where the wire waveguides protrude. The seals act to reduce leakages at the point of protrusion but also act to support the wire waveguide at a number of points along its length, reducing lateral movement and increasing the time to failure of the wire waveguides. Larger wire waveguides may also be accommodated in this ultrasonic apparatus by increasing the internal seal diameter in the housing. If necessary, one can also accommodate a medical grade catheter at the ultrasonic housing tip by attaching it to the female connector lure located at the distal section of the housing where the wire waveguide emerges as seen in Figure 4-15.

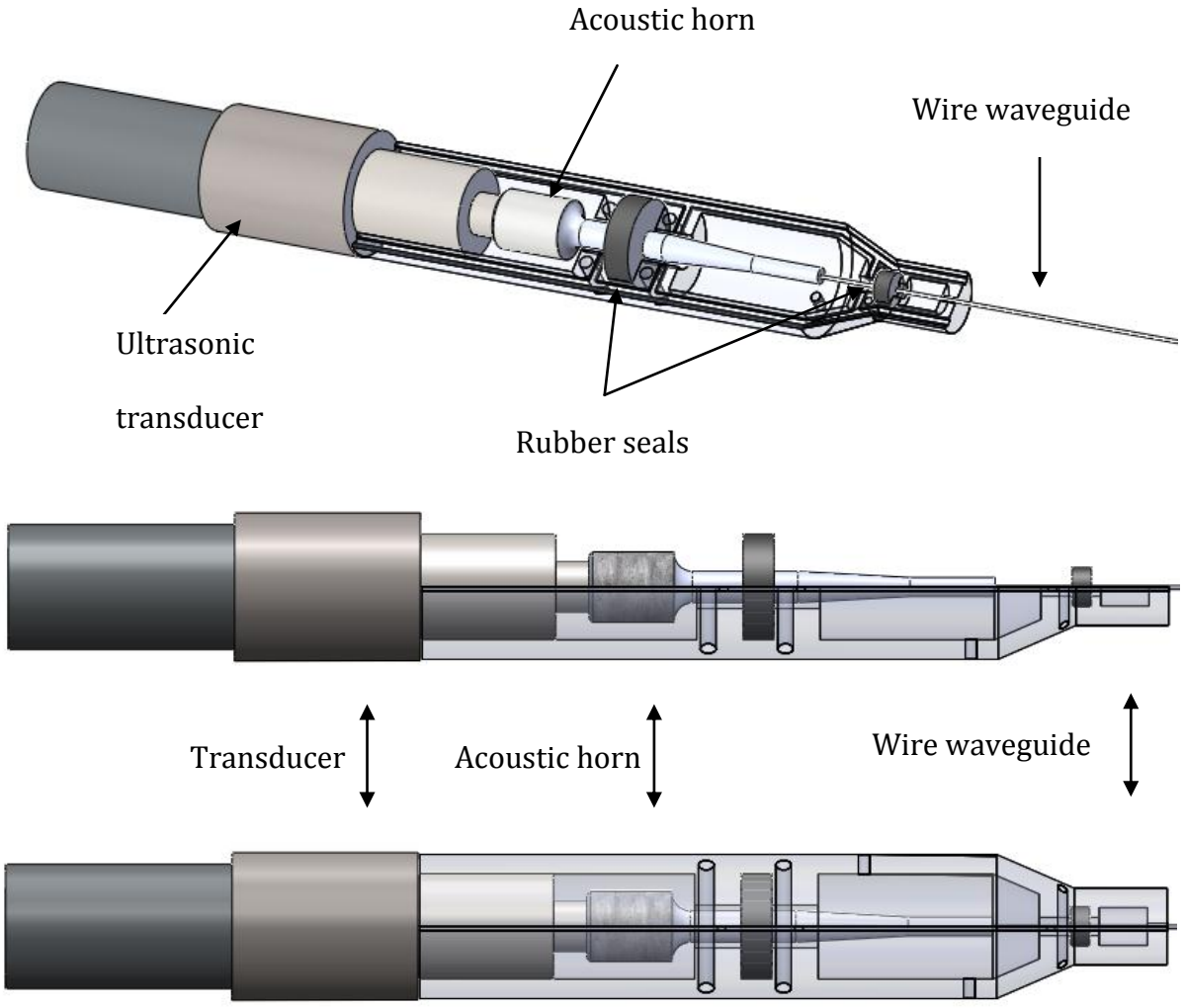

Figure 4-14 : Assembled housing and ultrasonic apparatus.

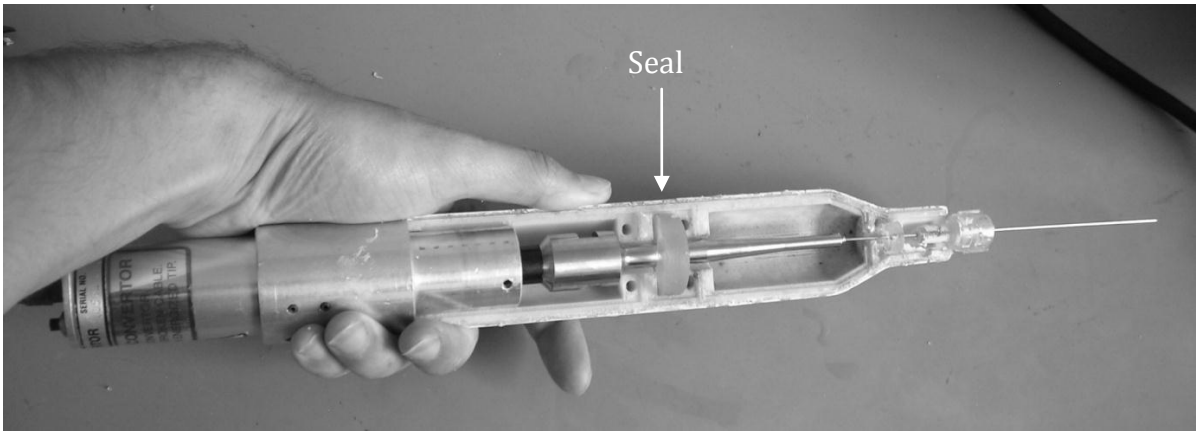

Figure 4-15 : Assembled ultrasonic apparatus (section view).

4.5 Test rig design

A test rig was designed and manufactured to advance the ultrasonic apparatus towards tissue samples and to control and measure a number of parameters. The design requirements for the test rig are also described in terms of functional, performance, design and operational requirements.

4.5.1 Test rig requirements

	Functional requirements
F.1.	The test rig *shall* allow for tissue testing using the ultrasonic apparatus.
F.2.	The test rig *shall* be capable of advancing the ultrasonic apparatus towards tissue samples in a controlled manner.
F.3.	The test rig *shall* have a thermostatic liquid tank incorporated
F.4.	The test rig *shall* provide force feedback of the tissue perforation.
F.5.	The test rig *shall* provide temperature measurement of the tissue when it is perforated by the ultrasonic wire waveguide.
F.6	The test rig *shall* incorporate a miniature hydrophone which is capable of detecting cavitation.
F7.	The test rig *shall* accommodate all sensing devices simultaneously and be interfaced and controlled using a Data Acquisition (DAq) system and CPU.

Table 4-6 : Functional requirements for test rig design.

	Performance requirements
P.1.	The test rig *should* be capable to performing over 200 tissue tests (energised and non-energised, i.e. no ultrasound). *Response to F.1.*
P.2.	The test rig *should* be capable of advancing the ultrasonic apparatus at feedrates between 0- 100 mm/min. *Response to F.2.*
P.3.	The test rig *shall* be able to advance the ultrasonic apparatus in the Z-axis, moving up and down, with a stroke length of 200 mm. *Response to F.2.*
P.4.	Thermostatic tank *shall* maintain the liquid environment at the core human body temperature of 37 ^{o}C ± 0.5. *Response to F.3.*
P.5.	The force feedback *shall* be capable of measuring up to 15 N ± 0.01. *Response to F.4.*
P.6.	The force feedback *should* be capable of measuring at a sample rate of 1k. *Response to F.4.*
P.7.	Thermocouple *should* be sensitive to 0.1 ^{o}C. *Response to F.5.*
P.8.	The hydrophone *shall* be capable of operating at a minimum frequency of 50 kHz. *Response to F.6.*

Table 4-7 : Performance requirements for test rig design.

	Design requirements
D.1	The ultrasonic apparatus *should* be held vertically (z-axis) in a bench top frame which masses no more than 20 Kg and is less than 1.5 m in height.
D.2.	The test rig *should* allow for quick and easy access to changing the attached ultrasonic apparatus. *Response to F.1.*
D.3.	The thermostatic tank *shall* fit beneath the ultrasonic apparatus and be capable of accommodating all sensing devices. *Response to F.7.*
D.4.	The test rig *should* allow for easy filling/draining and removal of thermostatic tank.
D.5.	The tissue sample holder cantilever beam *should* be capable of holding soft tissue samples in thickness no greater than 6.0 mm. *Response to F.4.*
D.6.	The cantilever tissue holder *may* be designed so that the tissue can be interchanged quickly between tests.
D.7.	The tissue sample holder cantilever beam *shall* accommodate a thermocouple which can take measurements less than 3.5 mm from the wire waveguide point of entry to the tissue. *Response to F.2, F.4 and F.5.*
D.9.	The hydrophone *shall* be capable of operation in a liquid tank at 37 ^{0}C. An armature *should* hold the hydrophone and place it in the tank orthogonally at a fixed position relative to the wire waveguide. *Response to F.6.*
D.10.	The Data Acquisition (DAq) system *shall* allow for multiple sensing devices to be operated simultaneously. *Response to F.7.*

Table 4-8 : Design requirements for test rig design.

	Operational requirements
O.1.	The test rig *should* be designed to be mobilised and carried by one person.
O.2.	It *shall* be possible for one operator to safely handle all parts of assembly and conduct tissue testing using the test rig. *Response to D5.*
O.3.	Activation and sonification of the apparatus *shall* not harm or damage the operator.
O.4.	The electronics and CPU *should* be safely situated so that water from the tank cannot make contact.
0.5.	The cost of manufacturing the test rig *shall* fall within the budget for this project.

Table 4-9 : Operational requirements for test rig design.

4.5.2 Experimental test rig

A schematic of the test rig is shown in Figure 4-16. The main design features include, accommodation of the ultrasonic apparatus to a vertical motorised lead screw assembly and a tissue sample holder capable of measuring the forces generated by an advancing ultrasonically energised wire waveguide. The rig was also extended to include hydrophone pressure measurement and temperature measurement. This assembly, including sensors were designed to be held in liquid at $\approx 37\ ^{0}$C.

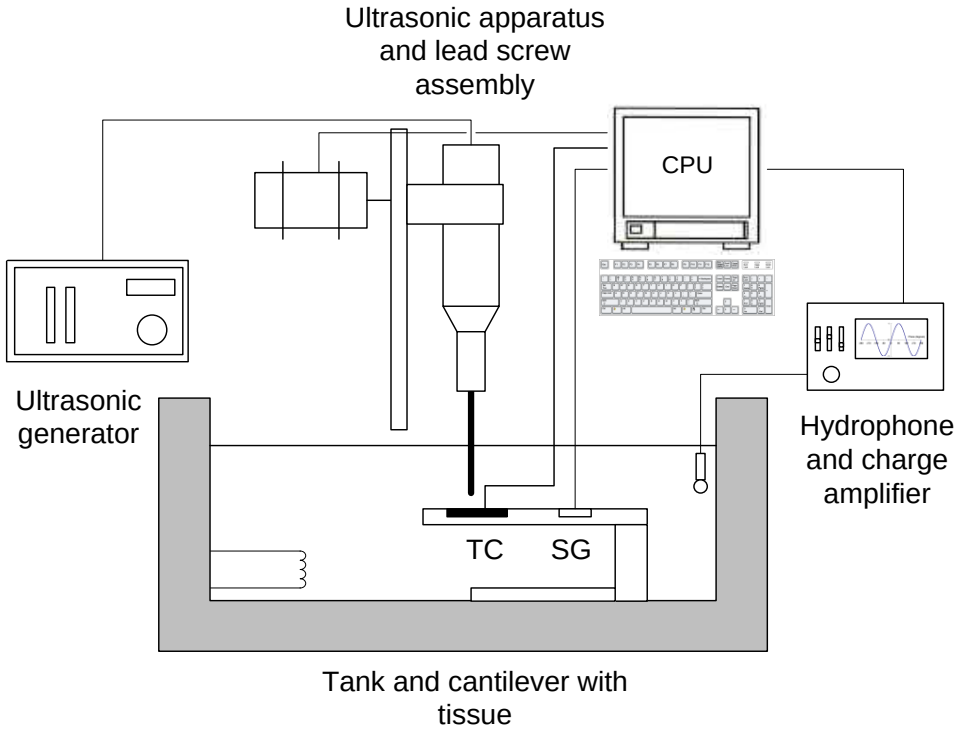

Figure 4-16 : Schematic of experimental rig with ultrasonic angioplasty apparatus, cantilever arrangement, strain gauge (SG), thermocouple (TC) thermostatic tank and DAq system.

4.5.2.1 Primary structure and lead screw assembly

The primary structure of the test rig was manufactured from extruded aluminium sections (ITEM). This is shown in Figure 4-17. The ultrasonic apparatus was attached to a linear lead screw system located vertically in the centre of the test rig structure. This was driven by a high torque stepper motor located above the lead screw assembly, behind the blue electronics box, which housed the stepper motor driver board (Uni-polar stepper driver board, 2 A, Greenwich Instruments Ltd, Kent, UK).

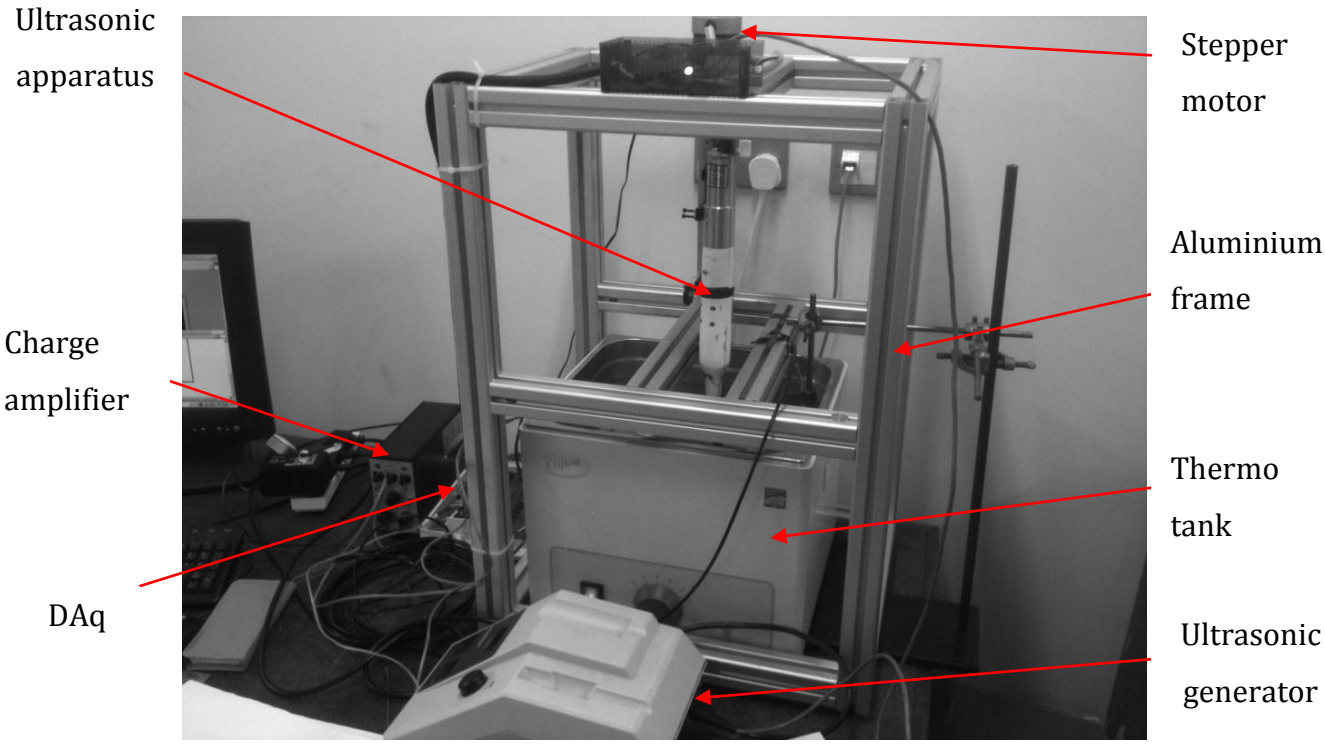

Figure 4-17 : Experimental test rig with ultrasonic apparatus attached.

4.5.2.2 Lead screw motor and thermostatic tank

A high torque motor (Hybrid stepping motor, 440-458, Radionics Ltd) with a step angle of 1.8^0 ±5 % was used. The speed of the motor was controlled by an adjustable onboard clock installed on the motor driver board. A flexible coupling from the stepper motor was used to drive the lead screw, as seen in Figure 4-18 . The pitch of the lead screw was such that one revolution gave 1.0 mm of travel. A pulse counter from the stepper motor drive card (one pulse per 1.8^0) was used to determine the distance travelled of the lead screw. This system was found to be capable of travelling between feedrates of 10 - 140 mm/min. The rig also incorporated a stainless steel thermostatic tank (Clifton 1000 Watt, model NE1B-14), with internal dimensions of 325 x 300 x 150 mm.

This tank was filled with tap water and saline. The temperature was held at 37^0C, this was found to be accurate to ± 0.2^0C. This tank would allow for the submersion of tissue samples and a strain-based force measurement sensor during tissue testing.

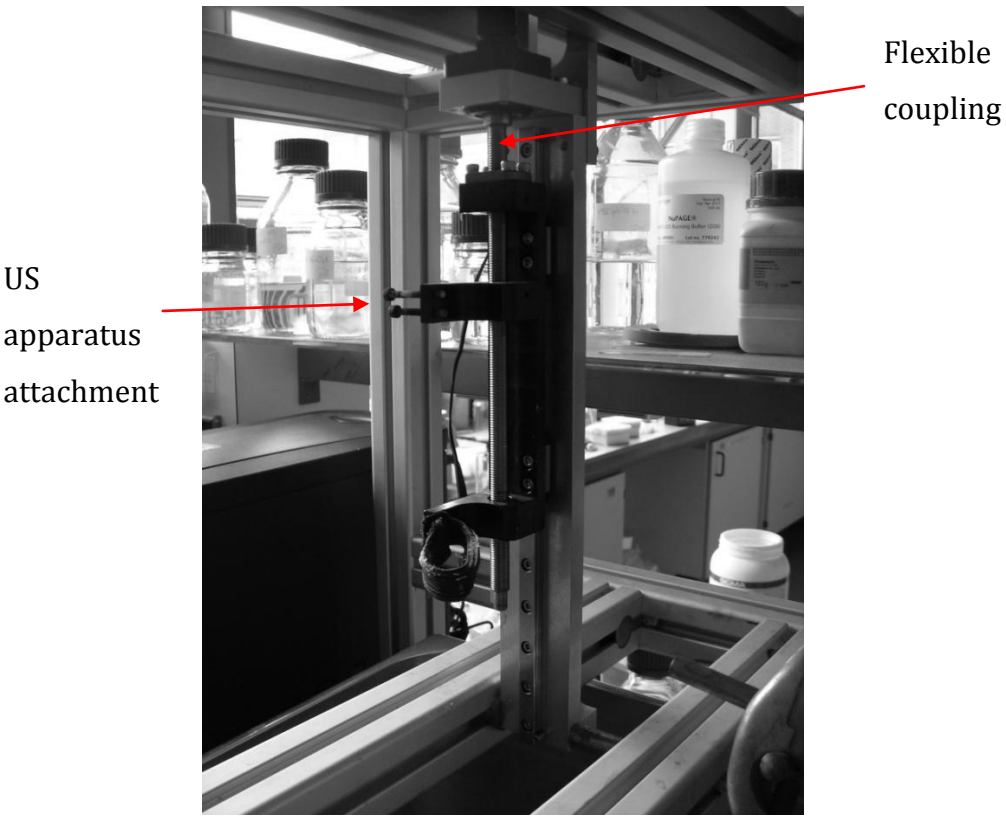

Figure 4-18 : Linear lead screw.

4.5.2.3 Cantilever tissue sample holder

The cantilever beam force measurement device was designed to hold tissue samples for testing. The beam had two plates which are bolted to the top and bottom of the cantilever. The lower plate contains the tissue in a guide slot (approximately 1.5 mm deep), as seen in Figure 4-19 (top).

The lower plate also includes a 3.0 mm diameter hole to allow for the wire waveguide to fully perforate the tissue. The upper plate which bolts to the top of

the cantilever beam supports the thermocouple, it also has a pilot hole for the wire waveguide to enter. This can be seen in Figure 4-19 (bottom left and right) also.

The cantilever beam assembly included strain gauges (KFG N10C2, Kyowa Electronic Instruments, Co, Ltd, Japan) and was calibrated to provide force feedback. A half-bridge temperature compensation strain gauge arrangement was used. This arrangement was then sealed using epoxy resin (Araldite, Huntsman Advanced Materials, USA).

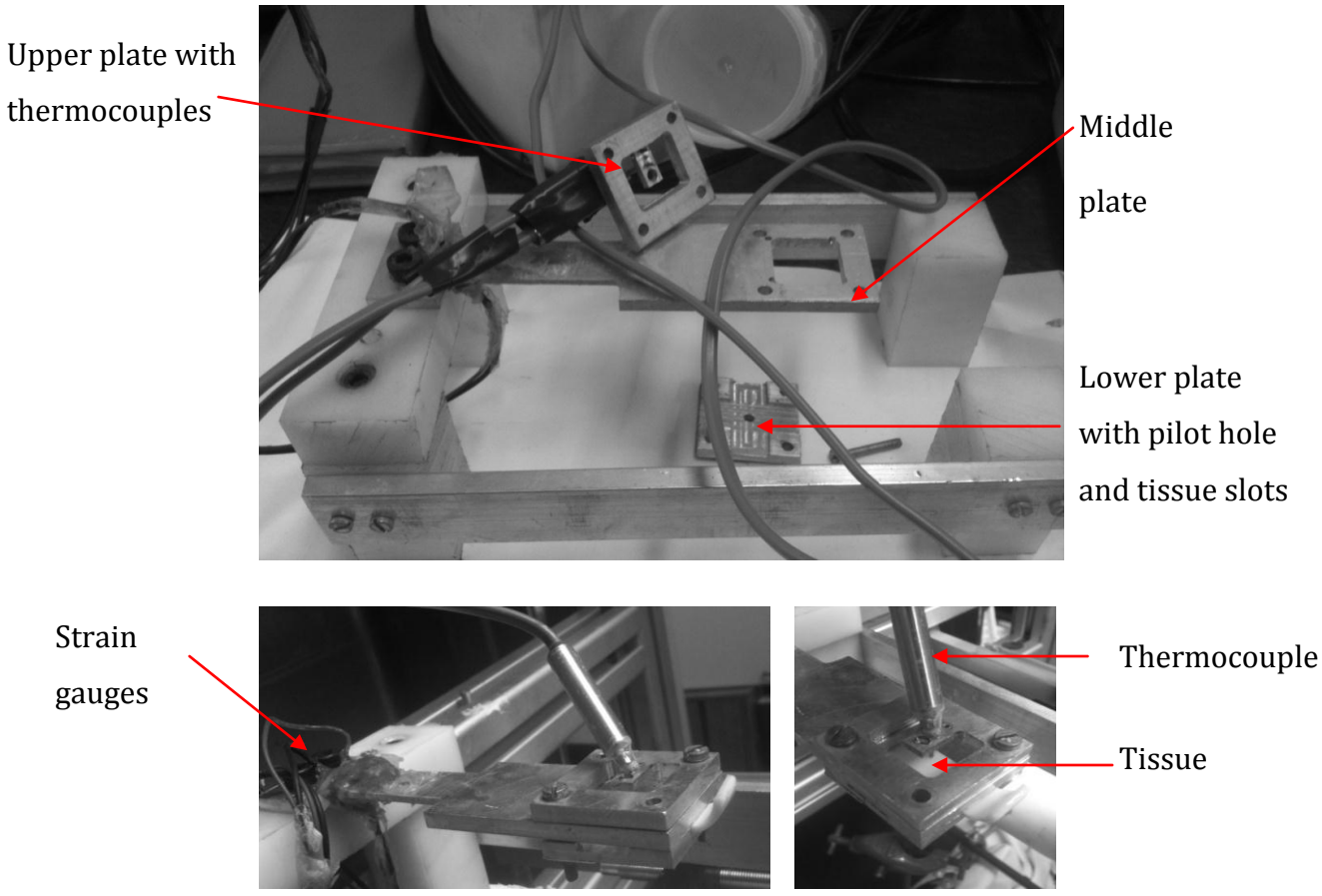

Figure 4-19 : Picture of cantilever beam tissue holder and strain gauge arrangement.

4.5.2.4 Calibration

Weights (masses) of known values were placed at the end of the beam where the tissue samples were to be held and tested. The strain reading (change in electrical resistance) for the range of weights could then be graphed and a constant conversion scale factor could be extrapolated. This factor was applied to all strain measurements to give force output. The gauge was then tested in the heated thermostatic tank to ensure that effects of temperature and buoyancy did not skew results. During calibration, the beam deflection, δ_{beam}, was determined via the force-deflection equation for the beam. i.e., for a given force, the beam deflection could be measured using a dial gauge, as shown in Figure 4-20. The force-deflection relationship proved to be approximately linear over the force range of interest (linear fit, $R^2 = 0.99$). This test was conducted six times (n = 6) and a mean linear fit of $y = 2.505x$ was recorded for forces of 0 - 10 N. The values are plotted in Figure 4-21.

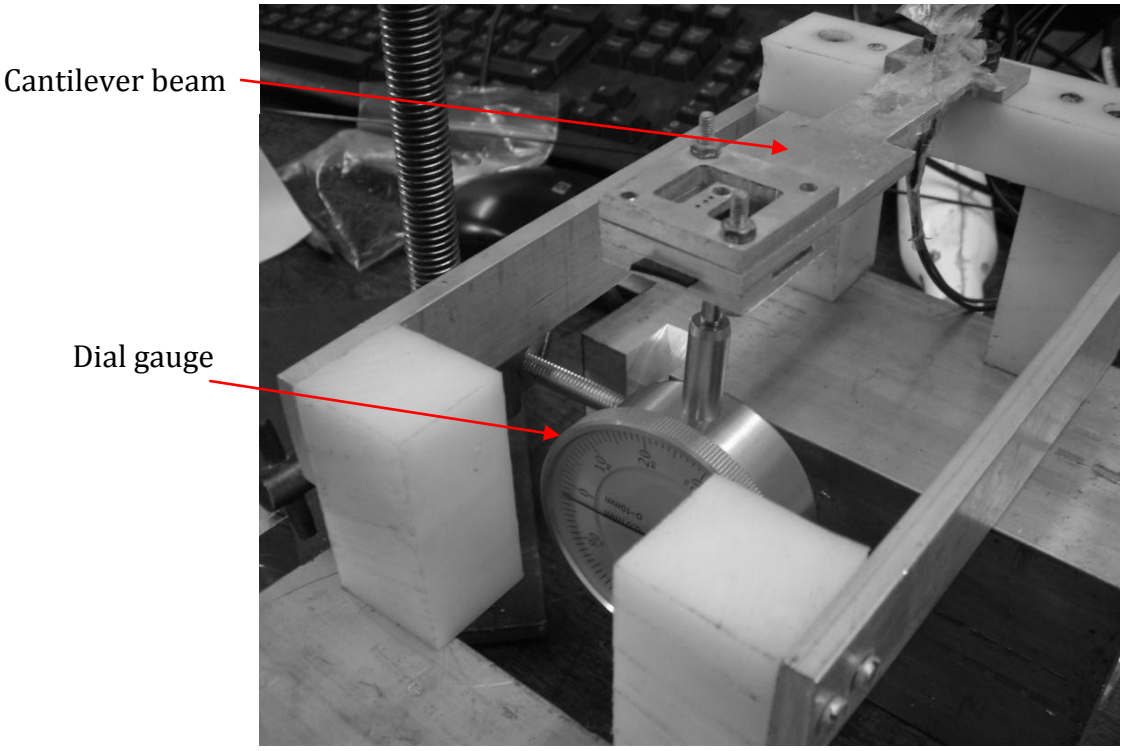

Figure 4-20 : Beam deflection measurement using dial gauge.

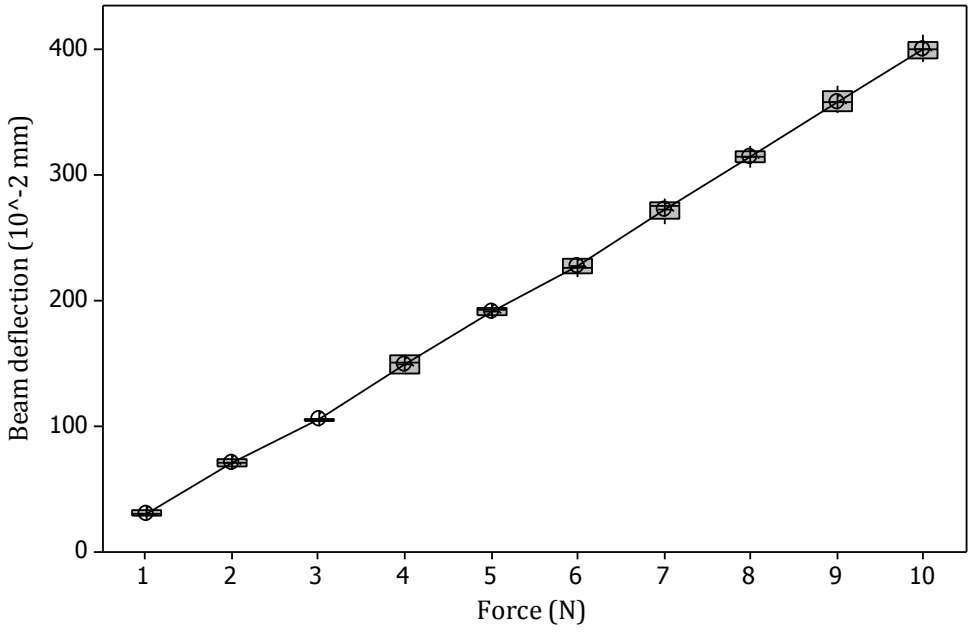

Figure 4-21 : Cantilever beam deflection versus force.

4.5.2.5 Mechanics of the cantilever tissue holder measurements

This dynamic system was designed to represent *in vivo* conditions, where the vessel would be allowed to extend somewhat before perforation. The cantilever beam essentially acts as a spring which produces an equal and opposite force acting against the wire waveguide as it perforates the tissue.

Results from the force measurement can be plotted as force versus time, however, by using the waveguide travel, δ_{tip} can also be calculated by converting time to distance using the constant feedrate (mm/min). By relating the force (or drop in force) to a deflection distance of the beam (mm), it was also possible to subtract the beam deflection from the distance travelled to give the wire waveguide indentation into the tissue, δ_i as seen in Figure 4-22. This provides more information than a static load cell system alone. Each time the tissue partially fails this has to be accounted for, as it results in a drop in applied force on the tissue and hence the beam, as shown in Figure 4-22. The wire waveguide indentation into tissue, δ_i, is given in Equation 19. Indeed, an additional benefit of this arrangement is the detection and quantifying of tissue failure depth in multiple stage tissue failure, as shown in Figure 4-23.

$$\delta_i = \delta_{tip} - \delta_{beam} - \sum\delta_{fail} \qquad \text{Equation 19}$$

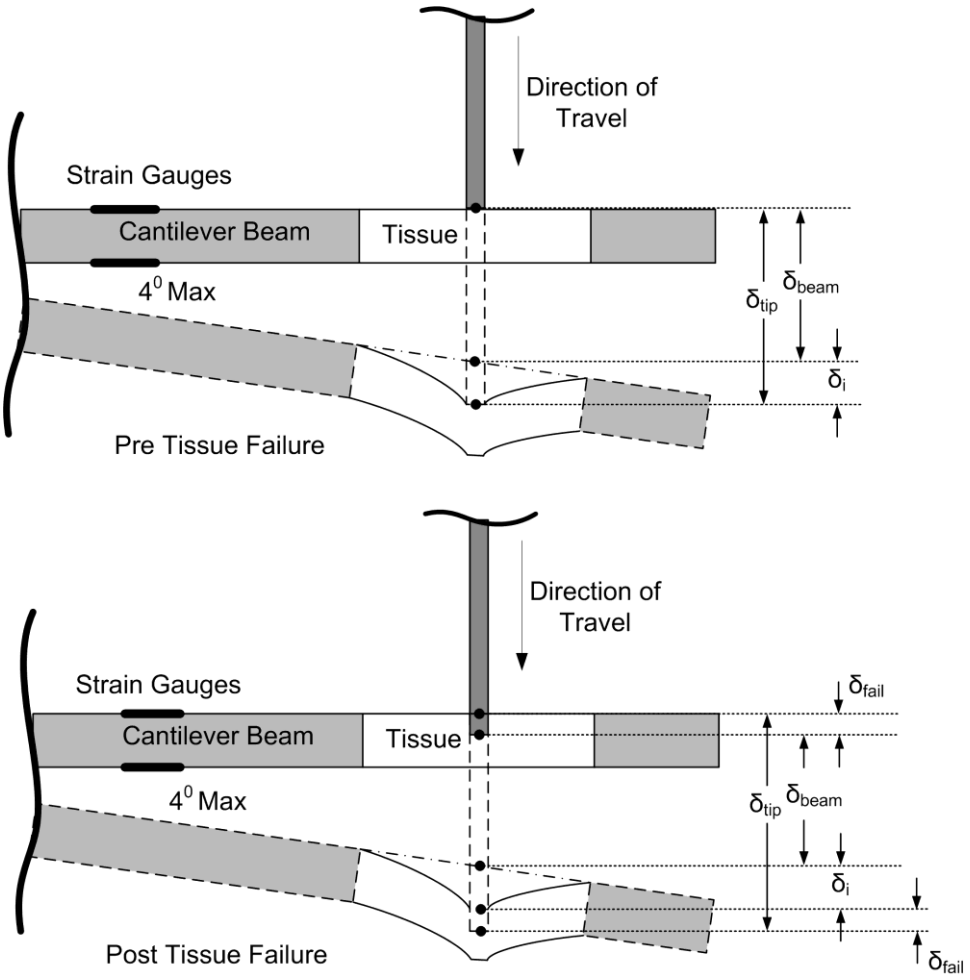

Figure 4-22 : Close up diagram of cantilever beam and tissue with displacement references. Note: the beam deflection in the diagram is exaggerated for visual purposes and does not exceed 4 degrees in practice.

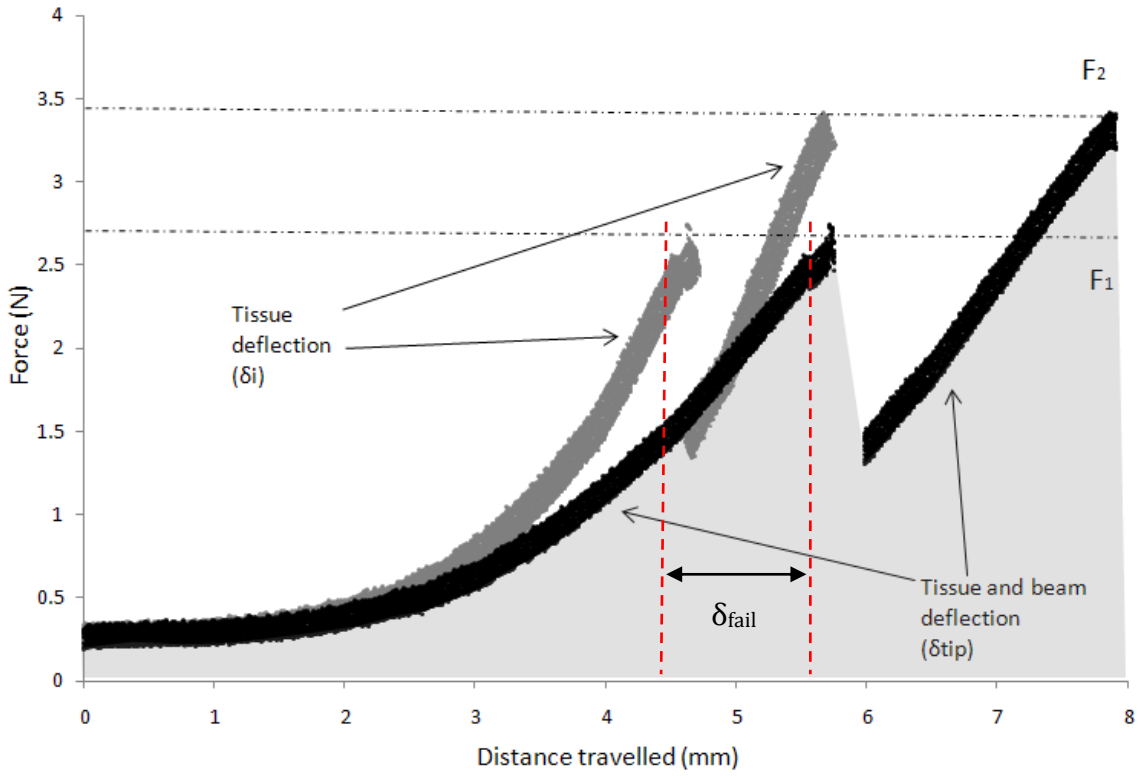

Figure 4-23 : Acquiring tissue deflection with respect to beam from tissue and beam deflection measurement, example of a two stage tissue failure. Tissue failure depth also illustrated.

4.5.3 Temperature measurement

The cantilever beam tissue holder allowed for the placement of two thermocouples close to the point of entry of the wire waveguide. They could be located 3.0 mm (centre to centre) from the pilot hole for the wire waveguide, and then placed 2.0 mm apart, as seen in Figure 4-24. A rapid response pot sealed 1.0 mm diameter, custom made K-Type mineral insulated thermocouple was used (TC Direct, Uxbridge, UK).

The Data Acquisition (DAq) system and thermocouple module has an onboard thermistor for cold-junction compensation for self calibration of the thermocouple. The thermocouples were also calibrated using the ice water technique outlined in ASTM E220-86 [164], to verify the cold junction accuracy.

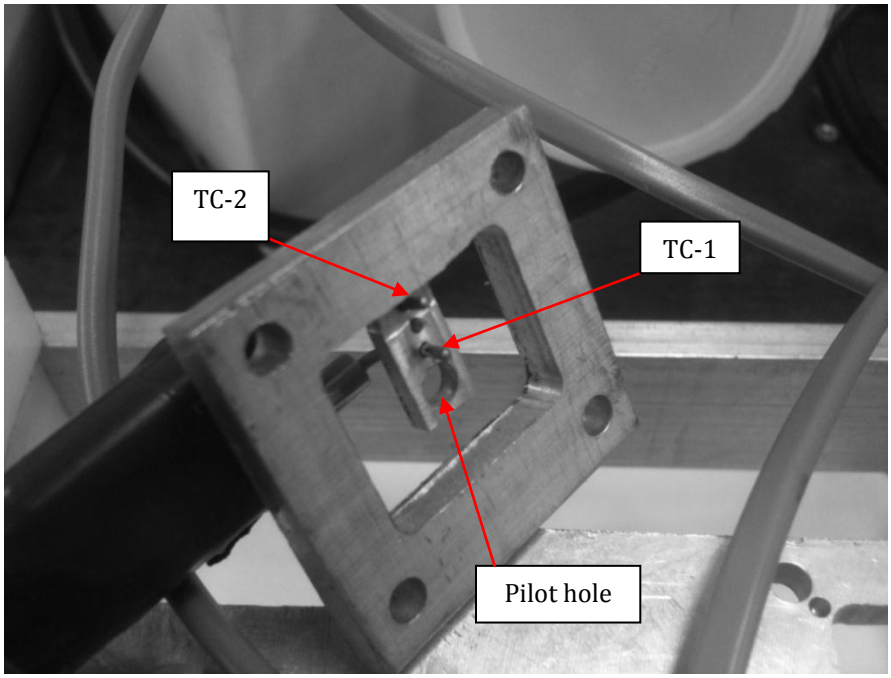

Figure 4-24 : Cantilever top plate with two thermocouples.

4.5.4 Hydrophone acoustic measurement system

The tank was fitted with a miniature hydrophone (Model B/200, Neptune Sonar Limited, Kelk Lake, East Yorkshire, United Kingdom, 9.0 mm diameter, unfocused), as seen in Figure 4-25. This hydrophone has a flat response up to 180 kHz and a resonant frequency of 240 kHz. The acoustic pressures generated by the vibrating wire waveguide distal tip in an open tank were measured using the hydrophone and charge amplifier (Brüel & Kjær, Charge amplifier Type 2635).

The charge conditioning amplifier (Brüel & Kjær, Charge amplifier Type 2635) was used to amplify the voltage signal from the hydrophone. This performs a time integration of the electric current, thus measuring the total electric charge, this was calibrated to 1 Pa = 1 mV. This voltage signal was then transmitted to an analogue port on the Data Acquisition (DAq) system for measurement. Sound and Vibration tool kit (National Instruments) was used to process and display the data, the sampling rate was 80 kHz.

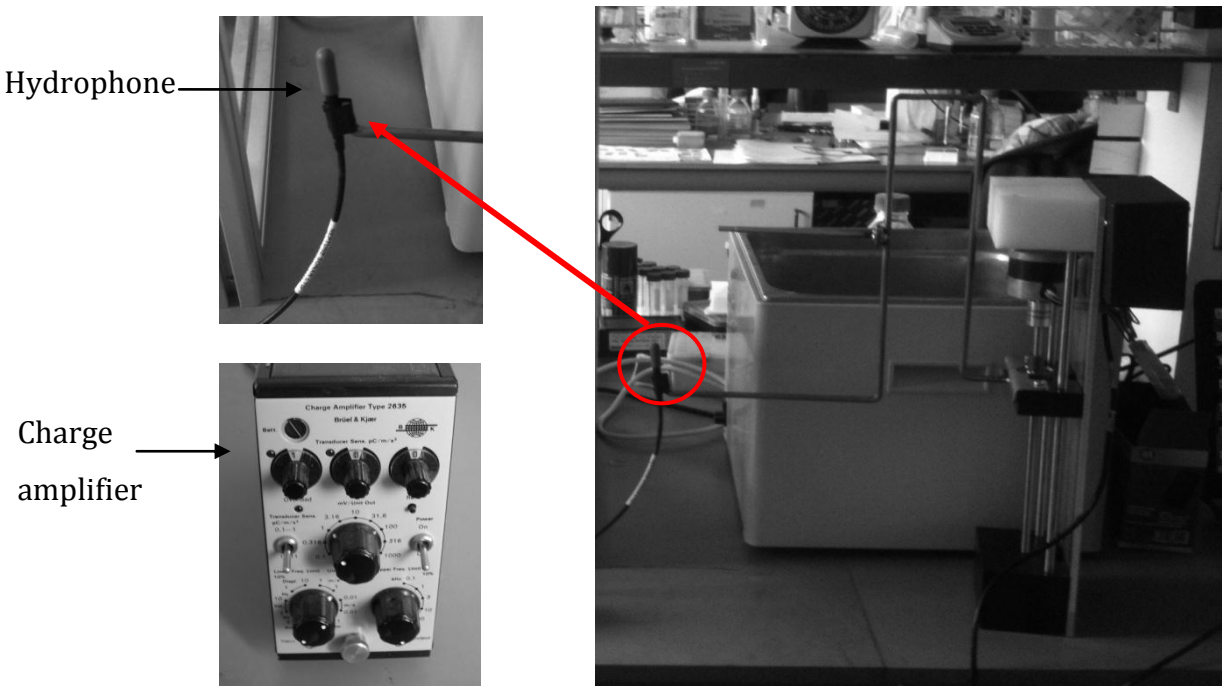

Figure 4-25 : (Bottom left) Charge amplifier. (Top left and right). Hydrophone and hydrophone assembly.

4.5.5 Data acquisition

The programming environment and hardware used to control the various instruments and Data Acquisition (DAq) was LabVIEW and National Instruments© PCI-6221 acquisition board and connector terminal block SCC-68. A Graphic User Interface (GUI) was created to allow easy control and measurement of all devices on the DAq system. The stepper motor was controlled using a driver board. Switching and control was performed using a LabVIEW function. The feedrate of the ultrasonic device, force feedback of the tissue-wire waveguide interaction and temperature increase in the tissue could be controlled and displayed on the monitor through LabVIEW. A screen shot of this graphical interface is shown in Figure 4-26. For strain measurement, a strain gauge module from National Instruments was used. This was module SCC-SG03 (half-bridge). Each channel of the SCC-SG module includes an instrumentation amplifier, a 1.6 kHz low-pass filter, and a potentiometer for bridge-offset nulling. Each SCC-SG module also includes a single 2.5 V excitation source.

Thermocouple modules (SCC-TC01) for temperature measurements could also be placed into the DAq. It also includes a 2 Hz low-pass noise filter and instrumentation amplifier with a gain of 100. The input circuitry of the SCC-TC01 modules also includes high-impedance bias resistors for open-thermocouple detection, as well as handling both floating and ground-referenced thermocouples.

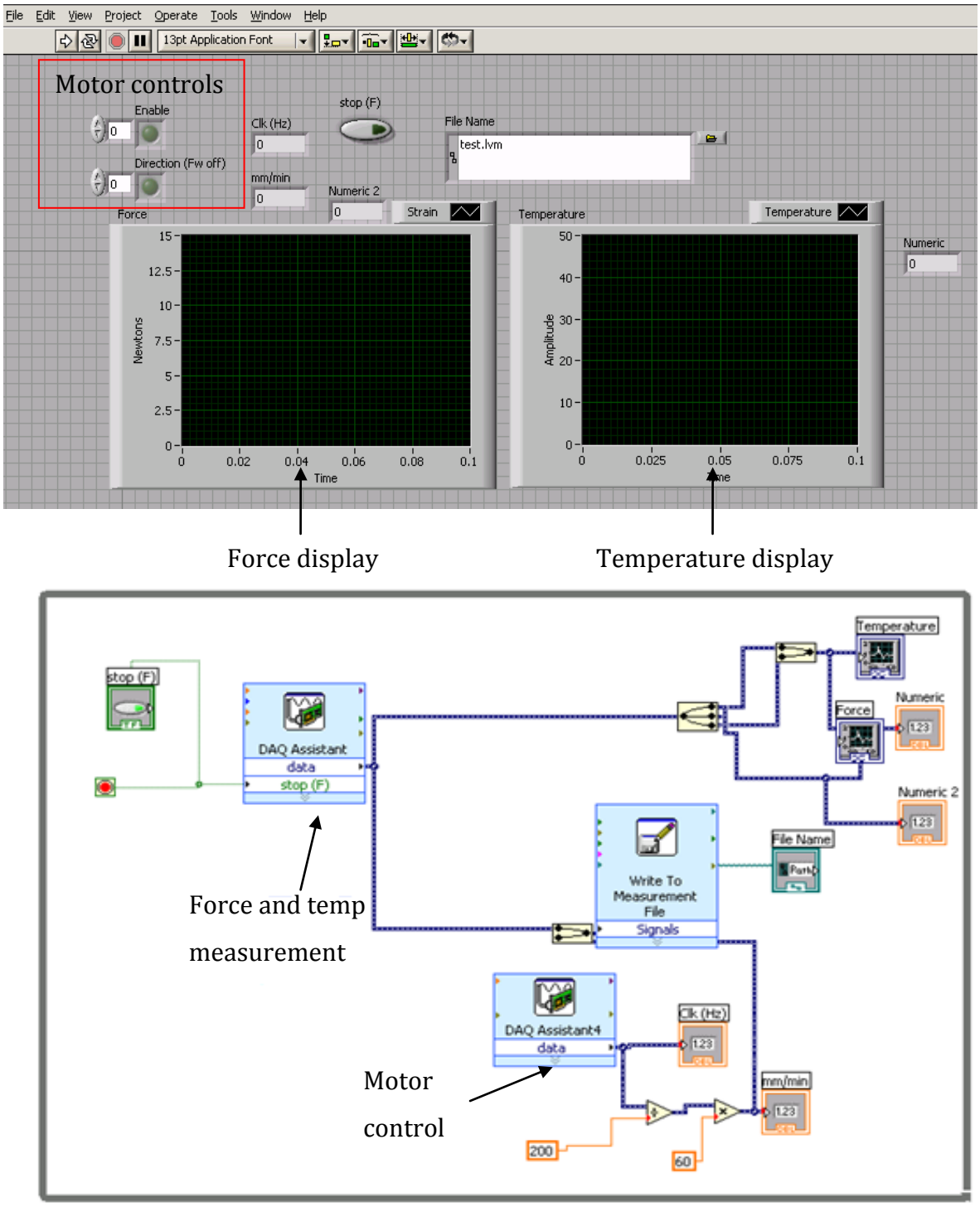

Figure 4-26 : (Top) GUI for DAq. (Bottom) Wiring diagram.

4.6 Characterisation of ultrasonic apparatus

4.6.1 Waveguide amplitude of vibration for power input

To ensure that the wire waveguide manufacturing technique and the seals in the housing did not affect the performance of the waveguides, characterisation of the waveguide distal tip amplitude of vibration for power input was carried out. The wire waveguide distal tip amplitudes of vibration were measured using an optical microscope and camera (Olympus BX60M, frame rate <90) and vision analysis software (Infinity Analyze). The high frequency vibration (22.5 kHz) is seen as a streak (maxima and minima) on the vision software. Measuring the distance between these two points gave the peak to peak displacement (i.e. amplitude of vibration x 2). It was also possible to measure streaks created by visible artefacts on the wire waveguide as datum points. A schematic representation of this measurement is shown below in Figure 4-27.

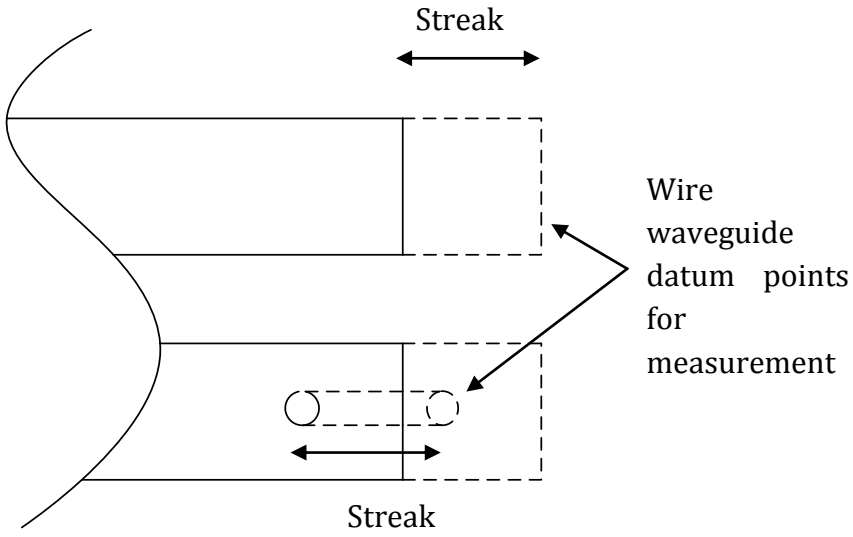

Figure 4-27: (Top) Maxima and minima at wire waveguide distal tip, (Bottom) artefact datum point creating a streak.

4.6.2 Methodology

For this test, the apparatus was held horizontally as shown in Figure 4-28. Visco-elastic foam was placed under the wire to stabilise the wire waveguide, thus making the optical measurements possible. The power input for settings 1-8 au were tested and the resulting wire waveguide distal tip displacements were measured. Using multiple 132 mm wires, no less than six tests (n = 6) were carried out for each power setting. Power settings greater than 5 au often resulted in premature failure of the wire waveguides, in that, the amplitudes of vibration were too great for the material to withstand.

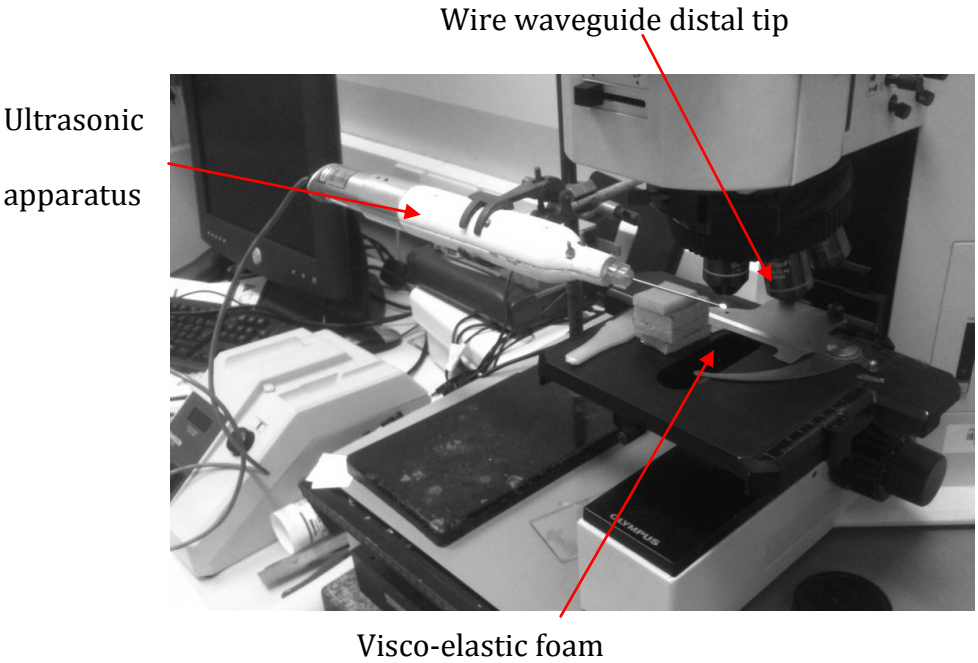

Figure 4-28 : Experimental set-up for characterisation of power input for wire waveguide distal tip amplitude of vibration.

4.6.3 Results

An image of the stationary wire waveguide distal tip is shown in Figure 4-29. A number of datum points which appear as distinct white dots are identified. The energised wire is shown in Figure 4-30. The points on the wire now appear as streaks which can be measured using the image analysis software. The results are plotted Figure 4-31. The acoustic intensity is also calculated and given in Table 4-10. The results display an approximate linear relationship in terms of input/output (i.e. power input/amplitude of vibration). Settings above 5 au are excluded from these results as they were deemed too unstable for tissue testing. From setting 0-1 au no power is transmitted and it was often the case that setting 1 au produced intermittent transmission. For tissue testing, setting 1 au was also excluded.

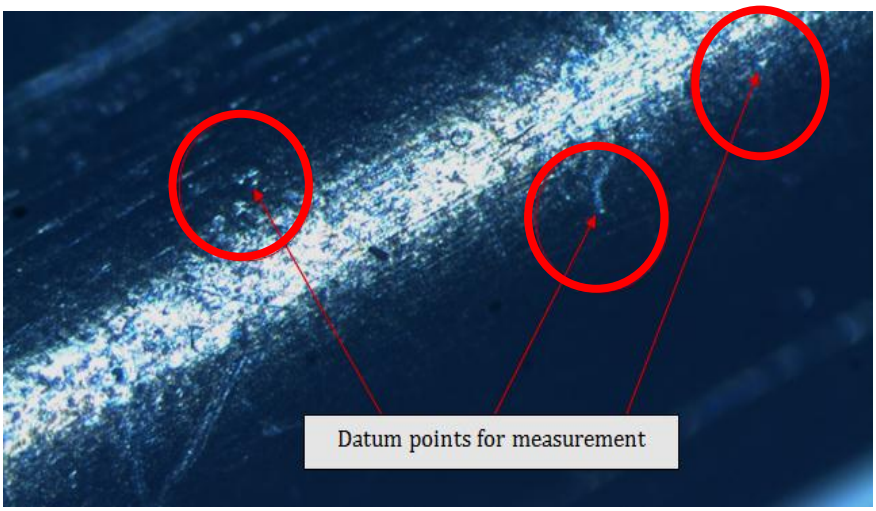

Figure 4-29 : Non-energised waveguide.

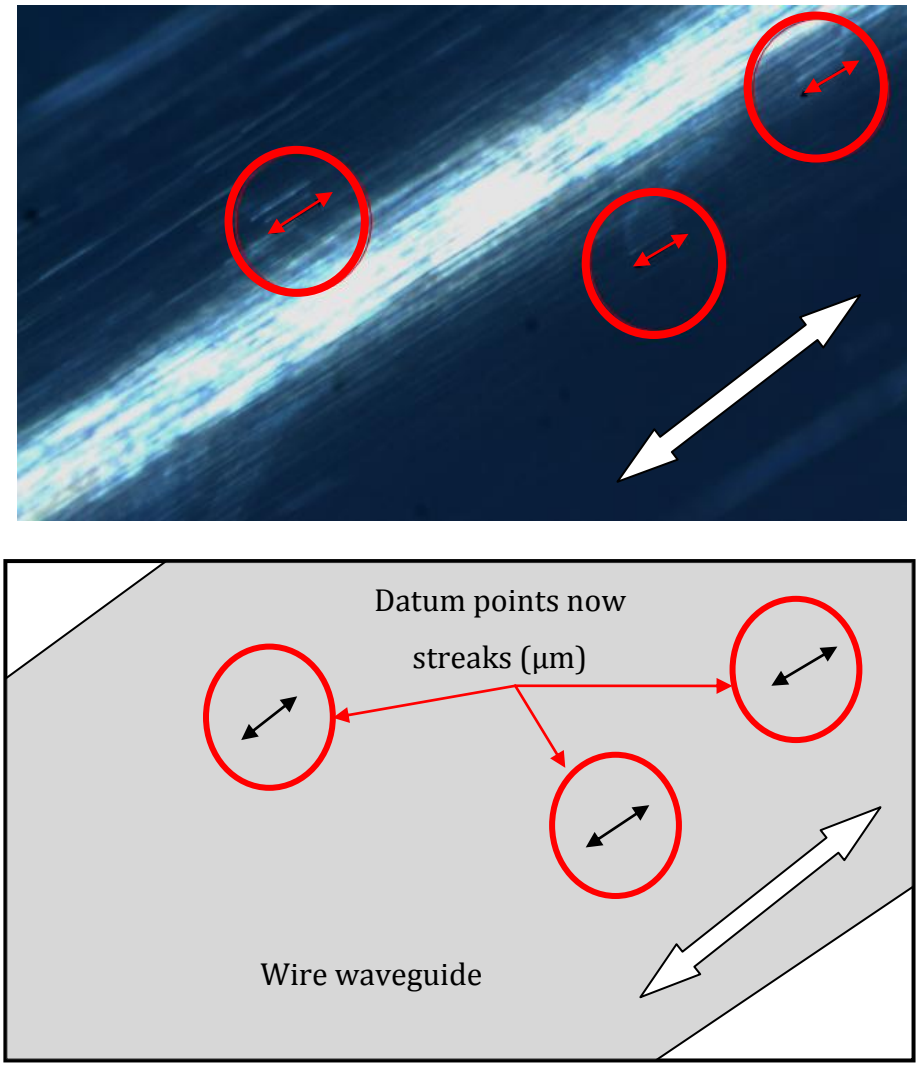

Figure 4-30 : (Top), energised wire waveguide with datum points. (Bottom) ,schematic of energised wire waveguide with datum points.

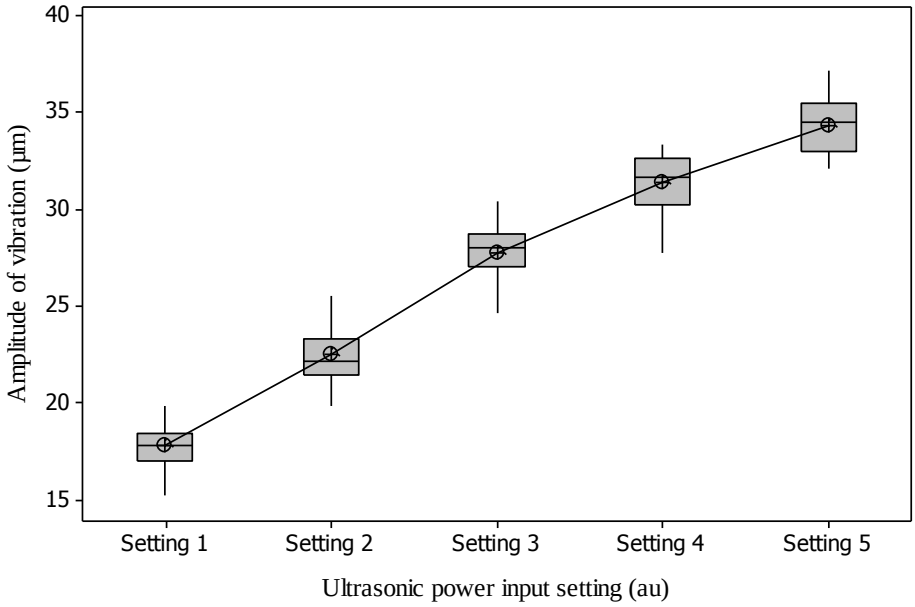

Figure 4-31 : Amplitude of vibration at wire waveguide distal tip for a given power input setting.

Power setting (au)	Amplitude of vibration (mean) (µm)	Acoustic Intensity (mean) (W/cm^2)
1	17.8 (σ = 1.19)	1.03
2	22.5 (σ = 1.5)	1.65
3	27.8 (σ = 1.43)	2.51
4	31.4 (σ =1.45)	3.21
5	34.3 (σ = 1.58)	3.83

Table 4-10 : Amplitude of vibration at wire waveguide distal tip and acoustic intensity for a given power input setting.

4.7 Fundamental frequency of operation measurement

The operational frequency of the ultrasonic transducer, as specified by the manufacturer, is 22.5 KHz. Since this sonifier has been altered by the addition of wire waveguides and the apparatus housing (seals), it was deemed necessary to experimentally verify if this was operating at this specified frequency. Using the hydrophone, a Fast Fourier Transform (FFT) on the acoustic spectrum was performed. Using this data, the fundamental frequency could then be determined.

4.7.1 Methodology

The ultrasonic apparatus (Flat 1.0 mm distal tip, 132 mm length) was attached to the test rig. This was then lowered into the thermostatic tank to a depth of approximately 50 mm. The tank was filled with tap water, heated to ≈ 37 ^{0}C and fitted with the miniature hydrophone which was lowered into the tank using a retort stand. This was situated orthogonally to the wire waveguide, approximately 30 mm deep into the water at a distance of 140 mm from the wire waveguide. A schematic of this experiment is shown below in Figure 4-32.

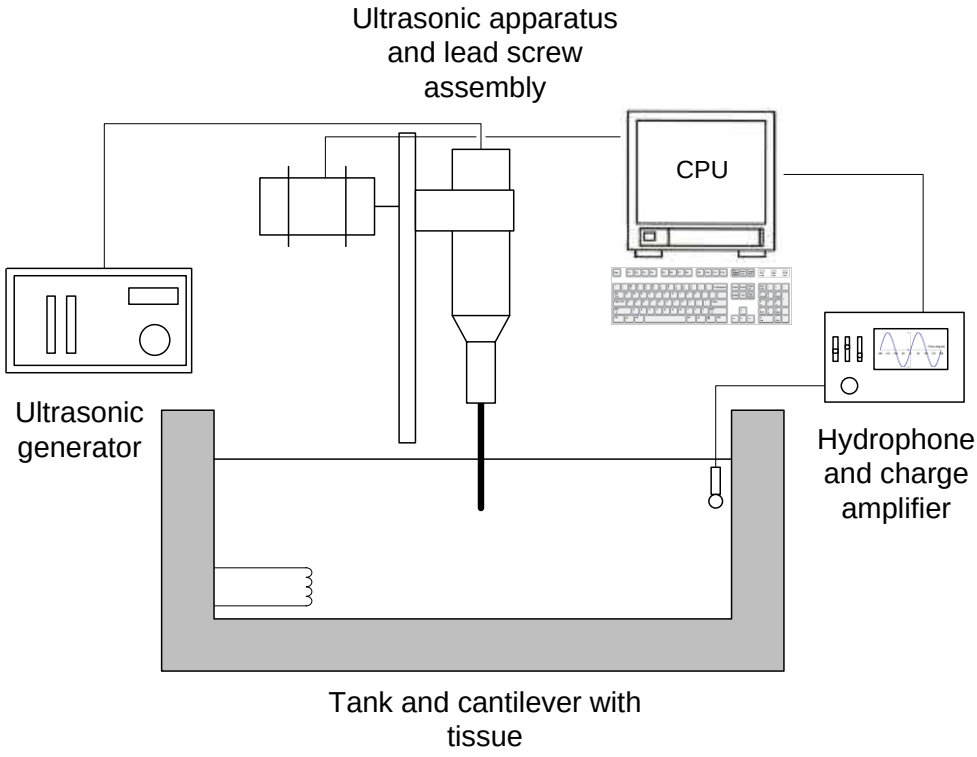

Figure 4-32 : Schematic of experiment for cavitation detection.

The ultrasonic generator was powered on but no energy was transmitted to the transducer (i.e. setting 0 au, no amplitude of vibration at wire waveguide distal tip). The signal from the hydrophone was conditioned via the charge amplifier and recorded as an analogue input to the data acquisition card and then to the CPU via the PCI bus. National Instruments Sound and Vibration tool kit was used to interrogate the input signal. An FFT was performed on the acoustic spectrum which is used to establish the peak amplitude at the dominant driving frequency. The sampling rate was 80 kHz. To reduce the spectral leakage, a Hanning window was applied to the FFT signal. This acts to minimise non-harmonic sinusoids of the fundamental and gives a better representation of the dominant frequency.

4.7.2 Results

When the generator was powered on, the FFT of the acoustic spectra revealed a spectral peak at the operating frequency of 22.5 kHz, as can be seen in Figure 4-33. The vibration from the generator at 22.5 kHz was received by the hydrophone in the liquid filled tank. This was most likely caused by the vibrations being transmitted through the bench top to the water tank. A peak at 50 Hz was also measured, a result of the surrounding electrical interference from the mains voltage signal.

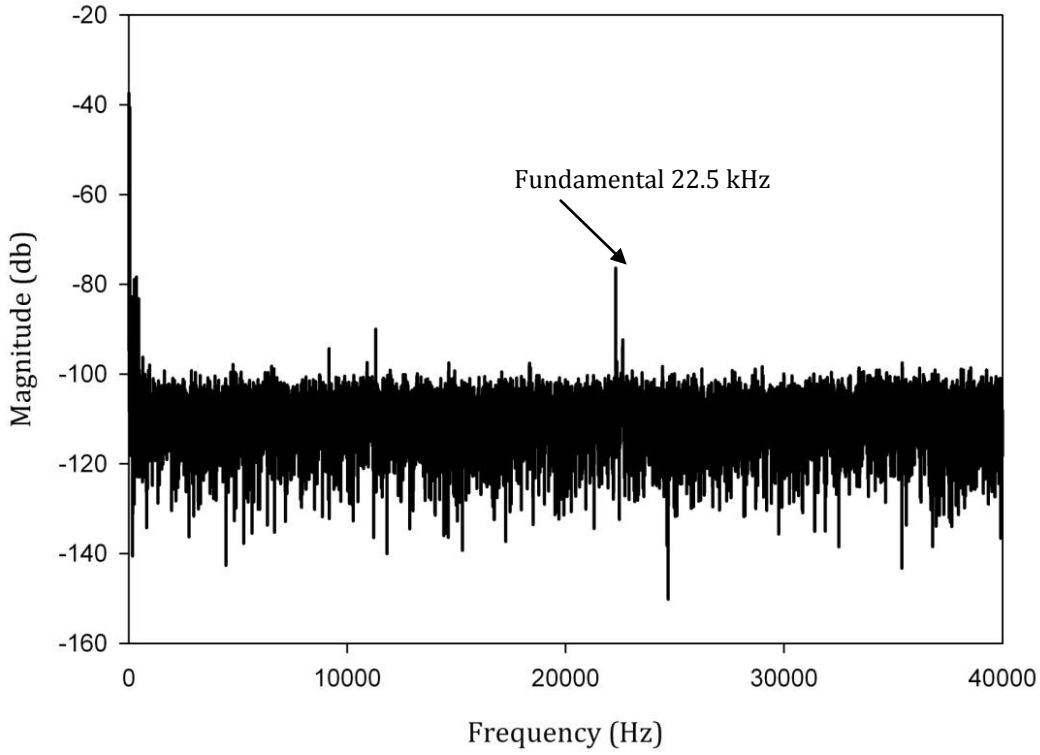

Figure 4-33 : FFT of acoustic spectrum, with peak at fundamental 22.5 kHz.

4.8 Cavitation detection using hydrophone

Cavitation can be measured as a secondary source of sound. By using a hydrophone placed in the tank but away from the cavitating region, one can determine if cavitation is present in the acoustic field. This method is commonly known as Passive Cavitation Detection (PCD). The goal of this experiment was to determine if the wire waveguides could produce sufficient pressures from the vibrating wire waveguide distal tip to cause stable and inertial cavitation.

Based on reports by others, characteristic markers of stable cavitation include sub (e.g. f/2), super (e.g. 2f) and ultra (e.g. 3f/2) harmonic peaks of the fundamental frequency (measured at 22.5 kHz) in the FFT spectrum [93, 99, 165, 166]. For inertial cavitation detection, a frequency band within the FFT signal absent of significant harmonics should be analysed. An increase and a levelling of the broadband noise (saturation) suggest operation in the inertial cavitation region [98, 167].

4.8.1 Methodology

The ultrasonic apparatus (Flat 1.0 mm distal tip, 132 mm length) was attached to the test rig. This was then lowered into the thermostatic tank to a depth of approximately 50 mm. The tank was filled with tap water, heated to ≈ 37 ^{0}C and fitted with the miniature hydrophone. This was lowered into the tank using a retort stand and was situated orthogonally to the wire waveguide, approximately 30 mm deep into the water at a distance of 140 mm from the wire waveguide.

The acoustic pressures generated by the vibrating wire waveguide distal tip in the open tank were measured using the hydrophone and charge amplifier. The power settings (au) were then increased from setting 1 – 8, corresponding amplitudes of vibration 0 - 40.8 μm. The majority of wire waveguides failed above amplitudes of vibration greater than 34.3 μm and for this reason there are a reduced number of test samples. For wire waveguides operating up to 34.3 μm, six test samples (n = 6) were recorded. For cavitation detection a Fast Fourier Transform (FFT) of the acoustic time signal was conducted. For stable cavitation detection, the entire acoustic spectrum was analysed at each setting. For inertial cavitation, a frequency band absent of any significant harmonics was extracted from the spectrum and analysed for indicators of inertial cavitation.

4.8.2 Results

Figure 4-34 shows an example FFT plot of the acoustic spectrum produced by an energised 1.0 mm flat wire waveguide distal tip with amplitude of vibration of 22.5 μm. The FFT of all acoustic spectra revealed a spectral peak at the operating frequency of 22.5 kHz. At all amplitudes of vibrations tested, harmonic peaks are evident, indicating that stable cavitation was present for all power settings. A number of frequency bands were extracted and examined for inertial cavitation. The frequency band of 16.5-17 kHz (a band absent of significant harmonics) is presented in Figure 4-35. The wire waveguide amplitude of vibration was increased and the noise power in this frequency band was recorded. This can be seen in Figure 4-36. An initial increase in broadband noise was first recorded as the wire waveguide was energised. This

noise power level reached saturation for values of amplitude of vibration greater than 31.4 μm (acoustic intensity of 3.21 W/cm^2) despite the fact that the wire waveguide distal tip amplitudes of vibration were still increasing. This is an indicator of operation in the inertial cavitation region. All bandwidths examined displayed this trend at amplitudes of vibration greater than 31.4 μm.

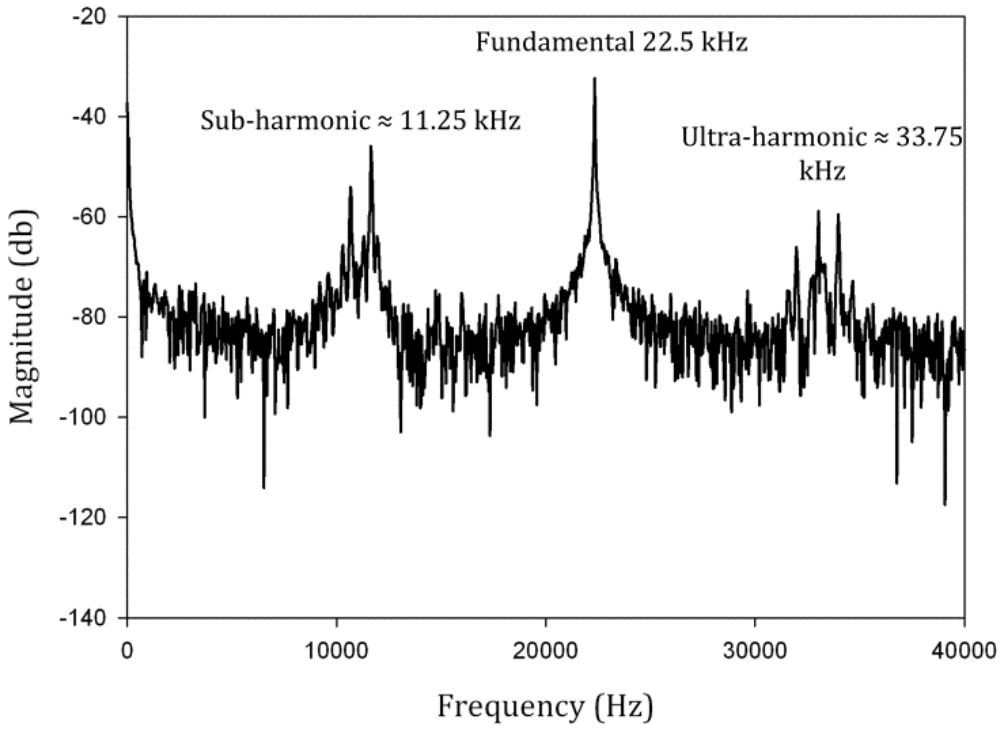

Figure 4-34 : FFT of acoustic spectrum. Wire waveguide delivering 22.5 μm amplitude of vibration.

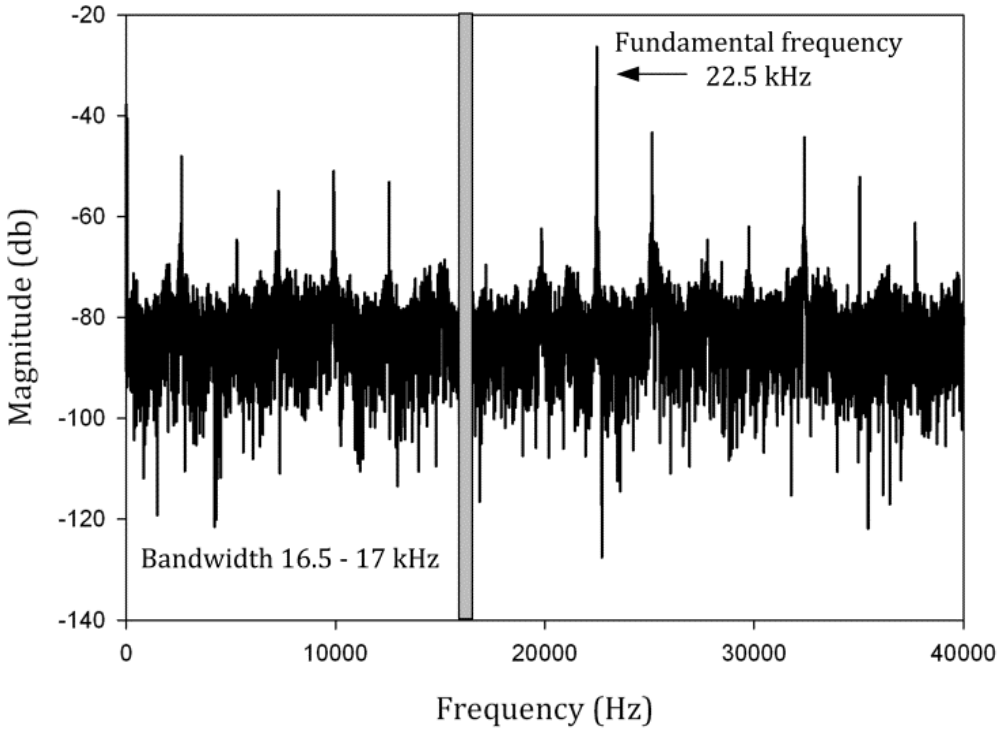

Figure 4-35 : FFT of acoustic spectrum with 1.0 mm wire waveguide energised, bandwidth 16.5 – 17 kHz extracted.

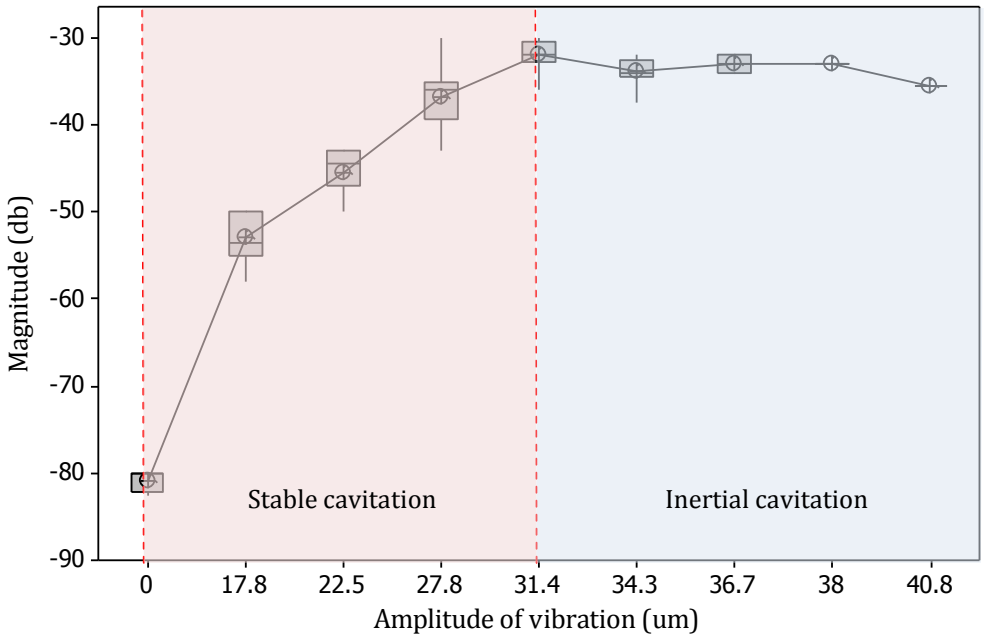

Figure 4-36 : Broadband noise power in frequency band 16.5-17 kHz.

4.9 Cavitation detection using diagnostic ultrasonic imaging device

To further validate the onset of cavitation (inertial), a B-mode ultrasonic imaging device (Philips ATL HDI 5000, L74 transducer) operating between 4-7 MHz was used to visualise the cavitation for amplitudes of vibration of 0 – 34.3 μm.

4.9.1 Methodology

The ultrasonic apparatus was held vertically using a retort stand and the flat 1.0 mm distal tip, 132 mm length wire waveguide was inserted into a length of PVC tubing of 15 mm internal diameter. This was then filled with tap water, 37 ^{0}C approximately. The B-mode emitter/receiver was coated with copious amounts of ultrasonic transmission gel and placed in contact with the PVC tubing at a height where the centre focus of the ultrasonic imaging device was focused on the wire waveguide distal tip, as shown in Figure 4-37. The ultrasonic generator was powered on and for each setting (1 - 5 au, 17.8 – 34.3 μm), a still image from the ultrasonic imaging device was recorded.

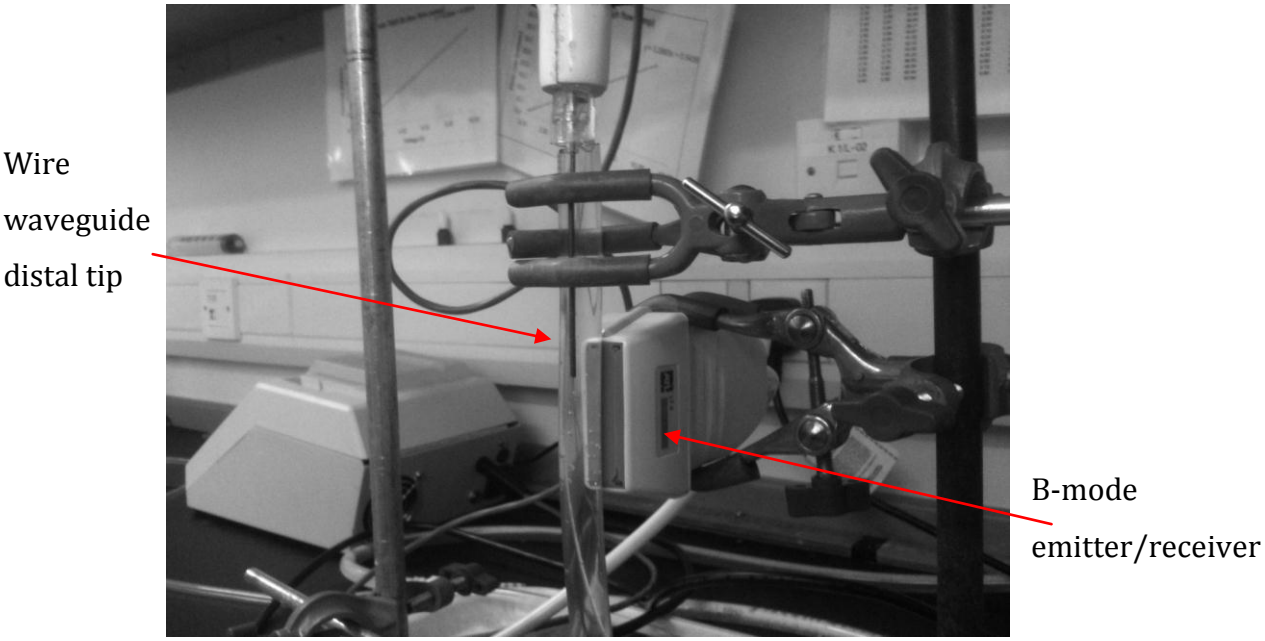

Figure 4-37 : Detection of cavitation using a B-mode ultrasonic imaging device.

4.9.2 Results

A schematic of the ultrasonic imaging display is shown in Figure 4-38. The wire waveguide distal tip is displayed in black. The PVC tubing of which the wire waveguide is inserted into is displayed in grey. No bubble activity was observed visually using the B-mode scanner for amplitudes of vibration of 0- 27.8 μm. An example of a non-cavitating wire waveguide can be seen in Figure 4-39.

Cavitation activity was observed at amplitudes of vibration greater than 31.4 μm and is shown in Figure 4-40. Dense bubble clouds are seen emanating from the wire waveguide distal tip at high velocities. Interference is also seen on the B-mode scanning image. The bubble stream direction was directly ahead of the wire waveguide distal tip for 3 - 4 mm approximately, this then coalesced on one side of the PVC tubing. The path of the bubble streaming is similar for all cavitating settings. Post sonification, the liquid was seen to have a number of bubbles which had not collapsed and were murky in appearance.

It was found that, for the 1.0 mm diameter waveguide, the cavitation threshold occurred above 31.4 μm amplitude of vibration, corresponding to an approximate wire waveguide distal tip acoustic intensity of 3.21 W/cm^2. This value correlates well with the cavitation threshold acquired via acoustic spectrum analysis using the hydrophone, values reported in the literature and the FEA results.

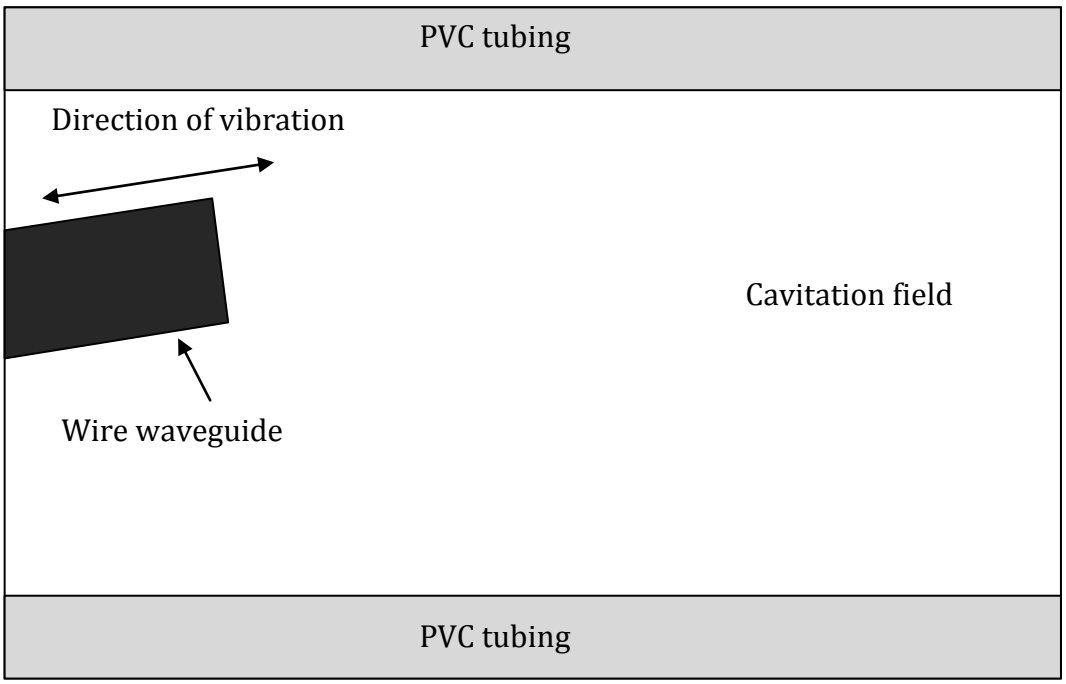

Figure 4-38 : Schematic of the ultrasonic imaging display for cavitation detection.

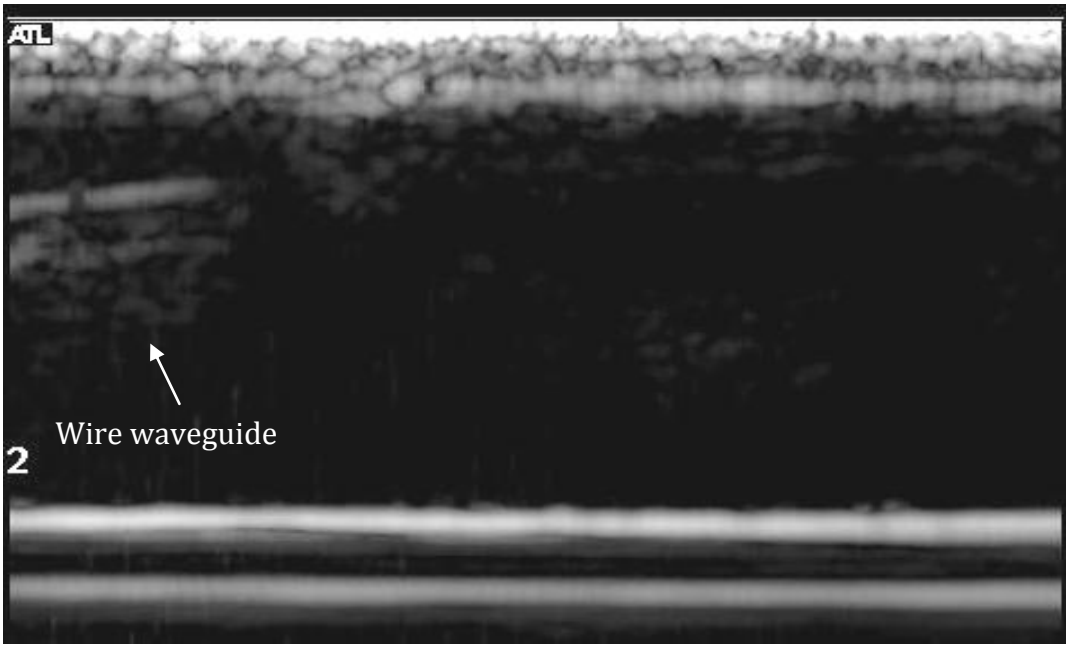

Figure 4-39 : B-mode image of wire waveguide, ≈ 20 μm, setting 1.5 au, non-cavitating.

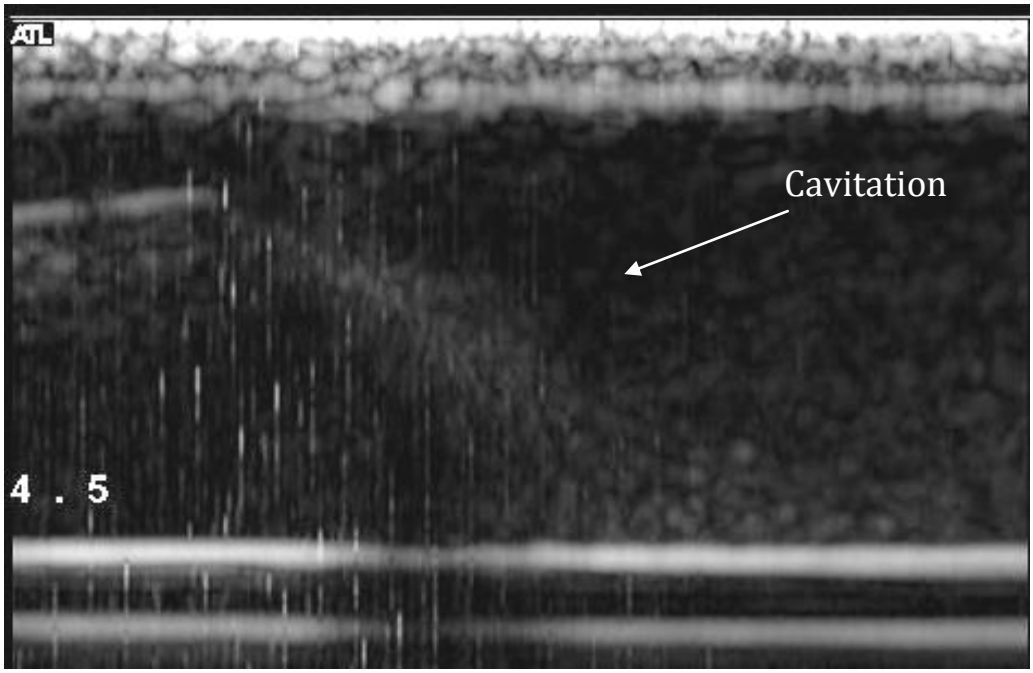

Figure 4-40 : Wire waveguide causing cavitation. Bubbles and interference observed using B-mode ultrasonic imaging, ≈ 33μm, setting 4.5 au.

4.10 Summary

- An ultrasonic apparatus which delivered ultrasonic vibrations through a wire waveguide was developed by Gavin [13]. This was an adapted sonifer which could deliver ultrasonic amplitudes of vibration to the distal tip of a wire waveguide. This ultrasonic apparatus was examined for its suitability for tissue testing.
- For this research, some of the design issues with the original ultrasonic device used by Gavin were addressed. A new method of manufacturing wire waveguides allowed for longer transmission times. A custom ABS housing was also designed and manufactured. This also allowed for longer transmission of ultrasound by providing additional support to the wire waveguide through a number of seals in the housing.
- The ultrasonic device operated at 22.5 kHz, as specified by the manufacturer. This delivered high frequency voltage to the transducer. This then converted the energy to mechanical vibrations. This was then amplified by an acoustic horn. The wire waveguides were then attached to the distal tip of the acoustic horn.
- The amplitudes of vibration at the wire waveguide distal tip are a function of the waveguide length. It was found that wire waveguides which operated between resonance and anti-resonant lengths transmitted best.

- Flat and radiused wire waveguide distal tip could be manufactured. Radiused distal tips were used in phase one testing. However, it was difficult to repeatedly produce radiused wire waveguide distal tips. For phase two and three tissue testing flat distal tips were chosen for tissue testing because of the ability to create a repeatable geometry and because they can deliver twice the acoustic pressures (required for cavitation) to that of the radiused tip (as shown in FEA, Chapter 3).
- A test rig was designed which could advance the ultrasonic apparatus towards tissue samples which are held in a force measurement cantilever. The force measurement cantilever included two thermocouples which could be inserted into the tissue. This arrangement could then be held in a liquid thermostatic tank. A hydrophone was also included in this test rig which could be used for cavitation detection. A Data Acquisition (DAq) system and LabVIEW environment was used to control and measure the sensing equipment.
- The cantilever beam tissue holder was designed to provide force feedback as the tissue samples are perforated. The beam was calibrated and beam displacement for a given force was also measured. Using this data the failure depth in multistage tissue failure can be calculated (i.e. recoil or reduction in force as the tissue partially fails is known to be a beam deflection distance).

- The amplitudes of vibration at the distal tip were measured using an optical microscope and image analysis software. Tests were conducted for power setting 1- 8 au. Artefacts on the wire waveguide were used as datum points. The artefacts were captured as streaks as the wire waveguide was vibrating. The wire waveguides could sustain amplitudes up to 34.3 μm (setting 5 au), after which wire waveguides regularly failed in a short period of time.
- The hydrophone and data processing was used to detect the operational frequency of the ultrasonic apparatus (22.5 kHz). The hydrophone was also used to detect the onset of cavitation. Stable cavitation occurred at all power settings (i.e. amplitudes of vibration). Inertial cavitation was deemed to occur above amplitudes of vibration greater than 31.4 μm (acoustic intensity 3.21 W/cm^2). According to the FEA of the flat wire waveguide, this amplitude of vibration produces approximately 0.3 MPa. This value was also verified by a B-mode ultrasonic imaging device.
- The apparatus was characterised for the following:

    - Amplitudes of vibration for given power input settings.
    - Operational frequency of the ultrasonic apparatus.
    - Cavitation detection.

- It was required that the ultrasonic apparatus operated similar to clinical devices. It was also required that the test rig could produce conditions suitable for the tissue tests. Some of the main design requirements which were verified are included in Table 4-11.

Description	Requirement	Verified
Operating frequency	20 – 50 kHz	22.5 kHz
Wire waveguide diameters (distal tip)	1.0 – 2.0 mm	1.0 mm
Amplitudes of vibration	0 – 60 µm	0 – 34.3 µm
Feedrates	0 – 100 mm/min	10 – 140 ± 2 mm/min
Thermostatic tank temp' (core human body temp')	37 ± 0.1 ^{0}C	37 ± 0.2 ^{0}C
Hydrophone DAq sampling rate (suitable for cavitation analysis)	≈ 50 kHz	80 kHz
Cavitation threshold 1.0 mm flat distal tip	Yes	amplitudes of vibration greater than 31.4 µm

Table 4-11 : Main design requirements for ultrasonic apparatus, test rig and sensing equipment.

CHAPTER

5 EXPERIMENTAL TISSUE TESTING

5.1 Introduction

Using the characterised ultrasonic apparatus, the test rig and sensing equipment, a suite of tissue tests were performed. The aim of the tissue tests was to examine the following:

i. The effect of the energised ultrasonically vibrating wire waveguide on soft arterial tissue perforation forces.
ii. The effect of increasing amplitudes of vibration at distal tip of the wire waveguide on soft arterial tissue perforation forces.
iii. The effect of cavitation at the wire waveguide distal tip on soft arterial tissue perforation forces.
iv. The effects of the increase of feedrate of the wire waveguide on soft arterial tissue perforation forces.
v. The effects of angled entry of the wire waveguide on soft arterial tissue perforation forces.
vi. The effects of the increase of wire waveguide distal tip amplitude of vibration on temperature elevation in the tissue.
vii. The effects of the increase of feedrate of the wire waveguide on temperature elevation in the tissue.

The experimental configuration is comparable to that of arterial perforation by an ultrasonically vibrating wire waveguide used for angioplasty, thrombolysis or other soft tissue cutting. For all tissue tests a 1.0 mm diameter wire waveguide was used, both radiused and flat distal tip.

Tissue testing was conducted in three phases. Based on initial testing and results from phase one, phase two and phase three experiments were then designed and conducted. Phase two and phase three experiments were aimed at examining the waveguide and tissue interaction in more detail, answering some of the questions resulting from phase one. The test phases are shown in Figure 5-1 and the test conditions are shown in Table 5-1.

- Phase one – The operating conditions of the ultrasonic apparatus were designed to act similar to that of devices used for thrombolysis and angioplasty. It was not yet known the effects, if any, of the ultrasonic wire waveguide on the healthy soft arterial tissue. This pilot tissue test phase was performed to examine if the ultrasonic apparatus and test rig performed as designed during tissue tests. It was important to establish if the ultrasonic apparatus had the ability to continually transmit ultrasonic vibrations under loading for the entire duration of the tissue test. Phase one testing was used to examine the maximum forces for complete tissue perforation using a non-energised and energised radiused distal tip wire waveguide (144 mm length) with increasing amplitudes of vibration (in the range of common distal tip amplitudes of vibration). The feedrate used for this test phase was 34 ± 2 mm/min. The

standard deviation from these results was then used for sample size estimation for phase two tissue tests.

- Phase two – Based on results from phase one, phase two experiments were then designed. Phase one testing displayed results which required further investigation (i.e. multistage tissue failure). Design of experiments, including sample size estimation, randomisation of experiments and statistical analysis (ANOVA) were employed during this phase using Minitab Statistical Software Package. Processing and manipulation of the resulting force data in phase two was also improved upon in an effort to extract more information from the force profile. The force profile was decomposed to describe stages of the tissue failure process (perforation initiation force, the force required for initial tissue failure). This was thought to be more representative of arterial failure whereby the elastic limit of the arterial wall was exceeded and a cut was initiated (i.e. irreversible damage). Perforation initiation energy and total energy for tissue perforation are also presented in phase two. The effects of cavitation on perforation force were also examined in phase two. Histological examination of tissue post perforation was applied to examine the tissue fibre damage and determine the cause of the multistage tissue failure. Initial thermal tests were also performed and recorded during this phase. Wire waveguide lengths of 132 mm were used for this suite of tests as they proved to be more reliable and were able to transmit the ultrasonic energy for long periods of time. All tissue

tests hereafter used 132 mm wire waveguide length. Feedrates of 38 ±2 mm/min were used during this phase.

- Phase three – These tests were designed to examine the effects of feedrate on perforation forces at constant power (amplitude of vibration) in conditions closer to that of clinical situations. A new tissue sample holder design facilitated angled entry approach to the tissue. The thermal effects of the wire waveguide over a range of power levels (amplitudes of vibration) were also examined. The ΔT and thermal profile were recorded and analysed from these test results.

22.5 kHz	**Waveguide Ø(mm)**	**Distal tip finish**	**Waveguide lengths (mm)**	**Amplitude of vibration (µm)**	**Cavitation threshold**	**Feedrate (mm/min)**
Ph 1	1.0 mm	Radiused	144	16 – 40	N/A	34 ±2
Ph 2	1.0 mm	Flat	132	22.5–34.3	> 31.4 µm	38 ±2
Ph 3	1.0 mm	Flat	132	22.5–34.3	> 31.4 µm	19-95 ±2

Table 5-1 : Summary of conditions used for tissue testing.

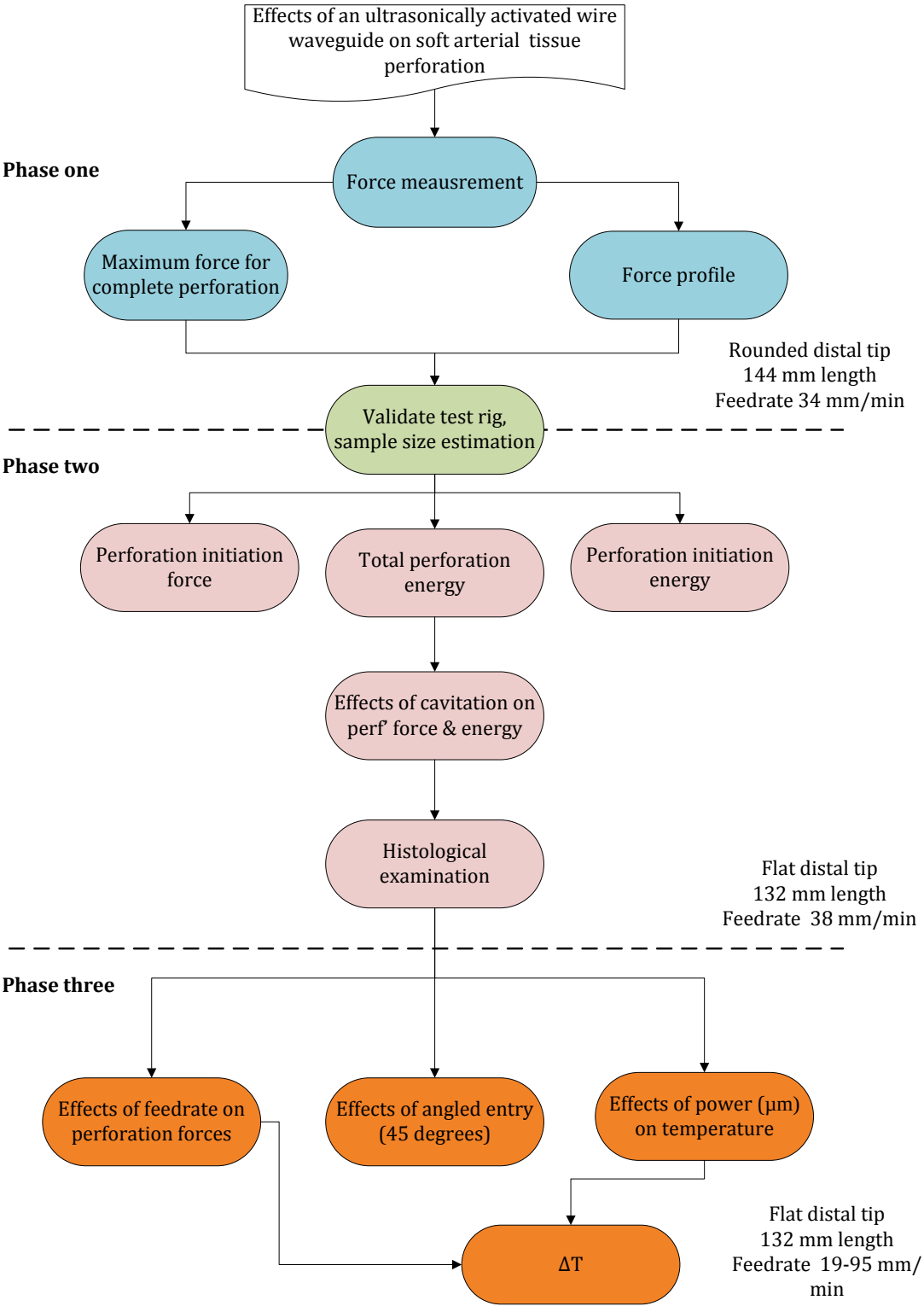

Figure 5-1 : Phases for experimental testing of the ultrasonic apparatus and soft arterial tissue.

5.2 Tissue preparation

For all tests healthy porcine vascular tissue was used as it is a close analogue to human vascular tissue [168]. Multiple porcine subjects were obtained from an abattoir and delivered within 24 hours after death. Tissue was stored and refrigerated in water until this point. Approximately 250 mm length of the descending thoracic aorta was extracted. Connective tissue was removed and 10 x 20 mm radial sections were cut from the tissue sample indicated in Figure 5-2. Sections which included branched arteries were rejected.

Sample tissue thickness ranged between 2.5 - 3.5 mm. Tissue sections were then stored in a 0.9 % refrigerated saline solution before testing (approximately 1-2 hours prior). In order for the tissue temperature to equalise with the liquid tank temperature of 37^0C ± 0.2, tissue samples were placed in a sealed container and lowered into the thermostatic tank. For each test, the aorta sections were then spread flat and clamped in the cantilever beam tissue holder (inner endothelium uppermost to represent an inside-out wire perforation) and submerged in the thermostatic tank.

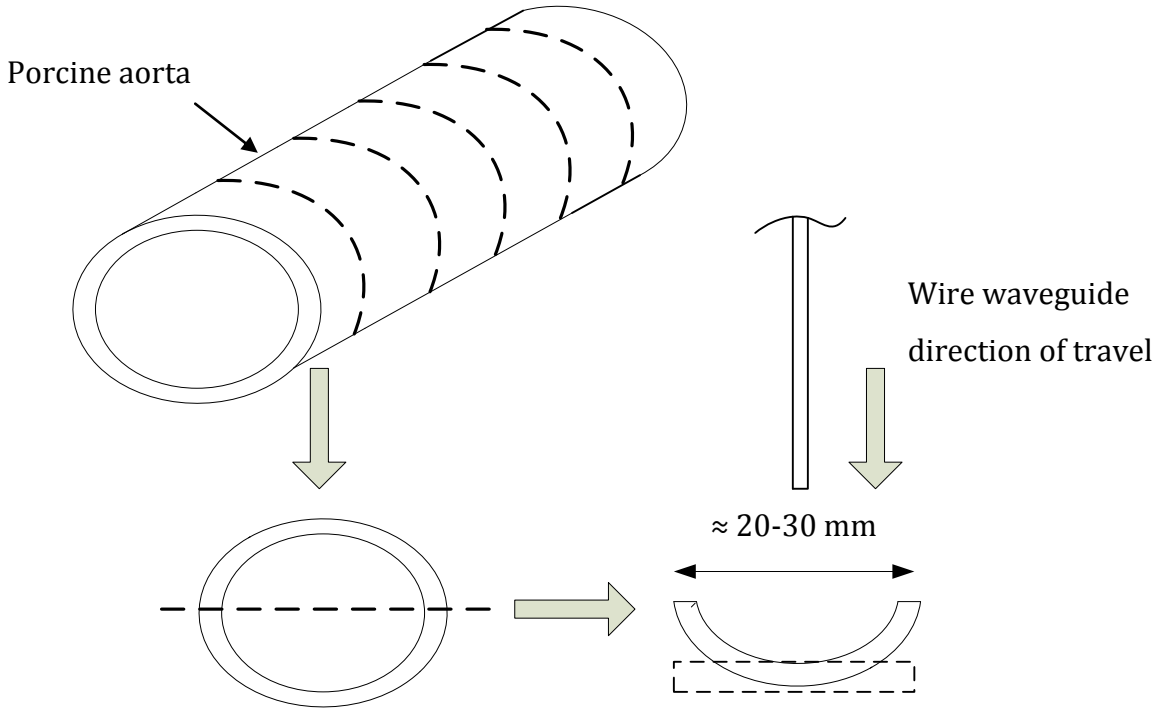

Figure 5-2 : Cutting of tissue test samples from porcine aorta sections.

5.3 Phase one tissue tests

5.3.1 Effects of amplitudes of vibration on tissue perforation forces

The ultrasonic apparatus was designed to act similar to that of devices used for thrombolysis and angioplasty. It was not yet known the effects, if any, of the ultrasonic wire waveguide on the healthy soft arterial tissue. It was also important to establish if the ultrasonic apparatus had the ability to constantly transmit ultrasonic vibrations under loading for the entire duration of the tissue test.

This comparative study was undertaken to examine the forces required to completely perforate the arterial tissue using a non-energised (no ultrasound)

and energised wire waveguide with a radiused 1.0 mm distal tip. With the energised wire waveguide, the effects of increasing distal tip amplitudes of vibration on tissue perforation were also examined.

5.3.1.1 Methodology

The tissue preparation protocol, as outlined in Section 5.2, was applied for these tests. 12 tissue samples were prepared, three tissue (n = 3) per amplitude of vibration (0, 16, 25 and 40 μm). Where 0 μm refers to a non-energised wire waveguide. A 1.0 mm radiused wire waveguide distal tip, 144 mm in length was used.

Each tissue sample was placed in the cantilever and submerged in the thermostatic tank which was filled with tap water and held at a temperature of approximately at 37 ^{0}C. The wire waveguide was advanced towards the tissue samples at a feedrate of 34 ± 2 mm/min. The ultrasound was operated in continuous mode at 22.5 kHz. For all tests the wire waveguide was advanced until arterial perforation occurred. This could be determined by monitoring the real time force profile data.

5.3.1.2 Results

5.3.1.2.1 Perforation force profile

Figure 5-3 shows examples of the perforation profiles achieved for the non-energised wire waveguide and for the energised wire waveguide for three distal tip amplitudes of vibration (16 μm, 25 μm and 40 μm). The force profile data has been filtered to exclude high frequency noise components superimposed on the force profile (> 100 Hz). For clarity, the force profiles are spread over the x -axis (time) so that each profile can be distinguished easily.

The force profile for the tissue perforation with a non-energised wire waveguide exhibits only one peak, i.e. single failure. A reduction in perforation force and multistage failure was evident when the wire waveguide was energised. It is also evident that when the waveguide is non-energised, there is a net reactive force on the waveguide after perforation due to contact friction between the wire waveguide and the tissue. This force is less in the tests with the ultrasound applied. The initial hypothesis, deduced from Figure 5-3, may be described as follows:

i. An initial rise in force as the wire waveguide contacts the tissue sample
ii. Peak one: This initial maximum peak force is thought to represent perforation of the intima-media layer (samples were set up so the internal arterial wall was penetrated, simulating the *in vivo* scenario).
iii. A secondary rise in force as the waveguide contacts the adventitia layer
iv. Peak two: Perforation of the adventitia layer and an associated reduction in force to a negligible value.

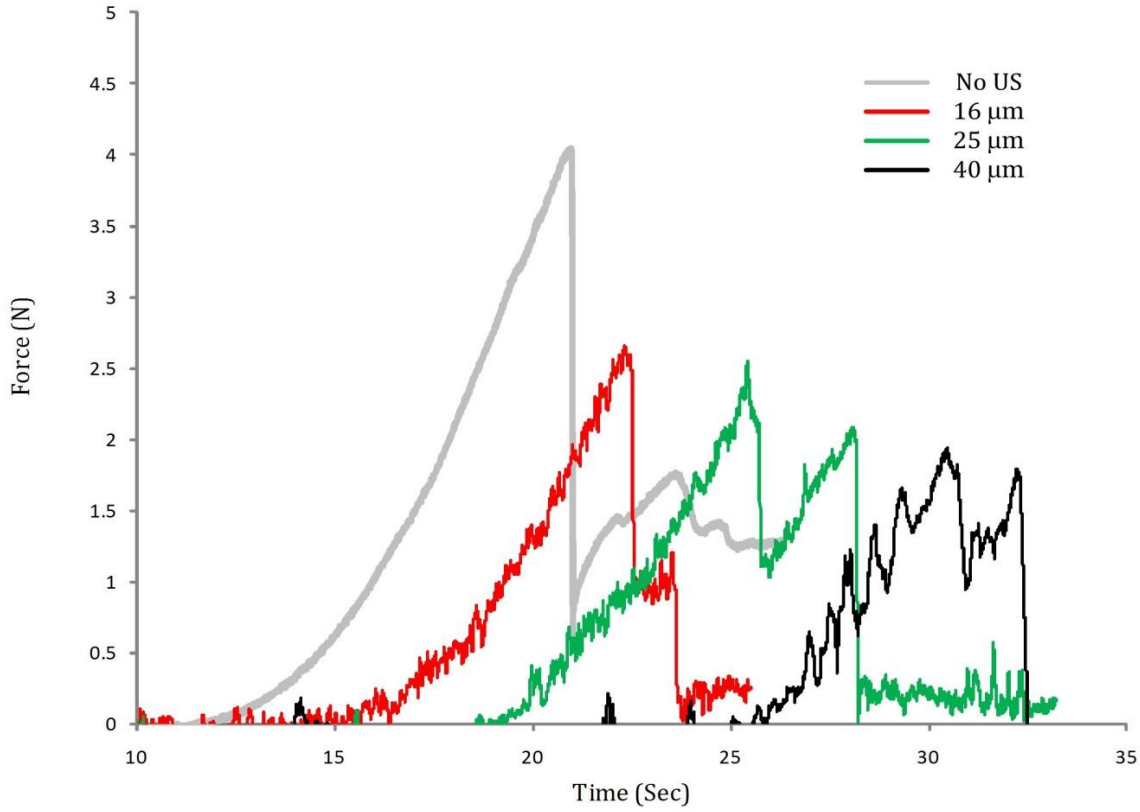

Figure 5-3 : Perforation force profiles with no ultrasound applied (0 µm, No ultrasound (US)) and for ultrasonic wire waveguide distal tip displacement of 16, 25 and 40 µm.

5.3.1.2.2 Maximum cutting force

The results of the maximum perforation force in all 12 experiments are shown in Figure 5-4. It was found that a force exceeding 3.8 N resulted in perforation of the healthy arterial tissue with a non-energised 1.0 mm radiused distal tip wire waveguide. The energised wire waveguide with increasing distal tip amplitude of vibration resulted in a lower force required to completely perforate the artery wall. A 30% reduction in mean perforation force (3.96 N vs. 2.67 N) was measured when the wire waveguide was energised at the lowest

ultrasonic power setting (16 μm). With the highest ultrasonic amplitudes of vibration tested here (40 μm), the perforation force was reduced to 2 N (σ = 0.1). It should be noted that in multistage failures of the tissue, the maximum force was not always the force first peak.

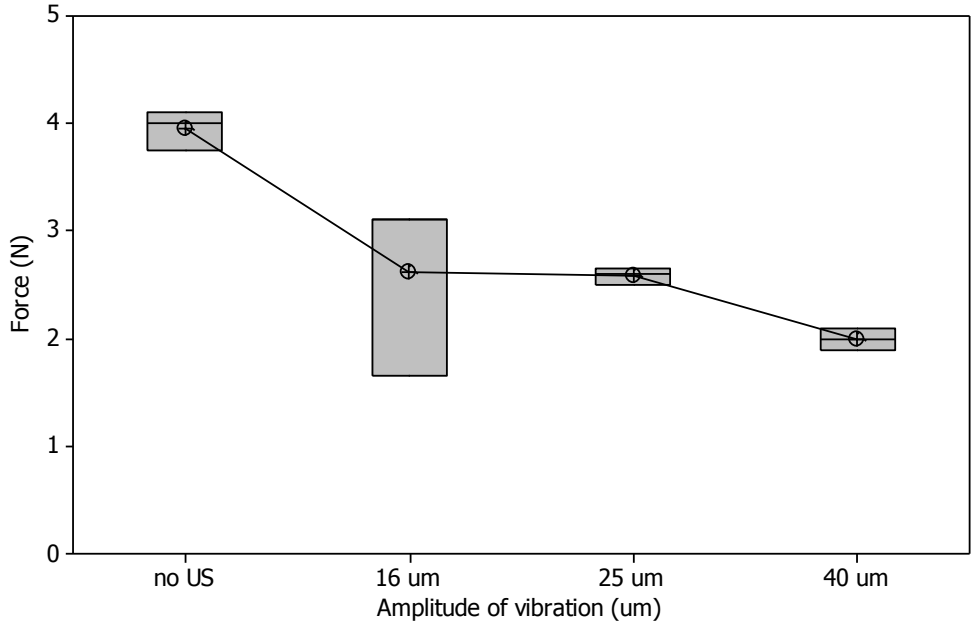

Figure 5-4 Maximum perforation force required with no ultrasound and with ultrasound at amplitudes of vibration of 16, 25 and 40 μm.

5.3.2 Conclusion of phase one tissue tests

Most work to date using therapeutic ultrasound has focused on high intensity applications in excess of 400 W/cm^2. This work focused on how low acoustic intensities, less than 4 W/cm^2 affect soft tissue perforation.

The results from the preliminary study indicate the following:

- There is a reduction in the force required (compared to a non-energised wire waveguide) to perforate the healthy elastic arterial wall at the wire waveguide amplitudes of vibration typically used to ablate and disrupt atherosclerotic plaques and thrombus.
- Multistage failure was evident when the wire waveguide was energised. By analysing the force profile for multistage failure, one may also partially perforate the tissue.
- The maximum force displayed in Figure 5-4 in some cases was the second peak. Initial failure of the tissue is a critical point of failure, i.e. the first force profile peak, so this should be examined in more detail.
- The sample size (n = 3) used for this test was low and deemed inadequate for statistically significant data. Larger samples would be needed for phase two tissue testing.

5.4 Phase two tissue tests

5.4.1 Examination of tissue failure forces using flat distal tip

This suite of tests (phase two) was designed to further examine the tissue perforation force profile in closer detail. A shorter wire waveguide (132 mm) was used for this suite of tests. This had a 1.0 mm diameter flat wire waveguide distal tip which could be easily and consistently replicated. It was also established through FEA (Chapter 3) that the flat distal tip can produce higher pressures than that of the 1.0 mm diameter radiused distal tip wire waveguide counterpart for the same amplitudes of vibration.

The amplitudes of vibration at wire waveguide distal tip for power input were experimentally measured, see Chapter 4. This length of wire waveguide was shown to be operating in the inertial cavitation region above amplitudes of vibration of 31.4 μm (mean). Due to tissue availability and storage, this phase of tissue testing was conducted over a number of weeks. The run order of tests was, therefore, randomised to mitigate the influence from any uncontrolled variables. The aims of this suite of tests were to:

- Examine the forces and energies for initial and total perforation.
- Examine the effects of cavitation on the perforation forces.
- Determine the cause of multiple failures in tissue via histological examination.

5.4.1.1 Methodology

For this test six tissue samples (n = 6) per amplitude of vibration (0, 22.5, 27.8, 31.4 and 34.3 μm) were prepared using the tissue preparation protocol as outlined in Section 5.2 (30 tissue samples in total). For each test, the tissue sample was secured in the cantilever and submerged in the thermostatic tank. The ultrasonic wire waveguide was advanced towards the tissue samples at a constant feedrate of 38 ± 2 mm/min for all tests. The ultrasound was transmitted in continuous mode at 22.5 kHz. The wire waveguides were advanced through the tissue samples until complete perforation occurred. The force profile and visual observation was used as an indicator that the tissue had been perforated fully.

The perforation initiation force was measured and refers to the first peaks (F_1 and F_2) as shown in Figure 5-5 for their respective profiles. While the perforation initiation forces (F_1 and F_2) are extremely informative they do not take the wire waveguide tissue indentation depth (δ_i) into account. The energy to initiate perforation (E_i) and totally perforate the artery wall (E_t) was therefore considered also.

The energy was calculated using Equation 1 from Chapter 2. The perforation initiation energy is represented by the shaded region in Figure 5-5. This method was also applied to the entire force profile to determine the total perforation energy.

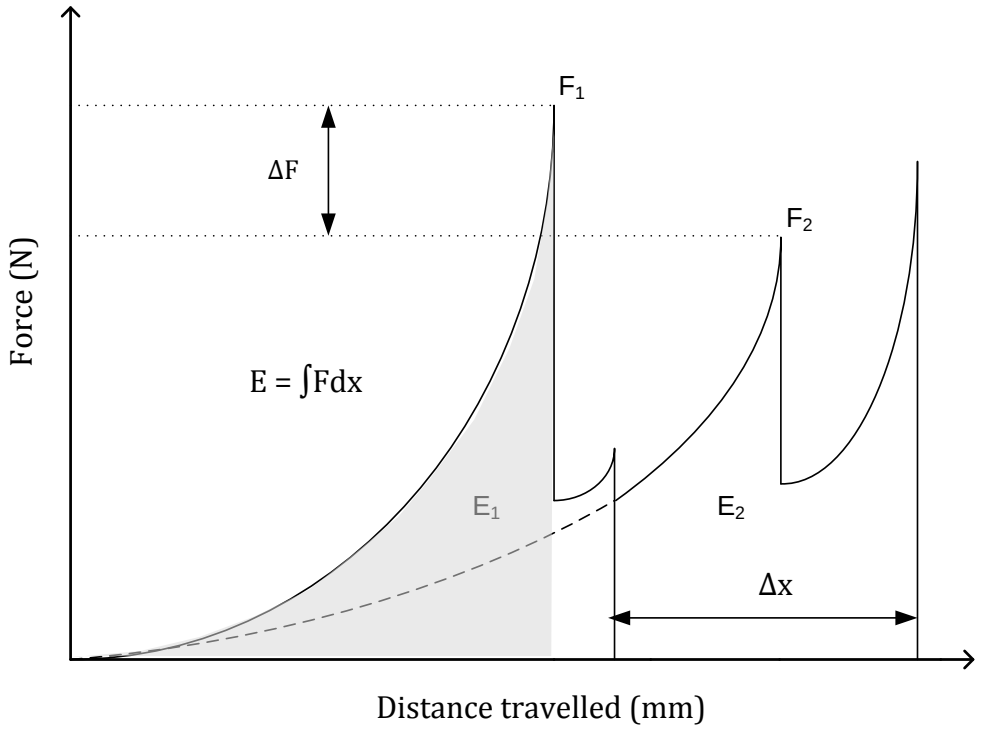

Figure 5-5 : Deriving perforation initiation energy from force and distance travelled.

5.4.1.2 Results

5.4.1.2.1 Perforation force profile versus waveguide indentation

Figure 5-6 shows examples of the tissue perforation force profile versus distal tip indentation into the tissue for each of the amplitudes of vibration (0 – 34.3 μm). The deflection of the cantilever beam has been subtracted from the overall deflection of the system (beam and tissue) to give waveguide indentation into tissue (δ_i). This was then used to calculate perforation energy. Generally, the force profiles can be described as having a number of features:

i. An initial rise in force up to a threshold value whereby the tissue fails and perforation of the tissue begins, the perforation initiation force, F_i.

The area under the curve up to this initial failure point represents the work done to initiate perforation, the perforation initiation energy, E_i, using the method similar to McCarthy *et al.* [28]. The total energy for perforation was also calculated from the force profile data by calculating the area under the entire curve. In the case of the non-energised wire all samples failed in a single stage. It should be noted that the magnitude of the perforation initiation force was not always the greatest force encountered during the perforation; in some cases the second or third peak was greater.

ii. With activation of the wire waveguide and, in particular, at higher amplitudes of vibration a multi-stage failure was evident. It was found that with amplitudes of vibration of 22.5 μm and greater, failure of the tissue occurs in multiple stages (two-three stages identified).

The results show a reduction in the perforation initiation force and energy required to initially perforate the tissue with increasing amplitudes of vibration. No more than three peaks were detected for any test. To ensure that the wire waveguide has contacted the tissue, a threshold of 0.3 N is allocated as the contact point, the data has also been decimated (50 points) to provide a clearer representation of the force profile, as seen in Figure 5-6.

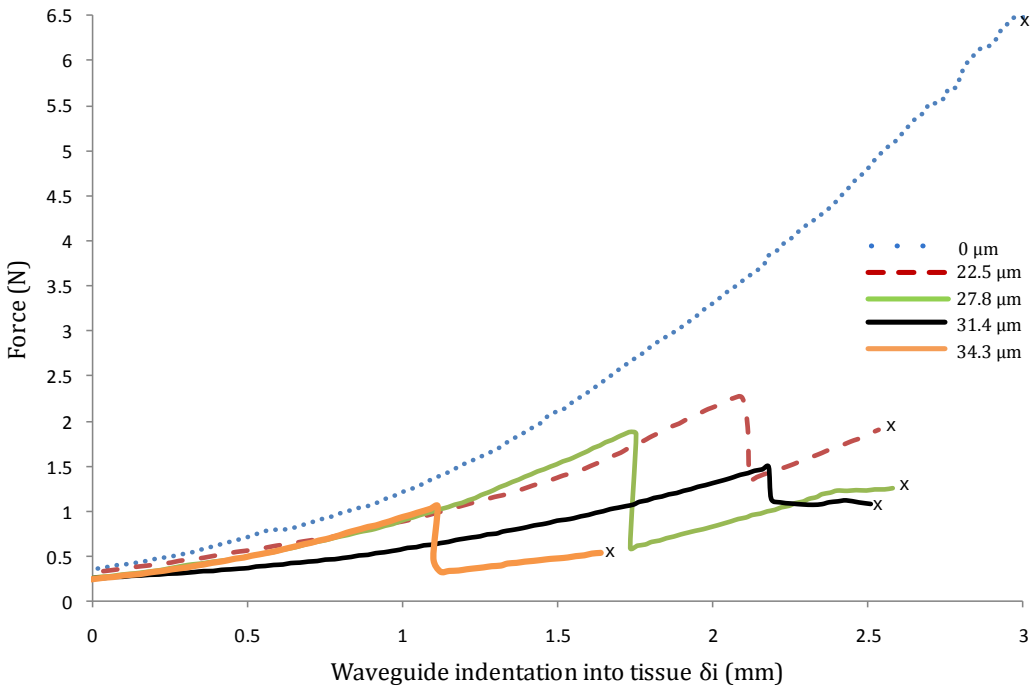

Figure 5-6 : Force versus distal tip indentation into tissue, δi, profiles for individual tests for a range of amplitude of vibrations. "x" indicates failure. Note: Non-energised is depicted as 0 µm.

5.4.1.2.2 Perforation initiation force

Figure 5-7 shows the results for the perforation initiation force for all tests (six tests per amplitude of vibration (n = 6), 30 runs in total). With the non-energised wire waveguide, the perforation initiation force is 6.13 N (mean, σ = 0.60 N). At the lowest amplitude of vibration of 22.5 µm, the perforation initiation force is reduced to 2.46 N (mean, σ = 0.49 N). The perforation initiation force is further reduced to 1.26 N (mean, σ = 0.14 N) with an energised wire waveguide while with the highest amplitude of vibration of 34.3 µm, an 80% reduction in force compared with the non-energised waveguide was found. The perforation initiation forces for amplitudes of vibration at 27.8

μm and above were not significantly different (CI = 0.95). There was also no significant reduction in the perforation initiation force when the wire waveguide was operating above the cavitation threshold amplitude of vibration of 31.4 μm. Standard deviation was lowest (both σ = 0.135 N) for the higher amplitudes of vibrations tested (31.4 μm and 34.3 μm). In comparison for a non-energised wire waveguide the deviation was much greater (σ = 0.60 N)

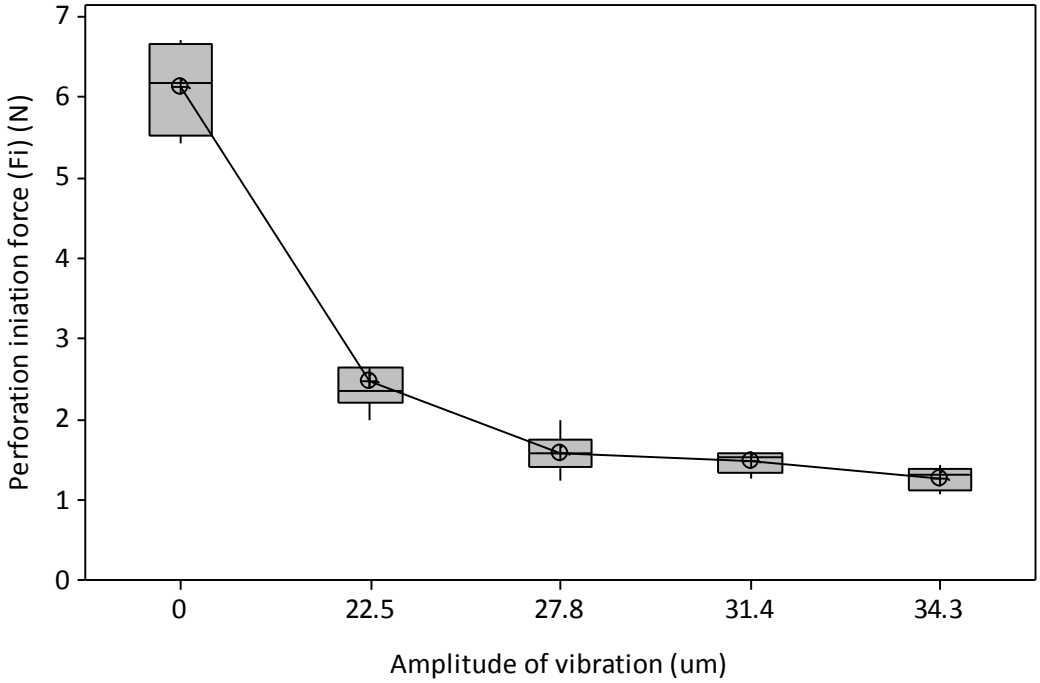

Figure 5-7 : Perforation initiation force (F_i) for a range of amplitudes of vibrations.

5.4.1.2.3 Perforation initiation energy

The resulting perforation initiation energy, E_i, was calculated and plotted in Figure 5-8. The energy for perforation initiation for a non-energised wire was 7.75 mJ (mean, σ = 1.41 mJ). This reduced to 2.38 mJ (mean, σ = 0.71 mJ) at the lowest amplitude of vibration of 22.5 μm. The minimum perforation initiation energy was measured as 1.02 mJ (mean, σ = 0.46 mJ) at the highest amplitude of vibration of 34.3 μm. The lowest standard deviation (σ = 0.22 mJ) was measured at amplitude of vibration of 27.8 μm, this increased for the higher amplitudes of vibration (31.4 μm, σ = 0.33 mJ and 34.3 μm, σ = 0.46 mJ).

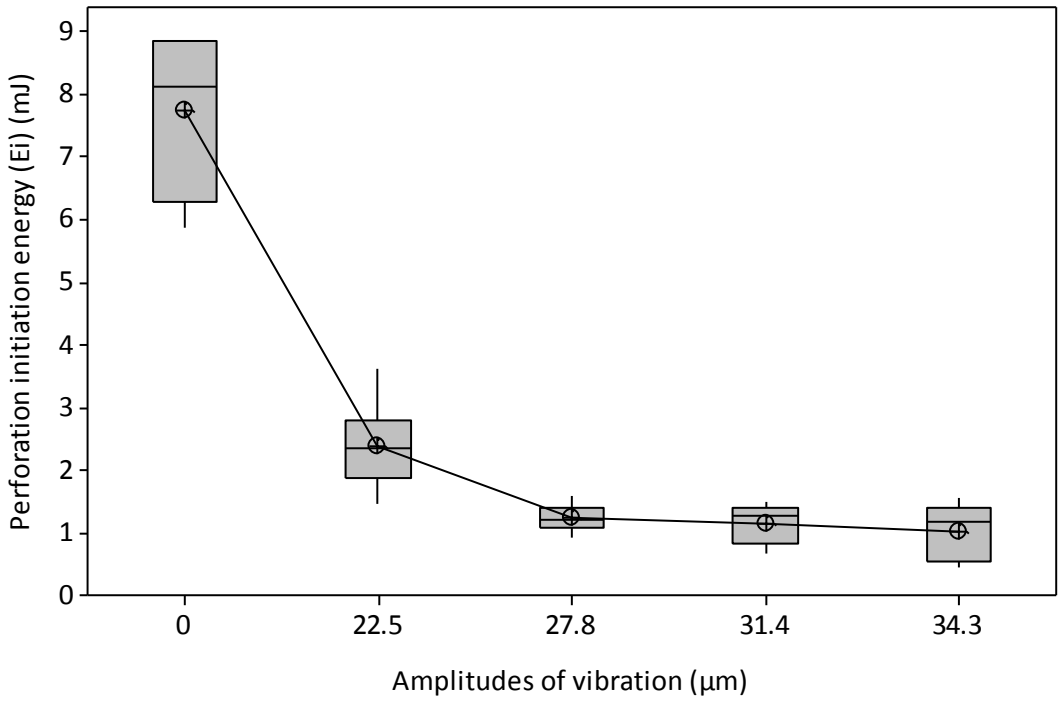

Figure 5-8 : Perforation initiation energy (E_i) for a range of amplitudes of vibration.

5.4.1.2.4 Total perforation energy

The total perforation energy (E_t) versus amplitude of vibration is plotted in Figure 5-9. For a non-energised wire waveguide, the total perforation energy was 7.75 mJ (mean, σ = 1.41 mJ, note: same as perforation initiation energy as failure occurred in one stage for all tests). This was reduced to 3.07 mJ (mean, σ = 1.49 mJ) at an amplitude of vibration of setting 22.5 μm. The energy required to completely perforate the tissue at the highest amplitude of vibration (34.3 μm) was reduced to 1.45 (mean, σ = 0.52 mJ). The perforation initiation force, energy and total perforation energy are also presented in Table 5-2.

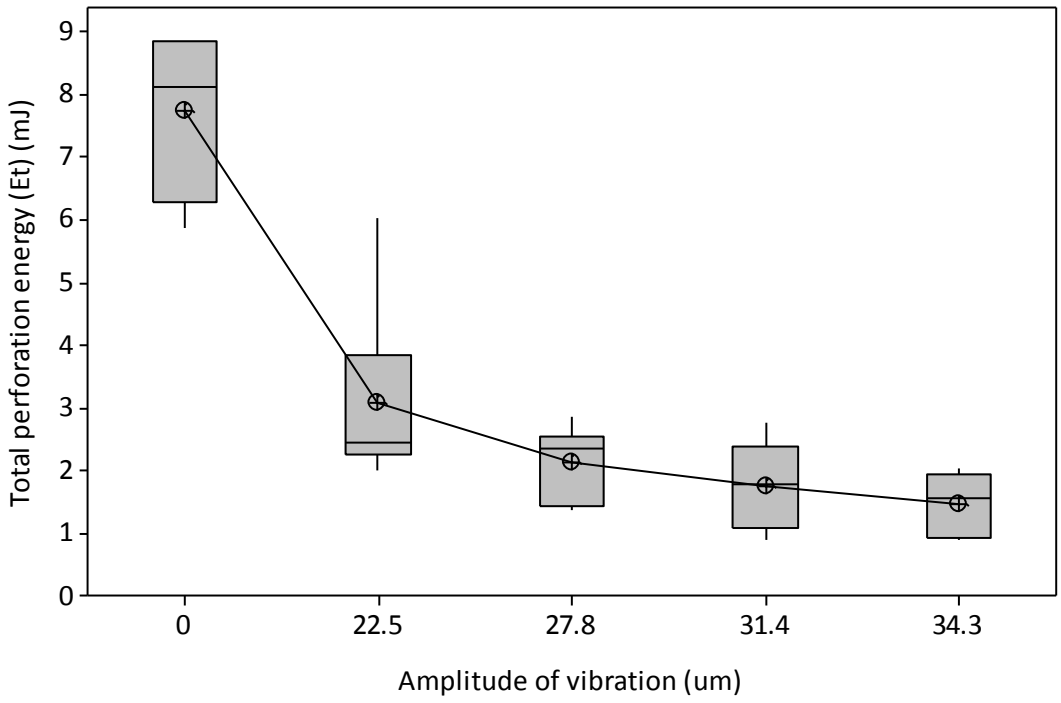

Figure 5-9 : Total perforation energy (E_t) for a range of amplitudes of vibration.

Amplitude of Vibration (μm)	Acoustic intensity (W/cm^2)	Perforation initiation force, F_i (N)	Perforation initiation energy, E_i (mJ)	Total perforation energy, E_t (mJ)
0	0	6.13 (mean, σ = 0.60)	7.75 (mean, σ = 1.41)	7.75 (mean, σ = 1.41)
22.5	1.65	2.46 (mean, σ = 0.49)	2.38 (mean, σ = 0.71)	3.07 (mean, σ = 1.49)
27.8	2.51	1.59 (mean, σ = 0.25)	1.23 (mean, σ = 0.22)	2.13 (mean, σ = 0.60)
31.4	3.21	1.48 (mean, σ = 0.13)	1.14 (mean, σ = 0.33)	1.75 (mean, σ = 0.71)
34.3	3.83	1.26 (mean, σ = 0.14)	1.02 (mean, σ = 0.46)	1.45 (mean, σ = 0.52)

Table 5-2 : Perforation initiation force (F_i), perforation initiation energy (E_i) and total perforation energy (E_t) for all amplitudes of vibration/acoustic intensities using a 1.0 mm flat distal tip wire waveguide at 22.5 kHz.

5.4.2 Histological analysis of tissue failure

Histological analysis was employed to answer some of the fundamental questions surrounding the perforation of the tissue with an ultrasonically energised wire waveguide. Before the tissue was subjected to testing, microscopic analysis was used to determine the composition of the porcine artery wall samples (intima, media and adventitia). A comparative analysis of tissue which was perforated by a non-energised and energised wire waveguide was also performed. Tissue samples were viewed at point of entry (plan view) and along the perforated hole (section view) as shown in Figure 5-10.

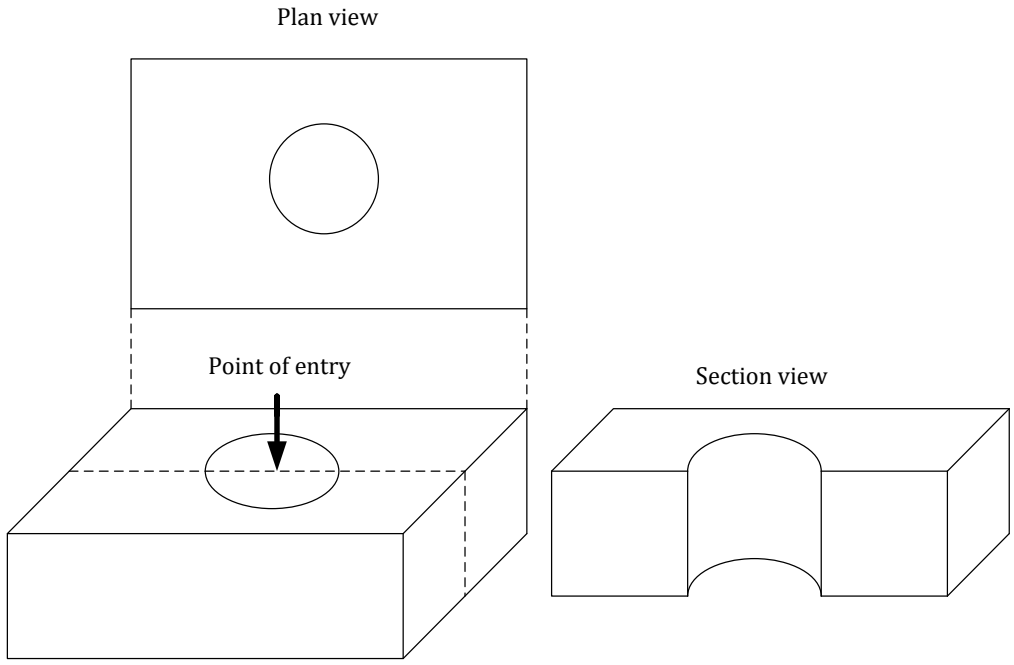

Figure 5-10 : Plan view (top) and section view (right) of tissue samples for histology.

5.4.2.1 Methodology

For this analysis, three different sets of tissue samples were histologically examined, as outlined below.

i. Negative controls (processed tissue but not perforated with any wire waveguide).
ii. Tissue sample perforated with a non-energised wire waveguide.
iii. Tissue samples perforated with an energised wire waveguide which exhibited multiple failures.

All tissues sample were stored in 10 % buffered formalin solution. The tissue was then processed to wax over a 12 hour period and is illustrated in the flowchart in Figure 5-11 . Water constituents were removed by alcohol, i.e. dehydration by ethanol. A hydrophobic clearing agent (Xylene) was then used to remove the alcohol and the tissue was finally infiltrated by molten paraffin wax. The hard wax tissue samples were then embedded in wax cassettes, top down for plan view and sideways for section view. The samples were then trimmed (20 μm) on a rotary microtome until the sections of interest were exposed. The cassette was then placed in an ice bath to cool.

For section view cuts it was important to get a representation of the cut approximately half way through the diameter of the hole. To achieve this several levels were taken. For each level, three to four 5 μm sections were cut and placed on a microscopic glass slide. The wax block was then trimmed for approximately 10 cuts of 20 μm. The next level of 5 μm sections was then cut. Up to seven levels were taken for some tissue samples.

For the plan view, the wax block was trimmed (20 μm) until section samples represented the point of entry at the upper tissue layer. One level of three to four 5 μm sections were then cut and placed on the microscopic glass slide. These samples were then de-waxed and stained using Haematoxylin and Eason (H&E) and Millers Elastic staining protocols. Samples could then viewed using light microscopy.

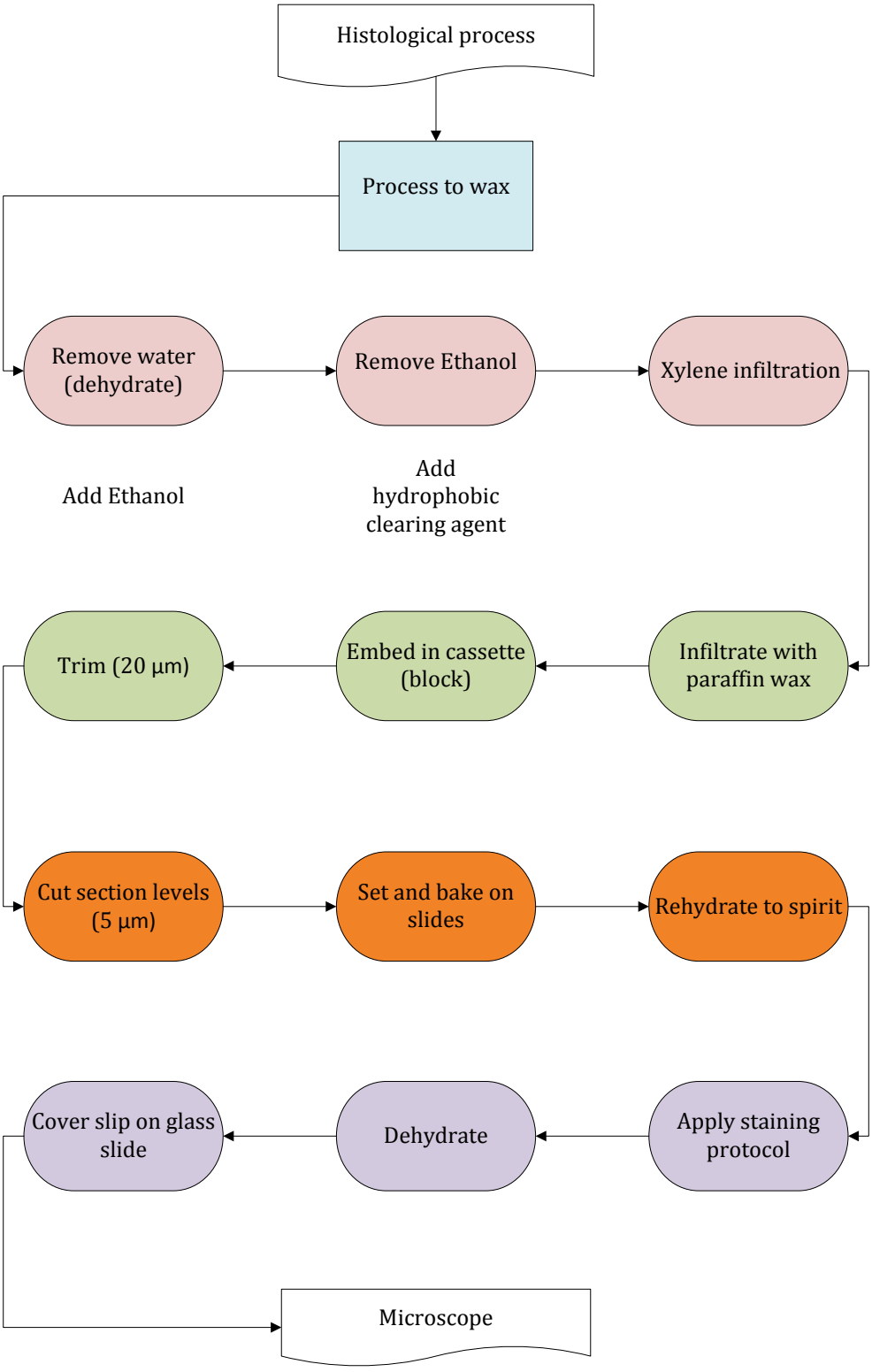

Figure 5-11 : Histological processing.

5.4.2.2 Results

5.4.2.2.1 Negative control tissue samples

A tissue sample which was prepared for testing but not tested on (control) was stained using Miller Elastic protocol is shown in Figure 5-12. The section view of the artery shows elastin fibres stained blue and collagen in the adventitia stained pink. Relatively thin adventitia layer is present surrounding the circumference of the tissue. The cut end of this artery section is also shown in Figure 5-13. The end section was dissected using a scalpel. The effects of this cut can be seen at where the fibres terminate. The fibres are sheared but are not de-bundled. This is an example of the shear failure.

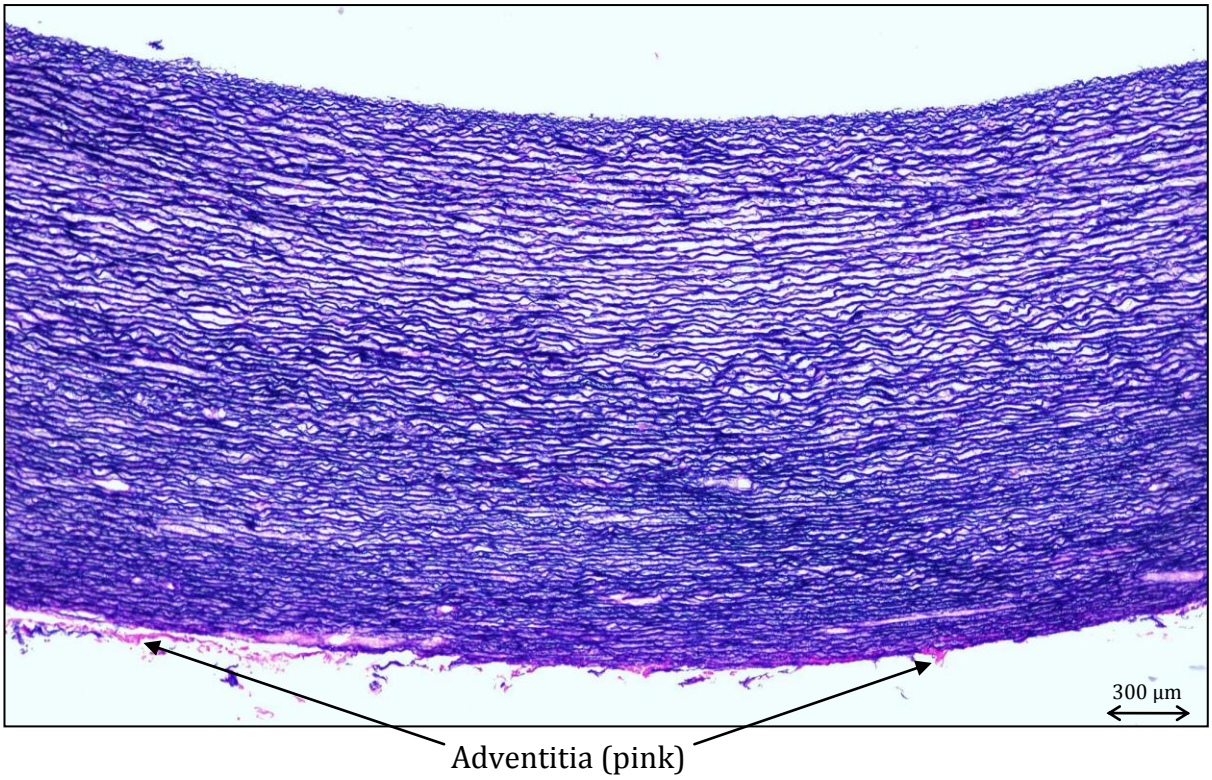

Figure 5-12 : Millers Elastic stain of artery wall, section view, 20x.

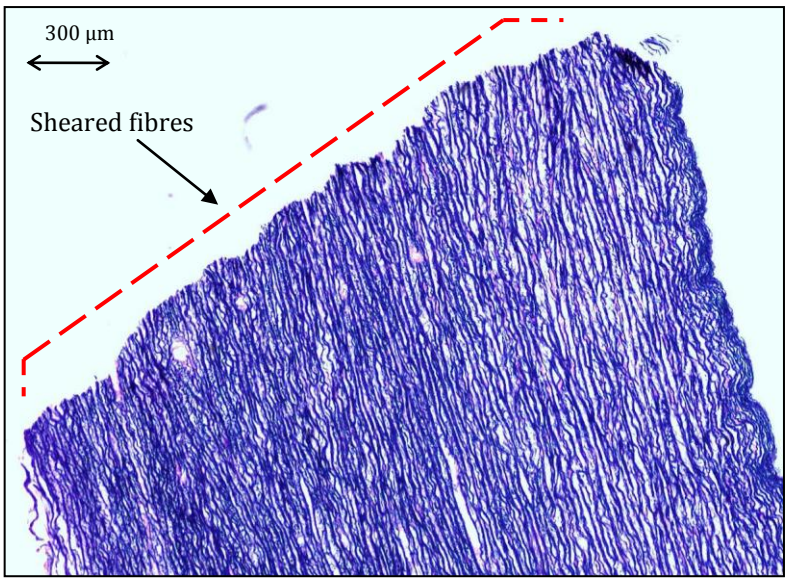

Figure 5-13 : End of artery section, 20x.

5.4.2.2.2 Non-energised wire waveguide perforation

Tissue samples which were perforated with a non-energised wire waveguide are shown in Figure 5-14. The plan view of the wire waveguide point of entry, stained with H&E, is shown Figure 5-14 (B). The 1.0 mm diameter wire waveguide does not produce a perfect circular entry hole; rather, the grain of the fibres has split in opposite points along the circumference of the hole. The forces to perforate the tissue using the non-energised wire waveguide are larger than that of the force when using an energised wire waveguide. The larger forces may cause more tissue damage akin to that of perforation by blunt trauma. Single tissue failures were seen on the force profile when the non-energised wire waveguides perforated the tissue. This single failure was also evident in the section view H&E tissue samples. Again the large forces seem to split the tissue (shear dissection) with minimal tissue removal when the wire waveguide is non-energised. The image of the shearing at points of tissue failure

in Figure 5-14 are in some respects comparable to Figure 5-13 where the tissue has been dissected by a scalpel. It should be noted that, due to the processing, some artefacts may get included on the slide or the tissue may get moved slightly by the addition of the cover slip.

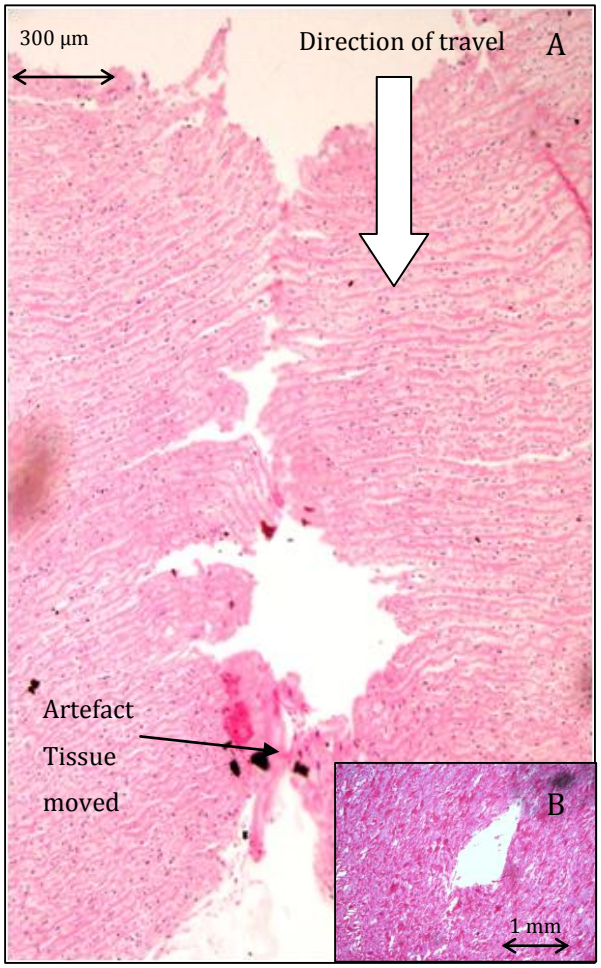

Figure 5-14 : A) Section view of tissue which was perforated by a non-energised wire waveguide, 20x, H&E stain. B) Plan view of point of entry of non-energised wire waveguide perforation, 4x, H&E stain.

5.4.2.2.3 Energised wire waveguide perforation

Tissue samples which were perforated with an energised wire waveguide operating with amplitudes of vibration of 27.8 μm are shown in Figure 5-15. A Haematoxylin and Eason stain was applied. The cross sectional profile of the hole parallel to the cut direction (A) clearly shows multistage tissue perforation. Three stage perforation was observed corresponding to the force profile data from the tissue test where three force peaks was measured. The histology images present strong evidence of tissue removal; the perforated hole remains after waveguide removal. At the tissue failure locations it can also be seen that the tissue has become striated and compressed or fused, with evidence of de-lamination in the vicinity. When the high frequency vibrations are applied to the wire waveguide, a well defined entry hole is created in the tissue (B). There is also evidence to suggest that lateral damage occurs away from the point of entry, this is shown in Figure 5-16. Similar de-striation of the fibres is seen, although no shearing of the fibres occurs.

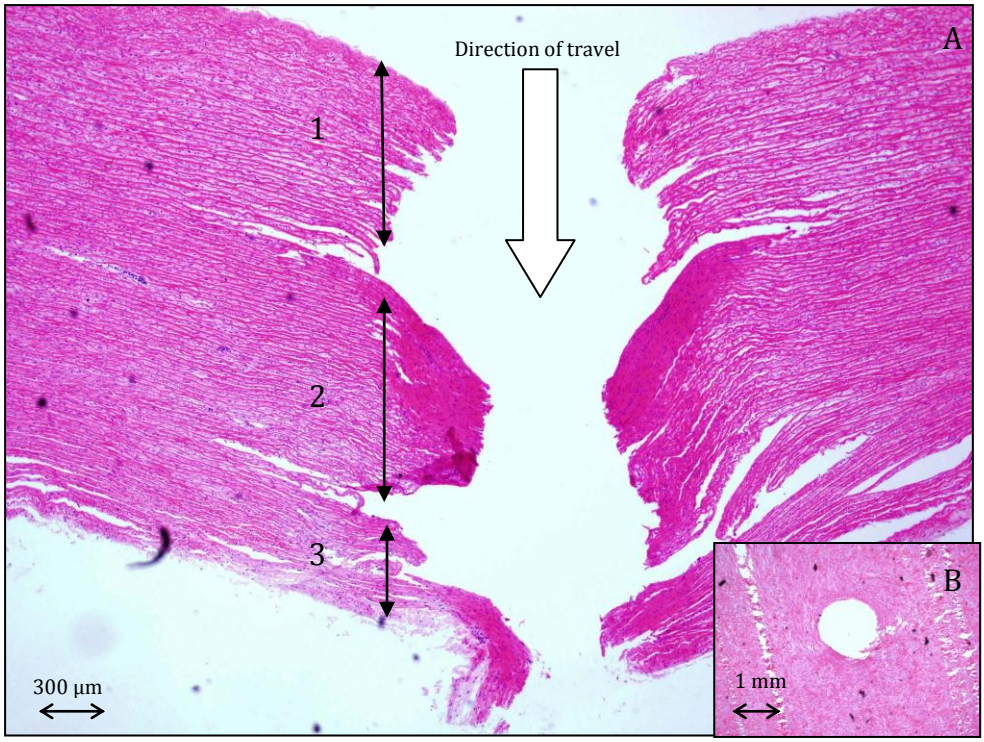

Figure 5-15 : A) Perforation of artery with energised wire waveguide, amplitudes of vibration of 27.8 µm, 20x. B) Plan view of point of entry, 4x.

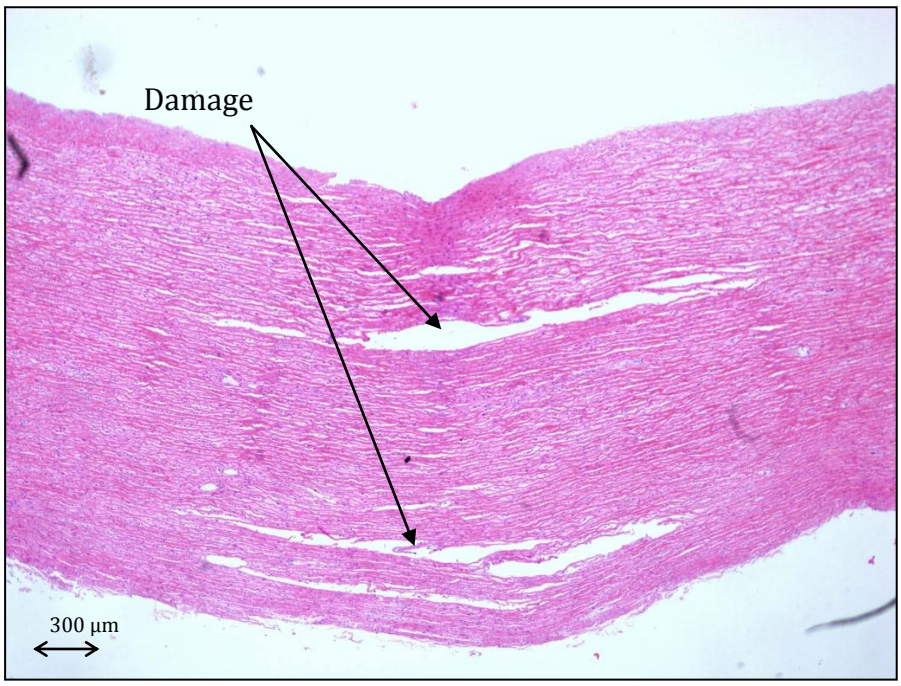

Figure 5-16 : Section cut from peripheral of point of entry. Lateral damage from a three stage perforation, 20x.

5.4.3 Conclusion of phase two tissue tests

- The phase two tissue tests show that the energised wire waveguide perforate the artery with lower forces than a non-energised wire waveguide. An increase in the wire waveguide distal tip amplitudes of vibration results in lower perforation forces.
- A significant reduction in perforation initiation force, perforation initiation energy and total perforation energy is measured with the energised wire waveguide at the lower amplitudes of vibration (< 27.8 μm). Increasing the amplitudes of vibration above this may not yield significantly lower perforation forces and energies.
- Inertial cavitation and its effects on the perforation forces were examined here. Operation of the waveguide in the inertial cavitation region appears to have no significant effect on the perforation force and energy. This ablation mechanism may however have a greater affect on hard brittle tissues, but for soft tissues, such as the aorta wall, direct mechanical contact between waveguide and tissue appear to be the primary tissue disruption mechanism.
- Histological examination of the tissue revealed a relatively thin adventitia layer in the porcine aorta when compared with the media layer. As a result, it was evident that there were multiple distinct failures within the media layer alone, ruling out the possibility that failure occurred at the boundaries between arterial layers (intima/media/adventitia), contrary to the initial hypothesis from phase one test results.

- When no ultrasound is applied, tissue fibres appear sheared. The forces applied by the wire waveguide may build up to a point where the elastic limit of the tissue is compromised and sudden failure occurs. These large forces appear to be great enough to then fully perforate the tissue.
- Histological examination show evidence of tissue removal when the tissue is perforated with an energised wire waveguide.
- Large variance in perforation force and energy is seen when the wire waveguide is non-energised. This may be attributed to the heterogeneity of the tissue samples. The standard deviation from the mean forces and energies are lower when the waveguide is ultrasonically energised. The lowest standard deviation occurring at amplitudes of vibration of 27.8 μm. This may suggest that, despite the tissues heterogeneity, the energised waveguide is performing a controlled cutting action, reaching its most efficient at amplitudes of vibration of 27.8 μm.
- With an energised wire waveguide, a more controlled cutting action appears to be occurring. Locally, the tissue may be failing from high strain rates and fatigue caused by the high frequency mechanical vibrations. The high frequency cyclic impact may be pounding and compressing the tissue until failure occurs.
- Although perforation occurs at lower forces with the energised wire waveguide when compared to the non-energised wire waveguide, tissue damage and removal both seem greater. Compression of the fibres is most evident with the second perforation stage, as seen in Figure 5-15. One possible explanation of this may be as follows.

i. Wire waveguide distal tip perforates the tissue initially. The first perforation initiation stage in then complete.

ii. As this fails the cantilever recoils upward and the second stage perforation begins. At this point the wire waveguide is now subject to loading both directly ahead and laterally (friction by tissue at sides of waveguide). This may impede the cutting action of the wire waveguide and cause larger forces for the second perforation. The compression of the fibres at this point is an indicator of this. It appears also that tissue removal is most evident in the initial perforation, whereas, the second and third perforation stages appear to have less tissue removal.

- This work shows that when high frequency vibrations are applied to waveguides, the range of forces and energy to perforate the tissue are more predictable. This may allow for greater control of tissue removal. The results may aid device design and power selection during precision tissue removal applications.

5.5 Phase three tissue tests

This tissue testing phase was designed to more closely represent *in vivo* conditions, whereby a range of feedrates and angle of approach would be more applicable. Phase three examines the following:

i. Effects of feedrate on tissue perforation forces.
ii. Effects of angled entry on perforation forces.
iii. Effects of feedrate and wire waveguide distal tip amplitudes of vibration on tissue temperature rise (ΔT).

5.5.1 Effects of feedrate on tissue perforation forces

Tissue failure is caused by a combination of the wire waveguide being driven into the tissue by the motor and lead screw but also by the cyclic impact from the vibrating wire waveguide distal tip. To this point, only the effects of ultrasound for a range of distal tip amplitudes of vibration on perforation force and energy at a fixed feedrate have been examined. This test is designed to examine the effects of feedrate on the perforation forces.

5.5.1.1 Methodology

For this experiment three different distal tip amplitudes of vibration were examined (0, 27.8 and 34.3 μm). For these three amplitudes of vibration settings the effects of a range of feedrates on perforation initiation force were examined (19, 38, 57, 76 and 95 ±0.2 mm/min), i.e. multiples of 19 mm/min. For each test run, six tissue samples (n = 6) were used. In total 90 tissue samples were tested, 30 samples per amplitude of vibration. Tissue samples for this test were processed according to the tissue preparation protocol outlined in Section 5.2

5.5.1.2 Results

5.5.1.2.1 No ultrasound, non-energised wire waveguide, 0 µm

The effects of the range of feedrates for a non-energised wire waveguide show no statistical difference in perforation initiation force (CI = 0.95). The results are plotted in Figure 5-17. The largest mean perforation initiation force and largest standard deviation (6.95 N, σ = 1.47 N) is seen with the slowest feedrate (19 mm/min), but it is not statistically different from all other feedrates (CI = 0.95). The mean perforation initiation force reduces by 1.7 N for the faster feedrate of 38 mm/min. For all other feedrates above 38 mm/min the mean value does not deviate by more than 0.4 N. The lowest standard deviation occurs at feedrates of 76 mm/min (σ = 0.72 N).

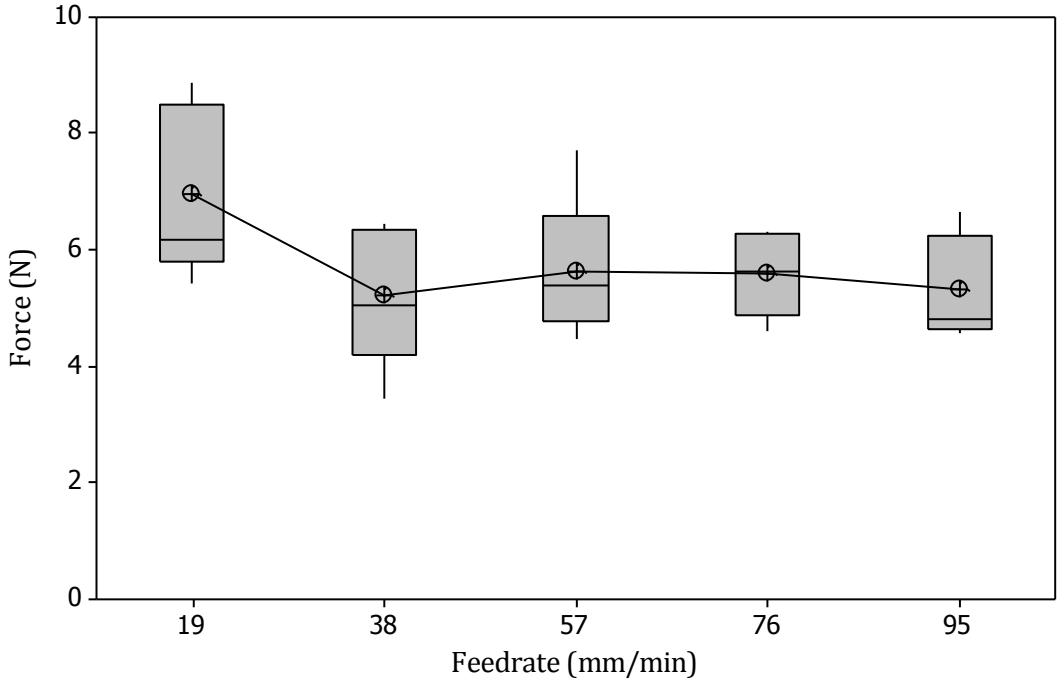

Figure 5-17 : Perforation initiation force for a range of feedrates (19-95 mm/min) for a non-energised wire waveguide.

5.5.1.2.2 Energised wire waveguide with amplitudes of vibration of 27.8 µm

With the energised wire waveguide producing amplitudes of vibration of 27.8 µm at the distal tip, the perforation initiation force for the range of feedrates (19- 95 mm/min) is shown in Figure 5-18. The perforation initiation force for the feedrate of 19 mm/min is statistically different from the perforation initiation force at 76 mm/min (CI = 0.95). Higher mean perforation forces (3.07 N mean, σ = 0.39 N) were again seen at the slowest feedrate of 19 mm/min. The lowest perforation initiation force and standard deviation (2.08 N, σ = 0.3 N) was seen at a feedrate of 76 mm/min. A 1 N (30%) reduction is measured between the highest and lowest mean perforation forces.

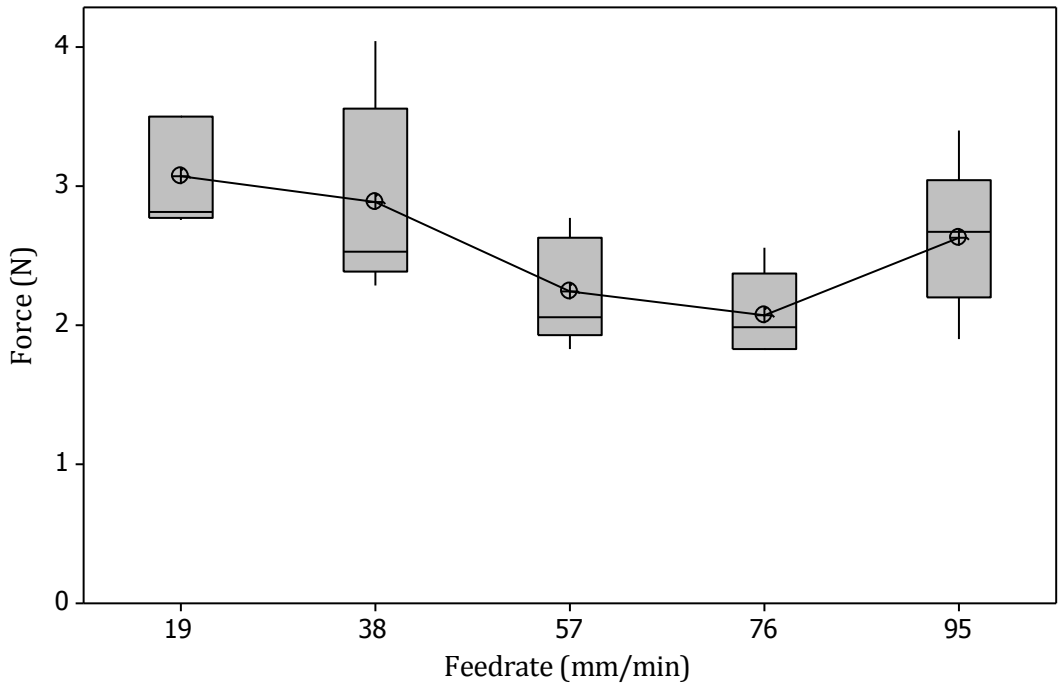

Figure 5-18 : Perforation initiation force for a range of feedrates (19-95 mm/min) for an energised wire waveguide with amplitude of vibration of 27.8 µm.

5.5.1.2.3 Energised wire waveguide with amplitudes of vibration of 34.3 µm

A reduction in perforation initiation force is observed for all feedrates, as expected, with the higher amplitude of vibration of 34.3 µm. No statistical difference was seen in the perforation initiation force for the range of feedrates, as can be seen in Figure 5-19 (CI = 0.95). The lowest mean perforation force and standard deviation occurred at a feedrate of 38 mm/min (1.26 N, σ = 0.1368). The greatest mean perforation initiation force (1.63 N, σ = 0.1871 N) was experienced at the higher feedrates of 95 mm/min.

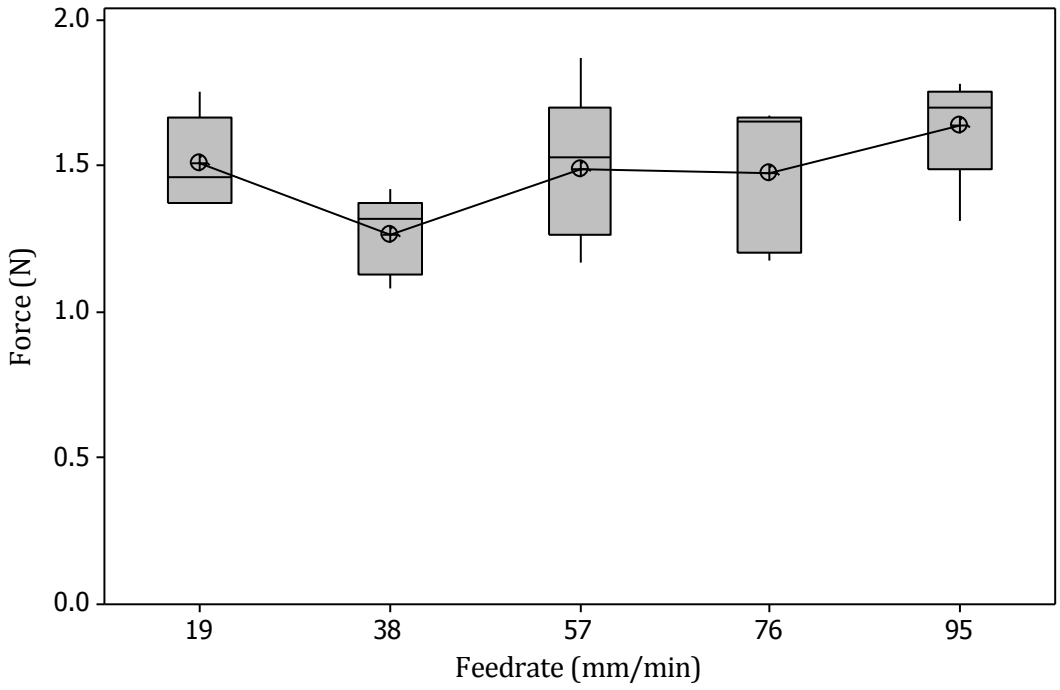

Figure 5-19 : Perforation initiation force for a range of feedrates (19-95 mm/min) for an energised wire waveguide with amplitude of vibration of 34.3 µm.

5.5.2 Effects of angled entry on perforation forces

The aim of this suite of tests was to examine the effects of angled entry on the perforation initiation force. This scenario may be more applicable to *in vivo* conditions whereby the wire waveguide may not approach the artery wall at 90 degrees. For this experiment a 45 degree angle of approach was examined, eccentric lesions may cause of such an approach. An illustration of this scenario is shown in Figure 5-20. One challenge for this test was to get the wire waveguide to engage the tissue at this angle rather than deflecting parallel to the wall and sliding along the inner lumen.

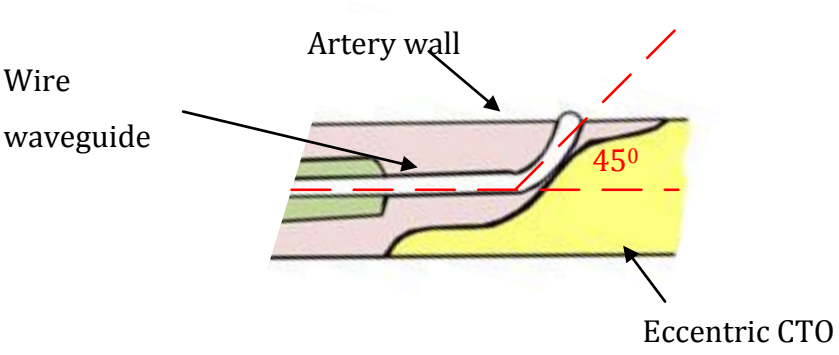

Figure 5-20 : 45 degree angle of approach.

5.5.2.1 Methodology

For this test, a tissue holder attachment was designed and manufactured which could be used with the current cantilever force measurement device. This is a 45 degree compensator. A schematic of this arrangement is shown in Figure 5-21. The cantilever strain gauge arrangement was re-calibrated to include the additional mass of this attachment. Tissue samples were placed in an 8.0 mm deep slot and were then secured by an upper plate. This attachment block and

the upper plate allowed for complete perforation of the tissue. An image of the cantilever with the 45^0 compensator is shown in Figure 5-22. The tissue was clamped by the upper plate in such a manner that it could not slip or be pushed from its position. To examine the effects of angled entry on the perforation initiation force, three amplitudes of vibration (0, 27.8 and 34.3 μm) were examined at a constant feedrate of 38 mm/min. Six tissue samples were tested (n = 6) for 45 degree and 90 degree. 36 test runs in total.

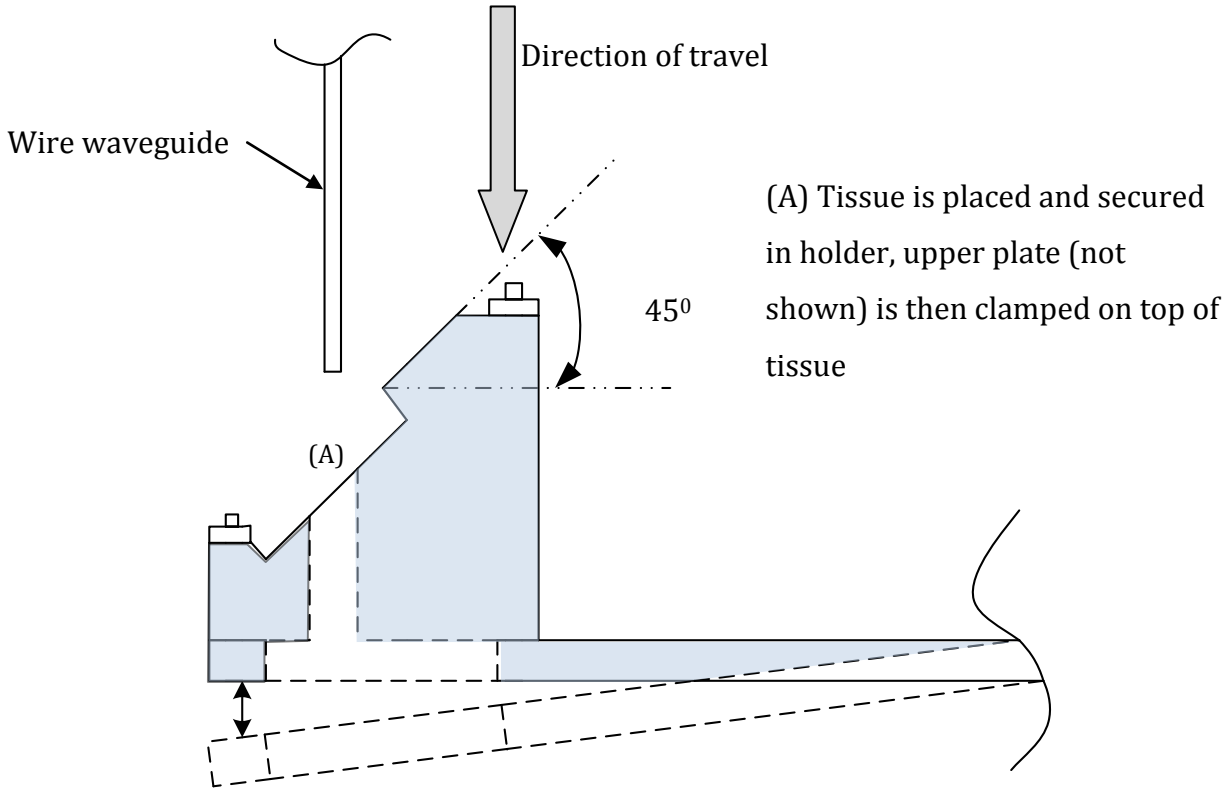

Figure 5-21 : Schematic of cantilever beam force measurement device with 45 degree angle compensator.

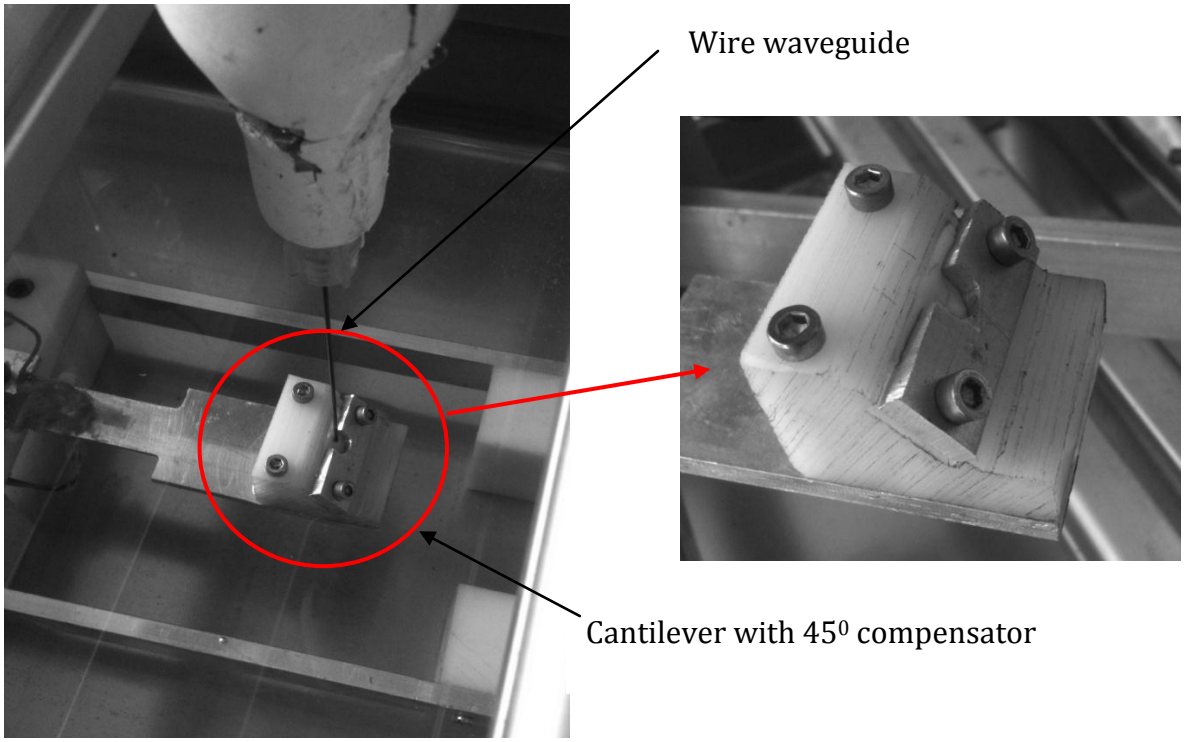

Figure 5-22 : Image of cantilever beam force measurement device with 45 degree angle compensator.

5.5.2.2 Results

Figure 5-23 shows the perforation initiation forces for the angled entry test for amplitudes of vibration of 0, 27.7 and 34.3 µm. For each set of amplitude of vibration, tests were carried out at a 45 degree and 90 degree angle of approach. The results for each set are contained in a red box.

In any case, the forces required for perforation initiation for both 45 and 90 degrees were not statistically different (CI = 0.95); the maximum difference in mean perforation initiation force for 90 degree and 45 degree differed by no more than 28 % (measured at 27.8 µm). For 0 µm and 27.8 µm the mean value for perforation initiation force was lower for 45 degrees (5.43 and 2.06 N respectively) than for the 90 degree angle of approach (6.1 N and 2.88 N). For tests using amplitudes of vibration of 34.3 µm, mean perforation initiation

forces were lower for the 90 degree angle of approach. The difference between the mean perforation initiation forces for 45 and 90 degrees at amplitudes of vibration of 34.3 µm was the smallest for all three distal tip settings (1.37 and 1.26 N, respectively).

The largest standard deviation (45 degree, δ = 0.59 and 90 degree, δ = 0.66) is present with 0µm (i.e. no ultrasound) and this may be related to the heterogeneity of the tissue. With ultrasound, the standard deviation is lowest, as can be seen with 34.3 µm (45 degree, δ = 0.29 and 90 degree, δ = 0.13).

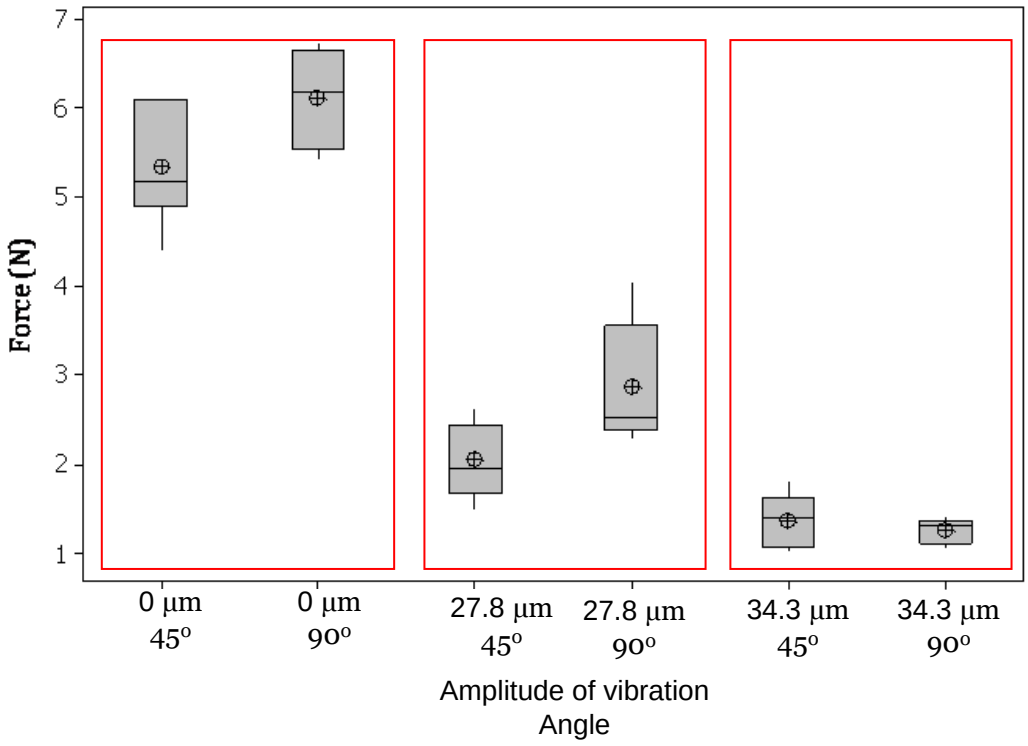

Figure 5-23 : Perforation initiation force for 0, 27.8 and 34.3 µm for 45 degree and 90 degree angle of approach to tissue.

5.5.3 Effects of feedrate and wire waveguide distal tip amplitudes of vibration on tissue temperature rise (ΔT)

Heating of tissue when using ultrasonic devices in medicine is commonly described. The aims of the thermal testing were to examine the temperature rise and its relationship with wire waveguide amplitudes of vibration and feedrates.

Tissue heating may be a result of:

i. Attenuation of the ultrasonic wave: For the higher intensity ultrasound, heating is often attributed to attenuation of the acoustic wave, depositing thermal energy as it passes through the medium. The high temperatures commonly observed are closely related to exposure time and operation duty.

ii. Wire waveguide internal friction: For the low frequency ultrasonic apparatus used for these tests, the emitter, the wire waveguide may also act as a heat source. The mechanical to thermal energy conversion caused by the high cyclic vibrations in the NiTi wire waveguide can cause the wire waveguide material to heat.

iii. Wire waveguide - tissue contact friction: Friction between the vibrating wire waveguide and surrounding tissue which is in contact with it can cause temperature increase which may be sufficient for cell and tissue necrosis.

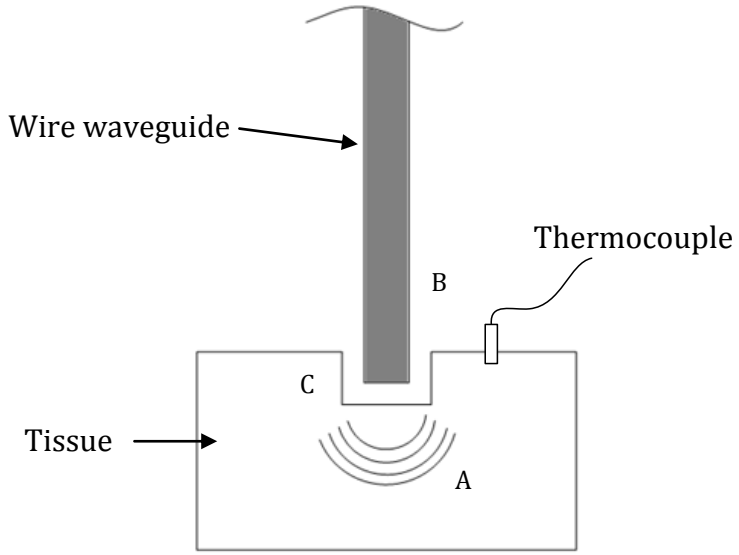

Figure 5-24 : Heating sources using ultrasonically vibrating wire waveguide. (A) Heating due to attenuation. (B) Wire waveguide as heat source. (C) Wire waveguide – tissue frictional heating.

5.5.3.1 Methodology

The measurements for the thermal tests were taken during the tissue perforation tests (phase two). A thermocouple was embedded into the surface of the tissue approximately 3.0 mm from the point of entry of the wire waveguide. Tissue samples were prepared according to the tissue preparation protocol outlined in Section 5-2; they were then placed in a container and held at thermostatic tank temperature (≈ 37 ^{0}C). It should be noted that the temperature measurement from the thermocouple lags behind the true temperature at the source as it is placed a few millimetres from the point of entry. For all tests, maximum temperatures are measured a few seconds after perforation. A drop in temperature was also used as an indicator that the maximum possible temperature had been reached.

5.5.3.1.1 Effects of amplitude of vibration on temperature

For this test, the temperature elevation (ΔT) was measured for a range of amplitude of vibrations (22.5, 27.8, 31.4 and 34.3 μm). The 1.0 mm flat distal tip wire waveguide was advanced at a constant feedrate of 38 ± 2 mm/min until the tissue was perforated. The ambient temperature (T_1) and maximum temperature during perforation (T_2) were measured. Six tissue samples were tested for each feedrate (n = 6), 24 tissue samples in total.

5.5.3.1.2 Effects of feedrate on temperature

For a constant amplitude of vibration (27.8 μm), the effects of feedrate on temperature rise (ΔT) were also examined. For this test, a range of feedrates were tested (19, 38, 57, 76, 95 ± 2 mm/min) using a 1.0 mm flat distal tip wire waveguide. Six tissue samples were tested for each feedrate (n = 6), 30 tissue samples in total.

5.5.4 Results

5.5.4.1 Effects of amplitude of vibration on temperature

The increase of amplitude of vibration at the wire waveguide distal tip resulted in an increase in ΔT. For a constant feedrate the maximum ΔT was measured at the largest amplitude of vibration of 34.3 μm. This mean value of the temperature increase was 1.8 ^{0}C (σ = 1.363). The lowest mean value temperature increase was measured with the lowest amplitude of vibration, this was 0.775 ^{0}C (σ = 0.48). The mean temperature increase (ΔT) doubled (0.852^{0}C, σ = 0.351 to 1.57 ^{0}C, σ = 0.68) from amplitudes of vibration of 27.8 μm to 31.4, respectively.

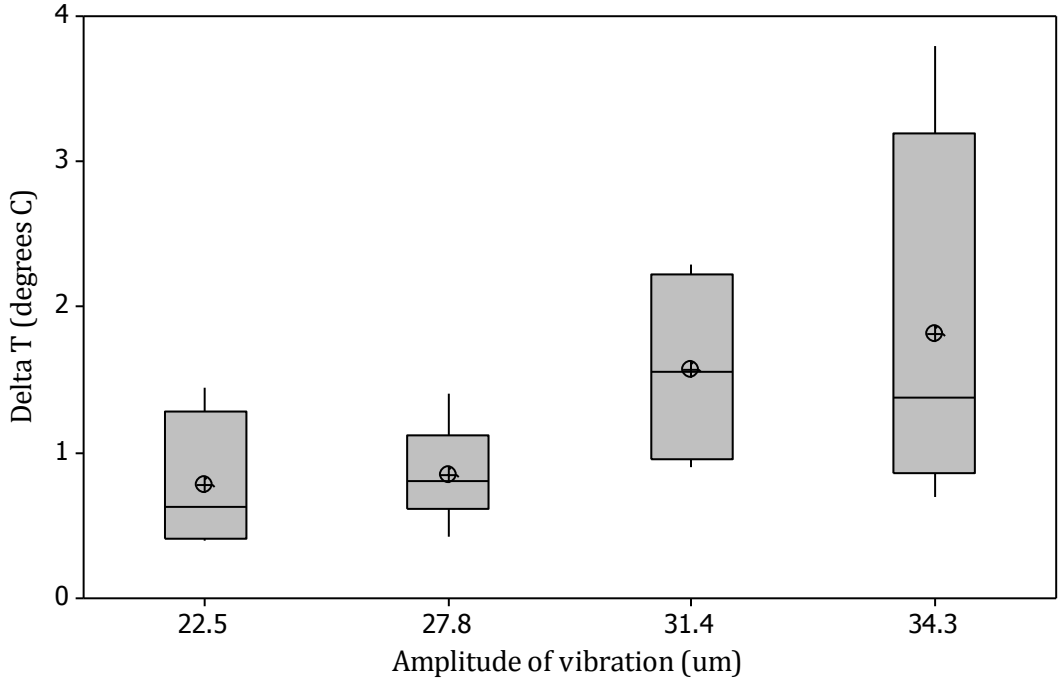

Figure 5-25 : Effects of amplitude of vibration on temperature elevation (ΔT), constant feedrate of 38 mm/min.

5.5.4.2 Effects of feedrate on temperature

The effects of feedrate on temperature are shown in Figure 5-26. The slowest feedrate of 19 ±2 mm/min resulted in the highest temperature increase of 1.7 ^{0}C (σ = 1.33, maximum 3.9 ^{0}C). Temperature increase values at 38 ±2 mm/min and 57 ±2 mm/min were very similar despite an increase in feedrate, the measurements were 0.83^{0}C (σ =1.33) and 0.88^{0}C (σ = 1.98). The lowest temperature increase was recorded at the fastest feedrate (95±2 mm/min), this was 0.437 ^{0}C (σ = 0.188). The temperature profile and force profile for a feedrate of 57 mm/min and amplitude of vibration of 27.8 μm are shown in Figure 5-27. In this example, the force and temperature profiles are closely matched. The force and temperature are related here. The multistage failure in the force profile is also evident in the temperature profile.

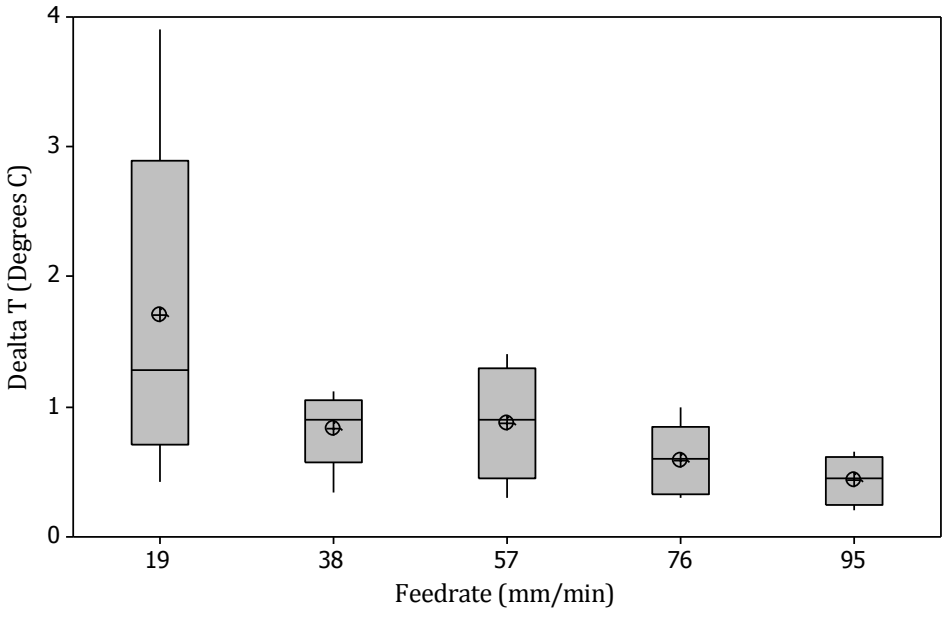

Figure 5-26 : Effects of feedrate on temperature elevation (ΔT), constant amplitude of vibration (27.8 μm).

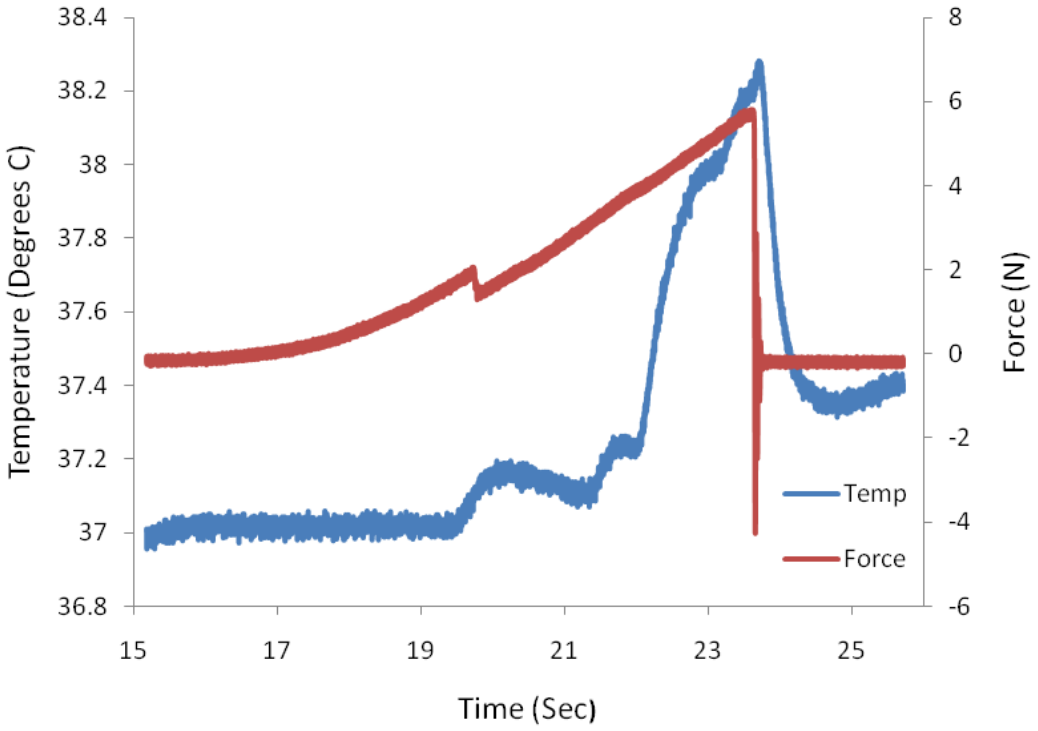

Figure 5-27 : Temperature profile and force profile example for feedrate of 57 mm/min and amplitude of vibration of 27.8 µm.

5.5.5 Conclusion of phase three tissue tests

5.5.5.1 Effects of feedrate on tissue perforation forces

A combination of feedrate and amplitude of vibration at distal tip may offer the most optimum cutting action, where efficient cutting can be attributed to lower perforation initiation forces. From these results, low perforation forces are associated with high amplitudes of vibration and slow feedrates. For amplitudes of vibration of 27. 8 µm the feedrate for lowest perforation initiation force is 76 mm/min. For tests using 34.3 µm the feedrate for lowest mean perforation initiation force has been reduced to 38 mm/min. This may suggest that at larger amplitudes of vibration at the wire waveguide distal tip the feedrate must be slower to achieve low perforation forces.

5.5.5.2 Effects of angled entry on perforation forces

No significant difference in perforation initiation force is seen with the angled point of entry. This may be explained by the soft elastic nature of the artery wall and the geometry which is perforating it. At some point, as the waveguide distal tip approaches and contacts the tissue at the 45 degree angle, one side of the distal tip will contact the tissue first and cause a stress concentration. Locally, because of the distal tip geometry, this has the effect of aligning the tissue towards the cutting face of the flat distal tip, as shown Figure 5-28. In comparison with hard tissue angled contact, the brittle nature of the tissue may cause failure at first point of contact providing a true 45 degree angle cutting. It is hypothesised that perforation *in vivo,* not only because of the elastic nature of the tissue but its anatomical position (vessel can extend in all directions) may be also well represented by a 90 degree angle entry when using flat tip wire waveguides.

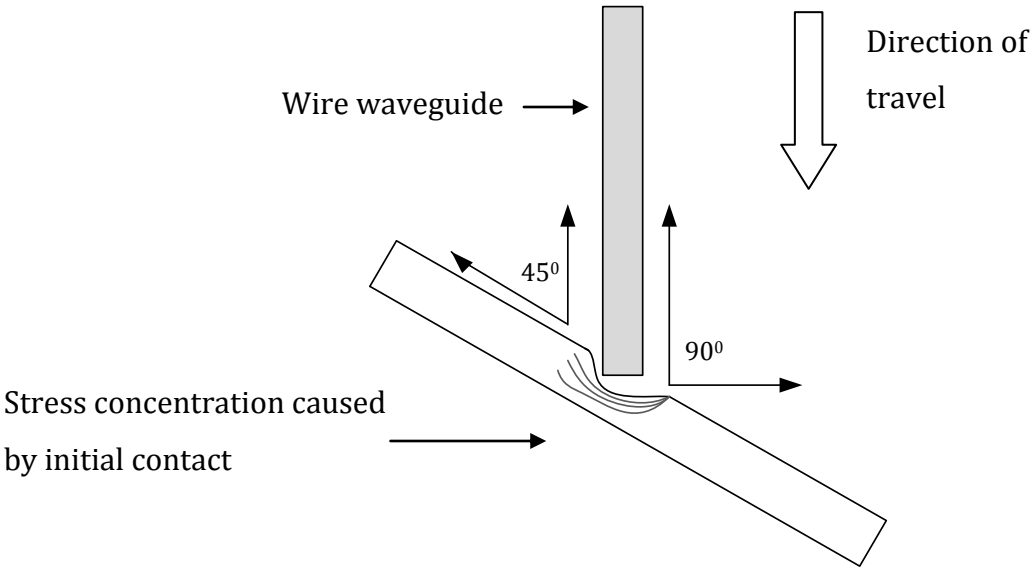

Figure 5-28 : Mechanics of soft tissue interaction with angled entry.

5.5.5.3 Effects of amplitude of vibration on temperature

It was evident that an increase in amplitude of vibration resulted in an increase in temperature of the tissue. The temperatures are not likely to cause thermal tissue damage. The temperature rose significantly after amplitudes of vibration of 27.8 μm. The temperature rise after may be attributed to cavitation heating. This form of additional heating is described in the application of phaco-emulsification. The adverse effect of this heating coupled with the force data from phase two testing may suggest that operating with amplitudes of vibration above this may not be significantly beneficial. No significant drop in perforation force is seen above 27.8 μm but there is a significant temperature increase. Since the frequency of operation is constant but amplitude of vibration is increasing, one may proffer that the temperature increase is most likely caused by lateral friction between the wire waveguide and tissue.

5.5.5.4 Effects of feedrate on temperature

For constant wire waveguide distal tip amplitude of vibration, slower feedrates resulted in a higher temperature rise. This would suggest that the temperature rise is a function of wire waveguide tissue contact time. A significant difference was seen at the slowest feedrate of 19 mm/min. For feedrates after this, the temperature increase remained relatively constant. When comparing the perforation initiation force for the same range of feedrates with the temperature data, one may offer the conclusion that heating is also closely related to the contact forces, this is evident in the force profile and temperature profile comparison, shown in Figure 5-27.

CHAPTER

6 CONCLUSION

6.1 Summary of results

The modified ultrasonic apparatus used in this research for tissue testing operates at a fixed frequency of 22.5 kHz and is capable of delivering ultrasonic amplitudes of vibration to a radiused and flat 1.0 mm wire waveguide distal tip for the extended periods of time required for tissues testing. Tests were conducted with a non-energised wire waveguide (0μm) and with an energised wire waveguide at four set amplitudes of vibration (22.5, 27.8, 31.4 and 34.3 μm). For feedrate tests the feedrates were 19, 38, 57, 76 and 95 mm/min. Over 222 arterial aortic tissue samples were tested in these studies. The aorta was extracted from over 30 porcine cadavers. The objectives set out in Figure 2-21 have all been achieved.

6.1.1 Tissue perforation force profile

- The force required to perforate the artery wall using a radiused distal tipped non-energised wire waveguide is 3.8 N mean, by ultrasonically energising the wire waveguide at low amplitudes of vibration (16 μm) the perforation force is reduced to 2.66 N mean (i.e. a 30 % reduction in force). Subsequent increasing of distal tip amplitudes of vibration results in no significant reduction in perforation force.

- The force required to perforate the artery wall using a 1.0 mm flat distal tipped non-energised wire waveguide is 6.13 N, mean. A 60 % reduction in perforation initiation force (3.67 N) is measured when the wire waveguide is ultrasonically energised at low amplitudes of vibration (22.5 μm). A further 35 % reduction in perforation initiation force can be achieved by increasing the amplitude of vibration by only 5.3 μm to 27.8 μm. Increasing the wire waveguide distal tip amplitudes of vibration further to 31.4 μm only results in a 7 % decrease in mean perforation initiation force.
- For all tests the largest standard deviation in perforation forces is measured when the wire waveguide is not energised (σ = 0.60 N). The lowest standard deviation in perforation initiation forces occurs with wire waveguide distal tip amplitudes of vibrations of 31.4 μm (σ = 0.13 N). The lowest standard deviation in perforation energy occurs with distal tip amplitudes of vibration of 27.8 μm (σ = 0.22 mJ).

6.1.2 The effect of feedrate on tissue perforation forces

- The perforation forces for a range of feedrates (19 - 95 mm/min) were measured for a non-energised wire waveguide and an ultrasonically vibrating wire waveguide (27.8 μm and 34.3μm).
- The lowest mean perforation forces with the non-energised wire were at a feedrate of 38 mm/min (5.25 N, mean). The perforation forces for the range of feedrates, however, were not statistically different (CI = 0.95).

- For an ultrasonically vibrating wire waveguide with distal tip amplitudes of vibration of 27.8 μm the lowest perforation initiation force is measured at a feedrate of 76 mm/min (2.08 N mean). This perforation initiation force is 30 % lower than the highest perforation initiation force (3.07 N, mean) measured for this range of feedrates and is statistically different from all other feedrates (CI = 0.95).
- For an ultrasonically vibrating wire waveguide with distal tip amplitudes of vibration of 34.3 μm the lowest perforation initiation force is measured at a feedrate of 38 mm/min (1.26 N mean). The highest perforation initiation force is measured at the fastest feedrate of 95 mm/min (1.63 N, mean). The perforation initiation forces across the range of feedrates are not statistically different (CI = 0.95).

6.1.3 The effect of cavitation on the tissue perforation forces

- Using a 1.0 mm diameter flat wire waveguide distal tip, inertial cavitation for the ultrasonic apparatus used in tissue testing occurs with amplitudes of vibrations greater than 31.4 μm. According to the FEA, for a flat wire waveguide distal this is predicted to be ≈ 0.3 MPa. This correlates well with the cavitation threshold from the literature.
- There is no statistically significant change in the perforation forces and energy above this cavitation threshold (CI = 0.95). There is an increase in temperature above the cavitation threshold, the mean temperature doubled (0.85 ^{0}C to 1.57 ^{0}C).

6.1.4 The effect of angled entry on tissue perforation forces

- Initially the artery was perforated at a 90 degree angle. No statistically different data was measured in the perforation initiation force when this angle was reduced to 45 degrees (CI = 0.95).
- For a non-energised wire waveguide the perforation initiation force is largest for 90 degree angle of approach (6.1 N, mean). The perforation initiation force reduced by 11% for the 45 degree angle of approach (5.4 N, mean).
- A 28% reduction in mean perforation initiation force was measured with wire waveguide distal tip amplitudes of vibration of 27.8 μm when angled at 45 degrees (from 2.88 N to 2.06 N).
- An 8% increase in mean perforation initiation force was measured with wire waveguide distal tip amplitudes of vibration of 34.3 μm when angled at 45 degrees (from 1.26 N to 1.37 N).

6.1.5 The effects of wire waveguide distal tip amplitudes of vibration on temperature

- The largest mean temperature increase (ΔT) was measured at the greatest amplitude of vibration (34.3 μm). This was 1.8 ^{0}C (mean). The largest ΔT measured at this amplitude of vibration was 3.8 ^{0}C. The lowest temperature rise (ΔT) was measured with the lowest wire waveguide distal tip amplitude of vibration (22.5 μm).

- Increasing the amplitude of vibration to 27.8 μm results in only a mean ΔT increase of 10%. Increasing the distal tip amplitudes of vibration further to 31.4 μm results in a mean ΔT increase of 45%. Increasing the amplitudes of vibration to 34.3 μm results in a mean ΔT increase of only 12 %.

6.1.6 The effects of feedrate and wire waveguide distal tip amplitudes of vibration on temperature

- The effects of feedrate on temperature increase, ΔT, were also examined. The feedrates tested were 19, 38, 57, 76 and 95 mm/min. The largest ΔT was measured with the slowest feedrate of 19 mm/min. This was a mean ΔT of 1.7 ^{0}C. The maximum ΔT was 3.9 ^{0}C at this feedrate. There was no statistically different ΔT for the range of feedrates 38 – 95 mm/min (CI = 0.95).

6.1.7 Numerical analysis

6.1.7.1 Mesh density analysis

For the frequency range (20 – 50 kHz) and wire waveguide distal tip amplitudes of vibration used in clinical and experiment testing of the ultrasonic wire waveguides (0 – 60 μm), the pressure profile was predicted and compared to an analytical solution for simple distal tip geometries. The mesh density required to model these devices was found to be 140 Elements Per Wavelength (EPW).

6.1.7.2 Effects of wire waveguide distal tip

- For a fixed frequency and wire waveguide distal tip amplitude of vibration a 1.0 mm flat wire waveguide distal tip produces double the maximum pressures which can be achieved by a 1.0 mm radiused distal tip. Increasing the diameter of the flat wire waveguide from 1.0 mm to 2.0 mm produces double the maximum pressure at the distal tip.
- For a fixed frequency of 22.5 kHz, the maximum wire waveguide distal tip pressure for a 1.0 mm radiused distal tip can be as high as 350 kPa at amplitudes of vibration of 60 μm. With a cavitation threshold of 0.1 – 0.2 MPa, this wire waveguide will cause cavitation at amplitudes of vibration ≈ 25 – 40 μm.
- For a fixed frequency of 22.5 kHz, the maximum wire waveguide distal tip pressure for a 1.0 mm flat distal tip can be as high as 550 kPa at amplitudes of vibration of 60 μm. With a cavitation threshold of 0.1 – 0.2 MPa, this wire waveguide will generate cavitation at amplitudes of vibration ≈ 10 – 25 μm.
- Experimental data for the 1.0 mm diameter flat distal tip wire waveguide for the same frequency of operation (22.5 kHz) shows the inertial cavitation occurring above amplitudes of vibration of 31.4 μm. The FEA model predicts that this amplitude of vibration for these conditions produces maximum pressures of ≈ 0.3 MPa at the wire waveguide distal tip.
- Using 140 EPW the FEA model could accurately predict the standing wave amplitude of vibrations and nodes which were measured

experimentally by others. This model could account for wave interactions created by an air interface.

6.2 Conclusions from this work

- Ultrasonically energised vibrating wire waveguides can perforate the artery at lower forces than non-energised wires.
- Increasing wire waveguide distal tip amplitude of vibration results in decreasing perforation forces. There is a significant decrease in perforation force at low distal tip amplitudes of vibration but no significant drop in perforation force is seen above amplitudes of 27.8 μm. The additional power will not reduce the perforation force but does cause heating which, over longer periods of time, can cause tissue damage.
- Single event failure of the artery wall occurs with non-energised wire waveguides. Ultrasonically energised wire waveguides produce multiple sequential failures in the media layer of the artery wall during perforation suggesting that the tissue is failing locally. This is evident in both the force profile and histological examination.
- Operation of the wire waveguide in the cavitation region does not seem to play a primary role in perforation force and energy reduction. It may however contribute to heating. Further investigation on its effects in temperature increase and residual tissue damage is therefore required.

- Pushing and probing of the ultrasonically energised wire waveguide over a range of feedrates is also more applicable to *in vivo* conditions. For the range of feedrates examined here (19 – 95 mm/min) there is no significant change in the artery wall perforation forces for both the non-energised and ultrasonically energised wire waveguide. A trend of low mean perforation forces for a particular feedrate may be observed from the data, more tests are required to establish significant changes in the perforation force. Generally, for non-energised and ultrasonically energised wire waveguides higher perforation forces are measured with lower feedrates (19 mm/min).
- Histological analysis of aortic tissue, which have been perforated by the ultrasonically energised wire waveguide, show tissue removal. Non-energised wire waveguide shear the tissue fibres and do not appear to remove tissue.
- When using non-energised wire waveguides there is a large standard deviation in the perforation forces. The standard deviation in the perforation forces is reduced when the wire waveguide is ultrasonically energised at all settings.

- There is a temperature rise in the tissue when the artery is perforated by the ultrasonically energised wire waveguide. Increasing amplitudes of vibration and decreasing feedrate results in greater temperature increase of the tissue at the wire waveguide point of entry. There is also a doubling of the mean temperature rise as the device operates across the inertial cavitation threshold. It is not obvious whether this is a result of the increase of distal tip amplitude of vibration or the presence of cavitation.
- The temperature rise (ΔT) measured for increasing wire waveguide distal tip amplitudes of vibration over a range of feedrates for the duration of contact time is not sufficient to cause thermal tissue damage ($< 4\ ^{0}C$).
- Given the low acoustic intensity and low attenuation values for conditions encountered during use of ultrasonically energised wire waveguides on tissue, the temperature increase is most likely due to heat generated by frictional forces between the wire waveguide and the tissue and not attenuation of the ultrasonic wave.
- The goal of the experimental tissue testing conducted as part of this research is designed to gain insight into the soft tissue-wire waveguide interaction. The experiments were designed to represent these devices *in vivo* under clinical conditions but contain some generalisations. This experimental tissue testing is the first of its kind and is designed to examine these devices under highly controlled and repeatable conditions. Where one or more variable is manipulated to determine its effect on a dependent variable. For this

reason, the results are limited in terms of a direct comparison with what would be expected to occur *in vivo*.

- The acoustic Finite Element Analysis (FEA) of the wire waveguide distal tip can predict the acoustic pressures generated for typical frequencies and amplitudes of vibrations used in wire waveguide tissue ablation and disruption. This analysis shows that the FEA method can be used to predict the pressures generated by the wire waveguide distal tip in simulated *in vivo* conditions and therefore can be used as a design tool for development and improvement of these devices.
- With sufficient mesh densities a linear FEA acoustic model can accurately predict the pressures directly at the wire waveguide distal tip and can also predict the entire acoustic field, including the standing wave structure created by an interface of acoustic media with different attenuation properties. The FEA acoustic model is shown to accurately predict the pressures measured experimentally from a study of a simulated peripheral artery with multiple fluids.
- Using a cavitation threshold and the pressures predicted by the acoustic FEA, the wire waveguide distal tip amplitudes of vibration and frequency required to generate the pressures sufficient for cavitation can be predicted.
- The FEA acoustic model is an approximation of the system, the resolution of which is determined by the mesh density. The accuracy of the model is also highly depended on valid input material properties. This model assumed linear acoustic properties of the

liquid medium. The liquid medium representative of blood is also modelled as a homogenous liquid and does not take into consideration that blood is a suspension. Despite these assumptions, for the pressure ranges of interest, this FEA method can provide accurate solutions useful in the design and improvement of these devices.

6.3 Recommended future directions

- The ultrasonic wire waveguide device has been shown to perforate and remove soft tissue at lower forces than a non-ultrasonically vibrating wire waveguide. An investigation into the design of new MIS cutting devices using this technology would be extremely beneficial. This may include a new supporting catheter and an investigation into a number of new MIS cutting applications for a range of tissue types.
- Examining the perforation or cutting of thicker soft tissue samples using this device and methodology presented in this research may also be useful. Tissue fracture toughness for a range of tissue types may be then calculated when using the force data from the perforating ultrasonically vibrating wire waveguides. Experimental data for the tissue, such as fracture properties could then be used in FEA to model the tissue perforation.
- Establishing accurate attenuation coefficients for the acoustic medium (i.e. blood) at the low ultrasonic frequencies can also provide important data for numerically modelling acoustic streaming and heating.

- The failure mechanisms of the soft tissue subjected to ultrasonically energised wire waveguide perforation should also be investigated in more detail. There is evidence which suggests that cyclic mechanical impact of the wire waveguide and the artery may cause the arterial tissue to stiffen, an effect of high strain rate, causing fracture and removal of tissue fibres by fatigue failure.
- Testing larger tissue samples or entire sections of vessels would be beneficial in determining the perforation forces more representative of *in vivo* conditions. In some cases larger test sample sizes may identify acute differences between the perforation forces for the range of test variables examined during this research.
- For assessing the risk of arterial perforation using the ultrasonically vibrating wire waveguides in CTO recanalisation, it may be more realistic to examine the wire waveguide in a blocked artery with a CTO lesion or mock CTO lesion. Bends and bifurcations in the artery may cause the ultrasonically vibrating wire waveguide to deflect and contact the artery wall; this may also require further investigation.
- This study shows evidence of soft tissue removal when using ultrasonically vibrating wire waveguides; it may be possible to examine the particulate or debris size distribution.
- One MIS field where this knowledge might be useful is Natural Orifice Transluminal Endoscopic Surgery (NOTES). NOTES performs surgical interventions by accessing anatomical systems through natural orifices such as the mouth, ears and anus. The ultrasonically vibrating wire waveguides may be used for NOTES as it has been shown that soft vessel

walls can be accessed at lower forces. The forces and energies presented in this research may also prove useful in future development of robotic or haptic surgery using ultrasonically vibrating wire waveguides.

- Obtaining an accurate inertial cavitation threshold for blood *in vivo* at the frequencies typically used with these devices would help identify when cavitation is occurring in clinical applications. This threshold could be obtained experimentally using the hydrophone cavitation detection system outlined as part of this work.
- Acoustic streaming was not considered as a contributing mechanism in tissue perforation for this research programme. A quantitative analysis of the fluid flow velocities and its effects on soft tissue should be investigated.

7 REFERENCES

[1] N. G. William, W. Chen, P. Lee *et al.*, "Initial experience and safety in the treatment of chronic total coronary occlusions with a new optical coherent reflectometry-guided radiofrequency ablation guidwire," *The American Journal of Cardiology,* vol. 92, no. 6, pp. 732-734, 2003.

[2] R. J. Siegel, J. Gunn, A. Ahsan *et al.*, "Use of therapeutic ultrasound in percutaneous coronary angioplasty. Experimental in vitro studies and initial clinical experience," *Circulation,* vol. 89, no. 4, pp. 1587-1592, April 1, 1994, 1994.

[3] U. Rosenschein, A. Frimerman, S. Laniado *et al.*, "Study of the mechanism of ultrasound angioplasty from human thrombi and bovine aorta.," *American Journal of Cardiology,* vol. 74, pp. 1263-6, 1994.

[4] H. Al-Ameri, G. S. Mayeda, and D. M. Shavelle, "Use of high-frequency vibrational energy in the treatment of peripheral chronic total occlusions," *Catheter Cardiovasc Interv,* vol. 74, no. 7, pp. 1110-5, Dec 1, 2009.

[5] L. L. Demer, M. Ariani, and R. J. Siegel, "High Intensity Ultrasound Increases Distensibility of Calcific Atherosclerotic Arteries," *Journal of the American College of Cardiology,* vol. 18, pp. 1259-62, 1991.

[6] U. Rosenschein, L. A. Rozenszajn, L. Kraus *et al.*, "Ultrasonic angioplasty in totally occluded peripheral arteries. Initial clinical, histological, and angiographic results," *Circulation,* vol. 83, no. 6, pp. 1976-1986, June 1, 1991, 1991.

[7] I. R. S. Makin, and E. C. Everbach, "Measurement of pressure and assessment of cavitation for a 22.5-kHz intra-arterial angioplasty device," *Acoustic Society of America*, 1996.

[8] S. Atar, H. Luo, T. Nagai *et al.*, "Ultrasonic Thrombolysis: Catheter-Delivered and Transcutaneous Applications " *European Journal of Ultrasound,* vol. 9, no. 1, pp. 39-54, 1999.

[9] "Press Release: FlowCardia Inc. Receives European Regulatory Approval and Successfully Completes U.S. Feasibility Clinical Trial," FlowCardia Inc., 2005, p. Press Release.

[10] "Press Release: FlowCardia, Inc. Announces 510(k) Clearance for the CROSSER™ 14 Chronic Total Occlusion Recanalization System - A New, Minimally Invasive Option to Bypass Surgery," FlowCardia, Inc., 2007.

[11] B. Meier, *Current Best Practice in Interventional Cardiology*, p.^pp. 43-44: John Wiley and Sons, 2009.

[12] J. A. Grantham, S. P. Marso, J. Spertus *et al.*, "Chronic total occlusion angioplasty in the United States," *JACC Cardiovasc Interv*, 6, pp. 479-86, United States, 2009.

[13] G. P. Gavin, "Experimental and numerical investigation of therapeutic ultrasound angioplasty," School of Mechanical & Manufacturing Engineering, Dublin City University, Dublin, 2005.

[14] R. E. Klabunde, *Cardiovascular Physiology Concepts*: Lippincott Williams and Wilkins, 2005.

[15] N. V. Salunke, and L. D. T. Topoleski, “Biomechanics of atherosclerotic plaque,” *Critical Reviews in Biomedical Engineering,* vol. 25, pp. 243-285, 1997.
[16] J. M. Clarke, and S. Glagov, “Structural integration of the arterial wall. I. Relationships and attachments of medial smooth muscle cells in normally distended and hyperdistended aortas.,” *Journal of Laboratory Investigation,* vol. 40, no. 5, pp. 587-602, 1979.
[17] G. A. Holzapfel, "Collagen in arterial walls: Biomechanical aspects," *Collagen. Structure and Mechanics*, P. Fratzl, ed., pp. 285-324, Heidelberg: Springer-Verlag, 2008.
[18] T. C. Gasser, R. W. Ogden, and G. A. Holzapfel, “Hyperelastic modelling of arterial layers with distributed collagen fibre orientations.,” *Journal of the Royal Society Interface.,* vol. 3, no. 6, pp. 15-35, 2006.
[19] M. DeWood, J. Spores, R. Notske *et al.*, “Prevalence of total coronary occlusion during the early hours of transmural myocardial infarction,” *N Engl J Med,* vol. 303, no. 16, pp. 897-902, Oct, 1980.
[20] R. Ross, J. Glomset, and L. Harker, “Response to injury and atherogenesis,” *The American journal of pathology,* vol. 86, no. 3, pp. 675-84, 1977.
[21] H. C. Stary, “The sequence of cell and matrix changes in atherosclerotic lesions of coronary arteries in the first forty years of life.,” *European Heart Journal,* vol. 11, pp. 3-19, 1990.
[22] J. L. Goldstein, and M. S. Brown, “The low-density lipoprotein pathway and its relation to atherosclerosis.,” *Annual review of biochemistry,* vol. 46, pp. 897-930, 1977.
[23] E. Maher, A. Creane, S. Sultan *et al.*, "Tensile and compressive properties of fresh human carotid atherosclerotic plaques," *J Biomech*, 16, pp. 2760-7, United States, 2009.
[24] T. Matsumoto, H. Abe, T. Ohashi *et al.*, “Local elastic modulus of atherosclerotic lesions of rabbit thoracic aortas measured by pipette aspiration method,” *Physiol Meas,* vol. 23, no. 4, pp. 635-48, Nov, 2002.
[25] S.-i. Katsuda, M. Hasegawa, M. Kusanagi *et al.*, “Regional characteristics of the harmonic components of the pressure pulse wave in the atherosclerotic aorta of the Kurosawa and Kusanagi-hypercholesterolemic (KHC) rabbit,” *Pathophysiology,* vol. 5, no. 1, pp. 67-72, 1998.
[26] H. M. Loree, A. J. Grodzinsky, S. Y. Park *et al.*, "Static circumferential tangential modulus of human atherosclerotic tissue," *J Biomech*, 2, pp. 195-204, United States, 1994.
[27] A. C. Simon, I. Pithois-Merli, and J. Levenson, “Physiopharmacological approach to mechanical factors of hypertension in the atherosclerotic process,” *J Hum Hypertens,* vol. 5 Suppl 1, pp. 15-21, Aug, 1991.
[28] D. Wood, M. Chandavimol, and A. Lgnaszewski, “Tried and true: Hypertension guidelines,” *The Canadian Journal of CME*, pp. 99-108, 2003.
[29] G. B. McGuinness, M. P. Wylie, and G. P. Gavin, “Ablation of chronic total occlusions using kilohertz-frequency mechanical vibrations in minimally invasive angioplasty procedures,” *Critical Reviews in Biomedical Engineering,* vol. 38, no. 6, 2010.

[30] C. Godino, A. S. Sharp, M. Carlino *et al.*, "Crossing CTOs-the tips, tricks, and specialist kit that can mean the difference between success and failure," *Catheter Cardiovasc Interv,* vol. 74, no. 7, pp. 1019-46, Dec 1, 2009.
[31] R. J. Kirvaitis, L. Parr, L. M. Kelly *et al.*, "Recanalization of chronic total peripheral arterial occlusions using optical coherent reflectometry with guided radiofrequency energy: a single center experience," *Catheter Cardiovascular Intervention,* vol. 69, no. 4, pp. 532-40, Mar 1, 2007.
[32] Y. L. Han, Y. Li, S. L. Wang *et al.*, "Multi-wire plaque crushing as a novel technique in treating chronic total occlusions," *Chinese Medical Journal (Engl),* vol. 121, no. 6, pp. 518-21, Mar 20, 2008.
[33] C. Godino, A. S. Sharp, M. Carlino *et al.*, "Crossing CTOs-the tips, tricks, and specialist kit that can mean the difference between success and failure," *Catheterization and Cardiovascular Interventions,* vol. 74, no. 7, pp. 1019-46, Dec 1, 2009.
[34] J. P. Pigott, "Crossing CTOs With the Wildcat Catheter: Experiences using a new option for crossing difficult chronic total occlusions.," *Endovascular Today*, pp. 30-38, 2011.
[35] S. B. King, 3rd, "Why have stents replaced balloons? Underwhelming evidence," *Ann Intern Med*, 10, pp. 842-3, United States, 2003.
[36] "www.Lifesciencefacts.com/coronary-angioplasty."
[37] E. Folland, *Balloon Angioplasty*, Philadelphia, 1994.
[38] G. S. Mintz, J. J. Popma, A. D. Pichard *et al.*, "Limitations of angiography in the assessment of plaque distribution in coronary artery disease: a systematic study of target lesion eccentricity in 1446 lesions," *Circulation,* vol. 93, no. 5, pp. 924-31, Mar 1, 1996.
[39] A. Sambola, V. Fuster, and J. J. Badimon, "Role of coronary risk factors in blood thrombogenicity and acute coronary syndromes," *Rev Esp Cardiol*, 10, pp. 1001-9, Spain, 2003.
[40] P. W. Serruys, H. E. Luijten, K. J. Beatt *et al.*, "Incidence of restenosis after successful coronary angioplasty: a time-related phenomenon. A quantitative angiographic study in 342 consecutive patients at 1, 2, 3, and 4 months," *Circulation,* vol. 77, no. 2, pp. 361-71, Feb, 1988.
[41] G. Dangas, and F. Kuepper, "Cardiology patient page. Restenosis: repeat narrowing of a coronary artery: prevention and treatment," *Circulation,* vol. 105, no. 22, pp. 2586-7, Jun 4, 2002.
[42] R. Jaffe, B. Courtney, and B. H. Strauss, "Chronic total occlusions, The pathobiology of CTO," R. Waksman and S. Saito, eds.: Wiley.
[43] S. Aziz, and D. R. Ramsdale, "Chronic total occlusions- A stiff challenge requiring a major breakthrough: Is there light at the end of the tunnel," *Heart,* vol. 91, pp. 42-48, 2005.
[44] "http://www.bardpv.com/_vascular/product."
[45] M. Mauser, J. Ennker, and D. Fleischmann, "Dissection of the sinus valsalvae aortae as a complication of coronary angioplasty," *Z Kardiol,* vol. 88, no. 12, pp. 1023-7, Dec, 1999.
[46] L. K. Michalis, M. R. Rees, J. A. Davis *et al.*, "Use of vibrational angioplasty for the treatment of chronic total coronary occlusions: preliminary results," *Catheter Cardiovasc Interv,* vol. 46, no. 1, pp. 98-104, Jan, 1999.

[47] R. Waksman, and S. Saito, *Chronic Total Occlusions*: John Wiley & Sons, 2011.
[48] S. B. King, "Angioplasty from bench To benchside To bench," *Circulation,* vol. 93, pp. 1621-1629, 1996.
[49] Y. L. Han, Y. Li, S. L. Wang *et al.*, "Multi-wire plaque crushing as a novel technique in treating chronic total occlusions," *Chin Med J (Engl),* vol. 121, no. 6, pp. 518-21, Mar 20, 2008.
[50] O. C. Munoz, E. Soto-Cora, K. Ali *et al.*, "Successful treatment of chronic total occlusions with the wildcat catheter," *Vascular Disease Management,* vol. 7, pp. 159-165, 2010.
[51] J. Goodkind, V. Coombs, and R. A. Golobic, "Excimer laser angioplasty," *Heart Lung,* vol. 22, no. 1, pp. 26-35, Jan-Feb, 1993.
[52] T. A. Fischell, and M. L. Stadius, "New technologies for the treatment of obstructive arterial disease.," *Catheterization and Cardiovascular Diagnosis,* vol. 22, no. 3, pp. 205-233, 1991.
[53] E. Grube, G. Sutsch, V. Y. Lim *et al.*, "High-frequency mechanical vibration to recanalize chronic total occlusions after failure to cross with conventional guidewires," *J Invasive Cardiol,* vol. 18, no. 3, pp. 85-91, Mar, 2006.
[54] R. J. Kirvaitis, L. Parr, L. M. Kelly *et al.*, "Recanalization of chronic total peripheral arterial occlusions using optical coherent reflectometry with guided radiofrequency energy: a single center experience," *Catheter Cardiovasc Interv,* vol. 69, no. 4, pp. 532-40, Mar 1, 2007.
[55] B. J. O'Daly, E. Morris, G. P. Gavin *et al.*, "High-power low-frequency ultrasound: A review of tissue dissection and ablation in medicine and surgery," *Journal of Materials Processing Technology,* vol. 200, no. 1-3, pp. 38-58, 2008.
[56] C. H. Farny, R. Glynn Holt, and R. A. Roy, "The correlation between bubble-enhanced HIFU heating and cavitation power," *IEEE Trans Biomed Eng,* vol. 57, no. 1, pp. 175-84, Jan, 2010.
[57] A. D. Maxwell, C. A. Cain, A. P. Duryea *et al.*, "Noninvasive thrombolysis using pulsed ultrasound cavitation therapy - histotripsy," *Ultrasound Med Biol*, 12, pp. 1982-94, England, 2009.
[58] M. V. Volkov, and I. S. Shepeleva, "The use of ultrasonic instrumentation for the transection and uniting of bone tissue in orthopaedic surgery," *Reconstr Surg Traumatol,* vol. 14, no. 0, pp. 147-52, 1974.
[59] A. Cardoni, MacBeath, and L. A., M, "Methods for reducing cutting temperature in ultrasonic cutting of bone," *Ultrasonics,* vol. 44, no. Supplement 1, pp. e37-e42, 2006.
[60] B. S. Khambay, and A. D. Walmsley, "Investigations into the use of an ultrasonic chisel to cut bone. Part 2: Cutting ability," *J Dent*, 1, pp. 39-44, England, 2000.
[61] R. B. Vajpayee, R. Sinha, N. Sharma *et al.*, "Evolution of phascoemulsification," *Phacoemulsification surgery*, New Delhi: Vij, J.P, 2005.
[62] I. H. Fine, M. Packer, and R. S. Hoffman, "New phacoemulsification technologies," *J Cataract Refract Surg*, 6, pp. 1054-60, United States, 2002.

[63] A. Anis, “PhacoTmesis,” *Curr Opin Ophthalmol,* vol. 7, no. 1, pp. 49-52, Feb, 1996.
[64] R. S. Hoffman, I. H. Fine, M. Packer *et al.*, "Comparison of sonic and ultrasonic phacoemulsification using the Staar Sonic Wave system," *J Cataract Refract Surg*, 9, pp. 1581-4, United States, 2002.
[65] W. J. Hodgson, “The ultrasonic scalpel,” *Bull N Y Acad Med,* vol. 55, no. 10, pp. 908-15, Nov, 1979.
[66] C. Koch, T. Friedrich, F. Metternich *et al.*, "Determination of temperature elevation in tissue during the application of the harmonic scalpel," *Ultrasound Med Biol*, 2, pp. 301-9, England, 2003.
[67] J. A. Greenberg, “Harmonic ACE, Pistol grip,” *Reviews in Obstetrics and Gynecology,* vol. 1, no. 4, pp. 198-199, 2008.
[68] M. Sridharan, *Harmonic ACE 510(K)*, FDA, 2009.
[69] T. Tanaka, K. Ueda, M. Hayashi *et al.*, "Clinical application of an ultrasonic scalpel to divide pulmonary vessels based on laboratory evidence," *Interact Cardiovasc Thorac Surg*, 6, pp. 615-8, England, 2009.
[70] S. S. Ching, A. I. Sarela, J. D. Hayden *et al.*, “Randomized clinical trial of torsional versus linear mode ultrasonically activated devices for laparoscopic cholecystectomy,” *Surg Endosc,* vol. 23, no. 7, pp. 1506-11, Jul, 2009.
[71] M. Ariani, M. Fishbein, J. S. Chae *et al.*, “Dissolution of Peripheral Arterial Thrombi by Ultrasound,” *Circulation,* vol. 84, pp. 1680- 1688, 1991.
[72] M. Chikada, “An experimental study of surgical ultrasonic angioplasty: Its effect on atherosclerosis and normal arteries,” *The Annals of Thoracic Surgery,* vol. 77, pp. 243-6, 2004.
[73] G. Trubestein, C. Engel, F. Etzel *et al.*, “Thrombolysis by ultrasound,” *Clin Sci Mol Med Suppl,* vol. 3, pp. 697s-698s, Dec, 1976.
[74] R. J. Siegel, M. C. Fishbein, J. Forrester *et al.*, “Ultrasonic plaque ablation. A new method for recanalization of partially or totally occluded arteries,” *Circulation,* vol. 78, no. 6, pp. 1443-8, Dec, 1988.
[75] "http://bardpv.com/flowcardia/datasheets/Crosser-Data-Sht-S11778-Rev2.pdf."
[76] C. A. Boyd, *Vibratory catheterization apparatus and method of using*, United States, U. S. P. Office, 1969.
[77] R. Pflueger, H. Nita, S. Bacich *et al.*, *Ultrasonic angioplasty device incorporating an ultrasound transmission member made at least partially from a superelastic metal alloy*, United States,to Baxter International Inc, U. S. Patent, 1995.
[78] P. S. Levin, J. Saltonstall, L. Nguyen *et al.*, *Ultrasound transmission apparatus and method using same*, United States,to Angiosonics Inc, U. S. Patent, 1999.
[79] S. Atar, H. Luo, T. Nagai *et al.*, “Ultrasonic thrombolysis: Catheter-delivered and transcutaneous applications,” *European Journal of Ultrasound,* vol. 9, no. 1, pp. 39-54, 1999.
[80] R. J. Siegel, P. Gaines, J. R. Crew *et al.*, “Clinical trial of percutaneous peripheral ultrasound angioplasty,” *J Am Coll Cardiol,* vol. 22, no. 2, pp. 480-8, Aug, 1993.
[81] E. Grube, G. Sutsch, V. Y. Lim *et al.*, “High-frequency mechanical vibration to recanalize chronic total occlusions after failure to cross with

conventional guidewires," *Journal of Invasive Cardiology,* vol. 18, no. 3, pp. 85-91, Mar, 2006.
[82] W. W. Cimino, and L. G. Bond, "Physics of ultrasonic surgery using tissue fragmentation: Part 1," *Ultrasound Med Biol,* vol. 22, pp. 89-100, 1996.
[83] J. A. McGeough, *Micromachining of Engineering Materials*, p.^pp. 147-178, New York, 2002.
[84] P. S. Medis, and H. T. Henderson, "Micromaching using ultrasonic impact grinding," *Journal of micromechanics and microengineering,* vol. 15, pp. 1556-1559, 2005.
[85] P. G. Yock, and P. J. Fitzgerald, "Catheter-based ultrasound thrombolysis, shake,rattle and reperfuse," *Circulation,* vol. 95, pp. 1360-1362, 1997.
[86] G. Drobinski, D. Brisset, F. Philippe *et al.*, "Effects of ultrasound energy on total peripheral artery occlusions: Initial angiographic and angioscopic results," *Journal of Interventional Cardiology,* vol. 6, no. 2, pp. 157-163, 1993.
[87] U. Rosenschein, L. A. Rozenszajn, L. Kraus *et al.*, "Ultrasonic angioplasty in totally occluded peripheral arteries. Initial clinical, histological, and angiographic results," *Circulation,* vol. 83, no. 6, pp. 1976-86, Jun, 1991.
[88] H. Hasanzadeh, M. Mokhtari-Dizaji, S. Z. Bathaie *et al.*, "Evaluation of correlation between chemical dosimetry and subharmonic spectrum analysis to examine the acoustic cavitation," *Ultrasonics Sonochemistry,* vol. 17, no. 5, pp. 863-869.
[89] H. L. Liu, W. S. Chen, J. S. Chen *et al.*, "Cavitation-enhanced ultrasound thermal therapy by combined low- and high-frequency ultrasound exposure," *Ultrasound Med Biol*, 5, pp. 759-67, England, 2006.
[90] S. Cancelos, F. J. Moraga, R. T. Lahey *et al.*, "The effect of acoustically-induced cavitation on the permeance of a bullfrog urinary bladder," *The Journal of the Acoustical Society of America,* vol. 128, no. 5, 2010.
[91] W. L. Nyborg, "Basic physics of low frequency therapuetic ultrasound. ultrasound angioplasty," *Developments in Cardiovascular Medicine*: Kluwer Academic Publishers, 1996.
[92] J. P. Perkins, "Power Ultrasonic Equipment: Practice and Application," *Based on a paper presented at the Sonochemistry Symposium, Annual Chemical Congress, Warick University, UK*, pp. 8-11, 1986.
[93] D. M. Hallow, A. D. Mahajan, T. E. McCutchen *et al.*, "Measurement and correlation of acoustic cavitation with cellular bioeffects," *Ultrasound in Medicine & Biology,* vol. 32, no. 7, pp. 1111-1122, 2006.
[94] S. Datta, C.-C. Coussios, A. Y. Ammi *et al.*, "Ultrasound-enhanced thrombolysis using Definity® as a cavitation nucleation agent," *Ultrasound in Medicine & Biology,* vol. 34, no. 9, pp. 1421-1433, 2008.
[95] A. Tezel, and S. Mitragotri, "Interactions of inertial cavitation bubbles with stratum corneum lipid bilayers during low-frequency sonophoresis," *Biophysical Journal,* vol. 85, no. 6, pp. 3502-3512, 2003.
[96] J. Laborde, A. L.Hita, J. P. Caltagirone *et al.*, "Fluid dynamics phenomena induced by power ultrasounds," *Ultrasonics,* vol. 38, no. 1-8, pp. 297-300, 2000.
[97] "American National Standards Institute (ANSI) Technical report: Bubble detection and cavitation monitoring," Acoustic Society of America, 2002.

[98] J. Frohly, S. Labouret, C. Bruneel *et al.*, "Ultrasonic cavitation monitoring by acoustic noise power measurement," *The Journal of the Acoustical Society of America,* vol. 108, no. 5, pp. 2012-2020, 2000.
[99] S. Yoshizawa, and S. Umemura, "Cavitation detection with subharmonic emissions by low intensity sustaining ultrasound," in IEEE International ultrasonics symposium, Beijing, 2008, pp. 772-775.
[100] *International Commission of Radiation Units and Measurements. Tissue substitutes, phantoms and computational modelling in medical ultrasound*, 7910 Woodmont Avenue, Bethesda, Maryland, 20814, USA, 1998.
[101] M. M. Calor Filho, and J. C. Machado, "The ultrasonic attenuation coefficient for human blood plasma in the frequency range of 7 - 90 MHz," in 2004 IEEE International Ultrasonics, Ferroelectrics and Frequency Control Joint 50th Anniversary Conference, 2004.
[102] R. J. Siegel, T. A. DonMichael, M. C. Fishbein *et al.*, "In vivo ultrasound arterial recanalization of atherosclerotic total occlusions," *Journal of the American College of Cardiology,* vol. 15, pp. 352-3., 1990.
[103] G. G. Hartnell, J. M. Saxton, S. E. Friedl *et al.*, "Ultrasonic thrombus ablation: In vitro assessment of a novel device for intracoronary use," *Journal of Invasive Cardiology,* vol. 6, pp. 69-76, 1993.
[104] M. G. Curley, P. S. Hamilton, J. T. Walsh *et al.*, "An evaluation of methods for measuring cardiac output with volumetric heating," in IEEE Engineering in Medicine and Biology Society, Amsterdam, 1996, pp. 131-133.
[105] W. L. Nyborg, "Acoustic Streaming," *Physical acoustics*, pp. 265-331, 1965.
[106] J. Wu, and W. Nyborg, *Emerging Therapeutic Ultrasound*, Singapore: World Scientific Publishing Co Pte Ltd, 2006.
[107] S. D. Danilov, and M. A. Mironov, "Mean force on a small sphere in a sound field in a viscous fluid," *J Acoust Soc Am,* vol. 107, no. 1, pp. 143-53, Jan, 2000.
[108] W. L. Nyborg, "Biological effects of ultrasound: Development of safety guideline. Part 2: General review," *Ultrasound in Medicine & Biology,* vol. 27, no. 3, pp. 301-333, 2001.
[109] D. Lee, and B. G. Loh, "Smart cooling technology utilizing acoustic streaming," *IEEE Transactions of Components and Packaging Technologies,* vol. 30, no. 4, pp. 691-99, 2007.
[110] J. Wu, A. J. Winker, and T. P. O Neill, "Effect of acoustic streaming on ultrasonic heating," *Ultrasound in medicine and biology,* vol. 20, pp. 195-201, 1994.
[111] V. Frenkel, R. Gurka, A. Liberzon *et al.*, "Preliminary investigations of ultrasound induced acoustic streaming using particle image velocimetry," *Ultrasonics,* vol. 39, pp. 153-156, 2001.
[112] C. G. Lauer, R. Burge, D. B. Tang *et al.*, "Effect of ultrasound on tissue-type plasminogen activator-induced thrombolysis," *Circulation,* vol. 86, no. 4, pp. 1257-1264, October 1, 1992, 1992.
[113] T. D. Mast, S. M. Inder Raj, F. Waseem *et al.*, "Bulk ablation of soft tissue with intense ultrasound: Modeling and experiments," *The Journal of the Acoustical Society of America,* vol. 118, no. 4, pp. 2715-2724, 2005.
[114] C. T. McCarthy, M. Hussey, and M. D. Gilchrist, "On the sharpness of straight edge blades in cutting soft solids: Part I - indentation

experiments," *Engineering Fracture Mechanics,* vol. 74, no. 14, pp. 2205-2224, 2007.
[115] M. Mahvash, and V. Hayward, "High-fidelity Haptic synthesis of contact with deformable bodies," *IEEE Comput Graph Appl,* vol. 24, no. 2, pp. 48-55, Mar-Apr, 2004.
[116] T. Azar, and V. Hayward, "Estimation of the Fracture Toughness of Soft Tissue from Needle Insertion," in Proceedings of the 4th international symposium on Biomedical Simulation, London, UK, 2008, pp. 166-175.
[117] C. T. Leondes, *Biomechanical systems technology*, Singapore: World Scientific Publishing Company, 2007.
[118] R. Anschuetz, and H. R. Bernard, "Ultrasonic irradiation and atherosclerosis," *Surgery,* vol. 57, pp. 549-53, Apr, 1965.
[119] J. B. Herrick, "Landmark article (JAMA 1912). Clinical features of sudden obstruction of the coronary arteries. By James B. Herrick," *JAMA,* vol. 250, no. 13, pp. 1757-65, Oct 7, 1983.
[120] R. J. Siegel, D. C. Cumberland, C. Christopher *et al.*, "Ultrasound angioplasty," *Textbook of interventional cardiology*, E. J. Topol, ed., pp. 705-723: Saunders, 1999.
[121] Y. Bige, Y. Yanni, and Y. Jiangang, "Effects of thrombolysis with ultrasound on the structure of erythrocyte and its safety threshold," in Engineering in Medicine and Biology 27th Annual Conference, Shanghai, China, 2005.
[122] F. Philippe, G. Drobinski, C. Bucherer *et al.*, "Effects of ultrasound energy on thrombi *in vitro*," *Catheterization and Cardiovascular Diagnosis,* vol. 28, no. 2, pp. 173-178, 2005.
[123] V. Suchkova, F. N. Siddiqi, E. L. Carstensen *et al.*, "Enhancement of Fibrinolysis with 40-kHz Ultrasound.," *Circulation,* vol. 98, no. 10, pp. 1030-5., 1998.
[124] T. A. Fischell, M. A. Abbas, G. W. Grant *et al.*, "Ultrasonic Energy. Effects on Vascular Function and Integrity," *Circulation,* vol. 84, no. 4, pp. 1783-1795, October 1, 1991, 1991.
[125] U. Rosenschein, V. Furman, E. Kerner *et al.*, "Ultrasound imaging-guided noninvasive ultrasound thrombolysis: preclinical results," *Circulation,* vol. 102, no. 2, pp. 238-45, Jul, 2000.
[126] C. W. Hamm, J. Reimers, R. Koster *et al.*, "Coronary ultrasound thrombolysis in a patient with acute myocardial infarction," *Lancet,* vol. 343, no. 8897, pp. 605-6, Mar 5, 1994.
[127] C. W. Hamm, W. Steffen, W. Terres *et al.*, "Intravascular therapeutic ultrasound thrombolysis in acute myocardial infarctions," *Circulation,* vol. 80, pp. 200-204, 1997.
[128] U. Rosenschein, A. Roth, T. Rassin *et al.*, "Analysis of coronary ultrasound thrombolysis endpoints in acute myocardial infarction (ACUTE trial). Results of the feasibility phase," *Circulation,* vol. 95, no. 6, pp. 1411-6, Mar, 1997.
[129] R. J. Siegel, "Ultrasound augmentation of thrombolysis and tissue perfusion," *Clinical Physiology and Functional Imaging,* vol. 24, no. 3, pp. 156-163, 2004.

[130] R. J. Siegel, D. C. Cumberland, R. K. Myler *et al.*, "Percutaneous ultrasonic angioplasty:initial clinical experience," *Lancet,* vol. 2, no. 8666, pp. 772-4, Sep 30, 1989.
[131] C. R. Bard, *Clinical Trials: Crosser Enters The Right Arterial Lumen (CENTRAL),# NCT01205386*, 2011.
[132] T. A. Fischell, G. Derby, T. M. Tse *et al.*, "Coronary artery vasoconstriction routinely occurs after percutaneous transluminal coronary angioplasty. A quantitative arteriographic analysis," *Circulation,* vol. 78, no. 6, pp. 1323-34, Dec, 1988.
[133] S. K. Chokshi, A. J. Rongione, I. Freeman *et al.*, "Ultrasonic energy produces endothelium- dependent vasomotor relaxation *in vitro*," *Circulation,* vol. 80, pp. 565, 1989.
[134] G. P. Gavin, G. B. McGuinness, F. Dolan *et al.*, "Performance characteristics of a therapeutic ultrasound wire waveguide apparatus," *International Journal of Mechanical Sciences,* vol. 49, no. 3, pp. 298-305, 2007.
[135] D. Noone, G. P. Gavin, and G. B. McGuinness, "Design issues for therapeutic ultrasound angioplasty waveguides," in 25th International Manufacturing Conference, Dublin, Ireland, 2008.
[136] W. L. Nyborg, "Basic Physics of Low Frequency Therapuetic Ultrasound. Ultrasound Angioplasty," *Developments in Cardiovascular Medicine*: Kluwer Academic Publishers, 1996.
[137] G. F. Pinton, "Numerical methods for non-linear wave propagation in ultrasound," Department of Biomedical Engineering, Duke University, 2007.
[138] G. Porges, *Applied Acoustics*: Peninsula Publishing, 1977.
[139] P. M. Morse, "Vibration and Sound," *Journal of the Acoustical Society of America,* vol. 27, pp. 311-326, 1981.
[140] R. J. Siegel, V. N. Suchkova, T. Miyamoto *et al.*, "Ultrasound energy improves myocardial perfusion in the presence of coronary occlusion," *J Am Coll Cardiol*, 7, pp. 1454-8, United States, 2004.
[141] X. Shi, R. W. Martin, S. Vaezy *et al.*, "Quantitative investigation of acoustic streaming in blood.," *Journal of the Acoustical Society of America,* vol. 111, pp. 1110-21, 2002.
[142] A. Mal, F. Feng, M. Kabo *et al.*, "Interaction of high intensity focused ultrasound with biological materials," in SPIE's NDE and Smart Structures Symposium, San Diego, 2002, pp. 4702-40.
[143] K. L. Gentry, M. L. Palmeri, N. Sachedina *et al.*, "Finite-element analysis fo temperature rise and lesion formation from catheter ultrasound ablation transducers," *IEEE Transactions on Ultrasonics, Ferroelectrics and Frequency Control,* vol. 52, no. 10, pp. 1713-21, 2005.
[144] B. Anvari, S. Rastegar, and M. Motamedi, "Modeling of intraluminal heating of biological tissues: Implications for treatment of benign prostatic hyperlasia," *IEEE Transactions on Biomedical Engineering,* vol. 41, no. 9, pp. 854-64, 1994.
[145] G. P. Gavin, F. Dolan, M. S. J. Hashmi *et al.*, "A coupled fluid-structure model of a therapeutic ultrasound angioplasty wire waveguide.," *Journal of Medical Devices*, pp. 254-263., 2007.

[146] R. Hill, S. A. Forsyth, and P. Macey, “Finite element modelling of ultrasound with reference to transducers and AE waves,” *Ultrasonics,* vol. 42, no. 1-9, pp. 253-258, 2004.
[147] Y. Liu, “Wave propagation study using finite element analysis,” Electrical Engineering, University of Illinois, Urbana-Champaign, 2005.
[148] M. Zampolli, A. Tesei, and F. B. Jensen, "Finite element models for the solution of underwater acoustics problems."
[149] G. Wojcik, J. Mould, F. Lizzi *et al.*, "Nonlinear modeling of therapeutic ultrasound." pp. 1617-22.
[150] F. A. Duck, “Nonlinear acoustics in diagnostic ultrasound,” *Ultrasound in Medicine and Biology,* vol. 28, no. 1, pp. 1-18, 2002.
[151] M. Palmeri, A. C. Sharma, R. R. Bouchard *et al.*, “A finite-element method model of soft tissue response to impulsive acoustic radiation force.,” *IEEE Transactions on Ultrasonics, Ferroelectric and Frequency Control.,* vol. 52, no. 10, pp. 1699-712, 2005.
[152] J. Wu, and W. L. Nyborg, “Ultrasound, cavitation bubbles and their interaction with cells,” *Advanced Drug Delivery Reviews,* vol. 60, pp. 1103-1116, 2008.
[153] F. Mosser, L. Jacobs, and J. Qu, “Modelling elastic wave propagation in wave-guides using the finite element method,” *NDT & E International,* vol. 32, pp. 225-234, 1999.
[154] N. Abbouda, G. L. Wojcikb, D. K. Vaughanb *et al.*, "Finite element modeling for ultrasonic transducers."
[155] C. S. Zhang, D. H. Zou, and V. Madenga, “Numerical simulation of wave propagation in grouted rock bolts and the effects of mesh density and wave frequency,” *International Journal of Rock Mechanics and Mining Sciences,* vol. 43, no. 4, pp. 634-639, 2006.
[156] J. P. Lewis, S. Gardner, and L. Corp, “A 2D finite element analysis of an ultrasonic cleaning vessel: Results and comparisons,” *International Journal of Modelling and Simulation,* vol. 27, no. 2, pp. 181-85, 2007.
[157] P. Reynolds, and J. Mould, "Short course: Finite element modeling for ultrasonic applications: Part 2: Wave propagation."
[158] A. t. reference., "Chapter 8: Acoustics. ANSYS Documentation, 15317.," ANSYS Inc, Canonsburg, PA, 2009.
[159] “Instruction manual: Sonifier 150 - Ultrasonic cell disruptor and homogiser,” 1999.
[160] “Sonifier cell disruptor : Microtips,” 1998.
[161] C. A. Boyd, *Vibratory catheterization apparatus and method of using*, United States, U. S. P. Office, 1969.
[162] R. Pflueger, H. Nita, S. Bacich *et al.*, *Ultrasonic angioplasty device incorporating an ultrasound transmission member made at least partially from a superelastic metal alloy*, United States,to Baxter International Inc, U. S. Patent, 1995.
[163] R. F. J. Seidel, "Distributed systems," *An introduction to mechanical vibrations*, Wiley, ed., 1989.
[164] ASTM, "ASTM E220-86e1: Standard test method for calibration of thermocouples by comparison techniques," 1996.

[165] C. X. Deng, Q. Xu, R. E. Apfel *et al.*, "*In vitro* measurements of inertial cavitation thresholds in human blood," *Ultrasound in Medicine & Biology,* vol. 22, no. 7, pp. 939-948, 1996.
[166] ANSI, "Bubble Detection and Cavitation Monitoring," Acoustic Society of America, 2002.
[167] M. Hodnett, R. Chow, and B. Zeqiri, "High-frequency acoustic emissions generated by a 20 kHz sonochemical horn processor detected using a novel broadband acoustic sensor: a preliminary study," *Ultrasonics Sonochemistry,* vol. 11, no. 6, pp. 441-454, 2004.
[168] C. Lally, A. J. Reid, and P. J. Prendergast, "Elastic behavior of porcine coronary artery tissue under uniaxial and equibiaxial tension," *Ann Biomed Eng,* vol. 32, no. 10, pp. 1355-64, Oct, 2004.

8 APPENDIX

8.1 Histological images (H & E)

8.1.1 Non-energised wire waveguide perforation

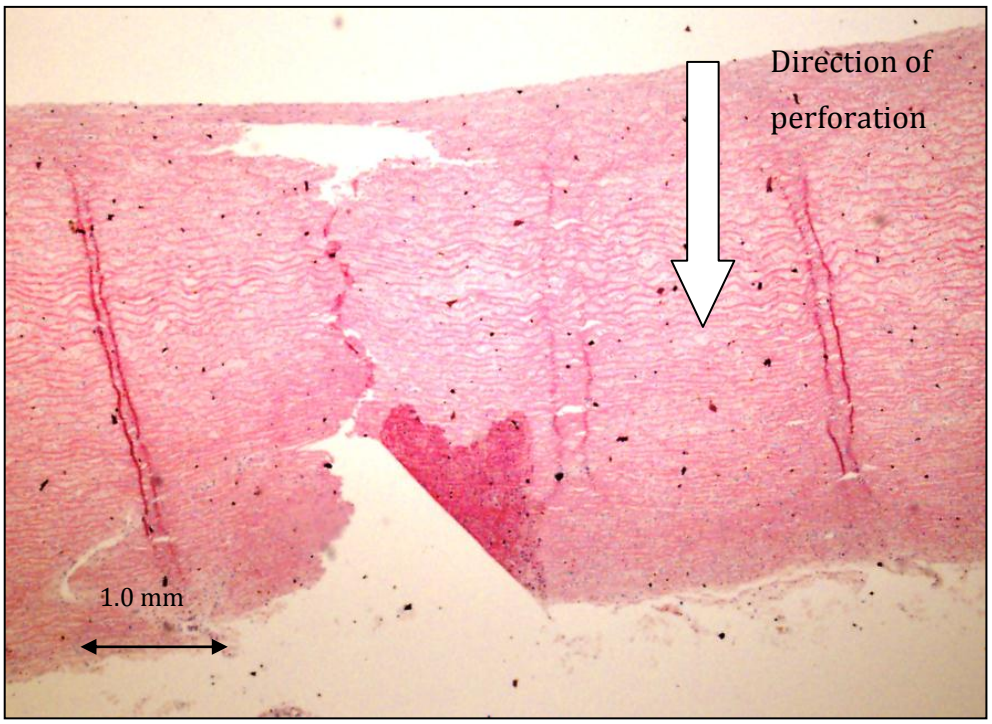

Figure 8-1 : Artery perforation with non-energised wire waveguide. 4x.

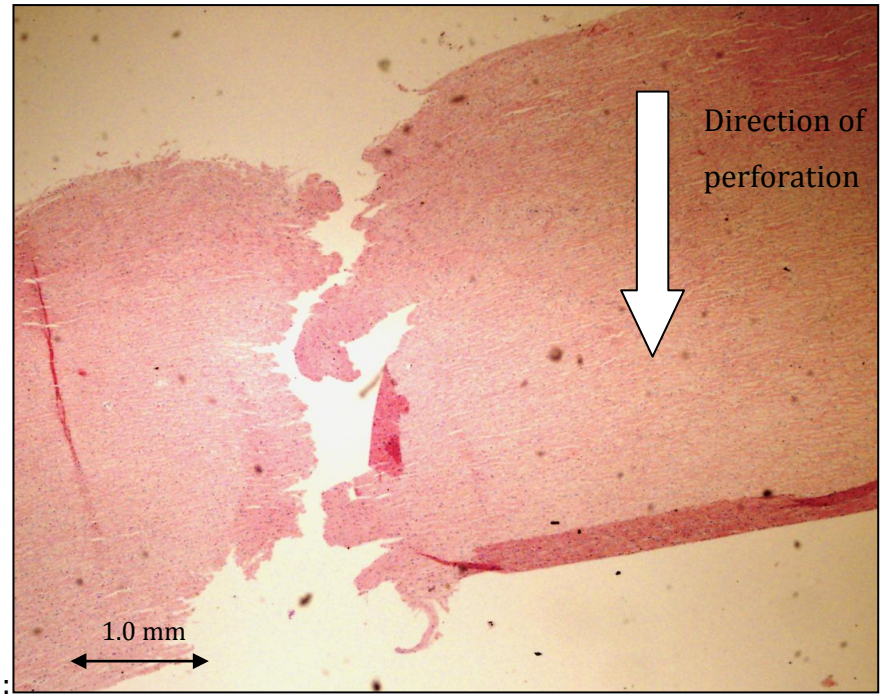

Figure 8-2 : Artery perforation with non-energised wire waveguide. 4x.

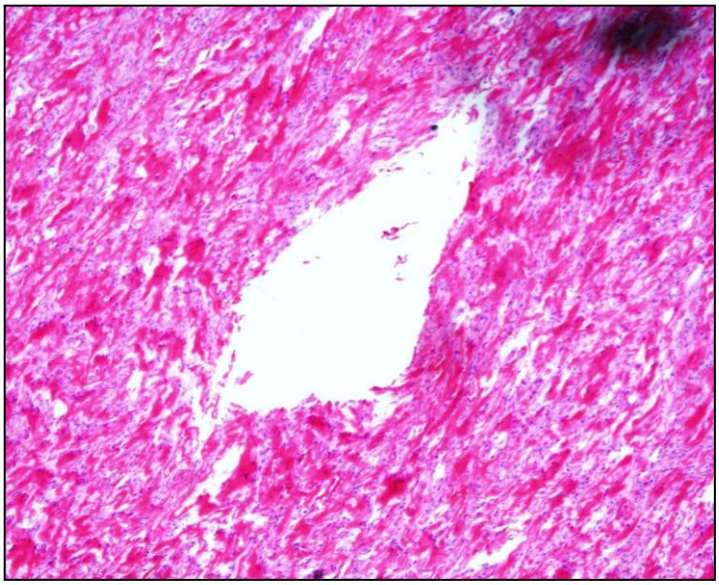

Figure 8-3 : Artery perforation with non-energised wire waveguide. 4x. Plan view.

8.1.2 Energised wire waveguide perforation

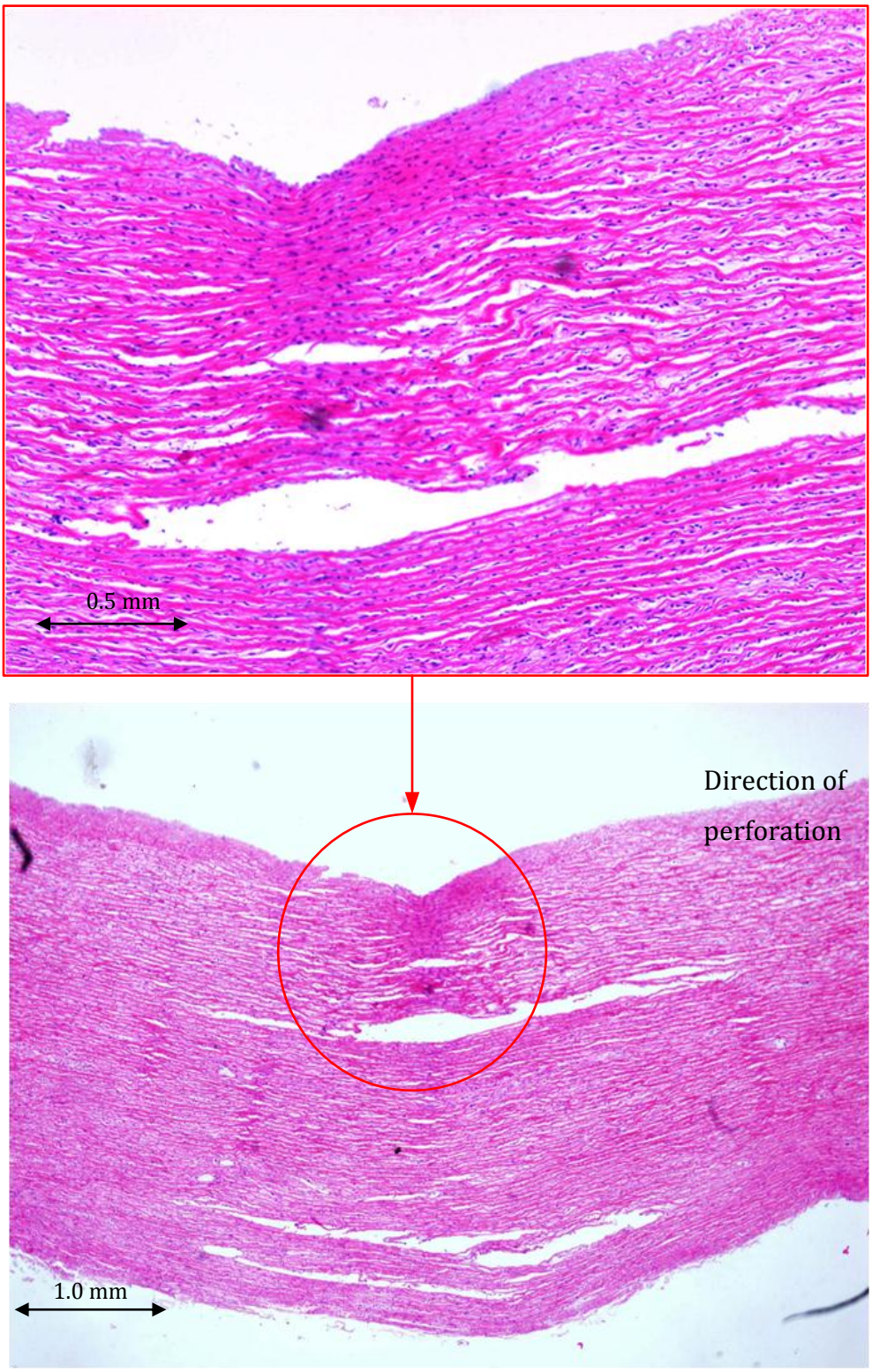

Figure 8-4 : (Top), magnification of fibre compression, 20x. (Bottom), evidence of residual damage with ultrasound.

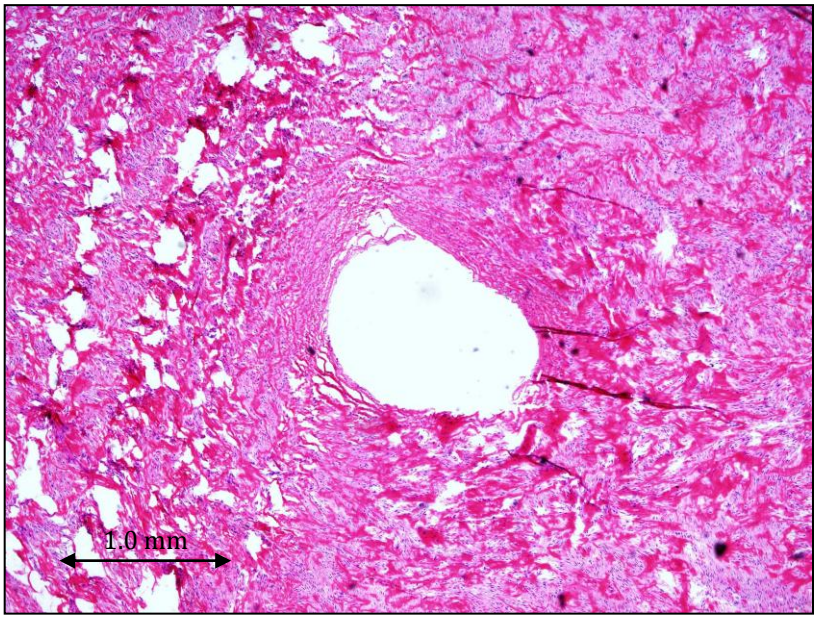

Figure 8-5 : Plan view of point of entry. 27.8 µm amplitude of vibration. 4x.

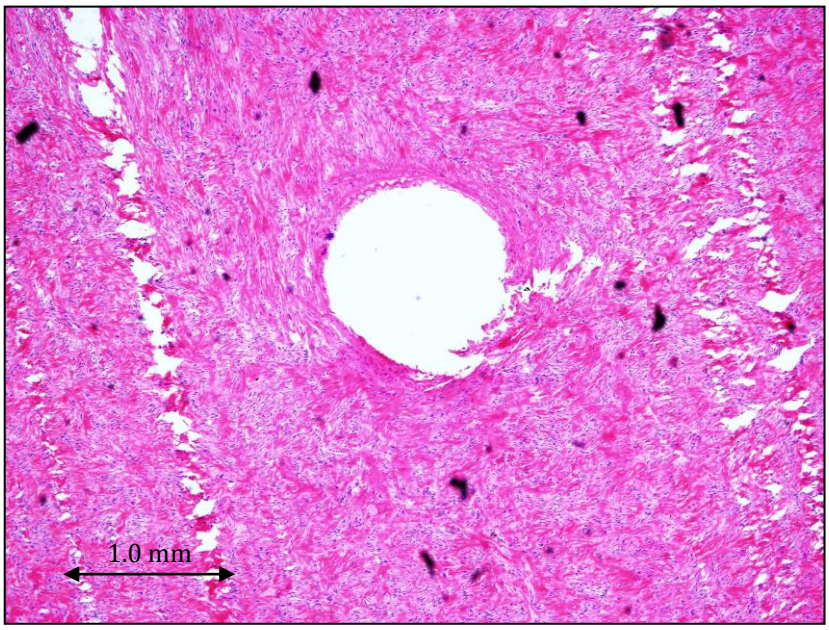

Figure 8-6 : Plan view of point of entry. 34.3 µm amplitude of vibration.4x.